QC
1
.P5812
v.56
no.8

THE PHYSICAL REVIEW

VOLUME 56 Second Series NUMBER 8

OCTOBER 15, 1939

Published for the

AMERICAN PHYSICAL SOCIETY

by the

AMERICAN INSTITUTE OF PHYSICS

LANCASTER, PA., AND NEW YORK, N. Y.

THE PHYSICAL REVIEW

A journal of experimental and theoretical physics established by E. L. Nichols in 1893

Published by the American Institute of Physics for the

American Physical Society

OFFICERS

President

JOHN T. TATE
University of Minnesota
Minneapolis, Minnesota

Vice President

JOHN ZELENY
Yale University
New Haven, Connecticut

Secretary

W. L. SEVERINGHAUS
Columbia University
New York, New York

Treasurer

G. B. PEGRAM
Columbia University
New York, New York

Local Secretary for the Pacific Coast

PAUL KIRKPATRICK
Stanford University
California

Editor

JOHN T. TATE
University of Minnesota
Minneapolis, Minnesota

BOARD OF EDITORS

JOHN T. TATE, *Editor* — J. W. BUCHTA, *Assistant Editor*

Associate Editors

K. T. BAINBRIDGE	A. L. HUGHES	W. BLEAKNEY
H. P. ROBERTSON	T. H. JOHNSON	G. BRETT
H. B. WAHLIN	F. A. JENKINS	D. M. DENNISON

Manuscripts for publication should be submitted to John T. Tate, University of Minnesota, Minneapolis, Minnesota.

Proof and all correspondence concerning papers in the process of publication, should be addressed to the Publications Manager, American Institute of Physics, 175 Fifth Avenue, New York, New York.

Subscription Price

United States and Possessions and Canada	$15.00
Foreign	$16.50

Back Numbers

Complete set: Series 2,[1] Vol. 1, 1913–Vol. 54, 1938—$390.00
Yearly rate: $16.50
Single copies: $1.50 each prior to July, 1929; $.75 each after July, 1929.

Subscriptions and orders for back numbers should be addressed to Prince and Lemon Streets, Lancaster, Pennsylvania, or to the American Institute of Physics, 175 Fifth Avenue, New York, New York.

Advertising is not accepted for the *Physical Review* but attention is called to the *Review of Scientific Instruments* and the *Journal of Applied Physics*, companion publications of the Institute, and media through which the field of physics can be reached most effectively. Rates and other information will be furnished on request.

Changes of address and complaints of failure to receive the *Physical Review* in the case of members of the American Physical Society, should be addressed to the Treasurer; in the case of other subscribers, to the Publications Manager.

[1] For Series 1 inquire of Physics Department, Cornell University, Ithaca, N. Y.

The Physical Review is published semi-monthly at Prince and Lemon Streets, Lancaster, Pennsylvania.

Entered at the Post Office at Lancaster, Pennsylvania, as second class matter.

Acceptance for mailing at special rate of postage provided for in section 1103, Act of October 3, 1917, authorized September 6, 1926.

THE
PHYSICAL REVIEW
A Journal of Experimental and Theoretical Physics Established by E. L. Nichols in 1893
VOL. 56, NO. 8 OCTOBER 15, 1939 SECOND SERIES

The Beta-Ray Spectra of Mg^{27}, Cu^{62} and the Nuclear Isomers of Rh^{104}

E. C. CRITTENDEN, JR.*
Cornell University, Ithaca, New York
(Received August 28, 1939)

The beta-ray spectra of several radioactive elements have been investigated by means of a cloud chamber in a uniform magnetic field. The spectrum of Mg^{27} gave an upper limit of 1.8 Mev on the basis of 586 tracks. The spectrum of Cu^{62} gave an upper limit of 2.6 Mev on the basis of 803 tracks. The spectra of the two nuclear isomers of Rh^{104} were found to have the same upper limit and the same shape within experimental error. Their upper limits are 2.3 Mev on the basis of 524 and 529 tracks. The similarity in shape of the two spectra indicates that a direct beta-transition from the 4.37-minute level does not occur to any appreciable extent and that as far as can be determined by this work the disintegration of the 4.37-minute isomer proceeds entirely by a gamma-ray transition to the ground state of Rh^{104} followed by a beta-transition to the ground state of Pd^{104}.

THE use of a cloud chamber in a magnetic field for the measurement of beta-ray spectra is ultimately limited by the scattering of the beta-particles in the gas which must necessarily fill the chamber and by the practical limitation on the number of tracks observable in a reasonable length of time. However, the method will give quite dependable spectra if sufficient care is exercised in the choice of tracks to be measured and if a fairly large number of tracks are utilized. This method was used to obtain the spectra of several beta-radioactive elements. The spectra of Mg^{27} and Cu^{62} have been investigated as well as the spectra of the two nuclear isomers of Rh^{104}. The latter two spectra are of particular interest as they give information concerning the course of the disintegration of the isomers.

Apparatus

The essential features of the design of the cloud chamber were taken from Kurie's modification[1] of the pressure operated sylphon chamber of Dahl, Hafstad and Tuve.[2] The active region of the chamber was 17 cm in diameter and 2.5 cm deep. The chamber was filled with helium at atmospheric pressure. Helium was employed as the gas with which to fill the chamber in order to decrease the scattering of the beta-particles. This gas was selected in preference to hydrogen as the low viscosity of the latter allowed the liquid droplets to fall too rapidly to permit sharp photography. Ethyl alcohol was employed as the liquid vapor in the chamber.

The magnetic field for deflecting the beta-particles was produced by a pair of Helmholtz coils capable of producing 900 oersteds under intermittent operation. The field was carefully checked for uniformity and found to be uniform within 2 percent over the visible region of the chamber. The magnitude of the field was measured by two independent methods agreeing within 0.5 percent.

* Now at Case School of Applied Science.

[1] F. N. D. Kurie, Phys. Rev. **47**, 97 (1935).
[2] O. Dahl, L. R. Hafstad and M. A. Tuve, Rev. Sci. Inst. **4**, 373 (1933).

Since the radioactivities investigated all had fairly short half-lives, the samples could not be placed directly in the cloud chamber. Instead, the samples were placed in a "well" in the top plate of the chamber and the beta-particles admitted through a thin aluminum window. This window had a thickness of 7 mg/cm² which was estimated to be equivalent to 0.01 Mev for electrons of 2 Mev.

The illumination for the cloud chamber was furnished by a bank of eight incandescent lamps of a type intended for series operation as street lamps on 32 volts and 6.6 amp. A lamp of this type has a double-coiled line filament and gave a fairly parallel beam when used with a cylindrical condensing lens. A Sept camera with an f: 3.5 lens was used for the photography. After development, the negatives were projected through a similar camera to give a full size image as determined by a template. No detectable distortion was introduced in the projection. The tracks were classified into groups differing in radius of curvature by 0.5 cm by the usual method of matching them to a series of circles. The lack of exact knowledge of the position of the tracks as a consequence of nonstereoptic photography introduced a small error in the radius of curvature. The maximum error from this cause was calculated to be 2.4 percent.

Several criteria were established which each track was required to satisfy in order to be considered acceptable for measurement. Most of these criteria have been discussed at some length by other writers[3, 4] and will be merely listed here. The criteria were as follows: (1) The track must be of the proper direction of curvature. (2) The track must be visible to 7 cm or more from the aluminum window. (3) The track must be visible to within 1 cm of the aluminum window. (4) The track must appear to have its origin in the source. (5) The track must suffer no detectable deflection from a circular path in 7 cm. In addition to the above criteria tracks which showed noticeable diffusion of the ions were excluded.

[3] E. R. Gaerttner, J. J. Turin and H. R. Crane, Phys. Rev. **49**, 793 (1936).
[4] J. R. Richardson and F. N. D. Kurie, Phys. Rev. **50**, 999 (1936).

The spectrum of Mg^{27}

Metallic magnesium was bombarded by 1.2-Mev deuterons from the cyclotron for the purpose of studying the spectrum of the 10-minute activity. The accepted reaction, assigned by Henderson,[5] is:

$$_{12}Mg^{26}+{}_{1}H^{2}\rightarrow{}_{12}Mg^{27}+{}_{1}H^{1},$$
$$_{12}Mg^{27}\rightarrow{}_{13}Al^{27}+\beta+\gamma.$$

Na^{24}, of 14.8 hours half-life, is also formed on bombardment of Mg by deuterons. On the basis of Henderson's[5] results on the excitation functions of Mg^{27} and Na^{24}, the excitation probability of Na^{24} is estimated to be less than 0.05 percent of the excitation probability of Mg^{27} for a deuteron energy of 1.2 Mev. The Na^{24} should thus not affect the spectrum observed for Mg^{27}.

The Mg samples which were prepared for cloud-chamber measurements were first cleaned to remove the oxide coating and then bombarded directly in the deuteron beam inside the vacuum of the cyclotron chamber. The target, when bombarded, collected some deposit of carbon from the pump-oil vapor recoiled onto its surface. This carbon gave N^{13} on bombardment which has an 11-minute *positron* period and thus is easily distinguished from the Mg^{27} *electron* spectrum. For the purpose of determining the half-life, the sample was covered with a thin aluminum foil to avoid deposition of carbon and bombarded as above. The activity of the target so prepared was measured with an Edelmann

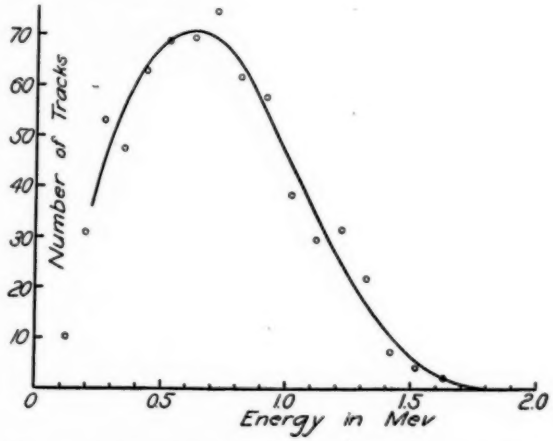

FIG. 1. Distribution in energy of 586 tracks for Mg^{27}.

[5] M. C. Henderson, Phys. Rev. **48**, 855 (1935).

electrometer and argon-filled ionization chamber. The same method of measurement was employed to obtain the data used in the other half-life determinations. For Mg, a half-life of 10.0±0.1 minutes[6] was obtained. This result is in agreement with the value of 10.25±0.25 minutes previously determined by Henderson.[4]

There were 586 acceptable tracks observed in the cloud chamber. The distribution in energy of these tracks appears in Fig. 1. Visual extrapolation of this curve to the energy axis gives an upper limit of 1.8 Mev. This is considerably lower than the results obtained by other workers using the absorption method. Henderson[4] obtained an upper limit of 2.05 Mev by the use of Feather's rule. Widdowson and Champion[7] also measured this upper limit by absorption and obtained 1.96 Mev.

K-U and Fermi plots were made for this spectrum. These led to end-points of 2.0 Mev and 1.7 Mev, respectively, the latter fitting a straight line possibly somewhat better than the former.

The spectrum of Cu^{62}

Metallic copper was bombarded by the high energy neutrons resulting from the bombardment of Li by 1.2-Mev deuterons and the beta-ray spectrum of the 10-minute activity studied. The accepted reaction, assigned by Heyn[8] is:

$$_{29}Cu^{63}+{}_0n^1\rightarrow{}_{29}Cu^{62}+{}_0n^1+{}_0n^1,$$
$$_{29}Cu^{62}\rightarrow{}_{28}Ni^{62}+\epsilon^+.$$

The bombardment of Cu by high energy neutrons, which in this case involves bombardment by neutrons of all lower energies, leads to a number of radioactive products. Only two of these products other than the one studied emit positrons. These are Cu^{64}, of 12.8 hours half-life, and Cu^{61}, of 3.4 hours half-life. These activities should not interfere with measurements on Cu^{62} as they should be excited only weakly under bombardment for a short time.

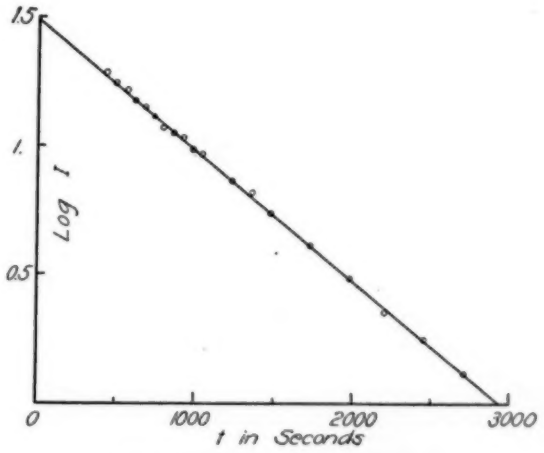

FIG. 2. Decay curve for Cu^{62}.

The samples to be exposed to the high energy neutrons were placed outside the vacuum of the cyclotron, separated from the Li target by a wall of copper 0.24 cm thick. The samples had a thickness of 192 mg/cm² which was estimated to be equivalent to 0.2 Mev for electrons of 2 Mev. Such a thickness of the sample should not appreciably alter the value obtained for the visually extrapolated end point. It may, however, cause the curve to approach the axis more slowly than if a thin source were used.

The samples were bombarded for 15 minutes with a deuteron current of 7 microamperes on the Li. The decay curve of one of the samples is given in Fig. 2. There is no evidence in this curve of the presence of the longer period activities. The half-life obtained was 9.92±0.05 minutes. This is in agreement with Ridenour and Henderson's[9] value of 10.0±0.1 minutes.

Measurements were made on 803 acceptable tracks. The distribution in energy of these tracks is plotted in Fig. 3. The curve extrapolates visually to an upper limit of 2.6 Mev. (K-U upper limit 3.0 Mev.)

The spectra of the isomers of Rh^{104}

Rh bombarded by slow neutrons gives rise to two electron activities with half-lives reported to be 44 seconds and 4.2 minutes.[10] These have

[6] The writer is indebted to Mr. B. L. Moore of this laboratory for these measurements on the Mg^{27} half-life, which were made in connection with other work. The error quoted here and for the other half-lives to be reported in this paper is the estimated error in drawing a straight line through the points in a plot of the logarithm of the intensity *vs.* time.

[7] E. E. Widdowson and F. C. Champion, Proc. Phys. Soc. **50**, 185 (1938).

[8] F. A. Heyn, Nature **138**, 723 (1937); Physica **4**, 160 (1937).

[9] L. N. Ridenour and W. J. Henderson, Phys. Rev. **52**, 889 (1937).

[10] E. Amaldi and E. Fermi, Phys. Rev. **50**, 899 (1936).

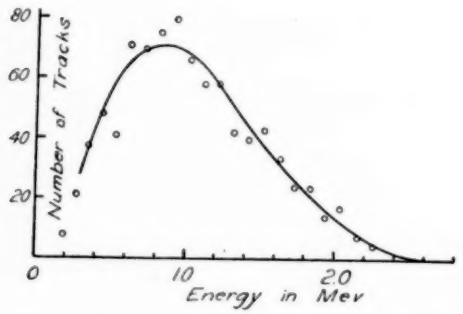

FIG. 3. Distribution in energy of 803 tracks for Cu^{62}.

been ascribed to isomers of the single isotope Rh^{104} in which one isomer represents a metastable state and the other isomer the ground state.[11] Pontecorvo[12] has found that the continuous spectrum of the 4.2-minute activity is accompanied by a homogeneous group of electrons of 35–60 kv. These he concluded are formed by internal conversion of gamma-radiation of about 80 kv emitted in a transition from the metastable state of Rh^{104} to the ground state. He further concluded that the 44-second beta-ray activity was due to transitions from the ground state of Rh^{104} to the ground state of Pd^{104}. This same transition would account for at least part of the continuous spectrum of the 4.2-minute activity.

An alternative process to the gamma-ray transition from the metastable state of Rh^{104} is a direct beta-transition to Pd^{104}. The occurrence of this direct beta-transition would probably leave the resultant Pd^{104} nuclei in one or more excited states, since a transition directly from the metastable state of Rh^{104} to the ground state of Pd^{104} would require a large change of spin. The superposition of this spectrum on the spectrum due to transition from the ground state of Rh^{104} would give the spectrum of the long period activity a shape different from that of the short period activity. A study of the shape of the spectra of the two isomers then affords a means of detecting the presence of the direct beta-transition.

Neutrons were produced by bombardment of metallic Li by 1.2-Mev deuterons. The Rh samples had a thickness of 184 mg/cm² which was estimated to be equivalent to 0.2 Mev for electrons of 2 Mev. These samples were placed about 4 cm from the neutron source and surrounded by paraffin. The decay curve after exposure for 17 minutes is shown in curve I of Fig. 4. Observations were taken with two instrument sensitivities indicated by the circles and crosses on the figure. The half-life of the long period activity was determined to be 4.37 ± 0.05 minutes. Subtracting the ordinates of the line from the ordinates of the decay curve for small values of the time resulted in the curve shown in curve II, Fig. 4. This gave a half-life of 42 ± 2 seconds for the short period activity. The ratio of initial intensities corrected to infinite bombardment time was determined to be 12 ± 1. This is in agreement with Pontecorvo's[11] value of 11 ± 0.7 obtained under bombardment by Rn+Be neutrons after passage through paraffin. A further measurement of the short period half-life using a bombardment time of 2 seconds gave a half-life of 41.8 ± 0.7 seconds.

For the cloud-chamber work the short period activity was separated by bombarding for 15 seconds and making the first expansion 24 seconds later followed by one expansion every 15 seconds up to 10 expansions. It was calculated that under these conditions 3.7 percent of all

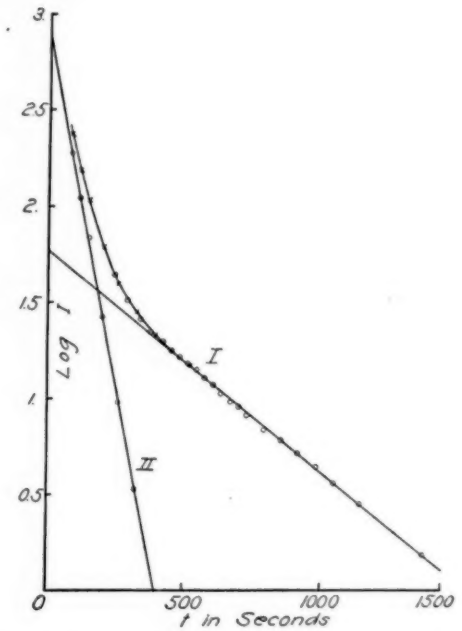

FIG. 4. Decay curves for Rh. I. Decay curve of both activities. II. Decay curve for short period activity.

[11] B. Pontecorvo, Nature **141**, 785 (1936).
[12] B. Pontecorvo, Phys. Rev. **54**, 542 (1938).

the tracks observed were due to the long period activity.

The long period activity was separated by bombarding for 17 minutes and making the first expansion 420 seconds later followed by one expansion every 15 seconds up to 40 expansions. Under these conditions 0.8 percent of all the tracks observed were due to the short period activity.

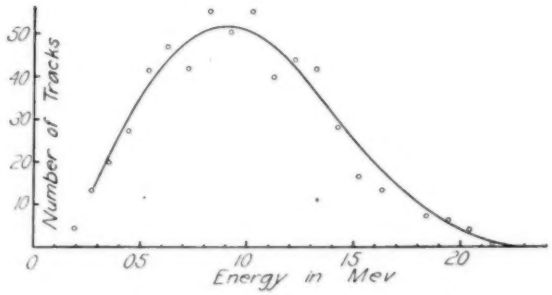

FIG. 5. Distribution in energy of 529 tracks for the short period activity of Rh.

The distribution in energy of the tracks from the short period activity is given in Fig. 5. This curve represents a total of 529 acceptable tracks. Visual extrapolation of this curve to the energy axis yields an upper limit of 2.3 Mev. The spectrum of this same activity has previously been investigated with a cloud chamber by Gaerttner, Turin, and Crane[3] who reported a K-U upper limit of 2.8 Mev. For comparison with their work a K-U plot was made for this spectrum which led to a K-U upper limit of 2.7_4 Mev.

The distribution in energy of the tracks for the long period activity on the basis of the observation of 524 acceptable tracks appears in Fig. 6. The visually extrapolated upper limit obtained from this curve is 2.3 Mev. This value is the same as the upper limit of the short period

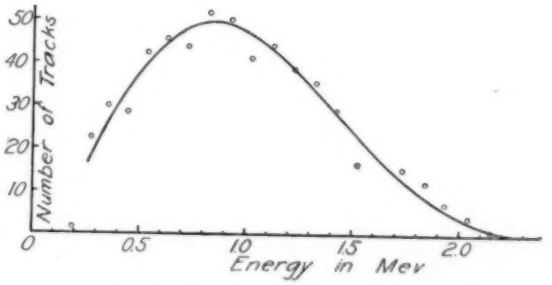

FIG. 6. Distribution in energy of 524 tracks for the long period activity of Rh.

activity. Furthermore the two spectra have shapes which are the same within experimental error, as briefly reported before.[13]

Some conclusions can be drawn from these results. (1) The common value for the upper limit of the two beta-spectra agrees with Pontecorvo's conclusion that the beta-transition from the ground state of Rh^{104} to the ground state of Pd^{104} is responsible for at least part of the continuous spectrum of the long period activity. (2) The similarity in shape of the two spectra leads to the conclusion that the direct beta-transition from the metastable state does not occur to any appreciable extent. Thus, as far as can be determined from this work, the long period activity proceeds entirely by a gamma-ray transition from the metastable state of Rh^{104} to the ground state, followed by the beta-ray emission to the ground state of Pd^{104}.

This work was aided by a grant from the Research Corporation which made possible the use of the cyclotron. The writer wishes to express his appreciation to Professor M. S. Livingston and Professor R. F. Bacher for frequent advice and helpful criticism.

[13] E. C. Crittenden, Jr. and R. F. Bacher, Phys. Rev. **54**, 862 (1938).

The Production of a Beam of Fast Neutrons

PAUL C. AEBERSOLD*
Radiation Laboratory, Department of Physics, University of California, Berkeley, California
(Received July 25, 1939)

Well-defined, intense beams of fast neutrons have been produced by using shields of paraffin and lead in conjunction with the 8-Mev deuteron-beryllium source of a cyclotron. Essentially, the beam is delimited by an outward tapering channel through a wall of paraffin (or water) over 50 cm thick. Accompanying gamma-radiation was greatly reduced by lining the channel with 3 cm of lead and by walling the outside of the hydrogenous shield with over 2.5 cm of lead. Gamma-rays from the source are suppressed by a 3-cm thick lead filter in the channel. Ionization measurements and photographs showed that the fast neutron effects are mainly localized to a collimated beam which radiates out along the projection of the aperture through the lead channel. To distinguish between neutron and gamma-radiations the responses of small ionization chambers with different walls were studied. The ionization produced by the fairly uniform background of gamma-radiation is only a few percent of that caused by fast neutrons in the beam. With an ordinary deuteron current of 60 μa the ionization produced in air at the beam outlet by fast neutrons alone is 1.14 e.s.u./cc per min. To produce a neutron beam of this intensity would require a Rn-Be source of over 10^5 curies. The beam was found suitable for many physical and biological experiments.

INTRODUCTION

FOR the use of fast neutrons in many physical and biological experiments it is desirable to employ the radiation as a collimated beam. Although collimation is readily achieved with x-rays through the use of lead diaphragms, there is no correspondingly effective absorber for fast neutrons. Limiting diaphragms for these penetrating rays must consist of channels through large thicknesses of matter. Special problems then arise concerning the scattering of radiation by the sides of the apertures and the production of secondary radiation by the material of the diaphragms.

The design of an arrangement to collimate fast neutrons will depend on the uses contemplated for the beam. In the present case a beam was sought that would be comparable with those used in x-ray therapy, for example, a beam having an area of 50 to 100 cm^2 at 70 cm from the source with only a small intensity of radiation outside of the beam. Consideration must also be given to the thickness and type of materials for shielding the regions outside the desired beam, to the reduction of scattered and secondary radiations, and to geometrical factors that determine the disposition of absorbing material.

A further essential consideration concerns the intensity available at the outlet. Since fast neutrons necessarily demand thick diaphragms, a beam with an intensity feasible for many interesting biological experiments cannot be gained by close approach to the source but must be attained by the use of an intense source. Fortunately, the source used for these experiments, a beryllium plate bombarded by deuterons accelerated to an energy of 8 Mev in the cyclotron of Lawrence and Cooksey,[1] was adequate for the purpose; for with the prevailing deuteron currents of 60 to 90 microamperes, it was determined that the outlet of the beam could be 70 cm or more from the source and still give good intensities. This allows a thickness of 60 cm or more of absorber in the diaphragming arrangement. Fortunately, too, this thickness of paraffin or water is quite effective in attenuating the intensity of neutrons.

DESIGN OF THE DIAPHRAGMING ARRANGEMENT

As a result of its greater hydrogen content, paraffin effects a greater reduction of fast neutron intensity for a given thickness than any other practicable material, making it the most efficient and compact shielding material. Water has about 85 percent as many hydrogen nuclei per cc as paraffin, and, according to Dunning *et al.*,[2,3] the mean free path of fast neutrons in water is 15

* Fellow of the Finney-Howell Foundation.

[1] E. O. Lawrence and D. Cooksey, Phys. Rev. **50**, 1131 (1936).
[2] J. R. Dunning, Phys. Rev. **45**, 586 (1934).
[3] Dunning, Pegram, Fink and Mitchell, Phys. Rev. **48**, 265 (1935).

percent greater than in paraffin (5.9 and 5.1 cm, respectively). Other advantages of paraffin are that it can be molded into special shapes and stacked in various arrangements, but, where large masses of shielding material are needed, water is more economical and more easily transferable.

The shielding to be expected of thick, extensive diaphragms cannot be calculated without taking into account the resultant scattered radiation. Values given by Dunning on the transmission of fast neutrons out of spherical absorbers are pertinent to the present problem. These may be used in estimating that a spherical shield of paraffin with a radius of 55 cm around the source will reduce the fast neutron intensity, measured on the basis of recoil proton ionization, by more than a factor of one hundred. Such a reduction was noted in preliminary measurements with the cyclotron source.

If an open channel to the source is put through the shield, fast neutrons can emerge from this channel and elsewhere most of them will have been slowed down and largely absorbed. Preliminary tests with a channel through a wall of paraffin showed that the fast neutron intensity at the outlet of the channel was much greater than the intensities aside from it, but the arrangement was unsatisfactory for general purposes because it afforded very little shielding against gamma-rays.

Not only do gamma-rays come from the source to the extent of one or more quanta per neutron, but ultimately every neutron is absorbed in a nucleus and may give rise to several quanta. Gamma-rays from the source with energies above one Mev will scatter through a paraffin shield to a much greater extent than fast neutrons. Gamma-rays created by neutron absorption in hydrogenous shields, 2.2 Mev quanta from the formation of deuterons, and those created in other surrounding materials will add in making a general gamma-ray background.

Whether lead, which is ordinarily used for gamma-ray shielding, should be used in this case depends on how much gamma-radiation is created in Pb by neutrons. Fleischmann found[4] that the "infinite" thickness yield of gamma-rays from Pb by slow neutron bombardment is but a third of that for paraffin, an eighth to a ninth of that for Fe and Cu, and about a twenty-fifth of that for Cd whereas it is only about twice that of the lowest emitters, B_2O_3 and C. Investigations of the excitation of gamma-rays by medium energy neutrons have all shown that the maximum cross section occurs in the region of atomic number 50 and that for Al and Pb the cross sections are around a fifth of the maximum. For higher energy neutrons, above 4 Mev, Grahame and Seaborg,[5] and also Soltan,[6] report cross sections for inelastic scattering that increase with atomic number and are about 0.4 of the total cross section for absorption plus total scattering given by Dunning. In most places where lead shielding would be employed, however, the average energy of the neutrons would not be high. In any event, the gamma-ray yield by neutron excitation from a thickness of lead required for a certain absorption of incident gamma-rays will be less than that for a thickness of a lighter material needed to cause the same absorption.

The most direct way of obtaining a region for experiments at the outlet of the neutron diaphragm that is fairly free of gamma-rays would be to build a lead-walled box or room outside the neutron shield. If, however, a thick lead wall is allowed to extend across the opening at the receiver end of the channel, the fast neutrons encounter a mass of lead as they emerge and can be scattered sufficiently to destroy much of the collimation effected by the channel. If, on the other hand, an opening is provided through the lead wall at the channel outlet, gamma-radiation from a large region of material around the channel is admitted past the gamma-ray shield. Both of these difficulties can be overcome by lining the channel and covering the target end of the channel with lead.

The question arises whether a lead lining, which should be a few cm thick for the necessary gamma-ray shielding, will make the channel unsuitable for neutron collimation. Although Pb nuclei are not so effective as H nuclei in slowing down neutrons, the average distances between

[4] R. Fleischmann, Naturwiss. **22**, 839 (1934).

[5] D. C. Grahame and G. T. Seaborg, Phys. Rev. **53**, 796 (1938).

[6] A. Soltan, Nature **142**, 252 (1938).

collisions in lead and in paraffin are not much different as has been shown by Dunning. Although the collisions in lead do not result on the average in nearly so much loss of energy, a neutron that undergoes even a fairly small angle of scatter in the lead will have a good chance of suffering its following collisions in the surrounding paraffin and there being robbed of its kinetic energy and absorbed. If the amount of lead used does not materially reduce the extent of paraffin shielding, the greater transmission of neutron energy that occurs in the lead will not be serious.

With these points in mind, an arrangement was set up in which some lead shielding was employed. The neutron diaphragm consisted mainly of a 55 cm thick wall of paraffin which occupied the available space between the coil tanks of the cyclotron magnet and which had a channel through it lined with an inch of lead. The receiver side of the paraffin wall was covered, except for the channel opening, with an inch of lead. To prevent energetic electrons ejected from the lead by gamma-rays, or the soft x-rays that follow ejection of electrons from Pb atoms, from affecting things exposed on the outside of the lead shield, the whole receiver side, including the end of the channel, was covered first with a sheet of Cu, 0.5 mm thick, and then a sheet of Al, 1 mm thick. At the target end of the lead-lined channel there was space provided for a filter, as much as 6 cm thick, to be penetrated by the radiation before entering the opening down the lead-lined channel. Generally a 3 cm thick lead filter was used at the target to insure that all the gamma-radiation coming from the source as well as that from the paraffin shield would be attenuated by at least an inch of lead before emerging on the receiver side of the collimation arrangement. The opening through the lead channel tapered from 3 cm by 5 cm at the target end to 7 cm by 7 cm at the receiver end. Because of the space allowed for filters at the source and for the lead shield on the outside of the paraffin, the end of the channel was 70 cm from the target. For reasons of convenience the channel was not directed along the forward direction of the deuteron beam but at an angle of about 30 degrees from it away from the cyclotron vacuum chamber. Gamma-ray shielding was not attempted in other directions than toward the source, the paraffin shield, and the cyclotron vacuum chamber. Shielding was thus not provided against gamma-rays coming from the 30-inch thick tanks of water that surround the cyclotron magnet for purposes of protection nor from parts of the cyclotron magnet and coils. Such shielding would have been heavy and awkward to handle, and it was not introduced after it was found from ionization measurements that the simple shielding already described was sufficient for many experiments.

Considerable use was made of this first arrangement, but the intensity at the outlet was less than expected. Measurements on the distribution of neutron intensity around the source showed that the intensity could be approximately doubled by having the direction of the channel coincide with the direction of the deuteron beam instead of at 30 degrees to it. Some obstructions were removed to permit this, and the second arrangement, shown in Fig. 1, was set up.

Other changes were also made in setting up the second arrangement. The central portion of the neutron diaphragm was changed from paraffin to a tank of water in order to allow draining for ease of removal. The tank also makes a support to which a double row of one-inch thick lead plates can be bolted, an increase of one inch over the first arrangement. The lead shielding is of larger extent, reaching over to the magnet yoke, which itself is a good shield. Paraffin blocks were put around the target between the magnet coils in order to slow down and absorb the neutrons at the rear of the target, thereby decreasing the amount of neutron and gamma-radiation scattered from matter outside the forward shielding and coincidentally the amount of gamma-radiation formed by neutron absorption in regions past the lead shields.

The outlet of the channel was increased to 10 by 10 cm and the opening at the target end was increased to 2.5 by 7.5 cm to allow the use of a greater portion of the deuteron beam. The source and channel are thus wider. For convenience in making clinical tests the end of the lead lining of the channel was designed to protrude 10 cm past the lead shield and to form a rounded, removable cone, the outlet of which is 70 cm from the target. When a tapered insert

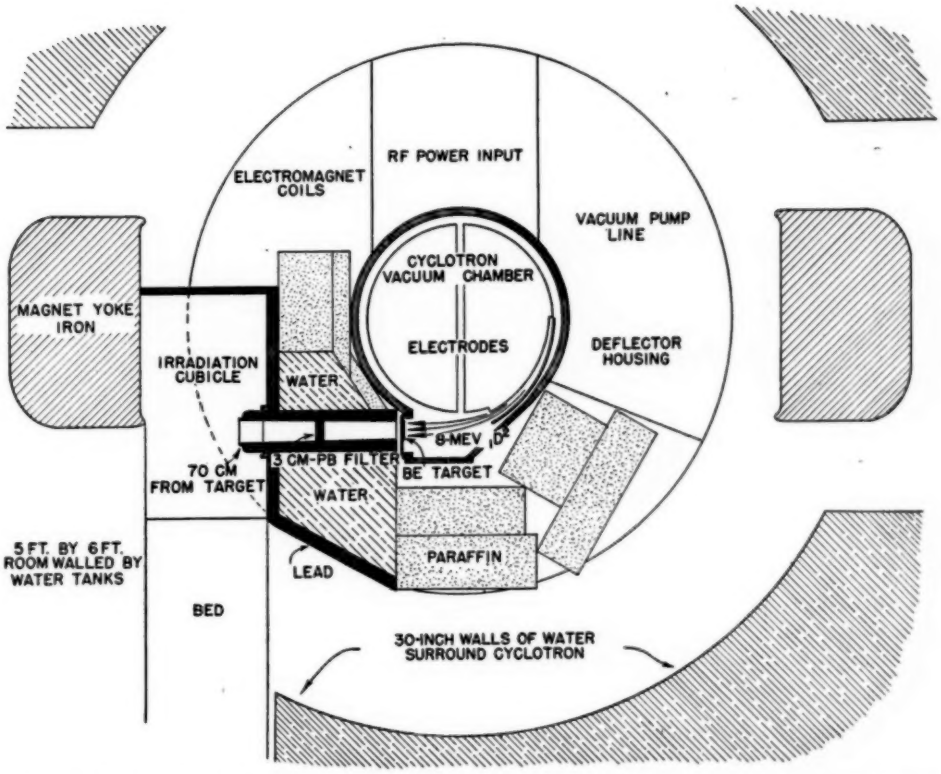

FIG. 1. Horizontal section of an arrangement used to obtain a beam of fast neutrons. In vertical directions, shielding is afforded by the poles, yoke, and coil tanks of the cyclotron magnet itself.

cone is put in the channel and a smaller sized end cone is used, a 7 by 7 cm outlet is obtained. In some experiments the removable cone can be left off and exposures can be made closer to the source. The removable cones and the lining of the channel (master cone) were cast in forms made of one-eighth inch brass sheet. This brass covering not only adds strength but eliminates any secondary electrons from the lead. Since 10 cm was taken up by protrusion of the cone and 5 cm by the lead shield, a tank of water only 50 cm thick could be used. The intensity is sufficient to allow a thicker tank, hence greater target-to-outlet distance, but the outlet then is too close to the magnet yoke for some uses. Rotation of the cyclotron chamber could avoid this.

MEASUREMENT OF THE BEAM BY IONIZATION

Because of the connection of this work with biological experimentation, the radiation measurements were made with small ionization chambers. Under conditions given by Gray[7] the ionization that occurs in a small chamber can be related to the energy absorbed from the radiation by the material of the wall. Accordingly, if the wall is comparable in composition with tissue, the ionization can be correlated with the energy absorbed from the radiation by tissue. Although accompanying gamma-rays also produce ionization in the chambers, the ionization caused by fast neutrons alone can be determined by a comparison of the ionization responses of chambers with various walls.

Technique of measurement

A series of thimble ionization chambers were made all identical in construction but of different materials. The hydrogenous materials chosen were amber, Bakelite, Celluloid, hardwood, and hard rubber. The nonhydrogenous materials suitable for the construction were carbon, aluminum, copper, brass, zinc, cadmium, tin, and lead. The chambers were cylinders with walls 1.0 mm thick, an internal diameter of 10.3 mm, a length of 21 mm, and a gas volume of 1.75 cc.

[7] L. H. Gray, Proc. Roy. Soc. London **A156**, 578 (1936).

The ionization produced in the chambers was measured by means of the Victoreen condenser-chamber and electrometer arrangement used for x-ray dosage measurements. Each chamber can be mounted coaxially on a cylindrical amber condenser of 48 cm electrical capacity which can hold several times more charge without significant leakage than the total charge (of one sign) on ions formed in the chamber by the exposures. The inner coating of the condenser is connected to an aluminum wire which extends into the chamber along its axis and serves as a collecting electrode. The outer coating of the condenser connects with the conducting part of the chamber wall, which for the hydrogenous walled chambers was an extremely thin layer of graphite. The system consisting of the collecting electrode of the chamber, the inner coat of the condenser, and the fiber of the electrometer is charged to 400 volts at the start of an exposure while the chamber wall, outer coat of the condenser, and the electrometer case always remains at ground potential. A collecting field then exists in the chamber of about 400 volts/cm at the walls and about 1000 volts/cm at the wire. During exposure to radiation this field causes a flow of ions that discharges the electrode system and the exposure or amount of ionization produced is proportional to the resultant change in potential of the system. When used with the Victoreen string electrometer of 12 cm capacity, a charge of 1.14 e.s.u./cc collected from the ionization chamber causes a shift of the electrometer fiber of one division or a change of potential of the system of condenser and electrometer of ten practical volts. In order to prevent discharge of the electrometer itself by extraneous radiation, the chamber and condenser are disconnected from the electrometer and exposed to the radiation while the electrometer is maintained charged. The only discharge is then caused by the ionization in the ionization chamber itself. At the end of an exposure the condenser and chamber are returned to connection with the electrometer and the reading is the same as if the connection had been maintained during irradiation and no ionization had occurred in the electrometer. In order to maintain an adequate collecting field, readings are not taken for a fall of potential below 200 volts. The amber insulation that is between the collecting electrode and the chamber wall is practically covered by an insert of the same material as the chamber wall to prevent amber from being the effective wall for this region of the chamber.

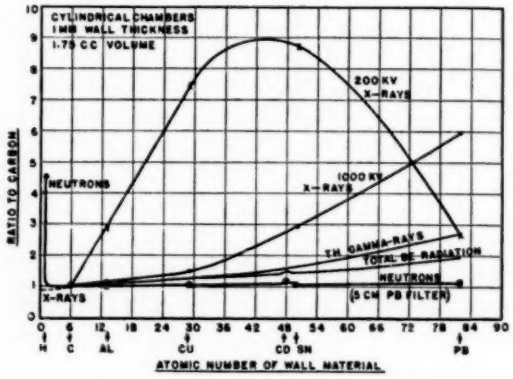

FIG. 2. Relative responses of thimble ionization chambers of different wall materials to various radiations.

Responses of the chambers to different radiations

Exposure of these ionization chambers to different kinds and qualities of radiation has shown that their relative responses are characteristic of the radiation and that a comparison of the responses is valuable in diagnosing the character of a radiation that arises for measurement. The results of exposing the chambers to x-rays, gamma-rays, and neutrons are shown in Fig. 2. The reading of each chamber relative to that of the carbon chamber for the same exposure is plotted against the atomic number of the material of its wall. The abscissa marked H does not represent a pure hydrogen wall but instead, amber, the material used having the most hydrogen per gram. The values for the latter were plotted at this position to indicate the effect on the response of adding H atoms to the wall material.

The curve marked 200-kv x-rays was obtained with the x-rays from a 200-kv x-ray apparatus after filtration through 0.5 mm of Cu. The average energy of the quanta was around 100 kev. One sees that there is a rapid rise of the response produced by changing the wall from C to Al to Cu, but that the rise from Cu to Sn is not large, while from Sn to Pb there is a large decrease in the response. The rapid rise is to be expected from an increased production of photo-

electrons, the production per electron increasing as the cube of the atomic number. The actual response does not increase nearly so rapidly as this because for x-rays of this energy the main response in C and even in Al is the result of Compton rather than photoelectric absorption. The reason for the apparent decrease in the response in this case for the elements above Cu is that the photoelectric absorption increases so rapidly that the rays are greatly absorbed in going through the millimeter thick wall before they reach the thin, inner effective region of the wall. In order to reduce the absorption the wall should be no thicker than the range in the material of the most energetic electrons produced and even then a small absorption correction enters. For the more penetrating radiations, encountered generally in the collimation tests, the absorption in the wall is not serious.

The curve labeled 1000-kv x-rays was obtained with the x-rays from a Sloan type generator[8] after filtration through about 3 mm of Pb. The average energy of the quanta was around 500 kev. The curve is lower and the rise with atomic number is less than for the softer rays, but the difference is not so large as would be expected from the photoelectric effect alone because for 500-kev quanta the Compton process plays a large part. Since the absorption in the wall is much less in this case the curve continues to rise even up to Pb, although the Pb value would be about 20 percent greater if there were no absorption.

A curve was also obtained with the gamma-rays from a mesothorium salt after filtration by 4 mm of Pb and 2 mm of brass. The average energy of the quanta was in the region of 1 Mev. As a consequence of this further increase in the hardness of the radiation there is less photoelectric response in Pb and the rise in response from C to Pb is seen to be less.

If the only process occurring were the Compton process, the total energy of recoil electrons released per unit number of electrons would be about the same in C and in Pb. The ratio of the ionizations in chambers of these materials would be, according to Gray, the inverse ratio of the stopping powers per electron for these materials. The stopping power per electron for particles of the speed concerned is possibly 20 percent smaller for Pb than for C. Thus, if only the Compton process occurred, the Pb chamber would still read a little greater than the C one. The difference in the readings will be mainly, however, a measure of the electrons arising from other processes.

On the basis of the photoelectric process a continual increase in the energy of the gamma-rays should result in a continual decrease in the difference of the Pb and C readings. However, at energies above 1.1 Mev the formation of electron-positron pairs occurs. Since the coefficient per electron for the formation of pairs increases as the atomic number, here again is a factor which makes the Pb chamber read higher than the C one. This coefficient increases with the energy of the quanta, becoming equal to the Compton coefficient at 5 Mev and far surpassing it at still greater energies.

Since the photoelectric and pair production processes vary in an opposite manner with quantum energy, one should observe a minimum in the difference of the Pb and C readings for quanta somewhere between say 1 and 5 Mev. A given difference in the Pb and C readings could be caused by quanta either below or above this minimum. The different variation of the processes with atomic number would allow one to tell by using chambers made of other elements whether the energy of the incident quanta were lower or higher than the value at which the minimum difference of Pb and C occurs. The relative responses of the chambers have not been calibrated at enough quantum energies to allow their use in estimating the energy of incident quanta, but the method might be employed. The relative responses have been useful, however, in determining the presence of gamma-radiation.

Special mention needs to be made of the responses of the hydrogenous walled chambers to x-rays and gamma-rays. If H atoms were added to the atoms of the C wall, the response would fall slightly as shown by the dotted line labeled x-rays. However, since oxygen and traces of heavier elements are present in the hydrogenous materials that were used, enough greater photoelectric response exists for the 200-kv case to make the readings 2 to 4 percent greater than for

[8] Stone, Livingston, Sloan and Chaffee, Radiology **24**, 153 (1935).

carbon. For hard rubber, in which there is sulphur, the reading was 2.6 times that for carbon. For the 1000-kv case, all of the hydrogenous chambers gave readings practically the same as for carbon, except hard rubber which gave a 1.5 percent greater response. The Al value was only 14 percent greater than the C one. For the gamma-rays the chamber with walls of any of these light materials gave practically identical readings. The difference in the responses of hydrogenous walled and carbon walled chambers to gamma-rays will be negligible in these measurements.

The chambers were first tested for responses to neutron rays by exposure to the unfiltered radiation coming from beryllium bombarded by 6-Mev deuterons. The exposures were made 20 cm from the target so that the chambers would be closer to the target than to surrounding sources of scattered or secondary radiation. The curve marked total Be radiation was obtained. It shows a rise in response from C to Pb which is less than that for the gamma-rays from the thorium. Because of the rise analagous to that for gamma-rays, it was suspected that this rise might be caused largely by the gamma-rays that accompany the production of neutrons in this type of source. A block of Pb 5 cm thick and of sufficient extent was placed back of the target so that the radiation emerging in a large solid angle about the source was filtered through the Pb block. The observed rise of response with atomic number was then much less, as shown in the plot labeled neutrons. The responses relative to carbon for this case are Al 1.02, Cu 1.10, Cd 1.15, Sn 1.08, Pb 1.23. A further 2.5 cm of Pb filter was introduced to see if the Pb to C ratio could be further decreased. The result was Cu 1.04, Cd 1.15, Sn 1.03 and Pb 1.18. The additional 2.5 cm of Pb produced only a few percent decrease in the values relative to carbon, indicating that the 5-cm Pb filter had already absorbed most of the gamma-rays coming directly from the source. Scattered and secondary gamma-rays could still reach the chambers, and these could readily account for the 18 percent greater reading observed for Pb than for C.

The slightly greater responses for the chambers of elements heavier than carbon could also be caused by the neutrons themselves if (1) disintegrations, or (2) gamma-rays were obtained by inelastic collisions in yields that increase with atomic number. The first cannot be justified from known nuclear reactions, but the second occurs, as was first shown by Lea.[9] Grahame and Seaborg[5] using neutrons with energies above 4 Mev found a yield of gamma-rays per atom that increased with atomic number, while Kikuchi, Aoki, and Husimi[10] using monokinetic neutrons of lower energy (2.4 Mev) and Grahame and Seaborg[5] using medium energy neutrons found a maximum yield in the region of atomic number 50 and much lower yields in C and Pb. For the relative chamber responses cited above there were neutrons of all energies incident on the chambers. Putting a 1-mm thick cylinder of Pb around the C chamber made no appreciable change in the response. In a Pb-walled chamber, however, there would be more absorption of the resulting gamma-rays and for Pb atoms internal conversion is more probable; consequently it is possible that a good share of the 18 percent greater reading found for the Pb than for the C chamber could be caused by incident neutrons rather than by incident gamma-rays.

In conclusion, it seems quite safe to assume that the difference will be quite small between the response of the carbon walled chamber and that of say the Pb chamber when the effects of other radiations than fast neutrons are excluded. Since the recoils from such walls will contribute little to the ionization in chambers of the size used, the main response can be attributed to the gas inside the chamber. In the case of air, the recoil nuclei of N and O will have an average range much smaller than the dimensions of the chamber and the air can be considered to be practically under conditions of particle equilibrium. That this conclusion is justified was determined by varying the air pressure in the chambers. The ionization per gram of air remained constant from atmospheric pressure, at which the chambers are normally used, down to pressures below one-tenth of an atmosphere. Thus, for neutrons the reading of the carbon chamber can be taken as the value for the

[9] D. E. Lea, Proc. Roy. Soc. London **A150**, 637 (1935).
[10] Kikuchi, Aoki, and Husimi, Proc. Phys. Math. Soc. Japan **18**, 115 (1936); H. Aoki, Proc. Phys. Math. Soc. Japan **19**, 369 (1937).

ionization produced in air. Since carbon is effectively an air wall for gamma-rays, the reading of the carbon chamber is a measure of the ionization in air by either or both neutrons and gamma-rays.

Of course, for neutrons the chambers having hydrogen in the wall material give much larger responses than the carbon and metal walled chambers. The value of 4.55 times the carbon response, shown in Fig. 2, is for the amber walled chamber when 5 cm of Pb filter was used. No change in the ratio was detected, within an accuracy of 2 percent, when the filter was increased to 7.5 cm of Pb. When no filter was used, the ratio was only 3.70 because of the gamma-rays.

Identification of ionization caused by neutrons and by gamma-rays

It is now evident how one can obtain the ionization caused by only the recoil protons from a hydrogenous walled chamber, i.e., solely a measurement of fast neutrons. The ionization in the carbon walled chamber will in general be the sum of the response caused by incident gamma-rays and the response caused by collisions of the neutrons with the nuclei of the air inside the chamber. Both of these responses will be the same for an amber chamber as for a carbon one. Subtracting the carbon reading from the amber reading in effect subtracts from the amber reading the gamma-ray response of the chamber and the neutron response of the gas in the chamber, the difference being the reading produced only by the recoil protons from the walls.

Since the neutron ionization of the air in the Pb and in the C chambers is also equal, a similar procedure for the Pb and C chambers gives the ionization resulting only from the excess production of electrons in Pb, by any means, over that produced in C. The latter, which may be called the Pb-C electron production, can be used as measure of the presence of gamma-rays, although a small part of it may be attributable to neutrons that undergo inelastic collisions in the walls.

The effects on the responses of these chambers caused by varying the enclosed gas, the gas pressure, and the collecting voltage have been tested.[11] The results of the tests and a discussion of the validity for these measurements of the conditions specified by Gray will be the subject of a subsequent paper. For the present purposes it is sufficient to use the difference of the amber and carbon chamber readings to measure fast neutron intensity and the difference of the lead and carbon chambers to indicate the presence of gamma-rays. It is of interest to note that the hydrogen content per gram of amber is almost 95 percent of that of water and that calculations show the recoil proton response of the amber walled chamber to be within 35 percent of that of a tissue walled chamber, making it quite suitable for biological tests. Accordingly, the character, intensity, and definition of the beams achieved with the previously described arrangements were tested with these chambers.

Beam produced by arrangement 1

The first arrangement, with the paraffin diaphragm, lead shield, lead-lined channel, and 3-cm thick lead filter, was found to give a well-defined beam of fast neutrons. The intensity was fairly uniform over the area of the outlet, decreased abruptly at the edges, and then fell off from the edges of the beam with increasing distance. At 5, 10 and 20 cm away from the edge of the outlet the intensities were, respectively, less than 3 percent, 2 percent and 1 percent of the value in the beam. Increase of intensity as the edge of the beam is approached is the result of radiation that comes through the channel obliquely and thus traverses less material by going through the corners of the outlet. Such diverging radiation in the channel may arise both from a broad source and from scattering in the material around the channel. The definition of the beam at 40 cm from the outlet was still quite sharp, except for a small spread due to the extent of the source. This maintenance of definition, together with the fact that the intensity along the beam was found to fall off only a little more rapidly than expected from the inverse square of the target distance, showed that there was not a great deal of scattered radiation spreading out from the channel. Thus, the arrangement is not only a diaphragm for delimiting a beam of fast neutrons,

[11] P. C. Aebersold and G. A. Anslow, Phys. Rev. **55**, 680 (1939).

but the tapered channel, by not allowing a large divergence, effects a collimation as well.

Attenuation of the beam by paraffin was tested by putting thicknesses up to 6 cm at the target end of the channel. From the recoil proton response of the amber chamber, the mean free path of the fast neutrons in the paraffin was found to be 5.2 cm, a result close to the value 5.1 cm found by Dunning under very different conditions. That most of the ionization produced by the beam when filtered through 3 cm of Pb is caused by fast neutrons can be concluded from the ratios of chamber readings observed at the outlet: amber/C=4.0 and Pb/C=1.3. Adding 3 cm more Pb filter only increased the amber/C ratio to 4.2 and decreased the Pb/C ratio to about 1.2. It is to be recalled that without any collimation arrangement the Pb/C ratio was over 1.9 with no Pb filter, and 1.18 with 7.5 cm of Pb filter. Consequently, with just the 3 cm of Pb filter the gamma-ray content of the beam is effectively reduced, for then only a few percent of the ionization in the amber chamber, hence in biological material, exposed to the beam is due to gamma-rays. In most experiments the use of more than 3 cm of Pb filter would be inefficient because fast neutron intensity would be sacrificed just to suppress a little further the remaining gamma-rays.

Although introduction of the lead shielding greatly reduced the gamma-ray effects existent with a paraffin diaphragm alone, the shielding was not sufficiently complete to eliminate a general background of gamma-radiation. Ten centimeters from the beam the amber/C chamber ratio was only 1.03 whereas the Pb/C chamber ratio was 1.8. Putting a box with walls of lead 2.5 cm thick around the chambers outside of the beam reduced both the amber and carbon chamber readings by a factor of 6, the Pb/C chamber ratio being reduced to 1.6. This shows that the main background ionization is caused by penetrating gamma-rays. Surrounding the lead box with cadmium decreased all of the readings by about 25 percent. Thus a small amount of the background ionization results from thermal neutrons, some of which may be due to disintegration of the nitrogen of the air in the chambers.[11] The reading of the amber chamber 10 cm from the beam was 5 percent of its value in the beam. Since 5 percent or less of the reading of this chamber when in the beam is also due to gamma-rays, the gamma-ray intensity both in and out of the neutron beam is about the same. This is because there is so much scattering and production of gamma-rays in the paraffin and other surrounding materials that a nearly uniform background results. By placing lead blocks in various positions about the chambers it was found that the gamma-radiation came largely from directions in which shielding had not been attempted. If the one-inch thick lead shielding wall had been extended to form a complete box or room outside of the paraffin diaphragm, the gamma-ray ionization outside of the beam would have been less than 1 percent of the ionization in the amber chamber in the neutron beam.

Beam produced by arrangement 2

The beam of fast neutrons produced by the second arrangement, Fig. 1, also emerges from the channel and proceeds with well defined edges, but the background of neutrons outside the beam is considerably larger than for the first arrangement. The intensity drops abruptly at the edges of the outlet by a factor of ten, then continues to fall off slowly aside from the outlet. At 2, 5, 10, 20, and 50 cm horizontally from the beam the intensities are approximately 8 percent, 6 percent, 4 percent, 2.5 percent, and less than 1 percent, respectively, of the intensity in the beam. Tests showed that this larger neutron intensity out of the beam is the result of several factors: (1) a wider channel, which allows radiation to come more obliquely through the corners of the outlet, (2) the lesser neutron shielding afforded by the use of water instead of paraffin and of smaller thicknesses than 50 cm in places, and (3) a protruding end cone, from which radiation can be scattered laterally. Because the source extends only 2.5 cm vertically, whereas it is 7.5 cm wide horizontally, neutrons come through the channel less obliquely in vertical planes, and it is found, therefore, that the upper and lower edges of the beam are sharper and that the intensity near these edges is not so large. Also on the side on which the water tank is thicker the intensity is a little smaller.

The character of the beam was tested by chamber responses and by absorption. The

amber/C chamber ratio was 4.25 and the Pb/C chamber ratio was 1.22. The addition of 3 cm further Pb filter in the channel did not change these ratios within the experimental accuracy, showing that already with the initial Pb filter only a small fraction of the ionization in the chambers is caused by gamma-rays. From the chamber responses and from ionization measurements in gases exposed to the beam, it is estimated that only about 10 percent of the C chamber reading (air ionization) and 2.5 percent of the amber chamber reading in the beam are caused by gamma-rays. The transmission of the beam through paraffin, C, and Pb absorbers placed in the channel was tested with the recoil proton ionization. The mean free path of the fast neutrons in paraffin was found to be 5.1 cm, agreeing with both the value from the first arrangement and that given by Dunning. For C (density 1.5) and Pb the values were 9.8 and 6.8 cm, respectively, which were also found with the first arrangement, but which are considerably higher than Dunning's values. The latter disagreements with Dunning's results could be explained by a difference of neutron energies, the paraffin values agreeing because of little dependence of the cross section of H nuclei with energy.

The background ionization by gamma-rays as compared with the neutron intensity in the beam is less with this arrangement than with the first for two reasons: (1) The neutron yield was about doubled by moving the channel to the forward direction of the deuteron beam, whereas the gamma-ray yield, which is nearly homogeneous around the target, remained the same. Accordingly, the gamma-ray contribution to the ionization in the beam was about halved, being approximately 2.5 percent of the amber chamber reading in the beam. (2) The lead shielding was extended and increased. The gamma-ray intensity outside of the beam behind the two-inch thick lead shield is in some regions about half that in the beam. In other regions where the shielding is less complete the value is about the same as in the beam. By providing one-inch thick lead walls against the coil tanks above and below the irradiation cubicle, the gamma-ray background could be reduced by over a factor of two. In any event, for most of the uses of the neutron beam this background is not important.

Although part of the more intense neutron beam obtained with the second arrangement could have been the result of increased target area, measurements of the distribution of neutron intensity around the target showed that the 30-degree change in the direction of the beam could account for the whole increase. It would have been convenient to use the neutron beam at 90 degrees to the deuteron beam, but with the uncollimated source the neutron intensity in this direction was found to be only a fifth of that in the forward direction. The greater flux of neutron energy in the forward direction of the deuteron beam is in agreement with the formation in the target reaction of a temporary B^{11} nucleus which, while moving with the momentum acquired from the deuteron impact, emits the neutron. At still higher bombarding energies of the deuteron the forward concentration of neutron energy flux will in itself be an aid in collimation.

Ionization effects by slow neutrons

The slow neutrons that occur with these arrangements need also to be considered, for they can result in ionization in two ways, first, by charged particle emission following absorption in the receiver itself and, second, by gamma-rays coming from absorption in the shields and other surrounding materials.

Although the first process occurs to a large extent in Li or B, it occurs only slightly in N and rarely in other elements. Thus, in tissue and most hydrogenous materials little ionization would be expected as a result of the slow neutrons present in the beam. This point was tested by putting B_4C or B_2O_3 screens, more than a cm thick, over the outlet of the beam or around the amber chamber in the beam. Effects of only a few percent were noted, which, because they could be duplicated with C screens, were attributed to scattering of the fast neutrons. Out of the beam, a small part of the ionization measured was ascribable to slow neutron disintegrations in the nitrogen of the air in the chambers. However, since the relative concentration of nitrogen in air is much larger than in tissue and since the biological effects of slow neutrons have not as yet been demonstrated, no serious attempt was made in this case to absorb the slow neutrons.

Since each neutron produced in the source can

eventually give rise to a penetrating gamma-ray by the second process, this may be of more consequence in regard to the shielding than the first. Boron, because of its large cross section for slow neutron absorption (1500 times that of a proton) and its small gamma-ray emission, could be dispersed throughout the paraffin and water shields to reduce the resulting gamma-ray background. Simultaneously, the slow neutron background would be reduced. A test was made by adding borax to the water tank of Fig. 1 until a saturated solution was obtained. An inappreciable change was observed in the gamma-radiation observed beyond the thick Pb walls on the water tank. The test was not made without the Pb walls, for these are needed for shielding against gamma-rays from the source. Thus, unless a much greater concentration of boron could be used and unless it could be distributed throughout more of the regions around the source, little reduction of the gamma-ray background would be afforded by this method over that already produced by the necessary Pb walls. The borax did make a small difference in the slow neutron background, the ionization in a Li-lined chamber being reduced by 35 percent. Cd wrapped directly around the chamber, however, reduced the reading by over a factor of ten. Hence, the simplest and most direct way of shielding against slow neutrons, when it is desired, is to surround the receiver with a suitable absorber. Cd was found to give rise to a large gamma-ray emission, making B a much better absorber for this work. In conclusion, then, the slow neutron effects are best taken care of at the receiver, the resultant gamma-rays by Pb and the slow neutrons themselves by B.

Intensity of the neutron beam

The ionization produced in the small chambers filled with air measured at the neutron beam outlet (Fig. 1) in e.s.u./cc per microampere-hour of deuteron bombardment is 5.40 for the amber chamber, 1.27 for the carbon chamber, and 4.13, the difference, for the recoil proton response. At an ordinary steady running current of 60 microamperes the air ionization is 1.27 e.s.u./cc per min, or, subtracting a 10 percent gamma-ray contribution, 1.14 e.s.u./cc per min by neutrons alone. The strength of a Rn-Be source needed to produce this neutron ionization can be calculated from estimates given the author by Dunning which place the ionization by recoils in air at 30 cm from a one-curie Rn-Be source as approximately 1500 ion pairs/cc per sec. This is equivalent to 0.8×10^{-5} e.s.u./cc per min. at 70 cm from the source, the distance of the Be target from the channel outlet. Thus, a source of over 10^5 curies of Rn-Be would be needed to produce the above neutron beam. A beam that would require 10^6 curies of Rn-Be is readily obtainable. It should be remarked here that in comparing yields on the basis of the total number of neutrons emitted from the source the increasing forward concentration of neutron flux with increasing deuteron energy needs to be taken into account. Also in comparing the relative ionizations produced, it is to be noted that the ionization by the gamma-rays from a Rn-Be source exceeds by more than two thousand times the ionization produced by the emitted neutrons.

Photographs of the Neutron Beam

The photographic response was found to give valuable information in this work. Maps of the intensity of radiation in and around the beam outlet were quickly obtained by exposing films large enough to cover the whole region. Ordinary radiographic film was wrapped in black paper

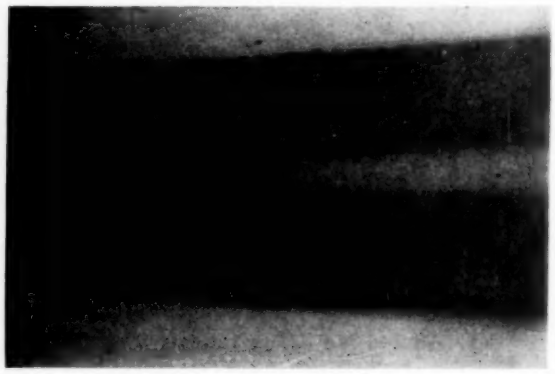

Fig. 3. Reduced reproduction of a film exposed along the axis of the fast neutron beam that emerges from the channel of the arrangement of Fig. 1. The darkly exposed region is the beam, and the lighter strip extending centrally along the beam is the shadow cast by a 3-cm thick strip of paraffin purposely inserted in the mouth of the outlet. The beam had traversed a 3-cm thick lead filter before incidence on the paraffin strip. The edges of both the shadow and the cone of radiation radiate out along sharp lines directed from the source.

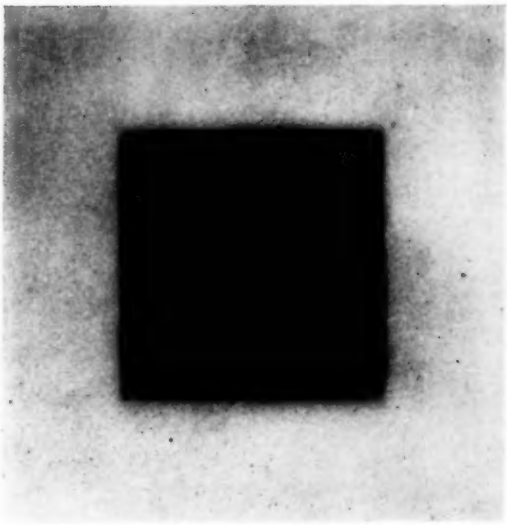

FIG. 4a. Half-scale reproduction of a film exposed perpendicularly to the beam at the outlet of the first arrangement. This film was at the surface of a body of paraffin over 20 cm deep in order to include the scattered and secondary radiations from such an irradiated body. The area exposed to the beam is seen to be sharply demarcated.

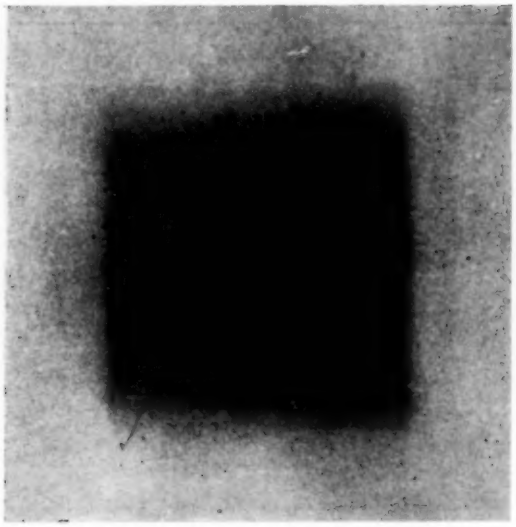

FIG. 4b. Film exposed simultaneously with that of Fig. 4a but at a depth of 11.5 cm below the surface. It is seen that a beam is maintained even through this depth of paraffin. Fuzziness of two of the edges is the result of the width of the source.

and exposed without the intensifying screens or cassettes employed in radiography. Under conditions in which mainly gamma-rays and fast neutrons are incident upon the film, the darkening can be assumed roughly proportional to the energies released in the emulsions by the radiations. A qualitative distinction of gamma-ray and neutron effects can be made by using absorption schemes or by placing emitters of secondary particles in contact with the film. The beauty of the photographic method lies in the graphic depiction of detail that is obtainable in a single exposure; also the results are more directly perceptible than those of a large number of ionization measurements. The neutron intensity could be mapped by the exposure of sheets of material susceptible to induced radioactivity, but, because of the special sensitivity of such detection to neutrons in certain energy ranges, this method is more selective than that desired in the preliminary work. If one were interested in the distribution of neutrons of specific qualities the induced activity method would be applicable.

A film was exposed in a vertical plane along the axis of the beam that emerges from the arrangement of Fig. 1. A strip of paraffin 3 cm thick was placed in the mouth of the collimating cone for the purpose of casting a shadow. In the reduced reproduction, Fig. 3, the beam appears as the darkly exposed region and the shadow cast by the paraffin is seen as a central lighter strip extending along the beam. That the beam is well collimated can be seen from the fact that the edges of both the shadow and the cone of radiation radiate out along sharp lines directed from the source. In the original the beam is 10 cm wide at the outlet and the film is 30 cm long.

Tests showed that fast neutrons are responsible for the darkening of the film along the beam. First, as seen in Fig. 3, after the radiation has traversed the 3 cm Pb filter a marked shadow is cast by 3 cm of paraffin. Second, ionization measurements showed a large difference in fast neutron intensity, but only a small difference in gamma-ray intensity, in and out of the beam. Third, thin pieces of C, Al, Cu, Pb, and paraffin placed in contact with the film gave no effects indicative of gamma-rays. Fourth, slow neutrons were eliminated as a cause of the exposures by taking pictures with the film between B_4C screens; moreover, the slow neutrons form a diffuse background. The contrast between the

beam and the outer regions, which are affected mainly by gamma-rays, is not so large as it should be because of darkening due to unremoved silver, shown by development of unexposed films.

The photographic effect of the fast neutrons on the film can be readily ascribed to the recoil protons that arise in the film, the emulsion, and the paper envelope, all of which are rich in hydrogen. The exposure for the film of Fig. 3 as measured in terms of ionization at the outlet was 34 e.s.u./cc in the amber chamber (8 e.s.u./cc ionization of air). A comparison of the sensitivity of the film to neutrons and gamma-rays would be of interest, but this has not yet been undertaken. Although with high voltage x-rays only a few e.s.u./cc in air is a sufficient exposure, the exposure needed with gamma-rays would be considerably greater; consequently, it can be estimated that roughly the same ionization density in the film with both fast neutrons and high energy gamma-rays will produce the same darkening.

Penetration of the beam into a body of paraffin was demonstrated by the simultaneous exposure of one film on the surface and a second at a depth. Fig. 4a is a reproduction of a film exposed at the surface of a paraffin body consisting of slabs $3.5 \times 30 \times 30$ cm stacked to a depth of over 20 cm. Fig. 4b is from the film exposed simultaneously with that of Fig. 4a but between slabs at a depth of 11.5 cm. The beam of the first arrangement, 7×7 cm at the outlet, was directed through the body so as to pass perpendicularly through both films and thus give a cross section of the beam on each. At the outlet the beam is seen to be sharply demarcated. At the depths the intensity in the region defined by the projection of the channel is much more than that outside of it. The edges of the beam at the depths have a spread due to the extent of the source. Although scattered and secondary radiations result in about a doubling of the ionization intensity outside of the beam over that present without the paraffin, a primary beam is maintained through the paraffin that is traceable to large depths. At the 11.5 cm depth the reading of the amber chamber was about 25 percent of its reading on the surface, and the surface reading was about 10 percent greater with than without the presence of the paraffin.

FIG. 5. Epilation produced on the back of a rabbit exposed to the fast neutron beam of Fig. 4*a*. The epilation started in two weeks and was complete after six weeks. The effect is seen to be sharply limited.

BIOLOGICAL TESTS OF THE BEAM

The suitableness of the beam for biological experiments that necessitate localized administration was tested by exposing the backs of rabbits to the 7×7 cm field of the first collimating arrangement. Graded exposures were given, and the region of exposure was watched every few days following the irradiation. In two to six weeks the hair on rabbits given sufficient exposure began to fall out of the exposed region. On those given large enough dosage the epilation in the region was complete after about six weeks. Fig. 5 shows one of the rabbits thus treated. The region of exposure is sharply demarcated. The small background dose of gamma-rays and slow neutrons caused no noticeable ill effects upon the rabbits as a whole, and they lived for over six months, regrowing their hair in most instances and appearing normal in all respects.

Mice could be exposed so that only their tails extended into the beam, the mice, of course, being quite close to the edge of the beam. Doses sufficient to cause the tails eventually to degenerate, about ten times the whole body lethal dose, could be given without any apparent illness of the mice.

Exposures of the human skin to the beam gave well demarcated regions of erythema, tanning, and epilation, followed by recovery.

The doses required for the rabbit epilation were between five and six hundred e.s.u./cc in the amber chamber. Tests with x-rays showed that a dose three to four times as great measured by ionization in the same chamber would be needed if the radiation coming from the outlet were x-rays or gamma-rays. Whether the effectiveness of the fast neutrons will also be greater when the dose is measured in terms of the ionization resulting in the tissue is of considerable importance and, although investigations thus far indicate an increased effectiveness that is dependent on the biological object employed, the important point for the present is that for the measurements as made the biological effectiveness of fast neutrons is greater. As a result the gamma-ray background will have less biological importance, making the biological dose in the beam from fifty to one-hundred times that outside of it.

Conclusion

Although enough arrangements have not been tried to arrive at the best choice and disposition of materials for the collimation of fast neutrons, these preliminary tests lead to some general conclusions: (1) A beam of fast neutrons that is satisfactory for some purposes can be obtained by means of a channel through a wall of paraffin. The wall should be 60 cm or greater in thickness and of large extent around the source. (2) Shielding is needed against gamma-radiation that originates not only in the source along with the neutrons but in surrounding materials as the result of absorption and inelastic scattering of neutrons. Several centimeters of Pb is sufficient to reduce the ionization caused by gamma-rays from the high energy deuteron-beryllium source to a small fraction of the ionization caused by the fast neutrons. Likewise, the scattered and secondary gamma-rays can be well suppressed by using Pb several centimeters thick to line the collimating channel and to form shielding walls outside the paraffin diaphragm. (3) The Pb lining of the channel is also satisfactory for delimiting a beam of fast neutrons and, because of a different angular scattering of neutrons in Pb, it may even be better for the collimation than just a paraffin channel. (4) The smaller the source and the longer the channel, the more sharply the beam will be defined. For the best collimation the channel should taper out radially from the source to the outlet. The effect of scattering material at the back and at the sides of the source in increasing the effective size of the source needs to be considered. Also in connection with scattered, as well as with secondary, radiation the effect of the position in the channel of the gamma-ray filter is still to be investigated. (5) To reduce effectively the production of gamma-rays by slow neutron absorption, boron would have to be dispersed throughout all the materials around the source in sufficient amount to be the predominant absorber of slow neutrons in all regions. This would also reduce materially the background of slow neutrons, but for this purpose alone the more direct method is to surround the receiver with walls rich in boron. (6) By taking advantage of the greater energy and number of the neutrons emitted from beryllium in the forward direction of a deuteron beam of high energy, not only is the most efficient use made of the source but the neutron beam is more intense relative to the gamma-ray background and the collimation is enhanced.

The advice, the interest, and the encouragement of Professor E. O. Lawrence have been of great value to the author. It is also a pleasure to acknowledge the cooperation extended by members of the laboratory. The author was enabled to participate in this work originally by a fellowship created by the Christine Breon Fund for Medical Research and to continue with it through a fellowship awarded by the Finney-Howell Foundation. The research has been generously supported by grants from the National Advisory Cancer Council and the Rockefeller Foundation. Acknowledgment is made of services rendered by Works Progress Administration, Project No. 10,695.

The Magnetic Moments of the Proton and the Deuteron

The Radiofrequency Spectrum of H_2 in Various Magnetic Fields *

J. M. B. KELLOGG, I. I. RABI AND N. F. RAMSEY, JR.
Columbia University, New York, New York

AND

J. R. ZACHARIAS
Hunter College, New York, New York

(Received July 31, 1939)

The molecular-beam magnetic-resonance method for measuring nuclear magnetic moments has been applied to the proton and the deuteron. In this method the nuclear moment is obtained by observing the Larmor frequency of precession ($\nu=\mu H/hI$) in a uniform magnetic field. For this purpose HD and D_2 molecules are most suitable because they are largely in the state of zero rotational momentum. Very sharp resonance minima are observed which makes it possible to show that the observed values of ν/H are independent of H, and to make a very accurate determination of the ratio μ_P/μ_D. With molecules of ortho-hydrogen in the first rotational state a radiofrequency spectrum of six resonance minima was obtained. This spectrum when analyzed yields a set of nine energy levels from which are obtained (1) the proton moment from its Larmor precession frequency; (2) the proton moment from the magnitude of the dipole interaction between the two proton magnetic moments (the directly measured quantity is μ_P/r^3); and (3) the value of the spin orbit interaction constant of the proton moment with the rotation of the molecule or the magnetic field H' produced by the rotation of the molecule at the position of the nucleus. The numerical results are $\mu_P=2.785\pm0.02$ nuclear magnetons; $\mu_D=0.855\pm0.006$ nuclear magneton; $(\mu_P/\mu_D)=3.257\pm0.001$; $H'=27.2\pm0.3$ gauss; $\mu_P/r^3=34.1\pm0.3$ gauss which gives $\mu_P=2.785\pm0.03$ nuclear magnetons. To within experimental error there is no disagreement of the results of these direct measurements with those from atomic beam measurements of the h.f.s. $\Delta\nu$ of the ground states of H and D.

INTRODUCTION

IN this paper we shall describe experiments in which the magnetic moments of the proton and deuteron are measured to a much higher precision than heretofore. In addition there will be presented some experimental results which throw light on the inner dynamics of the hydrogen molecule, such as the magnetic field at the position of the protons which is produced by the rotation of the molecule as a whole. The magnetic moments will be deduced from two independent quantities: (1) the Larmor precession frequency of the proton or the deuteron in an externally applied magnetic field, (2) the mutual magnetic energy of interaction of the two proton moments in the hydrogen molecule. The first of these two measurements depends on principles briefly described in the first paragraph of the section on method and more adequately in a paper by Rabi, Millman, Kusch and Zacharias.[1] The results are given in the first part of the section "Evaluation of Experimental Results."

In a previous paper[2] called "The Gyromagnetic Properties of the Hydrogens," experiments were described which measured the h.f.s. separation of the normal states of atomic hydrogen and deuterium. The magnetic moments of the proton and the deuteron were evaluated from these measurements by the application of the Dirac theory of the hydrogen atom. These calculations depend on the assumption that the interaction of the nuclear spin with the external electron is purely electromagnetic in nature. The values which were obtained from this experiment were 2.85 and 0.85 nuclear magnetons for the proton and deuteron, respectively, with a precision of about 5 percent.

These values, particularly that of the proton are to be compared with the earlier value of 2.5 given by Estermann and Stern[3] as a result of a

* Publication assisted by the Ernest Kempton Adams Fund for Physical Research of Columbia University.

[1] I. I. Rabi, S. Millman, P. Kusch and J. R. Zacharias, Phys. Rev. **55**, 526 (1939).

[2] J. M. B. Kellogg, I. I. Rabi and J. R. Zacharias, Phys. Rev. **50**, 472 (1936).

[3] I. Estermann and O. Stern, Zeits. f. Physik **85**, 17 (1933).

straightforward molecular beam deflection experiment with molecular hydrogen. Since this value was not claimed to be accurate to better than 10 percent the results of the two experiments, which differ entirely in principle, could be said to agree within the limits of error. A value of the proton moment was also given by Lasarew and Schubnikow[4] who measured the variation of the diamagnetic susceptibility of liquid hydrogen with temperature. They interpret the change in susceptibility as a paramagnetic effect of the nuclear moment and from measurements at three different temperatures obtain two values 2.7 ± 10 percent and 2.3 ± 10 percent. However, later experiments by Estermann, Simpson, and Stern[5] yielded a value of 2.46 ± 3 percent. They used the same method as in the previous experiments of Estermann and Stern, but with a more refined technique, which they applied to both H_2 and HD molecules.

The wide divergence between the values 2.85 and 2.46 is quite outside the sum of the limits of error. As an explanation the possibility of some sort of spin interaction between electron and proton not electromagnetic in character was suggested. Another possibility was a breakdown of the Dirac equation for the electron in the hydrogen atom.

These considerations which bring into question the fundamental entities of nuclear and atomic physics make a further experimental study of the proton moment a matter of great interest, particularly if the methods are independent. Further interest is added to these studies by recent theoretical investigations[6] of the nature of the proton and neutron moment and their composition in the deuteron.

Method

The method we employ is the molecular-beam magnetic-resonance method[1] modified to apply to gas molecules. As used in our experiment this method provides a means of observing the reorientations of molecular and nuclear moments which may occur with respect to a constant homogeneous magnetic field when an oscillating or rotating magnetic field is superposed. In our experiments this oscillating magnetic field will be weak compared with the constant field and perpendicular to it in direction. In the absence of any interaction between the molecular constituents this reorientation will occur when the Larmor frequency of precession,

$$\nu=\mu H/hI \tag{1}$$

and the frequency of the oscillating field are in resonance.

More generally, when there are interactions between the molecular constituents, the resonance reorientations occur when the frequency of the oscillating field is in resonance with the frequency given by the Bohr relation

$$h\nu_{nm}=\Delta E_{nm}=E_n-E_m, \tag{2}$$

where E_n and E_m represent the energies of two states of the whole molecular system in the homogeneous magnetic field. There are selection rules which govern these transitions, and in the cases which we will discuss this selection rule is $\Delta m=\pm1$ where m is the magnetic quantum number of the system. It is to be emphasized that the method detects not only transitions from state n to m, but also the inverse transition m to n. One of these corresponds to absorption of radiation and the other to stimulated emission. As Einstein has shown these two processes are equally probable. The above two descriptions are equivalent in the absence of interactions within the molecule because the energy differences between the successive states of spin quantization are then all equal to $\mu H/I$, whence the Bohr frequency is the same as the frequency given by Eq. (1).

To detect the reorientations, a beam of molecules is spread by an inhomogeneous magnetic field and refocused onto a detector by a subsequent inhomogeneous field. The transitions between the states of different space quantization are produced in the homogeneous field of an electromagnet placed in the region between the two deflecting magnets. In the gap of this electromagnet is placed a loop of wire which is connected to a source of current of radio frequency to produce the oscillating field at right

[4] B. G. Lasarew and L. W. Schubnikow, Physik. Zeits. Sowj. **11**, 445 (1937).
[5] I. Estermann, O. C. Simpson and O. Stern, Phys. Rev. **52**, 535 (1937).
[6] J. Schwinger, Phys. Rev. **55**, 235 (1939), Abs. 13; H. Fröhlich, W. Heitler and N. Kemmer, Proc. Roy. Soc. **166A**, 154 (1938).

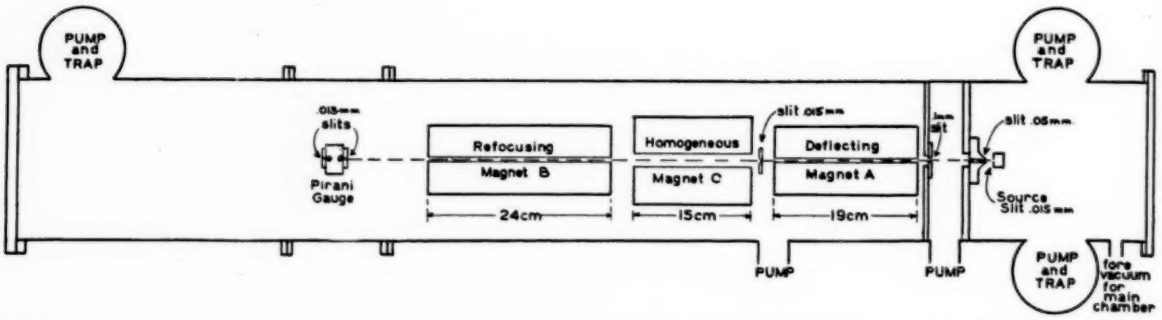

FIG. 1. Schematic diagram of apparatus. Longitudinal dimensions from source to detector are drawn to scale. Flattened copper tubes 13.5 cm long to carry radiofrequency current are not shown. They should appear between the pole pieces of magnet *C*.

angles to the steady field. If a reorientation of spin occurs in this field the subsequent conditions in the second deflecting field are no longer correct for refocusing and the intensity at the detector goes down. The experimental procedure is to vary the homogeneous field while maintaining some given value of the frequency of the oscillating field until a resonance is observed by a drop in intensity at the detector and the subsequent recovery when the resonance value is passed.

APPARATUS

The apparatus used in these experiments is similar to that used by R. M. K. Z.,[1] the chief modifications being those which result from the use of gas molecules in the beam. The present apparatus is shown schematically in Fig. 1. The outer 6″ brass tube is divided into three parts to facilitate pumping, each part having its own high vacuum system. In the source chamber, where much gas emerges from the source, a pressure of 4×10^{-5} mm of mercury is maintained by two brass oil-diffusion umbrella-type pumps with dry-ice-cooled helical baffles. The pumping speed measured at the position of the source slit is 100 liters of air per second. In the separating chamber, which is connected to the source chamber only by a slit 0.05 mm wide and 3 mm high through which the molecular beam passes, and to the main chamber by a slit 0.1 mm wide and 6 mm high, the pressure is of the order of 10^{-6} mm. The purpose of the separating chamber is to provide vacuum isolation of the main chamber from the gas in the source chamber. Finally in the main chamber, where the magnets are located and where the molecules are for the greatest length of time, a pressure of better than 5×10^{-7} mm is maintained with another brass oil-diffusion pump with a speed of 50 liters per second and with a glass pump of the Zabel design.[7] To diminish pressure fluctuations in this chamber, an extra section of brass tube 3 ft. long and 7″ in diameter is added beyond the Pirani gauge detector to provide ballast volume. All the diffusion pumps of the separating and main chambers pump into a glass pump which in turn pumps into the source chamber which serves as its fore vacuum. The two brass pumps of the source chamber are backed by a glass pump which in turn pumps into a Leybold three stage mercury diffusion pump capable of pumping against 10 mm of pressure. The gas from the Leybold pump goes back to the source feed line so that it is used over again. With this recirculation system as little as 6 cc of gas at NTP is required for a day's run and, if desired, even that amount may be recovered at the end of the day for subsequent use.

The source is mounted at the bottom of an Invar Dewar to which it is soldered. The molecules being investigated must pass through a long 2-mm tube in the Dewar before entering the source so their temperature becomes approximately that of the refrigerant in the Dewar. The Dewar is supported at the top by a ground brass joint so mounted that the trap can be moved both transversely and vertically under vacuum. The ground joint permits rotation about a vertical axis. This motion is necessary because of the canal effect of the slit jaws. In addition to the support at the top of the trap,

[7] R. M. Zabel, Rev. Sci. Inst. **6**, 54 (1935).

two long Invar screws pass through the sides of the outer brass tube and are used to clamp the source rigidly in place. This was found to be necessary to prevent random 0.001 mm lateral motions of the source. The gas pressure inside the source is usually of the order of 4 or 5 mm of mercury. The source slit is 0.015 mm wide, 3 mm high, and 0.25 mm thick. Although the source slit is made vertical optically before the apparatus is pumped out, slight changes of its angle with the vertical can be made under vacuum by clamping the source box with the Invar screws and then moving the top of the Invar trap. This procedure bends the trap a bit and thus changes the angle of the slit with the vertical.

The collimator consists of two sharp slit jaws 0.015 mm apart mounted eccentrically on a vertical ground joint. Small rotations of the joint therefore make possible slight adjustments of the collimator position while large rotations completely remove the collimator from the path of the molecular beam. Although the geometry of the apparatus is such that the collimator cannot conveniently be put halfway between the source and the detector, it is placed as near to this position as possible, since, as pointed out by Manley,[8] this is the optimum position. The total beam length, source to detector, is 77 cm.

The detector is of the Stern-Pirani type and is shown diagrammatically in Fig. 2. The most important difference between this detector and the Pirani gauges previously used[2] is that use is made of all four arms of the Wheatstone bridge, two electrically opposite arms being in the detector chambers and two in the balancing chambers whereby the sensitivity is increased. Each set of gauge chambers, which must be of small volume to diminish the time lag of the detector, is formed by inlaying in solder two 1.6-mm (inside diameter) copper tubes in a rectangular trough cut in the surface of a brass block. A transverse hole is drilled from the outside through both tubes to form the interconnecting channel shown in the diagram. The faces of the block are then surface ground and lapped. The slit jaws shown in the diagram are carefully lapped brass blocks screwed to the lapped faces of the gauge block. The slit itself is formed by forcing these slit blocks together against 0.015 mm spacers of aluminum foil to form a channel 0.015 mm wide, 2 mm high, and 4.5 mm long. The gauge wires are made of nickel ribbon 9 cm long, 0.25 mm wide, and 0.004 mm thick. These ribbons are kept taut by small spiral springs of 6-mil nickel wire formed on the point of a needle. Nickel leads are brought out of the ends of the gauge chambers through small glass tubes which are ground to fit snugly into the copper tubes. The ends are then sealed with a drop of clear glyptal lacquer. Finally, the gauge is baked at a temperature of 150°C for three days.

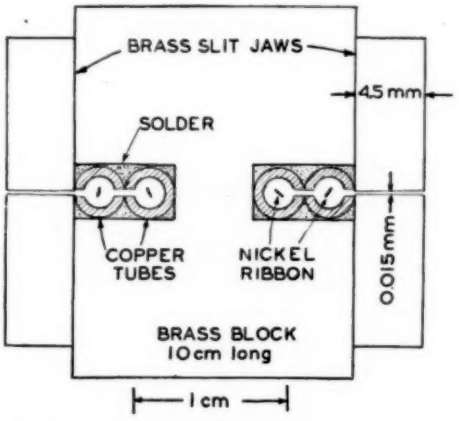

FIG. 2. Horizontal cross section of the detector. The block and tubes are 10 cm long.

To prevent electrical disturbances in the detector circuit when the oscillator is turned on, the entire circuit is well shielded and by-pass condensers are attached between the leads of the hot wire arms of the bridge and ground.

The portion of the outer brass tube near the detector is surrounded with rubber tubing through which is circulated water from a large tank which stays at the average room temperature. The whole system is lagged with crumpled Alfol (aluminum foil) to provide thermal insulation. This is necessary to diminish the large galvanometer drifts which accompany even small changes of the detector temperature. After the apparatus has been opened to air, it takes about a week for the detector to outgas sufficiently for accurate measurements to be possible. Therefore one oil diffusion pump and a mechanical pump are left running all the time so that "sticking" vacuum is maintained even when the apparatus is not in use.

[8] J. H. Manley, Phys. Rev. 49, 921 (1936).

The inhomogeneous deflecting magnets A and B (Fig. 1) are of the type described by Millman, Rabi, and Zacharias.[9] They are 19 cm and 24 cm long, respectively. The gaps are bounded by two cylindrical surfaces, one convex of radius 1.24 mm and the other concave of radius 1.47 mm. The gap width is 1.06 mm. Each magnet is wound with four turns of heavy, water-cooled copper. With 300 amperes the field is about 12,000 gauss and the gradient of the field about 90,000 gauss/cm.

The magnet C producing the homogeneous magnetic field is a single yoke magnet of Armco iron carefully annealed in a hydrogen atmosphere. It is wound with 9 turns of heavy, water-cooled copper. The surfaces of the air gap are 0.6 cm apart, 3.2 cm high, and 15 cm long. They are surface ground and lapped, and the gap is spaced with a ground and lapped spacer so that the air gap should be constant to about 0.05 percent.

Although the gradients of the two inhomogeneous magnetic fields must be in opposite directions for refocusing to be possible, it is essential[1] that all three magnetic fields be in the same direction and that the three magnets be close together to prevent reorientations of the molecules in the regions of weak rapidly changing field between the magnets. To further diminish these reorientations iron slabs are attached to the ends of the inhomogeneous magnets to increase the value of the magnetic field in the gaps between the magnets and to make the changes of field more gradual. With these precautions the refocused beam intensity in the present apparatus is about 95 percent of the beam intensity in the absence of the magnetic fields.

The high frequency magnetic field within the air gap of the C magnet is produced by a radio-frequency current in a "hairpin" of the type described in detail by Millman.[10] The two horizontal wires between which the beam passes are of flattened $\frac{1}{8}$ in. (outside diameter) copper tubing 13.5 cm long and 1 mm apart through which water flows for cooling purposes. This produces a magnetic field of about 3 gauss per ampere at the position of the beam. As much as 50 amperes of current at several megacycles have been used. The current comes from a single turn secondary inductively coupled to the tank coil of a conventional Hartley oscillator driven by an Eimac 250 TL tube. Frequencies between 0.5 and 16 megacycles have been used. The oscillator is sufficiently stable for the frequency to remain constant to 0.02 percent over the course of a day's run.

[9] S. Millman, I. I. Rabi and J. R. Zacharias, Phys. Rev. **53**, 384 (1938).
[10] S. Millman, Phys. Rev. **55**, 628 (1939).

Calibration

The measurement of gyromagnetic ratios by the method of this experiment depends on the absolute measurement of only two quantities as is shown by Eq. (1): (a) the frequency of the oscillatory magnetic field and (b) the strength of the homogeneous magnetic field.

The frequency is measured with the same General Radio Type 620-A heterodyne frequency meter used by R. M. K. Z.[1] with which frequencies can be measured to 0.01 percent. In our laboratory this meter was compared with another meter of the same type and found to agree with it to 0.01 percent.

The homogeneous magnet C is calibrated as a function of the exciting current in the magnet windings. The current is measured by the potential drop across a shunt through which the current passes. This potential drop is measured to 0.01 percent with a type K potentiometer. As the same shunt is used in the calibration and in the measurement of moments, its absolute resistance is of no importance.

In the process of calibration it was found that the field accompanying a current in the windings depended on the way the magnet was demagnetized. Therefore a standardized demagnetization procedure was used in both the calibration and the subsequent measurements. Calibrations were made for several values of the current in the A and B magnets. When this procedure was followed, the magnetic fields were found to be reproducible to 0.2 percent.

The calibration of the magnet was performed with flip coils, ballistic galvanometer and mutual inductance in the manner described by R. M. K. Z.[1] Two Leeds and Northrup 50-millihenry mutual inductances were used in the calibration. The values of these two mutual

inductances, rated by the manufacturer to ±0.5 percent, were found to vary about 0.5 percent depending on humidity. This uncertainty together with a slight uncertainty in the area of the flip coil is the chief source of error in the experiment. The absolute calibration of the field and hence the absolute values of the magnetic moments should be good to about 0.5 percent.

Since the moments of a number of nuclei have been measured[1, 11] on another apparatus with an independent field calibration, it is of interest to compare the results of the measurement of some one nuclear moment on the two apparatuses. For this purpose we chose fluorine which was available to us in the form of CCl_2F_2. We found resonance minima which may be ascribed to fluorine. While these minima were not as narrow as those of hydrogen and could not be located as accurately, it was still possible to measure the moment of fluorine to an accuracy well within the limits of error claimed for the calibration of the magnets of either apparatus. The fluorine moment we obtain[12] is 2.623±0.018 nuclear magnetons. This is to be compared with the value 2.622±0.013 nuclear magnetons previously reported by R. M. K. Z.

Procedure

Although the final values for the nuclear magnetic moments do not depend on the accuracy of the alignment of the apparatus or of the parallelism of the source, collimator, and detector slits, these adjustments must be carefully made in order that the beam intensity and deflecting power of the apparatus may be large enough. As in previous molecular beam experiments,[2, 9] much of the alignment is accomplished under vacuum with the beam, although part is done optically in advance. The three magnets are rigidly attached to a brass base plate which, together with the separating plate and foreslit between the separating and detector chambers, can be removed from the outer brass tube. As the magnets cannot be moved under vacuum, they, and the foreslit, are optically aligned on the base plate when it is outside the brass tube by running a tightly stretched number 40 copper wire down the line of the beam. The base plate and magnets are then inserted in the tube and clamped in position. The source slit, foreslits, collimator, and detector slit are approximately aligned optically and are carefully made vertical to make them parallel. The two wires which carry the high frequency current are set optically so that the beam passes between them. After these alignments have been made and the apparatus evacuated, gas is introduced into the source feed line and the beam is found by trial with the collimator removed from the beam path. The collimator is then introduced and the position of the beam relative to the magnetic field is found by moving the source, collimator, detector, and narrowest foreslit under vacuum. In this way the beam may be made to run parallel to the magnets and at any desired position in the air gap.

The best currents for use in the deflecting and refocusing magnets A and B are determined by trial. The ratio of the currents in the two magnets is first selected so that the refocusing is a maximum. Then with this ratio preserved the total current is adjusted to a value large enough so that most of the molecules which have a constituent moment reoriented in the C field are not refocused, and small enough so that the deflections of the molecules are not too large to preclude good refocusing when no reorientations occur. A careful adjustment of the total current is particularly important in the measurement of the deuteron moment with HD where the deuteron magnetic moment being studied is in the same molecule with a much larger proton moment.

The resonance minima are observed by keeping the currents in the A and B magnets and the frequency of the oscillator constant and varying the current in the C magnet which produces the homogeneous field. A measure of the number of molecular reorientations produced by the oscillating field is obtained from the change in beam intensity which occurs when the oscillator is turned off or on. As there is always some drift (of the order of ½ cm a minute) of the detector galvanometer spot, observations of the change in beam intensity are made by turning the oscillator

[11] P. Kusch and S. Millman, Bull. Am. Phys. Soc. **14**, No. 3, Abs. 35; S. Millman and P. Kusch, Bull. Am. Phys. Soc. **14**, No. 3, Abs. 36; P. Kusch, S. Millman and I. I. Rabi, Phys. Rev. **55**, 1176 (1939).

[12] J. M. B. Kellogg, I. I. Rabi, N. F. Ramsey, Jr. and J. R. Zacharias, Phys. Rev. **55**, 595 (1939), Abs. 24.

on and off at 15-second intervals for two minutes and then averaging the changes of the galvanometer deflection. In all of the experiments here described the Dewar to which the source is attached was filled with liquid nitrogen.

It is very important in these experiments that the correct high frequency current be used, since, as follows from the detailed theory of the reorientation probabilities as developed by Rabi,[13] the half-widths of the resonance minima are directly dependent on the strength of the oscillating magnetic field. If too much current is used the widths of the resonance minima increase proportionally to the current and if too little is used the depths of the minima decrease rapidly. The theoretical optimum strength of the oscillating field and the theoretical half-widths of the curves when this field is used are discussed in the next section. As is shown there, the optimum field depends both on the magnitude of the moment being measured and on the velocity and hence the mass of the molecule. In practice we usually determine the best values for the oscillatory current by trial. Since the positions of the minima are not affected by the magnitude of the oscillatory current, this determination is made only approximately.

Experimental Results

In this section we shall present our data in the form of typical curves which represent beam intensity at the detector as a function of the value of the field in the C magnet while a fixed frequency and amplitude of the oscillating current is maintained. These curves we call resonance curves and the minima of intensity which are observed, resonance minima. Of physical interest are the numbers, locations, depths, half-widths, and asymmetries of these resonance minima.

These curves are closely analogous to the absorption and stimulated emission lines of spectroscopy except for two distinct differences. First, instead of measuring the absorption of the radiation we measure the fraction of molecules which make transitions. Second, we employ a definite fixed frequency and shift the positions of the energy levels to correspond to this frequency by varying the magnetic field rather than scanning the spectrum through a range of frequencies at a fixed value of the field. Thus our results are analogous to what would be obtained if one measured the Zeeman pattern of a spectral line by measuring the absorption of some narrow spectral line as a function of the magnetic field in which the absorber is placed. The Zeeman lines would successively pass across this frequency interval and one would obtain an unusual set of absorption lines from which the Zeeman levels could be deduced. In the present experiment with hydrogen molecules, as the strength of the magnetic field is varied the resonance minima occur in groups, the positions of the groups being such that the Larmor precession frequency of a constituent magnetic moment of the molecule is near the frequency of the oscillating field. Since the regions of field that are of interest in the experiment are those in which the resonance minima occur, only these are included in the accompanying figures. It is to be emphasized, however, that between groups of minima there are large regions of the magnetic field intensity in which no resonance minima occur.

The gases used in these experiments were H_2, D_2 and HD, the latter having been purified for us by Drs. Brickwedde and Scott of the National Bureau of Standards. All experiments were performed with the source at liquid nitrogen temperature. For equilibrium at this temperature, the distributions of the molecules in the different rotational states are as given in Table I. The resultant nuclear spins to be associated with the different rotational states of H_2 and D_2 are also included in the table. These are different for even and odd rotational states since, as is dis-

Table I. *Relative abundance of different rotational states at 78°K. To obtain the abundance of a state with given I and J and m_I and m_J divide the concentration given by the statistical weight. The calculations were made assuming an ortho-para ratio of 3 to 1 for H_2 and 1 to 2 for D_2. For HD there is no quantum number of total spin.*

	H_2			D_2			HD	
J	Total Spin	Stat. Wt.	Rel. Conc.	Total Spin	Stat. Wt.	Rel. Conc.	Stat. Wt.	Rel. Conc.
0	0	1	0.248	0,2	6	0.559	6	0.628
1	1	9	.745	1	9	.328	18	.369
2	0	5	.003	0,2	30	.105	30	.003
3	1	21	.000	1	21	.004	42	.000

[13] I. I. Rabi, Phys. Rev. **51**, 652 (1937).

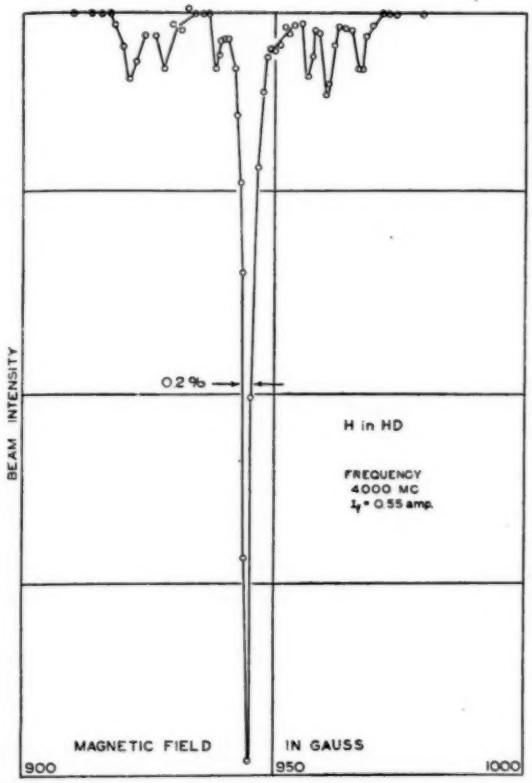

FIG. 3. Resonance curve for HD molecules chiefly showing transition of the proton spin for the zero rotational state.

cussed in the theories of the rotational specific heat of homonuclear hydrogen molecules, only para-H_2 and ortho-D_2 may exist in the even rotational states and vice versa for odd.

Figure 3 is a resonance curve taken with HD molecules at a frequency of 4.000 million cycles in a region of magnetic field varied from about 900 to 1000 gauss. In this region the Larmor precession frequency of the proton is near the oscillator frequency. The very deep minimum arises from the reorientation of the proton in this molecule when the molecule is in a state of zero rotation as will be made clear in the next section. The small fine structure on both sides is due to the same reorientation process, but in molecules which are in the first rotational state. The discussion of the results in the first rotational state and of the similar ones which arise from reorientations of the deuteron in the first rotational states of HD and D_2 molecules will be reserved for another paper. Fig. 4 is a curve similar to that of Fig. 3 but taken in an entirely different region of frequency and magnetic field, the region being such that the Larmor frequency of the deuteron is near the oscillator frequency. Here again the deep minimum corresponds to reorientations of the deuteron when the molecule is in the zero rotational state while the structure on the two sides arises from similar transitions but in the first rotational state. Fig. 5 is a curve obtained with D_2. The deep central minimum arises from the reorientation of the deuteron in molecules in the zero rotational state and the structure on either side is due to molecules in the first rotational state.

All of these groups of resonance minima have been observed at more than one frequency. It is found that the ratios of f, the frequency of the

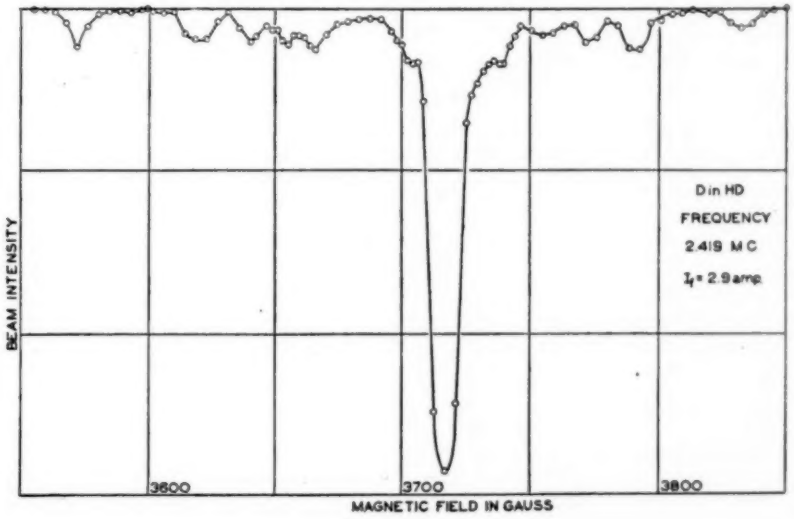

FIG. 4. Resonance curve for HD molecules chiefly showing transition of the deuteron spin for the zero rotational state.

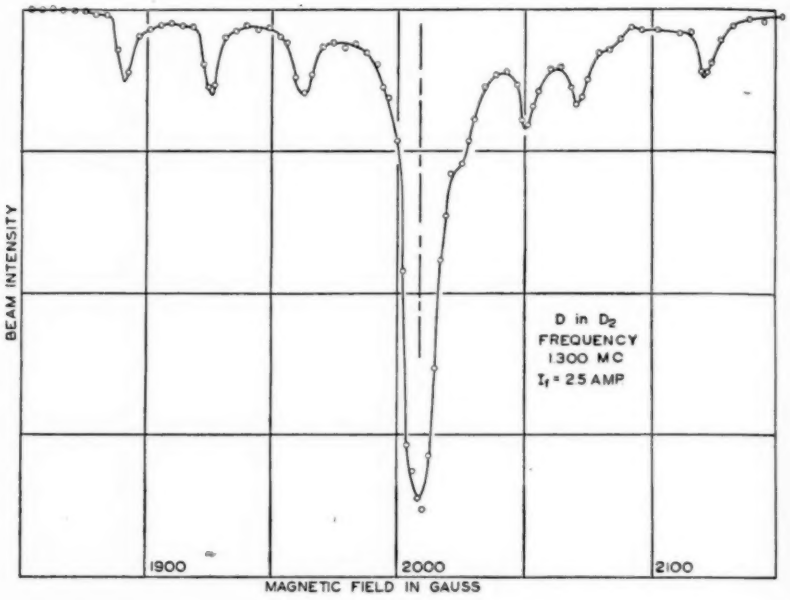

FIG. 5. Resonance curve for D_2 molecules showing transition of the resultant nuclear spin for the zero rotational state.

oscillating field, to H, the magnitude of the homogeneous field at which the principal minimum of any moment occurs, are constant. This constancy of f/H would be expected from Eq. (1) and is strong support for the assumption that the deepest minimum corresponds to the interaction of a magnetic moment with the applied magnetic field, since the constancy of f/H shows that the energy of interaction is proportional to the strength of the field.

The justification for identifying the resonance minima of Fig. 3 with proton reorientations and Fig. 4 with deuteron reorientations is that a group of minima with the same f/H as Fig. 3 is found in H_2, and a group with the same f/H as Fig. 4 in D_2 (see Fig. 5).

Each of these curves alone is slightly asymmetrical as would be expected from the discussion of Millman.[10] As pointed out by Millman, the signs of the moments can be deduced from the asymmetry. The signs of the proton and deuteron moments found in this way are positive in agreement with the results of K. R. Z.[2]

The depth of the minimum of H in HD corresponds to the occurrence of the reorientation process in about 75 percent of the molecules in the zero rotational state. That this quantity is not greater is to be expected on the basis of the theory given by Rabi and by R. M. K. Z. Since the molecules have a Maxwell distribution of velocity, some of the molecules are not under the influence of the oscillating field long enough, because of their high speed, to make the transition probability unity, while others, because of their low speed, are in the field too long and are partially returned to their original state. A discussion of the depths of the deuteron minima in HD and D_2 will be given in a later paper.

The minimal widths of the resonance minima are given approximately by the relation $t\Delta\nu \geqq 1$ where $t=L/v$ is the time spent by the molecules in the oscillating field and $\Delta\nu$ is related to the width of the minima in gauss by $\Delta\nu=\mu\Delta H/hI$. The minimal width of the resonance minima at half-intensity (half-depth) is therefore given by $\Delta H \geqq hIv/\mu L$. If the resonance minima are considerably broader than this it is an indication of lack of resolution or of fine structure in the minima. If the oscillating field is made very

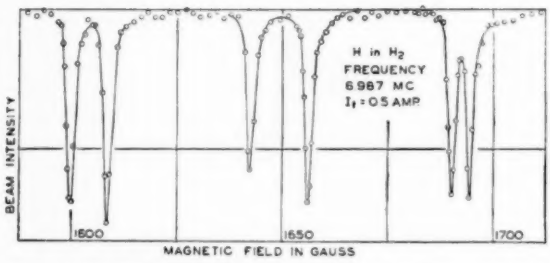

FIG. 6. Radiofrequency spectrum of ortho-H_2 molecules arising from transitions of the resultant nuclear spin. The path of the beam in the radiofrequency field is 13.5 cm.

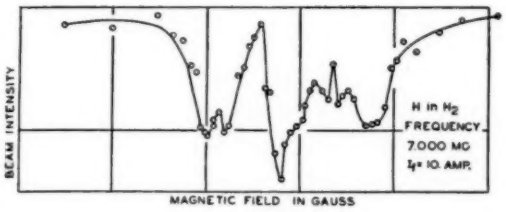

FIG. 7. Radiofrequency spectrum of ortho-H_2 molecules arising from transitions of the resultant nuclear spin. The path of the beam in the radiofrequency field is only 2.7 cm. The radiofrequency current was too large.

weak, the depth of the resonance minimum decreases, but its width is approximately unchanged; whereas, if the oscillating field is made too strong, the half-width of the minimum increases. The best value of the oscillating field for maximum depth of the resonance minimum and narrowest width when we deal with resolved lines is obtained when the amplitude of the oscillating field is approximately equal to $hIv/\mu L$. This relation was found to hold experimentally and is expected from the theory.[1]

In Fig. 6 we have a set of six resonance minima which arise from reorientations of the nuclei in H_2 molecules in the first rotational state. Since, as is shown in Table I, the zero rotational state has zero resultant nuclear spin, this state has no resultant nuclear magnetic moment and consequently gives rise to no nuclear resonance minima. The observed resonance minima can be located to within 0.5 gauss. The depths of the minima are approximately equal. The sum of the depths of the resonance minima is approximately equal to the total intensity of ortho-H_2 molecules which reach the detector. This is less than the amount to be expected under ideal conditions since each minimum is due to transitions between two states and in our experiment transitions from b to a are counted as well as those from a to b. Since, as will be shown in the next section, there are nine states all told and since the molecules are equally distributed amongst the states, the depth of each minimum should represent 2/9 of the intensity and the sum of the six minima 12/9 of the total intensity. The effect of the velocity distribution which was discussed above results in a 25 percent reduction of this intensity, so it is reasonable that the total depth should be approximately equal to the intensity of ortho-H_2 molecules as found experimentally.

Figure 7 represents a curve which was obtained with H_2 molecules in an earlier form of our apparatus in which the C magnet as well as the wires which produce the oscillating field were about a fourth as long as they are now. This curve was one of the first to be observed and a value of the oscillating field much greater than the optimum value discussed above was

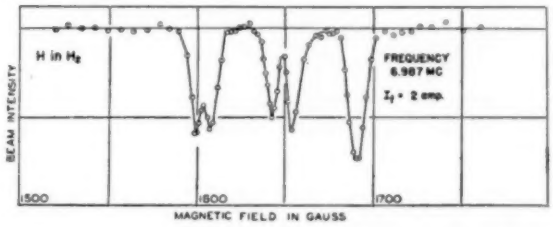

FIG. 8. Radiofrequency spectrum for ortho-H_2 molecules arising from transitions of the resultant nuclear spin. The path of the beam in the radiofrequency field is 2.7 cm. Optimum r.f. current for this case is 2 amp.

used. Fig. 8 is another curve on the same apparatus but with the use of the optimum oscillating field. A comparison of these two curves shows how the stronger oscillating field broadens the resonance minima and causes the curious overlappings which are responsible for the peculiar form of the curve in Fig. 7. By making the C magnet and the oscillating field four times longer, we were able to reduce the amplitude of the oscillating field by a factor of four since the time which the molecules are under its influence is four times as great. Fig. 6 when compared to Fig. 8 shows the effect of this improvement. The lines in Fig. 6 are much narrower and the resolution is consequently higher. There are six narrow and well separated minima, whereas in Fig. 8 there are only five separated minima.

Figure 9 shows how the positions of the H_2

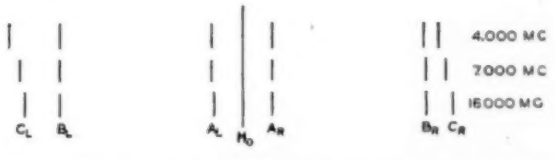

FIG. 9. Variation of radiofrequency spectrum with magnetic field to show the progress of the Paschen-Back effect. The spectra have been shifted to make the positions of H_0 coincide. H_0 was obtained directly by adding 10 percent of HD to the sample of H_2. In this way one can tell the shift in field of the individual lines.

resonance minima shift when observations are made at different frequencies. The vertical lines show the observed positions of the peaks at different frequencies. The positions of the different groups of minima in this figure are so adjusted that the field position marked zero is the position on the different groups at which the Larmor frequency of a proton is equal to the oscillator frequency. The reason for the shifts in the peak positions will be discussed in the next section.

Evaluation of Experimental Results

In this section we shall first deduce the magnetic moments of the proton and the deuteron from the locations in field and frequency of the deep resonance minima with HD and D_2 molecules as shown in Figs. 3, 4, and 5. Then we shall discuss in detail the results of the theory of the energy levels of ortho-H_2 in the first rotational state and apply them to the experimental results obtained from curves like Fig. 6. Finally we shall present a derivation of the formulae which we use.

When the molecule of HD or D_2 is in the state with rotational angular momentum, J, equal to zero, the internuclear axis is oriented in every direction with equal probability. Since these molecules have no resultant electronic moment ($^1\Sigma$ state) all interactions between each nucleus and the rest of the molecule become independent of the orientation of the nucleus in the external magnetic field. This follows because the axis of the molecule has all orientations with equal probability independent of the nuclear spin orientation. Further, the magnetic interaction between the two nuclear magnets averages out to zero, because the mutual energy of two dipoles averaged over all possible orientations of the line joining them is zero. Therefore, each of the two nuclei in the molecule has a definite energy in the external magnetic field depending on its own orientation but independent of the orientation of the other nucleus. These are exactly the circumstances under which the theory of Eq. (1) may be applied as well as the rigorous theory[13] for the transition probability in the oscillating field.

Table II. *Summary of data taken during the spring of 1938 for the determinations of the proton and deuteron moments. The magnet used for these measurements was calibrated with a flip coil and mutual inductance. The path in the r.f. field was only 2.7 cm.*

Substance	Moment Measured	Frequency in Megacycles	Field in Gauss	Nuclear Moment
H_2	H	5.662	1336	2.781
H_2	H	7.000	1655	2.775
H_2	H	8.923	2107	2.779
H_2	H	14.007	3299	2.786
HD	H	10.420	2456	2.785
HD	H	10.420	2461	2.780
HD	H	10.430	2457	2.786
HD	H	13.535	3180	2.793
HD	H	13.190	3106	2.787
HD	H	13.212	3106	2.791
D_2	D	2.103	3232	0.8536
D_2	D	3.143	4832	0.8537
D_2	D	2.103	3224	0.8560
HD	D	2.021	3106	0.8550

The experimental results show that these predictions are indeed true and that the half-widths and depths of the minima are as to be expected and that the ratio f/H is constant. From these values of f/H, from Eq. (1), and from the known results that the spin of the proton is $\frac{1}{2}$ and of the deuteron 1, we compute the value of the magnetic moments. The results are tabulated in Table II, and show that those obtained for the deuteron with D_2 and HD, and for the proton with H_2 and HD, are in close agreement.

These measurements were made when the homogeneous field magnet was the small one permitting a length of path in the radiofrequency field of only 2.7 cm. However, this magnet is the one that is carefully calibrated so that our values of the moments depend on this calibration. The averages, obtained by weighting proportionally to frequency, are 2.785 ± 0.02 nuclear magnetons and 0.855 ± 0.006 nuclear magnetons for the proton and deuteron, respectively.

The longer magnet, put into the apparatus later, was not directly calibrated at all. Its field is known only in terms of the proton moment.

A very careful determination of the ratio μ_P/μ_D was made with the longer magnet. The result is $\mu_P/\mu_D=3.2570\pm0.001$. This agrees with the value 3.259 ± 0.007 obtained with the short magnet. The difference in the precisions of the two results is chiefly due to the difference between the lengths of the two radiofrequency fields.

When the rotational quantum number is greater than zero, the various interactions mentioned in the previous paragraph are no longer

zero and the energy of a nucleus in the external magnetic field depends not only on its own orientation but also on the orientation of the other nucleus and on the orientation of the rotational angular momentum of the molecule. We shall discuss only ortho-H_2 in the first rotational state since, as discussed in the preceding section, this is the only state which contributes resonance minima when H_2 is observed at 78°K.

In ortho-H_2 the two nuclei are in a state where the spins of the two nuclei are "parallel," that is, the total nuclear spin angular momentum is 1. Transitions between this state and the state in which the total spin is zero cannot occur in our experiment for two reasons. First, such a change in spin involves a change from ortho-H_2 to para-H_2 and hence a change in rotational quantum number for which the energy difference is so large that it involves a frequency thousands of times as great as those we employ. Second, this transition is highly forbidden because it is of the triplet to singlet type.

From these considerations we see that in an externally applied magnetic field, in which the energy of the protons due to interaction with the field is much larger than the magnetic energy of interaction between the two protons and of the protons with the molecular rotation, we obtain nine energy levels. These correspond to the three orientations of the total nuclear spin I with each of which three orientations of the rotation vector J are possible. The resonance minima shown in Fig. 6 arise from the six transitions and their inverses which can occur between these nine magnetic levels subject to the restriction $\Delta m_I = \pm 1$.

The theory of the location of these levels is very similar to that of the magnetic levels of a multiplet of the Paschen-Back effect. If we assume that the orientation dependent energy of the ortho-H_2 is due solely to interactions with the external field and to the spin-spin magnetic interaction between the nuclei and the magnetic interaction between the nuclear spins and the molecular rotation, then the theoretical expression for the total energy of the ortho-H_2 molecule in the magnetic field (apart from constants independent of the orientation) becomes

$$E = -\mu_P(\boldsymbol{\sigma}_1+\boldsymbol{\sigma}_2)\cdot\mathbf{H} - \mu_R\mathbf{J}\cdot\mathbf{H} - \mu_P H'(\boldsymbol{\sigma}_1+\boldsymbol{\sigma}_2)\cdot\mathbf{J} + \frac{\mu_P^2}{r^3}\{\boldsymbol{\sigma}_1\cdot\boldsymbol{\sigma}_2 - 3(\boldsymbol{\sigma}_1\cdot\mathbf{r})(\boldsymbol{\sigma}_2\cdot\mathbf{r})/r^2\}, \quad (3)$$

where μ_P and μ_R are the proton and rotational magnetic moments, $\boldsymbol{\sigma}_1$ and $\boldsymbol{\sigma}_2$ the Pauli matrices for the nuclear spins, J, the rotational angular momentum in units of $h/2\pi$, and r the radius vector joining the two nuclei. The first term is the energy of the two proton moments in the external magnetic field H, which we take in the z direction. This term can also be written as $2\mu_P\mathbf{I}\cdot\mathbf{H}$ since, as has already been stated, the two proton spins, each of value $\frac{1}{2}$, combine to form a total proton spin I of value 1, and the two proton moments μ_p combine to form a total moment equal to $2\mu_p$. The second term is the energy arising from the interaction of the rotational magnetic moment of the molecule with the external magnetic field. The third term is the energy of interaction between the proton moment and the field H' caused by the rotation of the molecule at the position of the protons.

TABLE III. *Energy levels for the first rotational state of ortho-H_2 molecules in a magnetic field. $\alpha = \mu_r/2\mu_p$.*

m_J	m_I	ENERGY
1	1	$-2\mu_P\{\ H+\alpha H-\ H''/5\ +H'\}$
1	0	$-2\mu_P\{\ \alpha H+2H''/5\ -(3H''/5-H')^2/H(1-\alpha)\}$
1	−1	$-2\mu_P\{-\ H+\alpha H-\ H''/5\ -H'-[(3H''/5+H')^2+2(3H''/5)^2]/H(1-\alpha)\}$
0	1	$-2\mu_P\{\ H\ +2H''/5\ +(3H''/5-H')^2/H(1-\alpha)\}$
0	0	$-2\mu_P\{\ -4H''/5\}$
0	−1	$-2\mu_P\{-\ H\ +2H''/5\ -(3H''/5-H')^2/H(1-\alpha)\}$
−1	1	$-2\mu_P\{\ H-\alpha H-\ H''/5\ -H'+[(3H''/5+H')^2+2(3H''/5)^2]/H(1-\alpha)\}$
−1	0	$-2\mu_P\{\ -\alpha H+2H''/5\ +(3H''/5-H')^2/H(1-\alpha)\}$
−1	−1	$-2\mu_P\{-\ H-\alpha H-\ H''/5\ +H'\}$

This field is parallel to the rotational angular momentum J. The last term is the well-known expression for the interaction between two magnets separated by a distance r, which in this case is the internuclear distance.

From this form of interaction the energy levels of the molecule may be obtained by the Schrödinger perturbation theory. The calculation is given at the end of this section. The results, good to the second-order perturbation theory, are given in Table III, where the resultant energy levels are classified by the quantum numbers m_I and m_J, which are the magnetic quantum numbers of the total nuclear spin and of the molecular rotation, respectively, where each takes the values 1, 0 and -1.

The terms involving $(H')^2$ and $(H'')^2$ represent corrections to the energies which are inversely proportional to the external field. They arise because the magnetic field is not sufficiently large for the Paschen-Back effect to be complete. These corrections though small, are nevertheless measurable. The quantity H'' is the value of μ_p/r^3 and comes from the term which involves the mutual magnetic energy of the two protons and is independent of the value of the external field. H'' is thus the field at one proton due to the magnetic moment of the other.

This set of energy levels plus appropriate selection rules will give the observed spectrum at frequencies equal to the energy differences divided by h, as is shown by Eq. (2). At high fields where the first three terms in the energy expression are much larger than the last two, we have rigorous selection rules, namely:

$$\Delta m_I = \pm 1,$$

or

$$\Delta m_J = \pm 1.$$

The first corresponds to a change in the orientation of the total proton spin by one unit while the component of the rotational angular momentum remains unchanged; while in the second the orientation of the nuclear spin remains fixed while the rotational m_J changes. Since the above mentioned corrections are small compared with the other terms we obtain two groups of lines, one of which corresponds to transitions in which m_I changes and the other when m_J changes. The first set (of six) is grouped around the region where $f=2\mu_P H/h$ and the other set of six around the region $f=\mu_R H/h$.

In this paper only the first group will be discussed. The second group does not yield any new information except the magnetic moment of rotation and will be discussed in a paper devoted to the rotational moments of H_2, D_2 and HD. The six lines which we will consider correspond to the energy differences given in energy units in Table IV.

We must now recall that we use a fixed oscillator frequency, f_0, and vary the magnetic field in the neighborhood of H_0, where H_0 is defined by $H_0=hf_0/2\mu_P$. H_0 is thus the field at which the Larmor frequency of the proton would be equal to the oscillating frequency applied. Setting ΔE as given in Table IV equal to $2\mu_p H_0$ and dividing through by $2\mu_p$ it can be seen that resonances will occur for the values of the magnetic field listed in Table V.

Except for the effect of the small last terms in Table V, we see that the resonances are symmetrical about the position H_0. This circumstance permits us to deduce a value of the proton moment from the center of the pattern formed by the six resonance minima with the results given in Table II.

A unique identification of the transitions producing the minima of the curve of Fig. 6 makes possible an evaluation of the interaction con-

TABLE IV. *Changes of energy associated with a change of the orientation of the total nuclear spin by ±1 for ortho-*H *molecules in the first rotational state.*

m_J	Δm_I	ΔE
1	0→1	$2\mu_P\{H-(3H''/5-H')+(3H''/5-H')^2/H(1-\alpha)\}$
1	−1→0	$2\mu_P\{H+(3H''/5+H')+6H''/5(3H''/5+2H')/H(1-\alpha)\}$
0	0→1	$2\mu_P\{H+6H''/5+(3H''/5-H')^2/H(1-\alpha)\}$
0	−1→0	$2\mu_P\{H-6H''/5+(3H''/5-H')^2/H(1-\alpha)\}$
−1	0→1	$2\mu_P\{H-(3H''/5+H')+6H''/5(3H''/5+2H')/H(1-\alpha)\}$
−1	−1→0	$2\mu_P\{H+(3H''/5-H')+(3H''/5-H')^2/H(1-\alpha)\}$

TABLE V. *Magnetic fields at which resonances will occur for a fixed oscillator frequency* $f_0=2\mu_p H_0/h$.

m_J	Δm_I	MAGNETIC FIELDS	
1	0→1	$H_0+(3H''/5-H')$	$-(3H''/5-H')^2/H(1-\alpha)$
1	−1→0	$H_0-(3H''/5+H')$	$-6H''/5(3H''/5+2H')/H(1-\alpha)$
0	0→1	$H_0-6H''/5$	$-(3H''/5-H')^2/H(1-\alpha)$
0	−1→0	$H_0+6H''/5$	$-(3H''/5-H')^2/H(1-\alpha)$
−1	0→1	$H_0+(3H''/5+H')$	$-6H''/5(3H''/5+2H')/H(1-\alpha)$
−1	−1→0	$H_0-(3H''/5-H')$	$-(3H''/5-H')^2/H(1-\alpha)$

stants H' and H''. This identification is made possible by the asymmetry of the positions of the two outermost minima which is especially noticeable in low field. In fact Fig. 9 and Table VI show clearly that the minima labeled A_L, B_L, A_R and B_R are symmetrically located about H_0 at all frequencies, while C_L and C_R only approach symmetry at high frequency.

Setting $(1-\alpha)=0.843\approx 1$, reference to Table V reveals two things. First, if *four* minima are symmetrical and two asymmetrical, the asymmetrically situated minima marked C_L and C_R on Fig. 6 must be assigned to the transitions $m_J=1$, $m_I=-1\leftrightarrow 0$, and $m_J=-1$, $m_I=0\leftrightarrow 1$. Second, the quantity $(\frac{3}{5}H''-H')^2/H$ must be small. Reference to Fig. 9 shows that the shifts from symmetry produced by this second-order term in a field of 1000 gauss must be less than 1 gauss. Hence $(\frac{3}{5}H''-H')<(1000)^{\frac{1}{2}}$, and we must identify A_L and A_R with the transition $m_J=1$, $m_I=0\leftrightarrow 1$, and $m_J=-1$, $m_I=-1\leftrightarrow 0$. This leaves B_L and B_R as the remaining minima, and they must be assigned to the other two transitions.

Once the transitions are identified, the determination of the separations in field between corresponding minima gives:

$$A_R-A_L=2(\tfrac{3}{5}H''-H')=13.5 \text{ gauss},$$
$$B_R-B_L=(12/5)H''=81.8 \text{ gauss},$$
$$C_R-C_L=2(\tfrac{3}{5}H''+H')=95.2 \text{ gauss}.$$

This assignment satisfies the obvious requirement that $(C_R-C_L)=(B_R-B_L)+(A_R-A_L)$, and furthermore fixes the sign of H' as the same as that of H'', which is positive because the proton moment is positive. The experimental fact that at low fields the shifts of C_L and C_R are toward lower field serves only as a check on the correctness of the applicability of the theory.

The best values deduced from the results in Table VII are:

$$H'=27.2\pm 0.3 \text{ gauss} \quad \text{and} \quad \tfrac{3}{5}H''=20.5 \text{ gauss}$$
$$H''=34.1\pm 0.3 \text{ gauss}.$$

These values can be used to account quantitatively for the asymmetry. In fact, the term $(6/5)H''(\frac{3}{5}H''+2H')/(1-\alpha)H=3660/H$ if we use the value of the rotational moment given by Ramsey.[14] We compare the expected shift of 3.8 gauss with the experimental value (see Table VI) of 4 gauss from $(C_R+C_L)/2$ for the 4 Mc data.

The fact that the three intervals and the asymmetry can be accounted for to such accuracy by only two constants, strongly supports our theory. Furthermore, these values agree with similar results to be published by one of us (N. F. R., Jr.) using the resonances associated with transitions of the molecular rotation moment of H_2. These values for these same constants are:

$$H'=27.0 \text{ gauss},$$
$$H''=34.1 \text{ gauss}.$$

The quantity H'' is equal to $\langle\mu_P/r^3\rangle_{Av}$. We are indebted to Dr. Arnold Nordsieck for supplying us with the value of $\langle r^{-3}\rangle_{Av}$, which he obtained from the band spectrum analysis of H_2 by C. R. Jeppeson.[15] The asymmetry of the potential even

TABLE VI. *Displacements in gauss of minima for* H *in* H_2 *from center* (H_0) *obtained from* H *in* HD. *These displacements are considered reliable to* ±*0.5 gauss. Note that only* C_L *and* C_R *are unequal; that they approach equality in high fields.*

	DISPLACEMENTS IN GAUSS FOR OSCILLATOR FREQUENCIES OF		
	4.000 Mc	7.000 Mc	16.000 Mc
C_L	−51.8	−49.3	−48.9
B_L	−40.7	−40.8	−41.0
A_L	− 6.6	− 6.9	− 6.6
H_0	942.3	1649.1	3769.0
A_R	6.7	6.9	6.6
B_R	41.0	41.2	41.0
C_R	43.8	45.5	46.5

[14] N. F. Ramsey, Jr., Phys. Rev. **55**, 595 (1939), Abs. 26.
[15] C. R. Jeppeson, Phys. Rev. **44**, 165 (1933).

TABLE VII. *Displacements in gauss between corresponding minima of* H *in* H_2. *Note that the separations between corresponding minima are independent of oscillator frequency and that* $(A_R-A_L)+(B_R-B_L)=(C_R-C_L)$ *as expected theoretically.*

	Displacements in Gauss for Oscillator Frequencies of 4 Mc	7 Mc	16 Mc	Average	Assigned Theoretical Expression
C_R-C_L	95.5	94.8	95.4	95.2	$2(H'+3H''/5)$
B_R-B_L	81.6	82.0	81.9	81.8	$12H''/5$
A_R-A_L	13.2	13.8	13.3	13.5	$2(H'-3H''/5)$

for the lowest vibration state and the centrifugal effect of the first rotational level make the effective internuclear distance slightly larger than r_e, the equilibrium internuclear distance. This value of $\langle r^{-3}\rangle_{Av}$ of $2.438\times10^{+24}$ cm^{-3} combined with $H''=34.1$ yields a value of $\mu_P=1.403\times10^{-23}$ erg/gauss or 2.785 ± 0.03 nuclear magnetons, in too perfect agreement with the value obtained from the ν/H result. It is of interest to note that this serves as a check on the correctness of the calibration of the magnet, because if the calibration constant were changed the two values would change in opposite directions, and would disagree if the magnet were incorrectly calibrated.

Derivation of Table III

We shall now sketch a derivation of the formulae which are used to construct Table III, the table of energy levels obtained from the energy expression of Eq. (3). Since we use a high value of the external field, m_I and m_J are "good" quantum numbers and we will use the m_I and m_J representation. The diagonal elements of the first three terms on the right of Eq. (3) in this representation are

$$-2\mu_P H m_I-\mu_R H m_J-2\mu_P H' m_I m_J. \quad (4)$$

The matrix elements of the fourth term

$$\mu_P^2/r^3(IJm_Im_J \,|\boldsymbol{\sigma}_1\cdot\boldsymbol{\sigma}_2-3(\boldsymbol{\sigma}_1\cdot\mathbf{r})(\boldsymbol{\sigma}_2\cdot\mathbf{r})/r^2|\, IJm_I'm_J') \quad (5)$$

are evaluated from the nine wave functions of ortho-H_2. To a high approximation these wave functions are written as a product of the symmetrical spin functions of the two protons and the coordinate wave functions of the first rotational state. These wave functions are given by

$$\Psi_{m_Im_J}=\varphi_{m_I}\psi_{m_J} \quad (6)$$

$$\psi_1=-\tfrac{1}{2}(3/2\pi)^{\frac{1}{2}}\sin\vartheta e^{i\varphi},\quad \psi_0=\tfrac{1}{2}(3/2\pi)^{\frac{1}{2}}\cos\vartheta,$$
$$\psi_{-1}=\tfrac{1}{2}(3/2\pi)^{\frac{1}{2}}\sin\vartheta e^{-i\varphi},$$
$$\varphi_1=\alpha(1)\alpha(2),\quad \varphi_0=\sqrt{2}(\alpha(1)\beta(2)+\beta(1)\alpha(2))/2$$
$$\varphi_{-1}=\beta(1)\beta(2),$$

where α and β are the spin eigenfunctions for the spin components $\frac{1}{2}$ and $-\frac{1}{2}$, respectively.

The evaluation of these matrix elements is simplified by use of the following identity which may readily be verified by expansion:

$$\begin{aligned}&r^2\boldsymbol{\sigma}_1\cdot\boldsymbol{\sigma}_2-3(\boldsymbol{\sigma}_1\cdot\mathbf{r})(\boldsymbol{\sigma}_2\cdot\mathbf{r})\\&=-(3z^2-r^2)(3\sigma_{z1}\sigma_{z2}-\boldsymbol{\sigma}_1\cdot\boldsymbol{\sigma}_2)/2\\&-3\{\tfrac{1}{4}(\sigma_{x1}+i\sigma_{y1})(\sigma_{x2}+i\sigma_{y2})(x-iy)^2\\&+\tfrac{1}{4}(\sigma_{x1}-i\sigma_{y1})(\sigma_{x2}-i\sigma_{y2})(x+iy)^2\\&+\tfrac{1}{2}[\sigma_{z2}(\sigma_{x1}+i\sigma_{y1})+\sigma_{z1}(\sigma_{x2}+i\sigma_{y2})]z(x-iy)\\&+\tfrac{1}{2}[\sigma_{z2}(\sigma_{x1}-i\sigma_{y1})+\sigma_{z1}(\sigma_{x2}-i\sigma_{y2})]z(x+iy)\}. \quad (7)\end{aligned}$$

The matrix elements of the first term of Eq. (7) give all of the diagonal elements of Eq. (5) which are equal to[16]

$$(3m_J^2-2)(3\sigma_{z1}\sigma_{z2}-\boldsymbol{\sigma}_1\cdot\boldsymbol{\sigma}_2)\mu_P^2/5r^3.$$

For ortho-H_2, for which the three spin functions are symmetrical in the proton spin $\boldsymbol{\sigma}_1\cdot\boldsymbol{\sigma}_2=1$ and we then obtain for the diagonal elements of Eq. (5)

$$(3m_J^2-2)(3m_I^2-2)2\mu_P^2/5r^3.$$

The off diagonal matrix elements are used in our calculations to evaluate the second-order perturbations of the energies from complete Paschen-Back effect and give rise to the quantities listed in Table III. The off diagonal elements of Eq. (5) are easily calculated from the three spin and three angular wave functions. The values of the nonvanishing elements are:

$$(m_I, m_J \text{ to } m_I-1, m_J+1)=(2m_I-1)(2m_J+1)\times\{(m_I+1)(2-m_I)(1-m_J)(2+m_J)\}^{\frac{1}{2}}3\mu_P^2/5r^3,$$

$$(m_I, m_J \text{ to } m_I+1, m_J-1)=(2m_I+1)(2m_J-1)\times\{(1-m_I)(2+m_I)(1+m_J)(2-m_J)\}^{\frac{1}{2}}3\mu_P^2/5r^3,$$

$$(m_I, m_J \text{ to } m_I-2, m_J+2)=\{(1+m_I)m_I(2-m_I)(3-m_I)(1-m_J)\times(-m_J)(2+m_J)(3+m_J)\}^{\frac{1}{2}}3\mu_P^2/5r^3,$$

$$(m_I, m_J \text{ to } m_I+2, m_J-2)=\{(1-m_I)(-m_I)(2+m_I)(3+m_I)\times(1+m_J)(m_J)(2-m_J)(3-m_J)\}^{\frac{1}{2}}3\mu_P^2/5r^3.$$

[16] H. B. G. Casimir, "On the Interaction between Atomic Nuclei and Electrons," Prize Essay published by Teyler's Tweede Genootschap (1936), page 33.

The off diagonal elements of the term $\mu_P H'(\sigma_1+\sigma_2)\cdot\mathbf{J}$ are:

$$(m_I, m_J \text{ to } m_I+1, m_J-1) = \{(1-m_I)(2+m_I)(1+m_J)(2-m_J)\}^{\frac{1}{2}}\mu_P H',$$

$$(m_I, m_J \text{ to } m_I-1, m_J+1) = \{(1+m_I)(2-m_I)(1-m_J)(2+m_J)\}^{\frac{1}{2}}\mu_P H'.$$

The value of the perturbation energy which is to be added to the diagonal elements is obtained from the usual second-order perturbation theory. Since the only nonvanishing matrix elements are between states with the same value of m_I+m_J we have

$$W_{m_I, m_J}=\sum_{\delta}\frac{(m_I, m_J|E|m_I+\delta, m_J-\delta)\times(m_I+\delta, m_J-\delta|E|m_I, m_J)}{E_{m_I, m_J}-E_{m_I+\delta, m_J-\delta}}, \quad (8)$$

where the sum is over all permissible values of δ except zero. Into this equation are inserted the appropriate nondiagonal elements listed above and for E_{m_I, m_J} the diagonal elements of Eq. (4) without the term which involves H'. The second-order terms of Table III are thus obtained.

Discussion

The agreement between the measurements of the magnetic moment of the proton by two theoretically independent methods, i.e., the Larmor frequency in an external field and the magnetic interaction of the two proton moments makes our result quite certain. Our present result 2.785 ± 0.02 nuclear magnetons is in agreement with the previous atomic beam measurement of the proton moment through the hyperfine-structure of the normal state of atomic hydrogen. That result was 2.85 ± 0.15 nuclear magnetons which is well within the limit of error. To this extent there is no reason for supposing some breakdown of the Dirac equation for the electron nor the assumption of any novel interaction between proton and electron. A similar discussion holds for the deuteron. If we assume that the neutron moment is the difference[17] between the deuteron moment and the proton moment then its value is -1.93 nuclear magnetons.

The quantity H' which is the constant of spin-orbit interaction or the magnetic field at a nucleus produced by the molecular rotation is 27.2 gauss. Although no exact theory of this quantity exists in the literature a rough consideration shows it to be quite reasonable. The magnetic field produced by the orbital motion of one proton at the position of the other is $2ev/cr^2$ which can be written as $(2e/Mc)(Mvr/r^3)$. Setting Mvr equal to $h/2\pi$ we obtain $4\mu_n/r^3$ for this field, where μ_n is one nuclear magneton. Inserting numerical values this becomes 49.0 gauss. The effect of the electrons is in the opposite sense. Since our results show that H' is positive the magnetic field produced by the electrons is somewhat less than half that of the nuclei.

Our results show that it is possible to apply exact spectroscopic principles and procedures to spectral regions which correspond to ordinary radio waves. The accuracy to which the laws of quantum mechanics hold and the necessity of their application in a region of frequency in which one is accustomed to think classically we consider a striking confirmation of the theory.

This research has been aided by grants from the Research Corporation and the Carnegie Institution of Washington.

[17] However, see J. Schwinger, reference 6, for a discussion of the effect of the deuteron quadrupole moment on these considerations.

Note on the Scattering of Neutrons by Protons

C. KITTEL AND G. BREIT
University of Wisconsin, Madison, Wisconsin

(Received August 28, 1939)

Expansions for the computation of s wave scattering for square wells are arranged in a form convenient for numerical substitution. Effects of p wave scattering are estimated using Bethe's neutral form of meson theory. It is found that effects of the order of 50 percent in the angular distribution may be expected for 16-Mev neutrons.

INTRODUCTION

OBSERVATIONS on the scattering of neutrons by protons have been made[1–5] in the energy range 0–16 Mev. The present note compares the experimental results with theoretical calculations. Wigner's approximate formula[6] for a "square well" (potential having a constant value through a distance r_0) is amplified by the addition of three more terms in the range of force. It converges satisfactorily in the above energy region. The virtual level for the singlet state is introduced in such a way that corrections for the range of force can be conveniently made. The above calculations take account of s scattering only. The observations on fast neutrons fall below the theoretical curve for $r_0=e^2/mc^2$, the value for r_0 suggested[7] by experiments on the scattering of protons by protons.[8] These calculations are of a provisional character, since the interactions obtained from field theories should supplant the use of arbitrary potentials. The "cutting off" of potentials which has so far been found necessary in field theories makes the prediction of phase shifts doubtful, however, and the formula for the square well has been thought to be of interest as a temporary way of estimating effects of range and neutron energy.

The p wave phase shifts have been calculated using Bethe's "neutral" form of meson theory.[9] For a meson mass $\mu=177$ m the p wave scattering cross section is 0.12×10^{-24} cm^2 at 16-Mev neutron energy. This is to be compared with the experimental scattering cross section 0.6×10^{-24} cm^2 which includes the effects of all angular momenta and the s wave cross section 0.56×10^{-24} cm^2 for the square well with range e^2/mc^2. The p wave effects are seen to be appreciable and perhaps ultimately detectable for this μ. Proton-proton scattering experiments suggest,[10] on the other hand, $\mu=330$ m. Estimates for this shorter range of force ($\sim\hbar/\mu c$) give 0.01×10^{-24} cm^2 for the scattering cross section due to the p wave at a neutron energy of 16 Mev. This amount is practically undetectable. The presence of p scattering can be looked for by studying the angular distribution of scattered neutrons or of recoil protons. Some modifications of the usual phase shift analysis are necessary on account of the spin-orbit-spin coupling. These are discussed at the end of the note. An effect of ~50 percent on the angular distribution is expected at 16 Mev using $\mu=180$ m and roughly $\frac{1}{3}$ of this amount for $\mu=330$ m.

NOTATION

M = mass of proton or neutron (neutron-proton mass difference will be neglected throughout).
μ = mass of meson.
m = mass of electron.
E = kinetic energy of incident neutron.
E' = energy in frame of center of gravity $=E/2$.

[1] E. O. Salant, R. B. Roberts and P. Wang, Phys. Rev. **55**, 984 (1939).
[2] H. Aoki, Phys. Rev. **55**, 795 (1939).
[3] R. Ladenburg and M. H. Kanner, Phys. Rev. **52**, 911 (1937).
[4] E. T. Booth and C. Hurst, Proc. Roy. Soc. **A161**, 248 (1937).
[5] W. H. Zinn, S. Seely and V. W. Cohen, Phys. Rev. **56**, 260 (1939).
[6] E. Wigner, Zeits. f. Physik **83**, 253 (1933).
[7] G. Breit, H. M. Thaxton and L. Eisenbud, Phys. Rev. **55**, 1018 (1939). This paper is referred to as B. T. E. in the text.
[8] R. G. Herb, D. W. Kerst, D. B. Parkinson and G. J. Plain, Phys. Rev. **55**, 998 (1939).
[9] H. A. Bethe, Phys. Rev. **55**, 1261 (1939). We are indebted to Professor Bethe for communicating his results to us before publication.
[10] S. S. Share, L. E. Hoisington and G. Breit, Phys. Rev. **55**, 1130 (1939).

v = relative velocity of proton and neutron before collision.
r = distance between proton and neutron.
$\Lambda = h/(Mv/2)$; $k = 2\pi/\Lambda$; $\rho = kr$.
r_0 = radius of square well.
$F = r$ times radial wave function, normalized to unit amplitude at ∞.
D_1, D_3 = depths of square wells representing, respectively, proton-neutron interaction in the singlet and triplet states.
K_{01}, K_{03} = phase shifts for singlet and triplet partial waves of zero orbital angular momentum.
E_1 = energy of ^1S virtual level of deuteron.
$(-E_3)$ = |binding energy of deuteron in normal state|.
a_1, a_3 = intercepts on axis of r of tangents to F for zero energy neutrons, for singlet and triplet states. A positive a corresponds to tangent cutting axis on left of origin.
σ_1, σ_3 = scattering cross sections for singlet and triplet states.
θ = scattering angle in center of mass system.
$\sigma(\theta)$ = total scattering cross section per unit solid angle.
$\sigma = \int \sigma(\theta) d\Omega$.
E_1^0 defined by Eq. (8); ϵ defined by Eq. (10).

$\chi = (rdF/Fdr)_{r=r_0}$.
$\gamma_1 = 1 + E'/E_1$; $\gamma_3 = 1 - E'/E_3$.
$x_1 = [ME_1/\hbar^2]^{\frac{1}{2}} r_0$; $x_3 = [M(-E_3)/\hbar^2]^{\frac{1}{2}} r_0$.

S-Scattering

The total neutron-proton scattering cross section is given by

$$\sigma = \tfrac{1}{4}[3\sigma_3 + \sigma_1].$$

If the neutron energy is sufficiently low so that only the s $(L=0)$ partial wave need be considered,

$$\sigma_1 = (\Lambda^2/\pi) \sin^2 K_{01}; \quad \sigma_3 = (\Lambda^2/\pi) \sin^2 K_{03}.$$

For a square well, where the potential energy has the constant amount $-D$ for $r < r_0$ and is zero for $r > r_0$, one obtains

$$\sin^2 K_0 = (\rho \cos \rho - \chi \sin \rho)^2/(\rho^2 + \chi^2), \quad (1)$$

where the value of ρ for $r = r_0$ is used. Here

$$\chi = (rdF/Fdr)_{r=r_0} = [(M(D+E')/\hbar^2)^{\frac{1}{2}} r_0] \cot \times [(M(D+E')/\hbar^2)^{\frac{1}{2}} r_0]. \quad (2)$$

Triplet state

One wishes to obtain σ_3 as a function of the binding energy $(-E_3)$, E and r_0. It is first necessary to eliminate the well depth D_3; this is performed with the help of the series[7]

$$-\frac{D_3}{E_3} = \frac{\pi^2}{4x_3^2} + \frac{2}{x_3} + 1 - \frac{4}{\pi^2} + \left(\frac{32}{\pi^4} - \frac{8}{3\pi^2}\right) x_3 + \left(\frac{32}{\pi^4} - \frac{320}{\pi^6}\right) x_3^2 + \cdots. \quad (3)$$

Expanding Eq. (1) in a series in x_3, one obtains after a straightforward calculation:

$$\frac{\sin^2 K_{03}}{\rho^2} = \frac{1}{\gamma_3 x_3^2}[1 + x_3 + G_2 x_3^2 + G_3 x_3^3 + G_4 x_3^4 + \cdots], \quad (4)$$

where

$$G_2 = 1 - 4/\pi^2 - \gamma_3/4 = 0.5947 - 0.25\gamma_3;$$
$$G_3 = \tfrac{1}{3} - 4/\pi^2 + 32/\pi^4 + (1/\pi^2 - \tfrac{1}{3})\gamma_3 = 0.2566 - 0.2320\gamma_3;$$
$$G_4 = \tfrac{1}{3} - 4/\pi^2 + 48/\pi^4 - 320/\pi^6 + (-\tfrac{1}{4} + 2/\pi^2 - 8/\pi^4)\gamma_3 + (-1/48 + 1/2\pi^2)\gamma_3^2 = 0.0880 - 0.1295\gamma_3 + 0.0298\gamma_3^2.$$

Finally $\sigma_3 = (\Lambda^2/\pi) \sin^2 K_{03} = \dfrac{4\pi\hbar^2}{M(E' - E_3)} \times [1 + x_3 + G_2 x_3^2 + G_3 x_3^3 + G_4 x_3^4 + \cdots]. \quad (5)$

For $\gamma_3 = 2.3$ the term $G_2 x_3^2$ vanishes and the first two terms are a good approximation.

Singlet state

There is, according to present views, no stable singlet proton-neutron state. The depth D_1 can be determined from a knowledge of $\sigma_1(E=0)$, which results from the experimental value of σ for thermal neutrons and the computed $\sigma_3(E=0)$. (For the relevant formula see Eq. (8.6) of B.T.E.) It is, however, possible to avoid using D_1 in the expansion for σ_3 by the proper introduction of a virtual level. The definition of a virtual level is somewhat arbitrary; and the actual definition chosen for the problem in hand is designed to give the expansion for $\sin^2 K_{01}$ a form closely similar to Eq. (4) for $\sin^2 K_{03}$. Let the energy of the virtual level be defined as a positive energy E_1 such that

$$[(M(D_1 - E_1)/\hbar^2)^{\frac{1}{2}} r_0] \cot \times [(M(D_1 - E_1)/\hbar^2)^{\frac{1}{2}} r_0] = (ME_1/\hbar^2)^{\frac{1}{2}} r_0. \quad (6)$$

This definition may be compared with the condition for the stable ^3S normal level of the deuteron, namely

$$[(M(D_3+E_3)/\hbar^2)^{\frac{1}{2}}r_0]\cot \times[(M(D_3+E_3)/\hbar^2)^{\frac{1}{2}}r_0]=-(M(-E_3)/\hbar^2)^{\frac{1}{2}}r_0.$$

From Eq. (6) one finds

$$\frac{\sin^2 K_{01}}{\rho^2}=\frac{1}{\gamma_1 x_1^2}[1-x_1+G_2x_1^2 -G_3x_1^3+G_4x_1^4-\cdots],$$

which is similar to Eq. (4), and finally

$$\sigma_1=(\Lambda^2/\pi)\sin^2 K_{01}=\frac{4\pi\hbar^2}{M(E'+E_1)} \times[1-x_1+G_2x_1^2-G_3x_1^3+G_4x_1^4-\cdots], \quad (7)$$

where the G's are defined as in Eq. (4), but with γ_1 substituted for γ_3.

The virtual level is determined by the range and the quantity E_1^0, defined by

$$4\pi\hbar^2/(ME_1^0)=\sigma_1(E=0). \quad (8)$$

The quantity E_1^0 is the energy of the *virtual level for zero range*. One can evaluate $\sigma_1(E=0)$ from the experimental σ(thermal) and the computed $\sigma_3(E=0)$. Comparing Eqs. (7) and (8),

$$(1/E_1^0)=(1/E_1)(1-x_1+G_2^0x_1^2-G_3^0x_1^3+\cdots),$$

where the upper suffixes on the G's indicate that they are to be evaluated at $E=0$. One obtains the series

$$E_1=E_1^0[1-(E_1^0/\epsilon)^{\frac{1}{2}}+0.8447(E_1^0/\epsilon) -0.6666(E_1^0/\epsilon)^{\frac{3}{2}}+\cdots], \quad (9)$$

where

$$\epsilon=\hbar^2/(Mr_0^2). \quad (10)$$

The above series gives the virtual level for an assumed range in terms of the virtual level for zero range. For zero range, $E_1=E_1^0$, and the virtual level has a fairly direct physical meaning: for vanishing range of interaction the position of the virtual level determines $\sigma_1(E=0)$ in the same way as the binding energy $(-E_3)$ determines $\sigma_3(E=0)$.

Numerical formulae

Using the values of the fundamental physical constants as given by B. T. E., p. 1022, one may rewrite Eqs. (5) and (7) in a form convenient for numerical computation, if the range is kept fixed and the energy is varied.

$$\sigma_3=(\Lambda^2/\pi)\sin^2 K_{03}=\frac{5.21\times10^{-24}}{(E'-E_3)\text{ Mev}} \times[1+x_3+0.5947x_3^2+0.2566x_3^3+0.0880x_3^4 +\cdots+\gamma_3(-0.25x_3^2-0.2320x_3^3-0.1295x_3^4) +0.0298\gamma_3^2x_3^4+\cdots]\text{ cm}^2, \quad (11)$$

$$\sigma_1=(\Lambda^2/\pi)\sin^2 K_{01}=\frac{5.21\times10^{-24}}{(E'+E_1)\text{ Mev}} \times[1-x_1+0.5947x_1^2-0.2566x_1^3+0.0880x_1^4 +\cdots+\gamma_1(-0.25x_1^2+0.2320x_1^3-0.1295x_1^4) +0.0298\gamma_1^2x_1^4\cdots]\text{ cm}^2. \quad (12)$$

The fundamental physical constants are involved only in the number 5.21×10^{-24} cm^2. The pure numbers occurring inside the square brackets are independent of these constants. Graphs of the square brackets against energy are sufficiently linear to allow graphical interpolation. In each case the square bracket represents a correction for the range of force.

Using $E_3=-2.17$ Mev, and σ(thermal) $=14.8\times10^{-24}$ cm^2 reported by Simons,[11] one finds, with $r_0=e^2/mc^2$, the value $E_1=0.0978$ Mev for the position of the virtual level, while for zero range $E_1^0=0.112$ Mev. For these values of r_0, E_1 and E_3,

$$\sigma_3=\frac{5.21\times10^{-24}}{(E/2+2.17)\text{ Mev}}[1.974-0.1880\gamma_3 +0.00513\gamma_3^2-\cdots]\text{ cm}^2; \quad (13)$$

$$\sigma_1=\frac{5.21\times10^{-24}}{(E/2+0.0978)\text{ Mev}}[0.8738-0.00413\gamma_1 +0.0000104\gamma_1^2-\cdots]\text{ cm}^2; \quad (14)$$

$$\gamma_3=1+E/4.34; \quad \gamma_1=1+E/0.1956.$$

These series have been checked against exact solutions. For $E<10$ Mev, Eq. (13) gives results less than one percent too small, and Eq. (14) less than one percent too large. For $E=12$ Mev, $\sigma_{(\text{exact})}=0.789\times10^{-24}$ cm^2; $\sigma_{(\text{series})}=0.780\times10^{-24}$ cm^2. In Fig. 1, σ, σ_1, and σ_3 are plotted, using the above series, in the energy range 0–16 Mev.

[11] L. Simons, Phys. Rev. **55**, 792 (1939).

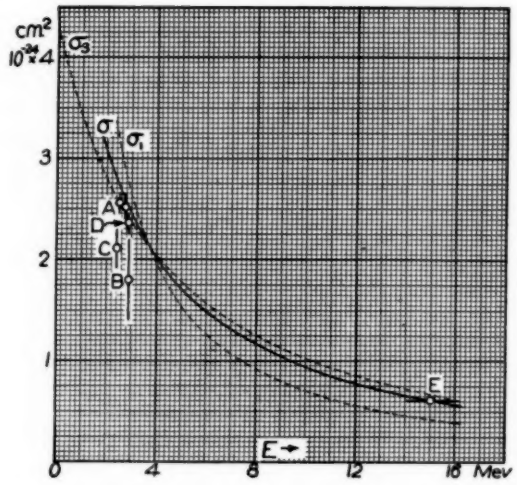

FIG. 1. *Abscissae:* energy of incident neutrons in Mev. *Ordinate:* neutron-proton scattering cross section for square well according to Eqs. (13), (14), with range $r_0=e^2/mc^2$. Only the effect of s waves is included. Curves σ_1, σ_3 are for singlet and triplet states, and $\sigma=\sigma_1/4+3\sigma_3/4$. *Experimental points: A*—Aoki; *B*—Booth and Hurst; *C*—Ladenburg and Kanner; *D*—Zinn, Seely and Cohen; *E*—Salant, Roberts and Wang.

With the same values of r_0, E_1 and E_3, one finds $D_1=11.52$ Mev, $D_3=21.0(2)$ Mev for the well depths; and $a_1=1.918\times10^{-12}$ cm, $a_3=-0.585\times10^{-12}$ cm for the intercepts.

The s wave scattering cross section for a square well with $r_0=e^2/mc^2$ is plotted in Fig. 1 as a function of the energy. The experimental value for the point E includes an unknown amount of d and p scattering. Estimates regarding the latter will now be discussed.

P-SCATTERING

The quadrupole moment of the deuteron indicates that nuclear potentials contain terms of the form $f(r)[3(\boldsymbol{\sigma}_1\mathbf{r})(\boldsymbol{\sigma}_2\mathbf{r})-r^2(\boldsymbol{\sigma}_1\boldsymbol{\sigma}_2)]$ so that different phase shifts are expected for ${}^3P_0$, ${}^3P_1$, ${}^3P_2$. The phase shift analysis of the experimental data must be made, therefore, taking into account the differences of these three phase shifts. It must also be modified[12] to take account of the fact that a d wave arises out of the s wave, and that for this d wave the angular distribution contains no terms in $(3\cos^2\theta-1)^2$, but only terms in $(3\cos^2\theta-1)$. The usual formulas for the angular distribution are not applicable, and the general formulas are complicated. Nevertheless it is possible to look for the effects of the p wave by determining the term in $\cos\theta$ in an analysis of the scattering cross section per unit solid angle, in the center of gravity system, in powers of $\cos\theta$.

Taking into account s and p waves only, one obtains for the cross section per unit solid angle in the center of gravity system

$$\begin{aligned}\sigma(\theta)=&\frac{3}{4}\left(\frac{\Lambda}{2\pi}\right)^2\Big\{\sin^2 K_{03}\\&+6\sin K_{03}\Big[\frac{5}{9}\cos(\delta_2-K_{03})\sin\delta_2\\&+\frac{3}{9}\cos(\delta_1-K_{03})\sin\delta_1\\&+\frac{1}{9}\cos(\delta_0-K_{03})\sin\delta_0\Big]\cos\theta\\&+(5\sin^2\delta_2+3\sin^2\delta_1+\sin^2\delta_0)\cos^2\theta\\&+\Big[-\frac{3}{4}(\sin\delta_1-\sin\delta_2)^2-\frac{1}{3}(\sin\delta_0-\sin\delta_2)^2\\&-3\sin\delta_1\sin\delta_2\sin^2\frac{\delta_1-\delta_2}{2}\\&-\frac{4}{3}\sin\delta_0\sin\delta_2\sin^2\frac{\delta_0-\delta_2}{2}\Big](3\cos^2\theta-1)\Big\}\\&+\frac{1}{4}\left(\frac{\Lambda}{2\pi}\right)^2\Big\{\sin^2K_{01}+6\sin K_{01}\cos(K_1-K_{01})\\&\times\sin K_1\cos\theta+9\sin^2K_1\cos^2\theta\Big\}.\end{aligned}\tag{15}$$

Here δ_0, δ_1, δ_2 are the phase shifts for ${}^3P_0$, ${}^3P_1$, ${}^3P_2$; and K_1 is the phase shift for ${}^1P_1$. The part of the expression in curly braces with the coefficient $\frac{3}{4}$ is due to triplet scattering. The s phase shifts for triplets and singlets are K_{03}, K_{01}, respectively. The last set of terms due to triplet scattering contains the factor $(3\cos^2\theta-1)$. These terms do not vanish for $\theta=\pi/2$ as is the case for $\delta_0=\delta_1=\delta_2$. The necessity of terms of this type may be seen by considering the special case $\delta_0\neq0$, $\delta_1=\delta_2=0$. The terms in $\sin^2\delta_0\cos^2\theta$ are then seen to cancel as they should since the P_0 part of the incident wave has no total angular momentum. The interference term in $\sin K_{03}\sin\delta_0\cos\theta$ is present, however, in agree-

[12] J. Schwinger, Phys. Rev. **55**, 235 (1939).

ment with the fact that the $^3S_1$ part of the incident wave has an angular momentum. The terms in $3\cos^2\theta-1=2P_2(\cos\theta)$ do not affect the integral of the cross section over all solid angles, and thus have no influence on absorption measurements. Since the d wave which is coupled to the s wave also gives rise to a term in $P_2(\cos\theta)$ for $\sigma(\theta)$ it is presumably not practical to try to disentangle these two contributions. The terms in $\cos\theta$ are, on the other hand, not affected by the d wave, and can be used as a direct test of a combination of effects of δ_0, δ_1, δ_2, K_1. Using the neutral form of theory given by Bethe, with $\mu=177$ m, numerical integrations for $E=16$ Mev give $\delta_0=-18.7°$, $\delta_1=23.7°$, $\delta_2=-5.2°$, $K_1=10.7°$. For these values of the phase shifts one has as the combined effect of s and p waves:

$$4\pi\sigma(\theta)=[1+0.56\cos\theta+0.62\cos^2\theta -0.17(3\cos^2\theta-1)]\times0.58\times10^{-24}\text{ cm}^2.$$

Here the first term in brackets represents the combined effect of ^3S and ^1S. The term $0.56\cos\theta$ is due to the interference between s and p waves, and the last two terms in brackets are due to the p waves. The contribution to $4\pi\sigma(\theta)$ in $\cos\theta$ is,

$$0.3(2)\times10^{-24}\cos\theta\text{ cm}^2,$$

which can be compared with the experimental value

$$\sigma=0.6\times10^{-24}\text{ cm}^2$$

for the average over solid angles of $4\pi\sigma(\theta)$. The analysis of $\sigma(\theta)$ into powers of $\cos\theta$ may be expected, therefore, to show an appreciable term in $\cos\theta$.

The above effect is sensitive to the range. Using a meson mass $\mu\sim330$ m numerical integrations give $\delta_0=-6.1°$, $\delta_1=3.7°$, $\delta_2=-1.8°$, $K_1=4.0°$. For these values the terms in $\cos\theta$ contribute $\sim0.1\times10^{-24}\cos\theta$ cm^2 to $4\pi\sigma(\theta)$, which is about $\frac{1}{3}$ of the amount for the cosmic-ray mass of the meson and at the maximum $\sim\frac{1}{6}$ of the solid angle average. The effect is obviously sensitive to the range of force; the important contributions to the p phase shifts come roughly from the regions $r=\hbar/\mu c$ to $r=3\hbar/\mu c$. The effect is not sensitive to the choice of the method of "cut-off" ("straight" or "zero").

The presence of p scattering affects σ. The contribution to σ at $E=16$ Mev due to the p wave is 0.12×10^{-24} cm^2 for $\mu=177$ m and 0.007×10^{-24} cm^2 for $\mu=330$ m, in a total of $\sim0.6\times10^{-24}$ cm^2. For the cosmic-ray mass of the meson one should, therefore, decrease the experimental value by ~20 percent at 16 Mev in order to obtain the net effect of the s and d waves. For the proton-proton range of force the correction is of the order of one percent and is insignificant. The interaction of $^3P_2$ and $^3G_2$ has been neglected above.

Appendix I

Effect of p wave

The usual scattering theory must be modified if the phase shifts are different for $^3P_0$, $^3P_1$, $^3P_2$, $^1P_1$. Since the meson interaction energy is diagonal in the spin of the two particles the incident wave may be considered as a statistical mixture in the proportions $\frac{1}{4}$, $\frac{3}{4}$ for singlet and triplet states. The cross section is then obtained as

$$\sigma(\theta)=\tfrac{1}{4}\sigma_1(\theta)+\tfrac{3}{4}\sigma_3(\theta).$$

For $\sigma_1(\theta)$ the usual considerations apply. For $\sigma_3(\theta)$ the incident wave may be considered as a statistical mixture of the three states

$$e^{ikz}S_1,\quad e^{ikz}S_0,\quad e^{ikz}S_{-1}$$

with weights of $\frac{1}{3}$ for each. Here S_1, S_0, S_{-1} are spin functions for the two particles corresponding to magnetic quantum numbers 1, 0, -1. The s and p parts of the above waves can be expressed in terms of linear combinations of products of angular and spin functions corresponding to the states $^3P_0$, $^3P_1$, $^3P_2$. Thus, for example,

$$\rho e^{ikz}S_1=F_0S_1+i(12\pi)^{\frac{1}{2}}F_1[(^3P_2)_1+(^3P_1)_1]/2^{\frac{1}{2}}.$$

Here $(^3P_j)_m$ is an angular-spin function for a ^3P state with total angular momentum j and magnetic quantum number m. The normalization is such that the integral over all solid angles of the sum over spin coordinates is unity. The customary notation for F_0, F_1 is used.[7] The interaction between the particles changes the differential equations satisfied by the radial factors. For $^3P_0$, $^3P_1$ there are then separate differential equations. For $^3P_2$ there is besides a coupling to $^3G_2$ which is neglected here. The scale with which the radial solutions must be introduced in place of F_0, F_1 must be chosen so that the resultant wave is $e^{ikz}+$part in $e^{i\rho}$. For large ρ this condition

determines completely the form of the radial functions in terms of the phase shifts.[13] Thus for instance $F_0=\sin\rho$ is replaced by

$$\sin\rho+e^{i(\rho+K_{03})}\sin K_{03}.$$

Proceeding in this way one obtains

$$(\rho e^{ikz}S_1)_{sc}=e^{i(\rho+K_{03})}\sin K_{03}S_1 + (12\pi)^{\frac{1}{2}}e^{i\rho}\{2^{-\frac{1}{2}}({}^3P_2)_1e^{i\delta_2}\sin\delta_2 + 2^{-\frac{1}{2}}({}^3P_1)_1e^{i\delta_1}\sin\delta_1\};$$

$$(\rho e^{ikz}S_0)_{sc}=e^{i(\rho+K_{03})}\sin K_{03}S_0 + (12\pi)^{\frac{1}{2}}e^{i\rho}\{(2/3)^{-\frac{1}{2}}({}^3P_2)_0e^{i\delta_2}\sin\delta_2 - 3^{-\frac{1}{2}}({}^3P_0)_0e^{i\delta_0}\sin\delta_0\};$$

$$(\rho e^{ikz}S_{-1})_{sc}=e^{i(\rho+K_{03})}\sin K_{03}S_{-1} + (12\pi)^{\frac{1}{2}}e^{i\rho}\{2^{-\frac{1}{2}}({}^3P_2)_{-1}e^{i\delta_2}\sin\delta_2 - 2^{-\frac{1}{2}}({}^3P_1)_{-1}e^{i\delta_1}\sin\delta_1\}.$$

Here the index *sc* means that the contribution to the scattered wave due to e^{ikz} is taken. The choice of signs of the linear combinations in $({}^3P_j)_m$ is made so that

$$({}^3P_2)_2=Y_1{}^1S_1;\quad ({}^3P_1)_1=2^{-\frac{1}{2}}(Y_1{}^0S_1+Y_1{}^1S_0);$$
$$({}^3P_0)_0=3^{-\frac{1}{2}}(Y_1{}^{-1}S_1-Y_1{}^0S_0+Y_1{}^{-1}S_{-1}).$$

The functions $Y_L{}^m$ are angular functions normalized to unity for integration over solid angles. The orbital angular momentum and magnetic quantum numbers are, respectively, L, m. The function $Y_1{}^0=(3/4\pi)^{\frac{1}{2}}\cos\theta$. The others are determined by the requirement that the angular momentum matrices have the standard form.[14] A computation of $\frac{1}{3}\Sigma_\mu((\rho e^{ikz}S_\mu)_{sc},(\rho e^{ikz}S_\mu)_{sc})$, with the scalar product applying to the spin coordinates only, gives the contribution to the triplet scattered wave which corresponds to the cross section used in the text (Eq. (15)).

Appendix II.

Calculation of small phase shifts due to concentrated potentials

If the potential causing the phase shift is sufficiently small, Taylor's formula is convenient. The meson potential responsible for the p waves is large at small r, but the phase shifts are small. In such cases a transformation of the radial equation is useful. This is first put in the form

$$d^2\mathfrak{F}/dx^2+g_0{}^2(x)\mathfrak{F}+g_1{}^2(x)\mathfrak{F}=0,$$

where x is r expressed in convenient units (such as $\hbar/\mu c$ in the present case). It is supposed that the solution of

$$d^2F/dx^2+g_0{}^2(x)F=0$$

is known, and the problem is to calculate the phase shift K of $\mathfrak{F}$ relative to that of F. Introducing

$$\eta=F^2\left(\frac{d\mathfrak{F}}{\mathfrak{F}dx}-\frac{dF}{Fdx}\right) \tag{II.1}$$

one finds

$$\frac{d\eta}{dx}+\frac{\eta^2}{F^2}+F^2g_1{}^2=0; \tag{II.2}$$

$$\tan K=\frac{-x/\rho}{(1/\eta)+(xG/\rho F)}. \tag{II.3}$$

One also has

$$\frac{d}{dx}\left(\frac{1}{\eta}+\frac{xG}{\rho F}\right)=\frac{F^2g_1{}^2}{\eta^2}. \tag{II.4}$$

Eq. (II.2) is used to obtain η by numerical integration. The occurrence of $F^2g_1{}^2$ is convenient, since in Taylor's approximation $\int F^2g_1{}^2dx$ is proportional to K. The method has an apparent disadvantage if the potential in addition to being large in absolute value locally has also moderate values over an appreciable distance. One must then play safe and integrate to sufficiently large x. If there is any phase shift the term in η^2/F^2 in Eq. (II.2) makes η variable. It is then convenient to use Eq. (II.4) because (a) the desirability of carrying the integration farther can be judged by estimating $\int F^2g_1{}^2\eta^{-2}dx$ which determines the relative change of the denominator in Eq. (II.3); (b) a numerical check can be obtained by carrying the integration of Eq. (II.2) to two large values of x and checking by means of Eq. (II.4) the two values of $1/\eta+xG/\rho F$.

[13] N. F. Mott and H. S. W. Massey, *Theory of Atomic Collisions* (Oxford Press, 1933), Chap. II.
[14] E. U. Condon and G. H. Shortley, *Theory of Atomic Spectra* (Cambridge Press, 1935).

On the Derivation of the Dispersion Formula for Nuclear Reactions

A. J. F. SIEGERT*
Stanford University, Stanford University, California
(Received August 31, 1939)

Kapur and Peierls gave a derivation of the nuclear dispersion formula which differed from other treatments in defining the compound states by means of wave functions in coordinate space. We have carried through the derivation starting out in a similar way, but avoiding certain disadvantages of their treatment, which mainly consist in too restricting assumptions.

THE dependence of the cross section for nuclear scattering on the energy of the incident particle is described by the nuclear dispersion formula. In this formula the cross section consists of two parts: One of them, the so-called "potential scattering," is a smooth function of the energy. The other part, the "resonance scattering," consists of a set of terms with resonance denominators containing the energy and decay constant of the compound states which cause the resonance phenomenon.

Derivations of this formula have been given by Breit and Wigner,[1] Bethe and Placzek,[2] Kalckar, Oppenheimer and Serber,[3] and Kapur and Peierls.[4] The authors mentioned first treat the problem by perturbation methods similar to the Weisskopf-Wigner theory of the dispersion of light by atomic systems. Kapur and Peierls have given a different treatment which they characterize as a perturbation calculation with perturbation of the boundary conditions rather than of the Hamilton operator. Their method promises to give a derivation which introduces the compound states in a simpler manner, by differential equations and boundary conditions in coordinate space rather than by inequalities between matrix elements.

The advantage of their treatment is that they can start from a simple model: one particle inside a potential wall. They show how one can generalize this model to cover all cases of nuclear reactions. As far as this generalization is concerned we take over their results. But we would like to improve on the treatment of the model itself, because there are certain disadvantages connected with their way of treating it.

The main objection is that Kapur and Peierls have made more stringent assumptions than the other authors to prove the dispersion formula. They assumed in fact that the width of all the compound states does not exceed their distance.[5] This would prohibit the application of the dispersion formula on actual nuclei and is, as we shall prove, an unnecessary assumption.

Another objection against Kapur and Peierls' treatment lies in the following fact: For mathematical convenience only, a radius r_0 is introduced outside of which the potential vanishes. Their distinction between resonance and potential scattering as well as their compound states turn out to be dependent on this parameter r_0: An increase of r_0 changes both resonance and potential scattering and only the total result is unchanged. We shall change the definition of the compound states slightly, thereby avoiding also another disadvantage of Kapur and Peierls' treatment, which consists in the dependency of energies and wave functions of the compound states on the energy of the incoming particle.

Our way of treatment differs from Kapur and Peierls' perturbation calculation mainly in that it is not an expansion in an orthogonal system. We investigate the singularities of the cross section which occur at certain complex values of the energy. Those singularities which lie near enough to the real axis, cause a sharp resonance maximum on the real axis and we can replace the cross section there by its singular part added to a smooth function of the energy. States with these singular values of the energy we call the

* Now with The Texas Company, Houston, Texas.
[1] G. Breit and E. Wigner, Phys. Rev. **49**, 519 (1936).
[2] H. A. Bethe and G. Placzek, Phys. Rev. **51**, 450 (1937).
[3] F. Kalckar, J. R. Oppenheimer and R. Serber, Phys. Rev. **52**, 273 (1937).
[4] P. L. Kapur and R. Peierls, Proc. Roy. Soc. **A166**, 277 (1938).
[5] Reference 4, p. 285.

compound states of the model. Their physical significance is easily seen: The cross section being the ratio of the intensities of outgoing and incoming wave becomes singular if there is only an outgoing wave. Our compound states are therefore the "radioactive" states of the system.

We use the same model and notation as Kapur and Peierls. For higher angular momenta, we only consider one particle moving with zero angular momentum in a potential $V(r)$. It is assumed that $V(r)=0$ for $r>r_0$. $\phi_E(r)$ is the wave function multiplied by r; it is a solution of the Schrödinger equation

$$\hbar^2\phi_E''/2m+(E-V)\phi_E=0 \qquad (1)$$

with the boundary condition $\phi_E=0$ for $r=0$. For $r>r_0$ we have

$$\phi_E=(I/k)\sin kr+Se^{ikr}$$

with $k=(2mE/\hbar^2)^{\frac{1}{2}}$. The scattering cross section is given by

$$\sigma=4\pi|S/I|^2.$$

We consider now S/I as function of E, including complex values of E. Expressing S and I by $\phi_E(r_0)$ and $\phi_E'(r_0)$ we have

$$\frac{S}{I}=\frac{\phi_E(r_0)\cos kr_0-\phi_E'(r_0)(\sin kr_0/k)}{\phi_E'(r_0)-ik\phi_E(r_0)}e^{-ikr_0}.$$

We look for singularities arising from vanishing denominator. The energies W_n for which the denominator vanishes are defined by the eigenvalue problem:

$$\hbar^2\phi_n''/2m+(W_n-V)\phi_n=0 \qquad (2)$$

with the boundary conditions

$$\phi_n=0 \quad \text{at} \quad r=0$$

and[6] $$\phi_n'-ik_n\phi_n=0 \quad \text{at} \quad r=r_0$$

with $$k_n=(2mW_n/\hbar^2)^{\frac{1}{2}}.$$

To obtain S/I in the neighborhood of a singularity W_n, we multiply (1) by ϕ_n and (2) by ϕ_E and subtract. We integrate the resulting equation

$$(\hbar^2/2m)(\phi_n''\phi_E-\phi_E''\phi_n)+(W_n-E)\phi_n\phi_E=0$$

between $r=0$ and $r=r_0$ and obtain, using the boundary conditions,

$$\frac{\hbar^2}{2m}\phi_n(r_0)[ik_n\phi_E(r_0)-\phi_E'(r_0)]+(W_n-E)\int_0^{r_0}\phi_n\phi_E dr=0.$$

This gives for the denominator in S/I:

$$\begin{aligned}\phi_E'(r_0)-ik\phi_E(r_0)&=\frac{W_n-E}{(\hbar^2/2m)\phi_n(r_0)}\int_0^{r_0}\phi_n\phi_E dr+i(k_n-k)\phi_E(r_0)\\&=\frac{W_n-E}{(\hbar^2/2m)\phi_n(r_0)}\left\{\int_0^{r_0}\phi_n\phi_E dr+i\frac{\phi_n(r_0)\phi_E(r_0)}{k_n+k}\right\},\end{aligned}$$

using

$$k_n-k=\frac{2m}{\hbar^2}\frac{W_n-E}{k_n+k}.$$

Assuming that the eigenvalue W_n is not degenerate we have in the limit $E\to W_n$: $\phi_E\to\phi_n$ and

$$\phi_E'-ik\phi_E\to(W_n-E)\frac{2m}{\hbar^2\phi_n}\left\{\int_0^{r_0}\phi_n^2dr+i\frac{\phi_n^2}{2k_n}\right\}.$$

For the numerator of S/I we obtain

$$\phi_E(r_0)\cos kr_0-\phi_E'(r_0)\sin kr_0/k\to\phi_n(r_0)e^{-ik_nr_0}$$

and finally

$$S/I=\frac{1}{W_n-E}\frac{(\hbar^2/2m)\phi_n^2(r_0)e^{-2ik_nr_0}}{\int_0^{r_0}\phi_n^2dr+i\dfrac{\phi_n^2(r_0)}{2k_n}}+f(E), \qquad (3)$$

where $f(E)$ is a regular function in the surrounding of W_n.

The factor multiplying $1/(W_n-E)$, and W_n itself, depend only on properties of the model not on E and they are invariant against changes of r_0, as long as $V(r)=0$ for $r>r_0$. To show this let us define a wave function φ_n by changing r_0 into $r_1>r_0$ in the definition of ϕ_n; this definition will be satisfied by $\varphi_n=A\phi_n$. The boundary condition is fulfilled since

$$\varphi_n(r)=A\phi_n(r)=A\phi_n(r_0)e^{ik_n(r-r_0)} \quad \text{for} \quad r>r_0.$$

[6] Taking here k_n instead of k makes the compound states independent of the energy of the incoming particle, and as we shall show later, it makes the distinction between resonance and potential scattering invariant against changes of r_0.

W_n is therefore unchanged. For the factor of $1/(W_n-E)$ we get

$$\frac{\varphi_n^2(r_1)e^{-2ik_nr_1}}{\int_0^{r_1}\varphi_n^2dr+i\dfrac{\varphi_n^2(r_1)}{2k_n}}$$

$$=\frac{\phi_n^2(r_0)e^{2ik_n(r_1-r_0)}\cdot e^{-2ik_nr_1}}{\int_0^{r_0}\phi_n^2dr+\phi_n^2(r_0)\dfrac{e^{2ik_n(r_1-r_0)}-1}{2ik_n}+i\phi_n^2(r_0)\dfrac{e^{2ik_n(r_1-r_0)}}{2k_n}},$$

which is obviously the same factor as in the original formula. In defining in the limit of long-life compound states contributions to the cross section due to the singular part of S/I as "resonance scattering," and those due to the regular part as "potential scattering," we have made a definition which is independent of r_0. We therefore can choose r_0 as large as we want and do not need to carry out additional considerations to include a screened Coulomb field or centrifugal forces, as Kapur and Peierls had to do.[7]

We can write the resulting Eq. (3) in a different form: From Eq. (2) and its conjugate complex we derive the equation

$$\frac{\hbar^2}{2m}|\phi_n(r_0)|^2=\frac{\gamma_n}{k_n+k_n^*}\int_0^{r_0}|\phi_n|^2dr, \qquad (4)$$

where γ_n is defined by $E_n-(i\gamma_n/2)=W_n$ with E_n and γ_n real. For sufficiently small values of γ_n we can multiply ϕ_n by a suitable constant A of absolute magnitude 1 so as to make $A\phi_n$ real in the region where it contributes (except for terms of the order γ_n) to the integral $\int_0^{r_0}|\phi_n|^2dr$.[8] We can thus write in this limit

$$\int_0^{r_0}A^2\phi_n^2dr=\int_0^{r_0}|\phi_n|^2dr.$$

With this fixed value for A we have then

$$A\phi_n(r_0)=|\phi_n(r_0)|e^{i(k_nr_0+\frac{1}{2}\delta_n)},$$

where δ_n is a phase determined entirely by the properties of the compound state n and independent of r_0. We thus obtain from (3)

$$S/I=\frac{1}{W_n-E}\times\frac{(\hbar^2/2m)|\phi_n(r_0)|^2e^{i\delta_n}}{\int_0^{r_0}|\phi_n|^2dr+\dfrac{i}{2k_n}|\phi_n(r_0)|^2e^{2i(k_nr_0+\frac{1}{2}\delta_n)}}$$

or, using (4)

$$S/I=\frac{\gamma_ne^{i\delta_n}}{W_n-E}\frac{1}{k_n+k_n^*+\dfrac{im\gamma_n}{k_n\hbar^2}e^{2i(k_nr_0+\frac{1}{2}\delta_n)}}. \qquad (5)$$

As γ_n tends towards zero k_n becomes real and the last term in the denominator of (5) becomes negligible, so that we have in this limit

$$S/I=\frac{\gamma_n}{E_n-\frac{1}{2}i\gamma_n-E}\frac{e^{i\delta_n}}{2k_n}+f(E). \qquad (6)$$

We now subtract from S/I the sum of all singularities with small γ_n. The difference

$$F(E)=S/I-\sum_n{}'\frac{\gamma_n}{(E_n-E)-\frac{1}{2}i\gamma_n}\frac{e^{i\delta_n}}{2k_n}$$

is a smooth function of the energy for real E. For the cross section σ we obtain the dispersion formula:

$$\sigma=4\pi\,|S/I|^2=4\pi\left|\sum_n{}'\frac{\gamma_n}{(E_n-E)-\frac{1}{2}i\gamma_n}\frac{e^{i\delta_n}}{2k_n}+F(E)\right|^2.$$

$F(E)$ is called the potential scattering term although it actually consists—at least partly—of contributions from broad levels.

We have thus proven the dispersion formula in the limit of long lifetime of the levels contributing to the resonance part. The existence of broad levels overlapping each other and any number of resonance levels does not affect our derivation.

The author is indebted to Professor F. Bloch and his nuclear seminar for the stimulus to this paper and for valuable discussions.

[7] Reference 4, p. 286.

[8] This is possible if the phase varies slowly in regions which contribute the main part of the integral. That this is the case can be easily proved.

The Identification of Characteristic X-Rays Associated with Radioactive Decay

PHILIP H. ABELSON*
Radiation Laboratory, University of California, Berkeley, California
(Received August 8, 1939)

An investigation has been made of the practicability of employing a bent rocksalt crystal spectrograph in the identification of x-rays emitted during radioactive decay. The spectrograph has been found to be a useable tool. X-rays associated with the disintegration of $_{31}Ga^{67}$ $_{29}Cu^{64}$, $_{35}Br^{80}$ and $_{43}Ma$ have been identified.

INTRODUCTION

RECENTLY it has been discovered that as a result of electron capture by the nucleus or internal conversion, many radioactive atoms emit characteristic x-rays in the process of disintegration. Alvarez,[1,2] who first demonstrated electron capture, has pointed out that many such cases should be found. He has also found internal conversion in Ga^{67}, where the coefficient is surprisingly high. Dancoff and Morrison,[3] in examining the theory of internal conversion for lighter elements, find that for energies less than 0.5 Mev and highly forbidden transitions, the coefficients may be $\gg 1$.

These writers point out eight instances of internal conversion. Additional examples have since been found, and it is quite probable that a systematic search would reveal a large number of such cases. A knowledge of the properties of x-rays emitted by decaying atoms can throw illumination upon the processes which are occurring. Thus, if a substance chemically identified as atomic number Z gives off characteristic radiation of an element $Z-1$ and no positrons, the process occurring is electron capture which may or may not be followed by internal conversion. If characteristic x-rays of element Z are emitted, one is dealing with nuclear isomerism. If the radiation is to be identified with an element $Z+1$, the process occurring is emission of a continuous beta-spectrum followed by internal conversion as the nucleus of element $Z+1$ falls from an excited to a lower state. In many cases the best method available for deciding between the three possibilities is identification of the x-rays which are given out in the process.

EXPERIMENTAL METHODS

Two methods are generally employed for identification of these x-rays—measurement by absorption, or by diffraction from a crystal. By far the best absorption method, and one which is usually adequate for needs of nuclear physicists, is that involving the use of critical absorption. When called upon to identify the radiation associated with any given radioactivity, the investigator knows that he is dealing with the characteristic x-rays of one of several elements. His measurements merely decide among the several possibilities.

The method of critical absorption has a number of disadvantages: Thin foils of most elements are not available; some of the elements needed are costly and difficult to obtain; the method works well only when the x-rays present belong to one element, and measurements carried out on complex radiations give confusing results. Clearly, then, the merits of the diffraction method for identification of x-rays bear investigation. In considering the practicability of using a diffraction method for identification of x-rays, the main question is one of intensities. Even with the tremendous intensities of radioactive materials available from the cyclotron, use of an ordinary x-ray spectrometer is impractical. The present work, however, has shown that by employing a bent crystal spectrograph, present intensities are sufficient to obtain pictures of x-ray lines from many elements.

BENT CRYSTAL SPECTROGRAPH

Some of the principles of design of a bent crystal spectrograph were discussed by DuMond

* Now at Department of Terrestrial Magnetism, Carnegie Institution of Washington, Washington, D. C.
[1] L. W. Alvarez, Phys. Rev. **52**, 134 (1937).
[2] L. W. Alvarez, Phys. Rev. **54**, 486 (1938).
[3] S. M. Dancoff and P. Morrison, Phys. Rev. **55**, 122 (1939).

and Kirkpatrick[4] in 1930. Johann[5] described a bent mica crystal spectrograph which he used successfully. Mlle. Cauchois[6] employed spectrographs having bent mica and gypsum crystals. Johansson[7] constructed a bent crystal spectrograph in which the crystal was both bent and cut in order to secure perfect focusing. Others have employed the bent crystal spectrograph for investigations of weak x-ray lines. The bent rocksalt crystal spectrograph used in the present investigation is essentially that described by Bozorth and Haworth.[8] The arrangement employed is shown in Fig. 1. Corresponding to any given wave-length λ there is a certain angle θ for reflection given by the well-known Bragg law:

$$n\lambda = 2d \sin \theta.$$

Here, since first-order reflection is used, n is one. If a radioactive sample which emits x-rays is placed along the focal circle, those rays satisfying the Bragg condition and striking the crystal will be brought to a focus on the focal circle on the opposite end of the crystal. Theoretically, in using x-ray film for a detector, one should bend the film to conform to the focal circle. However, by placing the film perpendicular to the x-ray beam, the radiant energy is concentrated on a smaller area. The energy per unit area (on which the x-rays fall) is increased by a factor of approximately $1/\sin \theta$. Part of this increase is offset by the fact that the x-rays pass through a smaller thickness of film and are hence less completely converted. Moreover, the film is supposedly in focus for only one λ. However, if one is seeking to identify radiation as being that of one of three neighboring elements, a lack of focal depth is not a serious handicap because the line width due to imperfections of the crystal is large enough to minimize the importance of the added width introduced through improper focusing.

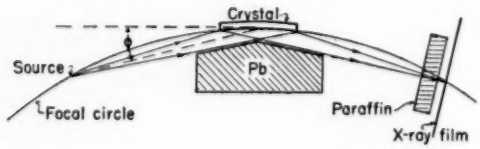

FIG. 1. The bent rocksalt crystal spectrograph. The crystal is bent to a radius of 30 cm and cut to a radius of 15 cm.

In this work two spectrographs were used. To obtain the lines from Ga^{67} and Cu^{64}, a spectrograph whose radius of focal circle was 15 cm was employed. This spectrograph was equipped with a crystal 2 cm by 3.2 cm, and the intensity of reflected radiation was quite high. Investigation showed that no ghost lines were obtained. The major imperfection lay in the width of the line appearing on the plate. This was associated with the fact that the image position was to a slight extent a function of source position. Through use of a fluorescent source of zinc x-rays, it was found that movement of the source could result in a displacement of the image by a distance corresponding to 0.02A. Since the separation of Zn and Cu is 0.11A, such a displacement is not serious. However, to eliminate possible artifacts through displacement of image, owing to displacement of source, special precaution was taken. When exposing the film to x-rays from a radioactive source, the source was made to cover a region on the focal circle corresponding to the three possible wave-lengths. In calibrating the film, the precaution was taken of having the fluorescent source cover the same region of the focal circle as was covered by the radioactive material. Under these circumstances any displacement of image with source is corrected for, since the calibration line and the line due to the radioactive substance are displaced in exactly the same amount.

The second spectrograph employed has a focal circle radius of 30 cm. The crystal, which is 3.4 cm long and 3.2 cm high, was supplied through the kindness of R. M. Bozorth. The characteristics of this spectrograph are quite different from those of the first one described. The principal disadvantages are lower intensity and the appearance of a ghost. The lower intensity arises from purely geometrical conditions, since in this case the source and image are farther removed by a factor of two. The ghost, which has an intensity about one-tenth that of the principal line, is well separated from it.

By taking the precaution of employing the same region of the focal circle as a source in

[4] J. W. M. DuMond and H. A. Kirkpatrick, Rev. Sci. Inst. **1**, 88 (1930).
[5] H. H. Johann, Zeits. f. Physik **69**, 185 (1931).
[6] Y. Cauchois, J. de phys. et rad. **3**, 320 (1932).
[7] T. Johansson, Naturwiss. **20**, 758 (1932).
[8] R. M. Bozorth and F. E. Haworth, Phys. Rev. **53**, 538 (1938).

obtaining the line from the radioactive material and in calibrating, the danger of a fictitious result is eliminated. The advantage of this spectrograph is its good resolving power. Moreover, the image line is practically independent of source position. In a test it was found that tellurium and antimony K_α are readily resolved. This spectrograph should be useful in determining x-ray wave-lengths as short as 0.35A. Elements emitting such K_α x-rays (K_α of $P^{59}=0.348$A) also send forth L_α radiation with a wave-length less than 2.5A. It is quite practical to identify L_α radiation in an air spectrograph for elements above 59 in atomic number. Accordingly the range in which a bent crystal spectrograph is useful at present appears to be from atomic number 23 to 92. By use of a vacuum, this range could be extended somewhat.

Experimental Results

Ga^{67}

The first x-rays examined with the spectrograph were those emitted in the decay of Ga^{67}. By critical absorption measurements, Alvarez[2] has shown that the radiation emitted by this activity can be described as characteristic zinc x-rays. This result was confirmed by the spectrograph,[8] and lines due to zinc K_α and zinc K_β were obtained. The calibration lines were obtained from copper and zinc. These elements were placed in the proper position on the source side of the focal circle and were exposed to continuous radiation from an x-ray tube. While the calibration lines were being obtained, the central portion of the film was shielded by lead. The 84-hour Ga^{67} was formed by deuteron activation of zinc. Gallium was extracted from the active zinc by means of a well-known ether extraction. The ether was evaporated to a volume of one cc, and the evaporation process was completed by allowing the ether to drop slowly upon a small piece of filter paper, thus transferring the gallium activity to the paper. The zinc bombarded was extremely pure, and it was not necessary to add gallium as a carrier. Accordingly the gallium activity present on the filter paper was free from elements which might have a large absorbing effect. The paper was of such length (1.5 cm) that when placed on the focal circle it covered the region corresponding to $\lambda=1.5$A to $\lambda=1.2$A. When exposing the film to radiation from Ga^{67} the calibration portion was, of course, covered with lead. The length of exposure of the film to the x-rays from the active substance was generally of the order of twice the half-life of the material.

Br^{80}

Another problem which can be solved by diffraction methods is the question of x-rays emitted during the decay of the 4.5-hour Br^{80}. These x-rays were found by A. H. Snell (unpublished) during the summer of 1938. Absorption measurements showed that the radiations were absorbed strongly by arsenic and weakly by selenium. According to the values of the wave-lengths of x-rays given by Siegbahn, the radiation could be either bromine or krypton. From the facts known at that time there was no strong reason for identifying the radiation with one of the two elements. Accordingly, the radiation was examined by the spectrograph and shown to be characteristic of bromine.[9] This provided a strong clue that the 4.5-hour Br^{80} was undergoing an isomeric transition to some other state. Segrè, Halford and Seaborg[10] have shown by means of an isomer separation that the 4.5-hour body decays into an 18-minute substance. Hence the x-rays result from the internal conversion of a gamma-ray which is emitted in the transition of the Br^{80} from the energy state corresponding to the 4.5-hour to an energy state corresponding to the 18-minute body. The energy of the γ-ray has been measured[11, 12] and the presence of x-rays confirmed.[12, 13]

The active bromine was obtained through irradiation of brombenzene by neutrons produced by a 100-μa hour bombardment of beryllium by deuterons. Active bromine was extracted from the brombenzene with water. Sodium sulfite was added to the aqueous solution together with silver nitrate. The resulting silver bromide precipitate was very thin, weighing a few milligrams per cm^2. This is important because self-absorption can cut

[9] P. Abelson, Phys. Rev. **55**, 424 (1939).
[10] E. Segrè, R. S. Halford and G. T. Seaborg, Phys. Rev. **55**, 321 (1939).
[11] G. E. Valley and R. L. McCreary, Phys. Rev. **55**, 666 (1939).
[12] R. E. Siday, Nature **142**, 681 (1939).
[13] L. I. Roussinow and A. A. Yusephovich, Phys. Rev. **55**, 979 (1939).

the intensity considerably. It is to be remembered that the average path the x-rays traverse in the source is $T/2 \sin \theta$ where T is the thickness. In exposing the film to the x-rays emitted by the bromine, it is necessary to eliminate the effect of scattered electrons. This could be done by use of a magnetic field or by selective absorption of the beta-particles. The latter method was employed; most of the electrons were absorbed in a 0.7 cm thick layer of paraffin, while the x-ray intensity dropped to a half. The silver bromide filter paper source was placed on the focal circle in such a way as to cover the region $\lambda = 1.15$A to $\lambda = 0.95$A, that is, the region corresponding to selenium, bromine and krypton K_α.

Cu^{64}

A third example of the use of the spectrograph was in the examination of the x-rays[9] emitted in the decay of Cu^{64}. Van Voorhis showed that a 12.8-hour activity is to be identified with Cu^{64} and that this body possesses a branching disintegration decaying either to Zn^{64} by negative electron emission or toe Ni^{64} by positron emission. Alvarez[2] later showed that x-rays were also associated with the decay of Cu^{64}. These x-rays were assumed to arise from electron capture, but no attempt was made to identify them. By use of the spectrograph the x-rays emitted by Cu^{64} have been shown to be characteristic nickel radiations. It appears, therefore, that Cu^{64} may decay by the three processes of negative electron emission, positron emission or electron capture. It could be argued that the nickel x-rays do not arise from electron capture but come as a result of internal conversion of a gamma-ray emitted after positron emission. However, the ratio of x-rays to positrons is close to that predicted on theoretical grounds.

In getting the picture of the x-rays from Cu^{64} the source was metallic copper itself which had been activated by 50μA hours of 8.0-Mev deuterons in the cyclotron. The source was placed on the focal circle covering a portion corresponding to $\lambda = 1.40$A to $\lambda = 1.70$A. In this case the best method of eliminating fogging due to beta-rays is certainly a magnetic field. However, even with the nickel radiation, it was possible to absorb almost all beta-rays with paraffin while cutting x-ray intensity to one-fourth. The spectrograph has since been rebuilt to facilitate use of a magnetic field for eliminating background due to beta-rays.

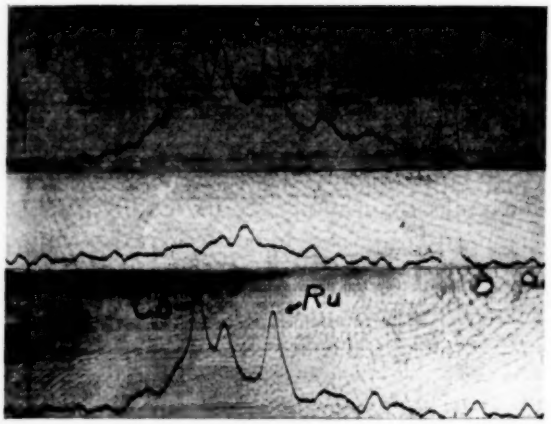

FIG. 2. A microphotometer trace of the K_α line of element 43. The three peaks of the upper and lower calibration traces correspond to the Cb, Mo and Ru K_α doublet. The main peak of the center trace is due to the K_α of element 43. The peak to the left is due to Mo K_α which arises from a two-day masurium activity.

The K_α line of element 43

A fourth picture obtained by the spectrograph was the K_α line of element 43. A microphotometer trace of this line is shown in Fig. 2. This radiation is associated with the decay of a 66-hour molybdenum activity which exhibits a branching decay. Of the order of one-fifth of the active molybdenum atoms disintegrate into a 6.6-hour masurium which drops to a lower energy state by gamma-ray emission. Another fraction of the molybdenum decays into a short-lived masurium which drops to a lower energy state by gamma-ray emission. In both cases the gamma-rays are internally converted and as a result characteristic x-rays of masurium are emitted. Segrè and Seaborg[14] have identified these radiations by critical absorption.

Because of the small intensity of x-rays (the internal conversion coefficient appears to be small) it was necessary to bombard the molybdenum 400μA hours with 8-Mev deuterons. The element was dissolved in nitric acid and precipitated with oxyquinoline following a procedure worked out by Perrier and Segrè.[15] The

[14] E. Segrè and G. T. Seaborg, Phys. Rev. **54**, 772 (1938).
[15] C. Perrier and E. Segrè, J. Chem. Phys. **6**, 155 (1939).

oxyquinoline precipitate was converted into molybdic oxide and placed on the focal circle to cover a wave-length region from 0.74A to 0.62A. This chemical procedure is desirable because deuteron bombardment of molybdenum yields a number of masurium activities. Among these is a two-day body which strongly emits molybdenum radiation probably as a result of electron capture.

I wish to thank R. M. Bozorth and the Bell Telephone Laboratories for the gift of a rocksalt crystal and Dr. L. W. Alvarez and Dr. E. Segrè for their advice and suggestions. I wish especially to thank Professor E. O. Lawrence, under whose direction this work was carried out, and the Research Corporation for financial support.

OCTOBER 15, 1939 PHYSICAL REVIEW VOLUME 56

On the Single Crystal X-Ray Diffraction Pattern of Calcite

FRANKLIN MILLER, JR.*
Ryerson Physical Laboratory, University of Chicago, Chicago, Illinois
(Received August 17, 1939)

The method of analysis of double spectrometer rocking curves developed by L. P. Smith is reconsidered. Although from Smith's very general viewpoint, six experimental curves are needed for a complete analysis, it is shown that for rocking curves from calcite, taken with the usual type of double spectrometer, it should be possible to deduce the shape of the single crystal diffraction pattern from two rocking curves, the (1,+1) and (2,+2). A method of modifying the equations of the instrument to allow for a simple type of mosaic structure is indicated.

The equations have been applied to rocking curves of Mo $K\alpha_1$ from calcite, supplied by L. G. Parratt. The method requires resolution of the observed curves into Fourier components, and a numerical method of doing this is described. The reliability of the components obtained can be tested by predicting the (1,−1) curve with them and comparing with experiment. In this way it is found that the curves are consistent as regards Fourier components of long period and large amplitude, but inconsistent in the short period, small amplitude components. A single crystal pattern is deduced, based mainly on the observed (1,−1) curve, with asymmetry as indicated by the (1,+1) and (2,+2) curves. It indicates that the crystals used do not have the flat-topped Darwin-Ewald-Prins diffraction pattern. Possible causes of the short period discrepancy have been investigated, but an adequate explanation has not been found.

INTRODUCTION

THE object of this work is to determine, from observed two-crystal spectrometer rocking curves, the shape of the single crystal x-ray diffraction pattern applicable to a certain pair of calcite crystals. This function, $g(\theta)$, represents the fraction of the incident intensity of a beam of parallel, monochromatic x-rays which is reflected by the crystal when incident at a glancing angle differing by θ from the corrected Bragg angle. Knowledge of $g(\theta)$ is desirable for two reasons. First, a comparison may be made with the Darwin-Ewald-Prins[1] theory. Such a comparison should shed valuable light on the nature of the imperfection of an almost-perfect crystal. Second, $g(\theta)$ may be applied as a correction to measured wave-length distributions. Because $g(\theta)$ has a finite width, an observed emission line, absorption edge, etc., is always distorted by the crystals. Data such as those of Parratt[2] show that the distortion is not a simple process, and knowledge of the entire shape of the diffraction pattern is therefore needed to make the correction. Although for many purposes crystals may be found, such as etched quartz, which possess adequate[3] resolving power in the second or even the first order, occasions arise when, because of intensity difficulties, imperfect crystals must be used. An example is the use of the two-crystal spectrometer as an approximate

* Now at Rutgers University.

[1] C. G. Darwin, Phil. Mag. **27**, 325 and 675 (1914); P. P. Ewald, Ann. d. Physik **54**, 519 (1917), Zeits. f. Physik **2**, 232 (1920), Physik. Zeits. **26**, 29 (1925); J. A. Prins, Zeits. f. Physik **63**, 477 (1930).

[2] L. G. Parratt, Rev. Sci. Inst. **6**, 387 (1935).

[3] L. G. Parratt, Phys. Rev. **46**, 749 (1934).

monochromator. Furthermore, for long wave-length work, relatively imperfect crystals of large grating space must be used.

Previous experimental study of the problem by Allison,[4] Parratt,[5] Renninger,[6] and others has been indirect. Observed values for the parallel position rocking curve width, percent reflection, and coefficient of reflection were compared with predictions of the Prins theory, for various crystals and wave-lengths. For a certain pair of calcites, Parratt and Miller[7] found fairly good agreement at long wave-lengths, but at $\lambda = 0.71$A the percent reflection was much too small, and the $(1, -1)$ width too great. An advance was made when L. P. Smith[8] pointed out the power of the Fourier transform method for the problems of the two-crystal spectrometer, and much of the work in this paper is based upon his analysis. Smith showed that the true wave-length distribution of an x-ray line, edge, etc., can be found from proper combination of six observed curves. His quite general treatment does not require specular reflection of each ray from the crystal face. As a result, the definition of $g(\theta)$ given above has no meaning; nevertheless functions closely related to the diffraction patterns of the two crystals, assumed different, could be found. No application was made to observed curves.

In this paper, simplifying assumptions, applicable to actual calcite specimens, are made in Smith's analysis, and the effects of a simple type of mosaic structure and of vertical divergence are included. It turns out that $g(\theta)$ can be found from two observed curves, the $(2, +2)$ curve being to a sufficient approximation the true line shape. Mosaic structure is introduced as follows: The crystal face is assumed to be covered by blocks which are large enough (say, 10^{-4} cm on an edge) so that no radiation completely traverses a block, and diffraction effects due to the finite number of planes in a block can be ignored. The function $g(\theta)$ is considered applicable to each block. A parallel incident beam is then reflected from the crystal face as a divergent beam, although specular reflection is assumed *for each block*. The amount of divergence depends on the probability distribution function for orientation of the blocks; by letting the distribution function become infinitely sharp we pass to the case of a perfect crystal.

Mathematical Theory

Following Smith, we will denote by upper case symbols the Fourier transforms of functions denoted by corresponding lower case symbols. Thus

$$\text{if} \qquad F(t) = \text{const.} \times \int_{-\infty}^{\infty} f(x) e^{itx} dx, \tag{1}$$

$$\text{then} \qquad f(x) = \text{const.} \times \int_{-\infty}^{\infty} F(t) e^{-ixt} dt. \tag{2}$$

The broad restrictions on $f(x)$ required for this inversion to be possible are fulfilled for the functions under consideration. We will also have use for a transform of the type

$$\mathfrak{F}(t) = \text{const.} \times \int_{-\infty}^{\infty} f(x) e^{itx^2} dx, \tag{3}$$

which may be called a Fresnel transform, denoted by corresponding script symbols.

For each of the three observed rocking curves an integral equation can be set up and the Fourier transform written down. The angles involved are illustrated for a parallel position in Fig. 1; the derivation of Eqs. (4) to (7) follows the general scheme of Chapter IX of *X-Rays in Theory and Experiment*, by Compton and Allison.[9] It is assumed that both crystals are rotated by equal amounts in recording the curves. By this method

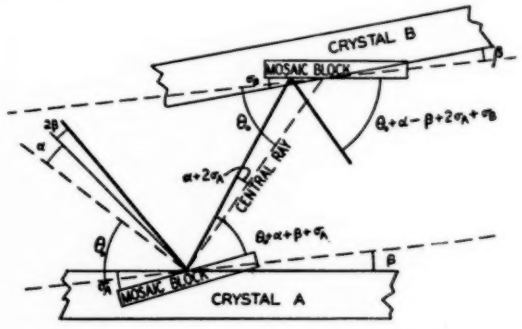

FIG. 1. Crystal arrangement in a parallel position.

[4] S. K. Allison, Phys. Rev. **41**, 1 (1932).
[5] L. G. Parratt, Phys. Rev. **41**, 561 (1932).
[6] M. Renninger, Zeits. f. Krist. **89**, 344 (1934).
[7] L. G. Parratt and F. Miller, Phys. Rev. **49**, 280 (1936).
[8] L. P. Smith, Phys. Rev. **46**, 343 (1934).
[9] A. H. Compton and S. K. Allison, *X-Rays in Theory and Experiment* (D. Van Nostrand Co., 1935). References are there given to contributions of Schwarzschild, Spencer, Laue, and others to the theory of the instrument.

of "double rotation"[10, 11] the effect of inhomogeneity in the focal spot or the crystal surfaces is almost completely eliminated. It must be remembered that if each crystal is rotated by an amount β about its own axis, either the x-ray tube must be rotated by 2β or crystal B must be rotated about crystal A, in order for the effective beam from the center of the focal spot to strike the same regions of the crystals. The two cases are identical mathematically, and the former is assumed in drawing Fig. 1. Vertical divergences, and vertical deviations of the mosaic blocks, are not shown in Fig. 1, and it is due to these that terms involving ϕ and ψ are introduced into the arguments of the g functions by considerations similar to those accompanying Fig. IX-11 of reference 9. The terms in ξ, which is a wave-length variable, recognize the fact that, according to the Bragg law, change in wave-length of an elementary ray can compensate for a change in the glancing angle introduced, say, by horizontal divergence. The nomenclature and resulting equations may easily be extended to positions $(n_1, \pm n_2)$, where $n_1 \neq n_2$.

For an $(n, -n)$ curve, we obtain from Fig. 1 the equation

$$\begin{aligned} p_n(\beta) = \text{const.} \times \int\int\int\int_{-\infty}^{\infty}\int\int\int\int & m(\alpha)s(\phi) \\ & \times j(\xi)f(\sigma_A)f(\sigma_B)f(\psi_A)f(\psi_B) \\ & \times g_A(\beta+\alpha+\sigma_A-a_n\psi_A{}^2-a_n\phi^2-a_n\xi) \\ & \times g_B(-\beta+\alpha+2\sigma_A+\sigma_B \\ & -2a_n\psi_A{}^2-a_n\psi_B{}^2-a_n\phi^2-a_n\xi) \\ & \times d\alpha d\phi d\xi d\sigma_A d\sigma_B d\psi_A d\psi_B. \quad (4) \end{aligned}$$

β = deviation of crystal B from the central position in which the glancing angle of the central ray is θ_0.

α = horizontal divergence of a ray from the central ray.

ϕ = vertical divergence of a ray from the central ray.

σ_A, σ_B = horizontal deviations of mosaic blocks from the cleavage plane.

ψ_A, ψ_B = vertical deviations of mosaic blocks from the cleavage plane.

$a_n = \frac{1}{2}\lambda_0(\partial\theta_0/\partial\lambda_0) = \frac{1}{2}\tan\theta_0$.

$\xi = 2(\lambda-\lambda_0)/\lambda_0$.

$p_1(\beta)$, $r_1(\beta)$, and $r_2(\beta)$ are the $(1, -1)$, $(1, +1)$, and $(2, +2)$ rocking curves, for double rotation.

$m(\alpha)$ and $s(\phi)$ are slit functions, determined by the geometry of the slits and the focal spot intensity distribution.

$f(\sigma_A)$, etc., are the mosaic distribution functions postulated in paragraph 3, and assumed similar for the two crystals.

$j(\xi)$ is the true emission line shape.

$g_A(\theta)$ and $g_B(\theta)$ are the crystal patterns of the two crystals.

The integrations are extended to infinite limits because all of the functions involved become zero sufficiently rapidly.

We must now assume $m(\alpha)$ to be "very wide" and hence constant over the effective range of α. This is justified since the rocking curves are only a few seconds wide, whereas the beam defined by the slits and focal spot is many minutes wide.[12]

Upon multiplication of Eq. (4) by $e^{2it\beta}d\beta$ and integration, the integral splits into 8 single integrals as follows:

$$\begin{aligned} & \int_{-\infty}^{\infty} p_n(\beta)\exp(2it\beta)d\beta = \text{const.} \\ & \times\int_{-\infty}^{\infty} s(\phi)d\phi\int_{-\infty}^{\infty} j(\xi)d\xi\int_{-\infty}^{\infty} f(\sigma_A)\exp(it\sigma_A)d\sigma_A \\ & \times\int_{-\infty}^{\infty} f(\sigma_B)\exp(it\sigma_B)d\sigma_B \\ & \times\int_{-\infty}^{\infty} f(\psi_A)\exp(-a_nit\psi_A{}^2)d\psi_A \\ & \times\int_{-\infty}^{\infty} f(\psi_B)\exp(-a_nit\psi_B{}^2)d\psi_B \\ & \times\iint_{-\infty}^{\infty} g_A(\beta+\alpha+\sigma_A-a_n\psi_A{}^2-a_n\phi^2-a_n\xi) \\ & \times\exp[it(\beta+\alpha+\sigma_A-a_n\psi_A{}^2-a_n\phi^2-a_n\xi)] \\ & \times g_B(-\beta+\alpha+2\sigma_A+\sigma_B-2a_n\psi_A{}^2 \\ & -a_n\psi_B{}^2-a_n\phi^2-a_n\xi)\exp[it(\beta-\alpha-2\sigma_A-\sigma_B \\ & +2a_n\psi_A{}^2+a_n\psi_B{}^2+a_n\phi^2+a_n\phi^2+a_n\xi)]d\alpha d\beta. \quad (5) \end{aligned}$$

or

$$P_n(2t) = \text{const.} \times F^2(t)\mathfrak{F}^{*2}(a_nt)G_A(t)G_B{}^*(t). \quad (6)$$

[10] J. W. M. DuMond and A. Hoyt, Phys. Rev. **36**, 1702 (1930).

[11] S. K. Allison, Phys. Rev. **44**, 63 (1933).

[12] This assumption is also made by Smith, and is surely valid for an $(n, -n)$ curve. For an $(n, +n)$ curve its validity is more certain in double rotation.

The asterisk indicates a complex conjugate. The derivation of Eq. (6) uses the fact that

$$\int\int_{-\infty}^{\infty} f_1(x+y+a)f_2(x-y+b)dxdy = \frac{1}{2}\left[\int_{-\infty}^{\infty} f_1(x)dx\right]\times\left[\int_{-\infty}^{\infty} f_2(x)dx\right].$$

For an $(n, +n)$ curve, (antiparallel position), the equation analogous to Eq. (4) is

$$r_n(\beta) = \int\int\int\int_{-\infty}^{\infty}\int\int\int\int m(\alpha)s(\phi) \times j(\xi)f(\sigma_A)f(\sigma_B)f(\psi_A)f(\psi_B) \times g_A(\beta+\alpha+\sigma_A-a_n\psi_A{}^2-a_n\phi^2-a_n\xi) \times g_B(\beta-\alpha-2\sigma_A-\sigma_B-2a_n\psi_A{}^2-a_n\psi_B{}^2 -a_n\phi^2-a_n\xi)d\alpha d\phi d\xi d\sigma_A d\sigma_B d\psi_A d\psi_B. \quad (7)$$

This yields

$$R_n(2t) = \text{const.}\times\mathfrak{S}(2a_nt)J(2a_nt)F^2(t) \times\mathfrak{F}(a_nt)\mathfrak{F}(3a_nt)G_A(t)G_B(t). \quad (8)$$

The parameter t is to be interpreted as the analogue of n when a periodic function $f(x)$ is written as a Fourier series $\Sigma A_n\cos(nx-\delta)$. Thus we speak of the "$t$th" component of a curve. Since our functions are not periodic, the parameter t has nonintegral values, and $P_n(2t)$, etc., are continuous functions of t.

For the present we will assume the pattern for crystal A to differ from that for crystal B only by a constant real factor. The validity of this assumption will be discussed below. Let $g_1(\theta)$ and $g_2(\theta)$ denote the single crystal patterns in the first and second orders. From the three experimental curves we get three equations in the parameter t:

$$(1, -1): P_1(2t) = \text{const.} \times F^2(t)\mathfrak{F}^{*2}(a_1t)G_1(t)G_1{}^*(t), \quad (9)$$

$$(1, +1): R_1(2t) = \text{const.} \times\mathfrak{S}(2a_1t)J(2a_1t)F^2(t)\mathfrak{F}(a_1t)\mathfrak{F}(3a_1t)G_1{}^2(t), \quad (10)$$

$$(2, +2): R_2(2t) = \text{const.} \times\mathfrak{S}(2a_2t)J(2a_2t)F^2(t)\mathfrak{F}(a_2t)\mathfrak{F}(3a_2t)G_2{}^2(t). \quad (11)$$

Elimination of J from Eqs. (10) and (11) gives

$$G_1{}^2(t) = \text{const.}\times\frac{R_1(2t)}{R_2(2a_1t/a_2)} \times\left[\frac{F^2(a_1t/a_2)}{F^2(t)}G_2{}^2(a_1t/a_2)\right]. \quad (12)$$

Also, we must have

$$|P_1(2t)|\times|R_2(2a_1t/a_2)| = \text{const.}\times|R_1(2t)| \times|\mathfrak{F}^{*2}(a_1t)F^2(a_1t/a_2)G_2{}^2(a_1t/a_2)|. \quad (13)$$

Since the effect of $\mathfrak{F}$ will be small compared with that of F, and since G_2 can be estimated from the $(2, -2)$ rocking curve, Eq. (13) offers a method of estimating the mosaic distribution function, and hence of determining the crystal pattern $g_1(\theta)$ from (12). To a very good approximation, for calcites of ordinary perfection, the expression in brackets in Eq. (12) can be regarded as constant, which amounts to assuming infinite resolving power in the second order and assuming perfect crystals.

It is instructive to discuss a few well-known properties of the instrument from the point of view of the Fourier transforms, Eqs. (9) to (13). No attempt is made to give references to the first discussions in the literature of some of these points. It must be borne in mind that the Fourier transform of a symmetrical function is real, while the Fresnel transform of even a symmetrical function is, in general, complex. Also, a narrow curve has a wide transform, and vice versa, since many high components are required to represent a sharp curve. Thus, in particular, the transform of a witch (Hoyt[13] curve) given by $1/(1+x^2/a^2)$, of half-width a, is proportional to $e^{-|at|}$.

(a) If the crystal patterns are identical in shape and there is no mosaic structure, then Eq. (6) shows that $P_n(2t)$ is real, and all the $(n,-n)$ curves are symmetrical. The converse is not true, however. If we write $G_A=G_A'+iG_A''$, etc., a real $P_n(2t)$ implies only that $G_AG_B{}^*$ is real, i.e., $G_A''/G_A'=G_B''/G_B'$. This can be satisfied in two ways: either $g_A(\theta)$ is proportional to $g_B(\theta)$, and the patterns (in general asymmetrical) have identical shapes, or $G_A''=G_B''=0$, in which case the patterns are both symmetrical, but not necessarily alike. The first case has been assumed in deriving Eqs. (9) to (13), since the $(n,-n)$

[13] A. Hoyt, Phys. Rev. **40**, 477 (1932).

curves are always observed to be symmetrical. It can easily be seen that if the second case is true, then Eq. (13) still holds, since then $G_B^*=G_B$, and G_2^2 becomes $(G_2)_A(G_2)_B$. Mosaic structure would not affect this conclusion, barring a fortuitous coincidence of the odd parts of $\mathfrak{F}$ and $G_AG_B^*$.

(b) If the vertical divergence is negligibly small then $\mathfrak{S}$ reduces to a constant. Vertical divergence has no effect on an $(n,-n)$ curve, but since $\mathfrak{S}(a_nt)$ is not always real, asymmetry will be introduced into an $(n,+n)$ curve even by a symmetrical slit function.

(c) The effect of mosaic structure will be to widen each curve, since F and $\mathfrak{F}$ surely decrease with increasing t for small t. Any positive function exhibits such a behavior.

(d) If the true line shape and diffraction pattern are both witches of widths w_i and w_g, respectively, then the $(1,-1)$ curve is a witch of width $w_p=2w_g$, and the $(1,+1)$ curve is a witch of width $w_r=w_i+2w_g=w_i+w_p$. This follows immediately from the properties of the exponential $e^{-w|t|}$, and the witch is obviously the only function for which the widths add in such a simple manner. Using the Fourier transform method, an observed curve can be corrected for the finite width of the diffraction pattern, by dividing the transform of the observed curve by the square of an assumed or derived single crystal pattern transform. Ordinarily a witch of half the width of the $(n,-n)$ curve will suffice for this correction. Methods based on assumptions of witches, error curves, etc., have previously been applied only to widths of emission lines.

Application to Actual Curves

Three rocking curves were recorded by Professor Parratt for Mo$K\alpha_1$ at 0.71A on the direct-reading spectrometer of Richtmyer and Barnes.[14] Maximum vertical divergence was 4.5×10^{-3} radian. Voltage was kept low enough so that radiation of half the wave-length studied was not excited. Background was 0.5 percent in the first order, and 4 percent in the second order. The crystals were A_5B_5 of reference 2, after repeated etching and grinding according to the method of Manning.[15] Crystals A_4B_4 of reference 2, of which an extended indirect study had already been made,[7] were found to have deteriorated badly since 1935. The percent reflection could be brought only to 40 percent compared with 66 percent in 1935. The crystals used have a percent reflection of 50 percent, and represent the most nearly perfect crystals available after an extended search. While not as nearly perfect as some specimens previously reported, they are comparable with crystals commonly used in x-ray spectroscopy.

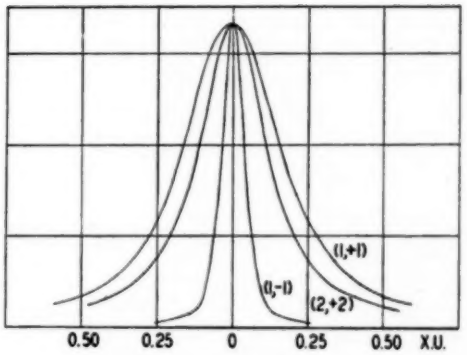

FIG. 2. Rocking curves of Mo $K\alpha_1$ on calcite, recorded by L. G. Parratt. All of the data for the wings are not plotted.

The observed curves are plotted in Fig. 2. From 70 to 100 ordinates were observed for each curve. The $(2,+2)$ curve, $r_2(\beta)$, was symmetrical, and accurately a witch of full width 0.268 x.u. Such a shape has been observed previously for Mo$K\alpha_1$, but is not typical of all lines. It is interesting to observe that both classical[16] and modern[17] theories predict such a shape for an x-ray emission line.[18] The $(1,+1)$ curve, $r_1(\beta)$, of width 0.384 x.u., was not a witch, and showed an extremely slight asymmetry which was probably real. The origin was taken as the intersection with the baseline of the locus of midpoints of horizontal segments; as so defined it differed by only 0.007 x.u. from the location of the peak. The odd part of $r_1(\beta)$ was thus very small (maximum value 3 percent of the peak) and its effect on $|R_1|^2=R_1'^2+R_1''^2$ was entirely negligible. Correction of the $(n,+n)$ curves for overlap of $K\alpha_2$ was important only for $r_1(\beta)$, and was carried out in a direct manner. The overlapping factor[11] was only 0.010 for $(1,+1)$ and 0.005 for $(2,+2)$. The correctness of the procedure was indicated by comparison of the two wings of a curve. No differences were found. The $(1,-1)$ curve, $p_1(\beta)$, was symmetrical, as expected, and had a width of 0.0868 x.u. All of the observed curves were found to decrease as the inverse square for abscissas farther than

[14] F. K. Richtmyer and S. W. Barnes, Rev. Sci. Inst. **5**, 351 (1934).
[15] K. V. Manning, Rev. Sci. Inst. **5**, 316 (1934).
[16] N. C. Mandersloot, Jarb. d. Rad. u. Elektrotek. **13**, 16 (1916); G. E. M. Jauncey, Phys. Rev. **19**, 68 (1922).
[17] V. Weisskopf and E. Wigner, Zeits. f. Physik **63**, 54 (1930); F. Hoyt, Phys. Rev. **38**, 860 (1930).
[18] See, however, remarks by A. Hoyt, reference 13.

about two full widths from the peak. E.g., for $r_2(\beta)$ a least-squares solution using 14 ordinates gave a value of -2.0 for the exponent.

A straightforward numerical method was adopted for the Fourier analysis, after trial showed the rolling sphere Henrici type analyzer to be unsuited to precise determination of short period components. The method of Robertson[19] was modified slightly as follows: A series of 1000 cardboard strips was prepared, each containing the sequence N, $N\cos 6°$, $N\cos 12°\cdots 0$, written from top to bottom to the nearest integer. To analyze a curve, ordinates were read off a large graph, spaced q units apart. Corresponding strips were hung, 15 at a time, on a plywood strip, and the appropriate products $f(x)\begin{matrix}\sin\\ \cos\end{matrix} tx$ read through diagonal rows of holes in a cardboard screen. The algebraic sums of the visible numbers were proportional to the real and imaginary parts of $F(t_0)$, where $t_0=\pi/(30q)$. By discarding alternate strips and using the remainder again, $F(\frac{1}{2}t_0)$, $F(\frac{1}{4}t_0)$, etc., were rapidly obtained. Three selections of ordinates at spacings of, say, 0.002, 0.0025, and 0.003 x.u. sufficed to give about 15 well spaced components,[20] and the area of the curve gave $F(0)$. The even and odd parts of a curve were analyzed separately, integration extending from 0 to $+\infty$. A formula for

$$\int_N^\infty x^{-n}\cos tx\,dx,$$

with n in general not an integer, was developed in such a form that the contributions of the wings to the Fourier components could be easily inserted in the analysis; for $\cos Nt=1$ and $Nt\gg 0$, the integral is $n/(t^2N^{n+1})$. As a check on this numerical method several arbitrary curves, including asymmetrical ones, were broken down into components with the aid of the strips, and then synthesized, also with the strips. Satisfactory agreement, to within about 1 percent, was obtained.

[19] J. M. Robertson, Phil. Mag. **21**, 176 (1936).

[20] Robertson's procedure for obtaining higher components amounts to using different screens. This must lead to error for high components; thus a sine component of 30 times the t value of the fundamental would have arguments spaced 180° apart and would vanish, regardless of the curve being analyzed. In Robertson's application to crystal structure work this is not serious.

Results and Conclusions

In Figs. 3 and 4 are shown the transforms of the three observed curves, plotted logarithmically. The t values are determined by the angular unit used in plotting the curves, which in this work was 34.29 seconds, corresponding to 1 x.u. in the $(1, +1)$ position. Since $p_1(\beta)$ was much narrower than the other two it was possible to be certain of $P_1(t)$ for much larger t values. The uncertainties represented by vertical lines indicate twice the *total* contributions of the wings to the transforms, using the inverse square assumption. This is a very liberal estimate, since the wings were observed to follow this rule out to abscissas much larger than those at which the numerical analyses were stopped. The error introduced by the numerical analysis itself is, for the components plotted, too small to be drawn. The fact that $r_2(\beta)$ is a good approximation to a witch is shown by the straightness of its transform when plotted in this manner.

In Fig. 4 is plotted also $\log_{10}|P_1R_2|$. If F, $\mathfrak{F}$, and G_2 are infinitely sharp, Eq. (13) shows that $\log|P_1R_2|$ should be parallel to $\log|R_1|$, as in the dashed line. It is seen that there is agreement among the components of long period and large amplitude (small t). Although definite disagreement is indicated among the components of short period, the amplitudes of these range from 1/5 to 1/100 of the most intense amplitudes. Lacking other sets of data, it seems best at present to interpret Fig. 4 as indicating a

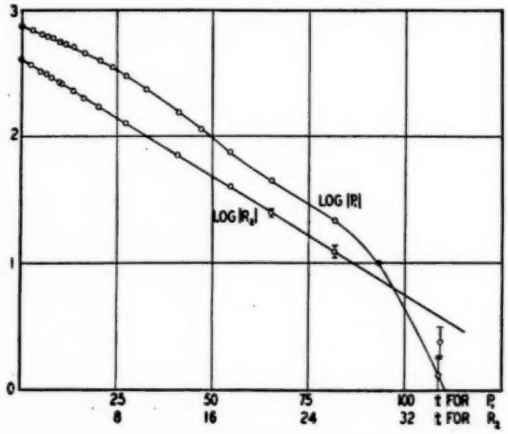

FIG. 3. Fourier transforms of the observed $(1, -1)$ curve, $|P_1|$, and of the observed $(2, +2)$ curve, $|R_2|$. The scale of ordinates is arbitrary.

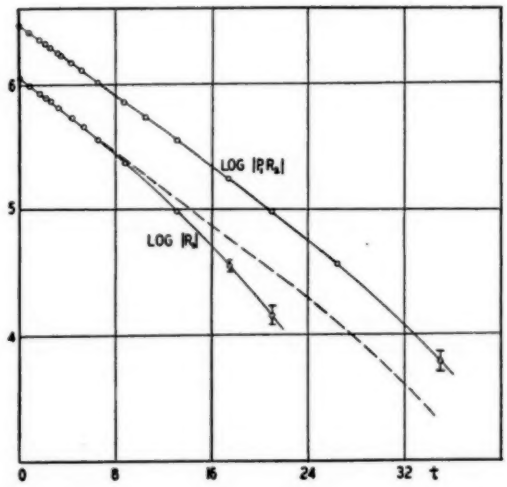

FIG. 4. Upper curve: Product of the curves of Fig. 3. Lower curve: Fourier transform of the observed (1, +1) curve, $|R_1|$. The dashed curve is parallel to the upper curve, and should coincide with the lower curve, according to Eq. (13).

general, but not detailed, confirmation of the theory of the double spectrometer.

In order to obtain the single crystal pattern $g_1(\theta)$, the most certain procedure is to obtain $|G_1|$ from the observed (1, −1) curve, using Eq. (9). The (1, +1) and (2, +2) data can then be used to find the ratio of real and imaginary parts of $G_1(t)$. Thus $G_1(t)$, and hence $g_1(\theta)$, are completely determined, and the pattern so found automatically predicts the correct (1, −1) curve. Of course, G_1 could be found directly from the (1, +1) and (2, +2) curves by Eq. (12), but the other method is more accurate since it places reliance upon the curve which is, in width, most nearly like the desired function.

Application of the first method yields curve *A* of Fig. 5. The observed percent reflection of 50 percent served to fix the scale of ordinates. This curve is almost symmetrical, since the (1, +1) curve showed only very slight asymmetry, and the (2, +2) curve none at all. The predicted Prins curve is plotted as *B* of Fig. 5, and is the average for the two kinds of polarization. Such an average is allowable for the small glancing angles involved here. The pattern derived from experiment shows no evidence for the flat top of the Darwin-Ewald-Prins theory. It should be mentioned that Fourier analysis of the (1, −1) curve was carried out to large enough t values (>500) to make certain that the round top of Fig. 5*A* is significant, and not due to neglect of higher components.

Curve *A* of Fig. 5 is derived by the most trustworthy method, and represents our best estimate of the single crystal pattern of the crystals used. Nevertheless, too much confidence should not be placed in the derived curve on account of the discrepancy of Fig. 4 among the higher components. That this discrepancy is serious becomes evident when the single crystal pattern is computed directly from the antiparallel curves. The resulting $g(\theta)$ is over twice as wide as curve *A*, and yields a (1, −1) width of 0.21 x.u. This is unthinkably large compared with the observed 0.087 x.u. The only reasonable explanation is that one, or both, of the observed antiparallel curves has been distorted in some unknown fashion. It is easiest to imagine that the true (1, +1) curve is narrower than that observed; a width of 0.31 x.u. instead of 0.38 would bring about agreement. (This figure was obtained from the slope of the dashed line of Fig. 4, allowing 0.01 x.u. for the (2, −2) width). It should be emphasized, however, that such an arbitrary correction is entirely outside of the observational error.

No adequate explanation for this inconsistency among the higher components has been found. Among the possible reasons for it which have been considered are: (*a*) Making the correction for finite resolving power in the second order tends to increase the discrepancy, and the correction would be only about a 4 percent change in the slope of the upper line of Fig. 4, in the wrong direction. (*b*) The effect of the perhaps oversimplified mosaic structure of para-

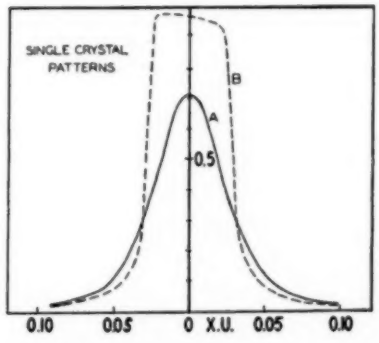

FIG. 5. *A*: Single crystal pattern deduced from the observed rocking curves. *B*: Diffraction pattern predicted by the Prins theory.

graph 3 will also tend to increase the discrepancy, since the mosaic distribution function is surely a positive function, and its transform decreases with increasing t. Qualitatively, the effect of mosaic structure can be seen as follows: Each of the three curves is widened by about the same amount by such a mosaic structure. Therefore one would expect the observed r_1 to be wider than the true r_1, but narrower than that predicted from the observed p_1 and r_2, since both of the latter have been widened. The opposite is observed. (*c*) The assumption that $m(\alpha)$ is "very wide" was made in deriving Eqs. (6) and (8). If there is mosaic structure, the effective range of α will no longer be of the order of the diffraction pattern width, but will be comparable to the width of $f(\sigma)$. As mentioned above, $f(\sigma)$ must be narrow, otherwise the $(1, -1)$ curve would be broadened. Hence the assumption of $m(\alpha)$ constant is justified. (*d*) For the slits used, the maximum vertical divergence is so small that at $t=20$ the function $\mathfrak{S}(a_1 t)$ is still 99.5 percent of its value at $t=0$, using a slit function $s(\phi) = 1 - |\phi/\phi_{\max}|$. (*e*) Possible dissimilarity of the two crystals is discussed above. It was shown that the only kind of dissimilarity consistent with the symmetry of the $(1, -1)$ curve would not affect the validity of Eq. (13), on which Fig. 4 is based. (*f*) Close consideration of the original curves and their treatment rules out explanations in terms of observational or computational error, improper correction for overlapping of Mo$K\alpha_2$, or incorrect treatment of the wings.

The essential point of the analysis presented here is that for ordinary calcite crystals the second-order resolving power is so high that only a small, easily estimated correction is needed to obtain the true line shape. In theory, at least, not only the single crystal diffraction pattern can be deduced, but also the distribution function of the mosaic blocks. When the method is applied to L. G. Parratt's precisely recorded rocking curves of Mo$K\alpha_1$, a general agreement among the long period Fourier components indicates that the theory of the double spectrometer is not entirely wrong. The serious and definite discrepancy among the short period components, however, is difficult to explain. The conclusion that the single crystal pattern (Fig. 5*A*) shows no evidence for the flat top of the Darwin-Ewald-Prins theory is valid regardless of this discrepancy, since the doubtful assumption concerns only the asymmetry of the pattern.

Acknowledgments

Sincere thanks are due to Professor Samuel K. Allison, whose continued interest in the theory of the two-crystal spectrometer led to the undertaking of this analysis. The author is deeply indebted to Professor Lyman G. Parratt, who painstakingly recorded the data, and with whom he has had several valuable discussions. Discussions with Professor Frank G. Dunnington, and assistance of Libuse Lukas Miller with the numerical work, were also of value.

The M_1 and M_2 X-Ray Absorption Edges of Lead

J. W. McGRATH*
State University of Iowa, Iowa City, Iowa
(Received August 7, 1939)

The M_1 and M_2 edges of lead, not having been previously measured, were investigated. They were found to occur at wave-lengths: M_1, 3.219A; M_2, 3.469A. A brief discussion of M edges is given and the fact that many M edges show discrepancies between observed and calculated values is noted. Methods of computing edge energies are discussed. The proposed explanation and meaning of these discrepancies are discussed with particular reference to lead.

INTRODUCTION

A KNOWLEDGE of the wave-lengths of the x-ray absorption edges of the elements is of importance in many connections. Many of the five M edges of 20 of the heavier elements have been measured.[1–13] The M_1 and M_2 edges have so far been measured in only eight of these elements, mainly because the experimental difficulties in observing them are greater than for the other M edges. It seemed worth while to attempt to photograph M_1 and M_2 edges. These edges of lead[6] had not been studied and it was chosen[14] for investigation because it lends itself to easy preparation in thin absorbing films.

THE METHOD

For edge contrast there is an optimum absorber thickness given by a formula derived by Sandström.[15] The values needed for the linear absorption coefficient on the short and long wave-length sides of the edge were obtained from Jönsson's[16] formula and tables[17] of Jönsson's values of the electron absorption coefficient. Computed optimum thicknesses for lead M_1 and M_2 edges were 7.3×10^{-5} cm and 6.9×10^{-5} cm, respectively. The screens used were from 5 to 13×10^{-5} cm thick.

The lead absorbing films were made by evaporation in a vacuum, and their thickness was governed, in a manner previously described.[9]

The self-rectifying x-ray tube and vacuum spectrograph have been described elsewhere.[5, 7] Only minor modifications were made. A.c. voltages on the tube were about 5100, currents of 50 to 200 milliamperes were used, and exposure times were from 2 to 12 hours depending on whether the photograph was one of emission or absorption.

The wave-lengths of the edges were obtained by measuring visually[18] with a traveling "one-power microscope" the distances between known emission lines and edges[19] and the lead edges on the photographs, and then interpolating with a formula given by Whitmer.[4]

RESULTS

In Table I are given the values of the edges in terms of wave-length and energy.

* Now of the Department of Physics, Michigan State College, East Lansing, Michigan.

[1] H. W. B. Skinner and J. E. Johnston, Proc. Roy. Soc. **161**, 420 (1937).
[2] V. H. Sanner, Zeits. f. Physik **94**, 523 (1935).
[3] J. A. Prins and A. J. Takens, Zeits. f. Physik **84**, 65 (1933).
[4] C. A. Whitmer, Phys. Rev. **38**, 1164 (1931).
[5] R. V. Zumstein, Phys. Rev. **25**, 747 (1925).
[6] E. Lindberg, Zeits. f. Physik **54**, 632 (1929); **56**, 402 (1929); **57**, 797 (1929).
[7] R. A. Rogers, Phys. Rev. **30**, 747 (1927).
[8] A. J. M. Johnson, Phys. Rev. **34**, 1106 (1929).
[9] J. W. McGrath, Phys. Rev. **56**, 137 (1939).
[10] W. D. Phelps, Phys. Rev. **46**, 357 (1934).
[11] D. Coster, Phys. Rev. **19**, 20 (1922).
[12] W. Stenström, Dissert., Lund., (1919).
[13] A table of wave-lengths of the M edges investigated before 1931 is given in M. Siegbahn, *Spektroskopie der Röntgenstrahlen* (Julius Springer, 1931), p. 277.
[14] An attempt was made to photograph Au M_2 (which had not been done (references 6, 8, 9)). However, the Ag $L\beta_1$ line (3.927A) was always present on the plate. Location and removal of the Ag source was not accomplished in the time available. But several gold absorption photographs were taken and it can be said that Au M_2 is very near the Ag $L\beta_1$ line.
[15] A. Sandström, Zeits. f. Physik **65**, 632 (1930).
[16] A. Jönsson, Dissert., Upsala, (1928).
[17] Reference 13, p. 470.
[18] Measurements were made visually rather than with a microphotometer for reasons given in reference 9.
[19] Reference lines were: Sb $L\beta_1$ (3.218A), Ag $L\gamma_2$ (3.300A), Sb $L\alpha_1$ (3.432A), Ag $L\gamma_1$ (3.515A), Ag $L\beta_2$ (3.694A); wave-length values from reference 13, p. 476. Sb lines were not used in M_1 photographs. The Ca K edge, from the gypsum spectrometer crystal, was very sharp and convenient so it was also used. Its gypsum crystal value of 3.059A as given by G. A. Lindsay and G. D. Van Dyke, Phys. Rev. **28**, 613 (1926) was used.

Discussion

After a consideration of possible apparatus and measurement errors it was estimated that these values are accurate to within: ±5.8 electron volts (±0.005A) for M_1, and ±5.3 electron volts (±0.005A) for M_2. These estimates are comparable with those of others who have operated this apparatus in this wave-length region.

It was found that absorbing screens slightly thicker than the calculated optimums gave better contrast. In agreement with these computed optimum thicknesses was the fact that greater thickness was required for M_1 than for M_2.

Siegbahn[20] has computed values of the M energy levels of the elements on the basis of known L edges and appropriate known emission lines. His values for lead are: M_1, 3840.5 electron volts; M_2, 3548.1 ev; M_3, 3058.0 ev; M_4, 2576.1 ev; M_5, 2474.6 ev. If one takes these as computed edge energies, there are apparent discrepancies between computed and measured values. For the lead edges here studied they are −8.5 ev for M_1 and 7.9 ev for M_2; these differences are probably not significant.

In other observed M edges significant discrepancies appear: usually for the M_4 and M_5 edges, fairly often for the M_1 edge, and occasionally for the M_2 and M_3 edges. Siegbahn[21] proposed that the M discrepancies arise because atomic electrons may not all go to the same final level in an absorption edge transition. Phelps[10] further suggested that the final levels are lattice levels.

Table I. *Lead M_1 and M_2 edges.*

Plate	M_1	M_2
16		3.471A
17		3.471
20	3.216A	
22	3.214	3.472
24	3.223	
25	3.217	3.470
26	3.223	3.471
27	3.221	3.468
29		3.465
31		3.464
Average Wave-length	3.219A	3.469A
Average Energy (Electron Volts)	3832.0	3556.0

[20] Reference 13, p. 346.
[21] M. Siegbahn, Zeits. f. Physik **67**, 567 (1931).

McGrath[9] found that when gold was alloyed with copper its M_4 and M_5 edges occurred at energies greater by several electron volts. Since the alloying changed the atomic spacing, which should in this case increase the energies of the lattice levels, he concluded that the final levels must be lattice levels. He gave a brief review of experimental results of others which indicated that, upon assigning to the low lattice levels the values of the quantum number l which the optical levels from which they originate have in free atoms, there are preferred atomic to low lattice level edge-giving transitions which are often given by $\Delta l = \pm 1$.

One should not expect, therefore, that the energies of the atomic levels, as calculated by Siegbahn,[20] would be the edge energies. Further, to obtain absolute term values one should not average calculations based on several different edges of the element since, in many cases, the final levels for these edge transitions are not the same. Ruark[22] computed absolute term values of several elements by a method seemingly better. To values of small x-ray terms obtained from optical spectra he added term differences obtained from x-ray emission lines. He estimated that the values obtained in this way are in error by not more than about 11 electron volts. So far as the author knows, there is not sufficient data to carry out this method of calculation for lead.

Since the atomic electrons do not all go to the same final level in the edge-giving transitions it is of interest to calculate the energies of the edges of an element using only one given edge and known emission lines. If these values are then compared to observed values any discrepancies arising are the energies of the final levels (which are lattice levels) with respect to the final level of the given edge transition.[23] The author has done this[24] for most of the edges

[22] A. E. Ruark, Phys. Rev. **45**, 827 (1934).
[23] While in recent years investigators of M edges have been concerned with these discrepancies and their meaning, so far as the author knows, no investigator of K or L edges has mentioned any such differences in them. Yet he has compared their observed values with his calculated values and finds, in several instances, discrepancies which appear to be significant. Probably, any such K and L edge discrepancies could also be explained on the proposal of Siegbahn[20] and Phelps.[10]
[24] The relations (in energy units) used for calculating the M edges, for example, were: $M_1 = L_3 - L_l$; $M_2 = L_3 - L\beta_{15} + (N_4 \rightarrow M_2)$; $M_3 = L_3 - L\beta_{15} + (N_4 \rightarrow M_3)$, and $M_3 = L_3 - L\beta_2 + (N_5 \rightarrow M_3)$ averaged; $M_4 = L_3 - L\alpha_2$; $M_5 = L_3 - L\alpha_1$.

of the heavier elements, using the L_3 edge as the given edge. Since values thus obtained are usually within 3 ev of those given by Siegbahn, with a few being as much as 10 ev different, the discrepancies noted on this basis are not much different in magnitude than those quoted on the basis of Siegbahn's[20] values by some M edge investigators.[4–10] The author's computed values for lead are: M_1, 3840.7 ev; M_3, 3052.6 ev; M_4, 2577.4 ev; M_5, 2475.9 ev; (there is not enough data for this calculation of M_2). Lindberg[6] found these energy values for the lead edges: M_3, 3058.0 ev; M_4, 2599.1 ev; M_5, 2494.9 ev. There appear, then, these discrepancies: M_1, -8.7 ev; M_2, 7.9 ev (on Siegbahn's value); M_3, 5.4 ev; M_4, 21.7 ev; M_5, 19.0 ev. The normal state of the lead atom is $^3P_0$, the outer electron configuration being $6s^26p^2$, according to Bacher and Goudsmit.[25] Upon assuming the previously mentioned edge-giving transition l selection rule, and assuming that the order of the low lattice and valence levels is the same as that of the free-atom optical levels[25] from which they originated, one would expect: negative and equal M_1, M_4, and M_5 discrepancies, but none for the M_2 and M_3 edges. However, if for some reason the $M_{4,5}$ electrons preferred the $O_{2,3}$ virtual level to the partially occupied $P_{2,3}$ level, on the same assumptions as before, one would expect the M_4 and M_5 discrepancies to be positive and equal. The discrepancy magnitudes cannot be estimated by this scheme. These expectations, with positive M_4 and M_5 discrepancies, are fulfilled.

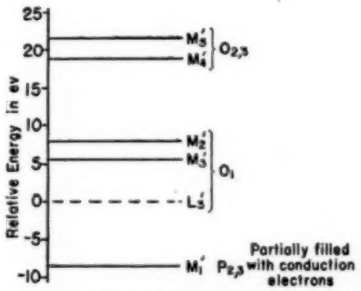

FIG. 1. Low lattice levels in lead as indicated by M edges.

In Fig. 1 a lattice energy level diagram is shown for lead as determined experimentally on the basis of M discrepancies. The primed letters indicate the final levels for the respective atomic electrons in edge transitions. The separations of the levels are drawn to scale but their widths are not indicated. There is probably some overlapping, especially for the M_2', M_3', L_3', and M_1' levels. While the last mentioned levels are shown as distinct the magnitudes of their separations from the L_3' level, with the possible exception of the M_1' level, are not significant. To the right are given virtual optical levels from which these lattice levels possibly originated.

It appears that continued study of the M edges and their discrepancies will contribute considerably in a roughly quantitative way to our understanding of lattice energy levels.

The author appreciates the kindness of the Department of Physics of the State University of Iowa, in extending the opportunity and facilities for this investigation.

[25] R. F. Bacher and S. Goudsmit, *Atomic Energy States* (McGraw-Hill, 1932), p. 356.

Structure of Iridium Lines

L. SIBAIYA
Department of Physics, University of Mysore, Bangalore, South India

(Received August 21, 1939)

The isotopic constitution of iridium was for the first time determined by Venkatesachar and Sibaiya from a study of the hyperfine structure of its arc line λ3513.67A. It was shown that iridium consists of two odd isotopes of mass numbers 191 and 193, the isotope 193 being twice as abundant as the isotope 191. This result was afterwards corroborated by Dempster's mass-spectrograph analysis. With the view of determining the ratio of the nuclear magnetic moments of the two isotopes, the hyperfine structure, arising from the nuclear spin moments of $(\frac{1}{2})(h/2\pi)$ and $(\frac{3}{2})(h/2\pi)$ of the isotopes 191 and 193, respectively, has been investigated for a few more iridium lines using an aluminized Fabry-Perot etalon. From the results obtained for the hyperfine level separations of the isotopes, it is concluded that the ratio of the nuclear magnetic moments of Ir (191) and (193) is −0.92.

IN an attempt to determine the isotopic constitution and nuclear spin of iridium, the hyperfine structure of some iridium lines has been previously investigated.[1] With a water-cooled hollow cathode source[2] and a quartz Lummer-Gehrcke plate 20 cm long and 3.45 mm thick, the structure of the Ir I 3513.67A revealed the existence of two odd isotopes in iridium with mass numbers 191 and 193. It was further inferred that their nuclear spin moments were $(1/2)(h/2\pi)$ and $(3/2)(h/2\pi)$, respectively. From estimates of the intensities of the components, Ir (193) was concluded to be nearly twice as abundant as Ir (191). These conclusions in regard to the isotopes and their abundance in iridium have been corroborated by Dempster[3] from a study of its mass spectrum. The wave number separation of the extreme satellites of λ3513.67 was found to be 0.217 cm^{-1}, which corresponds to 0.027A width. Some of the other lines that exhibited a similar structure could not be resolved by the Lummer plate employed. Thus the separation of the extreme satellites of these lines was less than that of λ3513.67. The present work was undertaken with a view of studying the hyperfine structure of other significant lines of iridium.

In the spectral region under observation silver films exhibit an absorption band, in consequence of which a silvered Fabry-Perot etalon could not be employed. For the study of lines in this region of the ultraviolet other investigators have used a coating of Hoch-heim alloy on the interferometer plates. As this alloy was not available, the etalon plates have been aluminized; these films also do not exhibit any absorption in the spectral region under study. The structure of the lines has been investigated with Invar distance-pieces of thickness 10, 15, 17.5, 20 and 23 mm between the etalon plates. The resulting increase in resolving power with increase of air-gap between the plates has enabled the determination of the hyperfine structure of some more iridium lines. The source

[1] B. Venkatesachar and L. Sibaiya, Nature **136**, 437 (1935); and Proc. Ind. Acad. Sci. **2**, 203 (1935).
[2] B. Venkatesachar and L. Sibaiya, Proc. Ind. Acad. Sci. **1**, 955 (1935).
[3] A. J. Dempster, Nature **136**, 909 (1935).

TABLE I. *Comparison of the structure of λλ3800.10 and 2924.81 with the structure of λ3513.67.*

LINE (A)	STRUCTURE (cm^{-1})					REMARKS
	Wing	*Wing*				
3513.67	+0.072	—	+0.000	−0.073	−0.145	Previous values
	(7)		(22)	(13)	(9)	
	+0.072	+0.032	0.000	−0.080	−0.151	New values
3800.10	+0.066	—	0.000	−0.053	−0.098	
2924.81	+0.060	—	0.000	−0.065	−0.118	
2849.74	0.082 (1)			0.000 (2)		Probably an isotope displacement
2639.70	0.083 (1)			0.000 (2)		

TABLE II. *Level separations.*

LEVEL[1]	Ir (191) ($\frac{3}{2}$)	Ir (193) ($1\frac{1}{2}$)
$A\ {}^4F_{4\frac{1}{2}}$	-0.150 cm^{-1}	0.162 cm^{-1}
$1°\ {}^4F°_{4\frac{1}{2}}$?	-0.052	0.056
$2°\ {}^4G°_{5\frac{1}{2}}$?	~-0.005	$\sim$0.006
$10°_{4\frac{1}{2}}$?	-0.032	0.036

[1] W. Albertson, Phys. Rev. **42**, 443 (1932).

employed was the same water-cooled hollow cathode previously described. The light from the source is focused on the Fabry-Perot etalon and a quartz achromat focuses the pattern on the slit of a Hilger E_1 spectrograph with quartz train.

Even with the highest resolving power employed, a complete resolution of some of the lines has not been possible. The structure of λλ3800.10 and 2924.81 are compared with the structure of λ3513.67 in Table I.

The lines λ2664.77 and λ2824.44, though they appear to be single even with the 23 mm etalon, are much wider than the lines λ2694.22 and λ2797.72; it must therefore be concluded that, at least in the former case, the resolving power is insufficient to resolve the structure of the lines. Consistent with the previous explanation of the structure of λ3513.67A, the values for the other level separations are given in Table II.

If H is the magnetic field at the nucleus arising from the optical electron and μ the magnetic moment of the nucleus of spin moment I, the distance between the extreme F levels of any gross structure term characterized by the quantum number J is given by

$$\Delta W=\mu H(2J+1)/J, \quad \text{when} \quad J\gtrsim I,$$

and $$\Delta W=\mu H(2I+1)/I, \quad \text{when} \quad I\gtrsim J.$$

The nuclear spins of iridium isotopes 191 and 193 are $\frac{3}{2}$ and $1\frac{1}{2}$, respectively, the sign of the former being negative; and hence for the iridium terms, whose total splittings have been computed above, $J>I$. It therefore follows that in these cases

$$\mu_{191}/\mu_{193}=\Delta W_{191}/\Delta W_{193}.$$

The values for the total widths of the hyperfine levels of the various terms lead to the conclusion that the ratio of the magnetic moments of Ir (191) and Ir (193) is -0.92. The ratio of the magnetic moments thus obtained for iridium is of the same order as that of μ_{199}/μ_{201} for mercury, *viz.*, -0.90; again in the case of xenon also μ_{131}/μ_{129} is -0.90.

OCTOBER 15, 1939 PHYSICAL REVIEW VOLUME 56

A $^1\Sigma\rightarrow{}^1\Sigma$ Transition of the C_2 Molecule

O. G. LANDSVERK
Ryerson Physical Laboratory, University of Chicago, Chicago, Illinois

(Received August 29, 1939)

The λ2300 "band" of the carbon arc, previously noticed by Bloomenthal and other investigators and measured by Hori, who attributed it to a C_3 molecule, has been accurately measured and analyzed, using photographs taken on the 30-foot, 30,000-line grating spectrograph. The analysis shows definitely that the structure consists of superposed (0,0), (1,1), (2,2), and (3,3) headless bands of a $\Sigma\rightarrow\Sigma$ transition of C_2 (or possibly C_2^+), in agreement with the earlier diagnosis of Mulliken and Dieke. Alternate lines are missing in each series, as expected in view of the zero spin of the carbon nucleus. Most probably the transition is $^1\Sigma_u^+\rightarrow{}^1\Sigma_g^+$ of C_2. The molecular constants are very nearly equal for the upper and lower electronic states. They correspond rather closely to the average values of the same constants for other known states of C_2. The following values were obtained for the more important constants: $B_e'=1.8334$ cm^{-1}, $B_e''=1.8223$ cm^{-1}, $\alpha'=0.0204$, $\alpha''=0.0195$, $r_e'=1.2382$ A, $r_e''=1.2419$ A, $\omega_e'=1748$ cm^{-1}, $\omega_e''=1774$ cm^{-1}, $\nu_0^{0,0}=43{,}227.25$ cm^{-1}. The ω_e values were obtained indirectly from the B and D values, since only one sequence of bands could be analyzed.

INTRODUCTION

BECAUSE of its importance in the study of molecular structure in general and in particular in the study of problems that arise in organic chemistry, the electronic transitions of the diatomic carbon molecule and the determination of related constants have been of considerable interest to the physicist and the

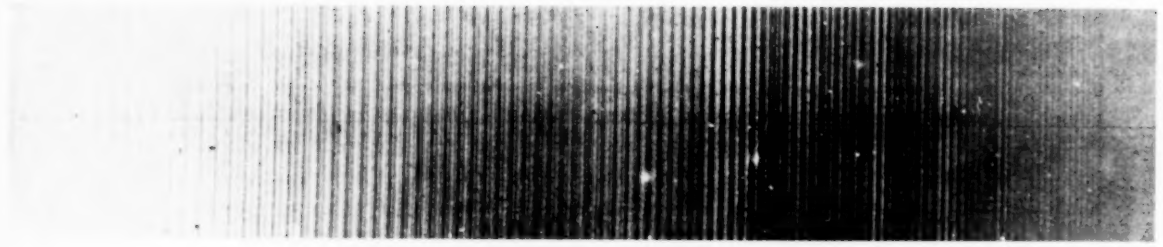

FIG. 1. The band at λ2300A reproduced from a picture that was taken with a Hilger E 1 spectrograph by Dr. S. Bloomenthal.

chemist alike. The subject of the present work is the analysis of a band which apparently occurs regularly in the spectrum of the carbon arc near λ2300A. So far as the writer is aware, the first published mention of this band is in an article by Mulliken[1] in 1930. The band was discovered in this laboratory by Dr. S. Bloomenthal in 1928–29, by using a carbon arc in hydrogen at low pressure in a search for boron hydride bands. It was also discovered independently by Professor G. H. Dieke. Later it was reported and measured by Hori.[2] It has also been reported by G. and L. Herzberg,[3] who state that they have made a partial analysis. Very likely the band has been noticed independently also by others.

Both Mulliken and Dieke interpreted the "band" as the $\Delta v=0$ sequence of a $^1\Sigma\rightarrow{}^1\Sigma$ transition of the C_2 molecule. However, attempts to confirm this view by rotational analysis have hitherto not been carried through. Dr. S. Bloomenthal and also S. D. Ginsberg did a considerable amount of work on the band in this laboratory but did not have sufficient dispersion and resolving power to accomplish a satisfactory analysis. Fig. 1 is a reproduction of one of Dr. Bloomenthal's pictures, which he has very kindly supplied. It was taken with a Hilger E 1 spectrograph.

As can be seen from Fig. 1, the λ2300 band has all the earmarks of a $\Delta v=0$ sequence of a transition with nearly zero change in moment of inertia and $\Delta\Lambda=0$.[4] The structure has a central minimum and a maximum on each side with no obvious heads. There are no other obvious bands of comparable intensity in the neighborhood which would correspond to $\Delta v=1$ or further sequences. This is what one expects if there is very little change in moment of inertia between upper and lower electronic states. The complex appearance of the band (presence of several series) is what would be expected if several members of the $\Delta v=0$ sequence are present. The fact that the bands usually appear with known C_2 bands, and the spacings of the lines in series indicating a B value about right for a C_2 molecule, provided alternate lines are missing in each series as required for a $^1\Sigma\rightarrow{}^1\Sigma$ transition in C_2, made the latter very probable. The present analysis bears out this diagnosis. Three bands identified as (0,0), (1,1), and (2,2) have been completely analyzed. The strongest portions of the (3,3) band have been measured.

There has existed hitherto only one published attempt at the analysis of these bands. This is in the paper by Hori referred to above. The strongest lines were arranged in a single series with no missing line at the center. Hori concluded from this last circumstance that the band cannot be due to a diatomic $^1\Sigma\rightarrow{}^1\Sigma$ transition and tentatively ascribed it to a C_3 molecule.

Hori's strongest series and the writer's (0,0) band are identical except across the central minimum. Here Hori uses the range from $R(12)$ to $R(28)$ of the writer's (3,3) band in place of lines $P(8)$ to $R(8)$ of the (0,0) band. It happens that $R(12)$ and $R(28)$ of the (3,3) band are not resolved from $P(8)$ and $R(8)$, respectively, of the (0,0) band. In this manner, Hori constructed an apparent series in which the intensities did not approach zero in the central region and in which no line was missing. When, however, a study was made of Hori's series, using the writer's more accurate measurements, it was found that at the two points at which Hori switched from one series to another, a sudden

[1] R. S. Mulliken, Zeits. f. Electrochemie **36**, 603 (1930).
[2] Takeo Hori, Zeits. f. Physik **88**, 495 (1934).
[3] J. G. Fox and G. Herzberg, Phys. Rev. **52**, 638 (1937).
[4] Cf. R. S. Mulliken, Rev. Mod. Phys. **3**, 149 (1931).

break occurred in the first differences. It was found possible, by departing from Hori's arrangement, to extend the series in such a way that the first differences progressed perfectly smoothly past these points. In this way, the true series comprising the (0,0) band was found.

Experimental Procedure

In all previous work on the λ2300 band the source has been an enclosed carbon arc. This was made necessary by the fact that, while the bands are produced at least as rapidly in air as in other gases, they are then overlain by bands of impurities, particularly CO bands. The CN bands are, of course, also strong, but do not extend to λ2300. Hori[2] used a metal cylinder for enclosing the arc. Bloomenthal in his work here used a Pyrex bulb. In both cases the graphite electrodes were placed so that their axes were in a straight line and the gap was adjusted by screws which extended to the outside of the bulb. Both experimenters ran the arc in hydrogen at pressures ranging from 8 to 50 cm of mercury. It was possible to use hydrogen since no CH bands appear in the λ2300 region.

In the present work the source was a carbon arc with the electrodes at right angles, enclosed in a five-liter Pyrex bulb. The apparatus was of conventional design except that air leakage was prevented by using sylphons fitted over bent rods the rotation of which operated the screw mechanism of the water-cooled electrodes.

Helium was found to be a suitable gas in which to operate the arc. In the first place, helium eliminates the danger of explosion. Further, the only spectrum produced by helium in the carbon arc is its line spectrum, which does not fall in the λ2300A region. Finally, it was found that sufficient purity of the gas could be obtained by merely confining tank helium for some time in a charcoal liquid air trap.

The pressure of helium was found not to be critical. The λ2300 band occurs at all pressures from 0.1 mm of mercury or less to atmospheric pressure. Using solid electrodes, a pressure of about 6 cm was found to give the best results. When hollow electrodes were used (see description below), the range from 0.5 to 2.0 cm of mercury produced a somewhat higher intensity with less background than other pressures. This pressure range was actually used for the final exposures.

In view of the close spacing and many blends indicated by the work of previous investigators, it was obvious that a matter of first importance was to increase the accuracy of measurement and the degree of resolution of the lines of the spectrum. It appeared that the high resolving power and especially the high dispersion of the laboratory's 30-foot, 30,000-line/inch grating spectrometer would be suitable for the purpose. Now the 30-foot spectrometer requires a very much longer time of exposure than the smaller instruments. Furthermore, the length of exposure which can be used is limited by the fact that, with full resolving power, only a minor change in barometric pressure is allowed. It, therefore, was necessary to have a light source of high intensity so that the time of exposure might be kept sufficiently short.

It was found that when solid graphite electrodes were used, enough intensity could not be attained. However, when $\frac{5}{32}''$ holes were drilled into the $\frac{3}{8}''$ electrodes, the cathode end of the arc, which wandered badly when solid electrodes were used, then settled into the cavity. When the arc was right-angled and the hollow cathode was placed facing toward the slit, not only did this produce a steady source of ideal dimensions for use with the 30-foot spectrograph, but also the heating effect was more concentrated and diffusion was retarded so that relatively more carbon vapor was available for the production of C_2 molecules. Also, the sputtering which takes place from a solid cathode and which consumes the cathode at a rate of about $\frac{1}{8}$ inch/hour was completely stopped. It is estimated that this change increased the intensity of the band at λ2300A by a factor of fifty or more, using a current of 20 amperes at 220 volts. It was found possible to produce a further increase in intensity of perhaps six times by raising the current to 30 amperes, but this was not necessary.

As previously mentioned, the 30-foot, 30,000-lines/inch grating spectrograph was used. The grating was ruled on speculum metal in this laboratory by Dean Henry G. Gale, and afterwards was given a thin coat of aluminum by evaporation, in order to increase its ultraviolet reflecting power. The grating is set up in Paschen

mounting and has six inches of ruled surface. The grating shows excellent resolving power. In the fourth order a resolving power of a least 420,000 has been observed by Dr. Beutler in an examination of mercury hyperfine structure.

The grating is so ruled that its maximum intensity for λ2300 is in the third order. This fact combined with the very favorable dispersion made it desirable to use the third order. It is then necessary to remove the second order of λ3450A, since under certain operating conditions the Swan bands of C_2 appeared strongly in this region, as also a certain amount of continuous light from the arc. For this purpose a quartz chlorine filter was used. An effective length equivalent to 1 cm of chlorine gas at atmospheric pressure was found to be suitable.

In the third order of λ2300A, the dispersion is about 0.25A/mm. Now the temperature of the carbon arc source of the λ2300 band is estimated to be at least 3500°C. If the emitter is assumed to be C_2, the Doppler width of the band lines from this source is calculated to be 0.02A (0.08 mm on the third-order plate). Therefore, a slit width of 0.04 mm ($=\frac{1}{2}$ Doppler width) is permitted because it reduces the resolution by only 10 percent. This gives an actual resolving power of about 60,000 in third order. This is much less than the grating could give but the high dispersion was very desirable. The slit width used in the present work was 0.04 mm, except in one case in which the width of 0.025 mm was used. As was expected, the smaller slit width merely increased the time required for exposure without increasing the resolution.

Three good exposures were made of two, five, and nine hours duration, and with respective slit widths of 0.04, 0.04, and 0.025 mm. The length of exposure was limited by continuous light which tended to mask the weakest lines. The exposures were made on Eastman type I–O plates, ultraviolet sensitized.[5]

The discharge of the carbon arc in helium when hollow electrodes, such as are described above, are used, exhibits certain interesting properties. If we assume, as is quite probable, that the lower $^3\Pi$ state of the Swan bands, which is thought to be the normal state, and the lower $^1\Sigma$ state of the λ2300 bands lie close together, the higher frequency of the λ2300 band indicates that the energy required to excite it must be greater than for the Swan bands. We would, therefore, expect the Swan bands to be produced strongly whenever the λ2300 bands appear. When, however, the hollow cathode carbon arc is used, the Swan bands disappear. The spectrum then consists only of the λ2300 bands, a few lines due to impurities in the electrodes, and the helium spectrum. This seems very strange, yet there can be no doubt that the λ2300 bands are produced by C_2, as is shown by the present analysis. (The possibility of C_2^+ is not thereby excluded.)

The fact that the helium spectrum appears strongly shows that electrons with energy approaching 25 volts are present in the discharge. The general appearance of the arc also suggests that the discharge is largely electronic.

Experimental Data

Below are presented the data on which the detailed analysis is based. Table I is a list of the measured values of the observed lines in cm^{-1} in vacuum. The probable errors of measurement, except for a few very weak lines, are well within ± 0.2 cm^{-1} (or 0.01A). Fully one-third of the lines, however, are blends. A major fraction of these are near the origins of the bands where intensities are low. There may be errors up to ± 1.0 cm^{-1} when such lines are fitted into series. The intensities, as estimated from the heights of peaks in microphotometer traces, are indicated in the column marked *I*. The columns that contain the *J''* assignments are labelled 0, 1, 2, 3 for the (0,0), (1,1), (2,2), and (3,3) bands, respectively.

Theory and Analysis of the Band Structure

As is well known, $^1\Sigma \rightarrow {}^1\Sigma$ transitions have simple *P* and *R* branches and no *Q* branch. When the molecule consists of two like atoms, the rotational states are classified as positive and negative as usual, but also as symmetrical and antisymmetrical (*s*, *a*). Transitions can occur

[5] These plates are decidedly grainy. They were, however, roughly five times as sensitive in the λ2300 region as Process or Eastman 33 plates. The Eastman Company states that they are as sensitive as Schumann plates down to 1800A. They are much more convenient to use.

TABLE I. *Wave numbers and identification of band lines of C_2 λ2313. Numbers under the headings 0, 1, 2, 3 (each heading denotes $v'=v''$) are J'' for the lines. Intensities I are estimated from microphotometer traces.*

ν(VAC)	I	0	1	2	ν(VAC)	I	0	1	2	3	ν(VAC)	I	0	1	2	3	ν(VAC)	I	0	1	2
43,026.8	0				43,140.4	4		18			43,230.9	0	0		14		43,322.3	1		30	
37.3	0				41.2	6	26		10		34.2	2		8			25.0	5	24		
45.4	2				47.1	7	24	16			36.8	3				22	27.5	1			38
50.5	2	62		40	48.2	0			8		37.9	1					30.5	2		32	
54.5	4	60		38	53.0	6	22	14			38.3	2	2				33.4	5	26		
56.4	2				55.0	00			6		38.8	0			16		35.8	1			40
58.6	2	58			56.0	0					42.3	3		10			39.0	2		34	
60.3	0		46	36	59.5	6	20	12			44.5	2				24	41.6	5	28		
62.9	3	56			61.5	00			4		45.7	3	4				44.3	0			42
65.5	0		44		65.7	6	18				46.8	2			18		49.4	1		36	
67.3	2	54		34	66.4	1		10			50.1	2		12			50.1	5	30		
69.1	1				68.8	000			2		52.4	2				26	52.4	0			44
70.5	1		42		72.2	5	16				53.3	4	6				55.8	1		38	
72.2	1	52			73.5	1		8			54.7	2			20		58.6	6	32		
72.7	2			32	76.5	00				6	57.6	3		14			60.9	00			46
76.1	2		40		78.8	5	14				60.3	3				28	64.5	1		40	
76.8	3	50			80.2	1		6	0		60.7	5	8				67.4	4	34		
78.4	3			30	83.2	000				8	62.5	2			22		69.3	0			48
81.5	5	48	38		85.3	5	12				65.6	3		16			72.8	1		42	
84.4	3			28	86.8	00		4	2		68.5	6	10			30	75.8	3	36		
86.7	5	46	36		90.1	000					70.4	10			24		77.5	1			50
90.6	3			26	92.0	4	10				72.0	10					81.6	0		44	
91.6	4	44			93.8	00		2	4		73.4	3		18			84.6	3	38		
92.3	4		34		95.8	000					75.6	1					86.1	0			52
96.7	4	42		24	98.9	3	8			12	76.3	6	12			32	90.2	0		46	
97.8	3		32		43,200.9	0			6		78.3	2			26		93.3	2	40		
43,102.1	3	40		22	03.3	000					81.4	3		20			98.7	0		48	
03.7	2		30		05.8	3	6	0		14	84.4	6	14				43,402.0	2	42		
07.3	3	38			08.6	0			8		86.6	2			28		02.9	0			
08.7	1			20	10.0	0					89.5	3		22			07.1	2		50	
09.7	4		28		12.8	2	4	2			92.4	6	16				11.1	1	44		
12.7	4	36			13.5	0				16	94.7	1			30		15.7	1		52	
15.5	4		26	18	14.8	1					97.4	3		24			19.8	2	46		
18.2	5	34			16.3	0			10		43,300.3	6	18				24.4	0		54	
21.6	5		24	16	16.9	1					02.8	2			32		28.6	1	48		
23.6	5	32			18.2	0					05.8	3		26			37.6	1	50		
27.7	5		22	14	19.8	1	2	4			08.4	5	20				46.4	1	52		
29.4	5	30			21.3	1				18	11.1	1			34		55.3	1	54		
34.0	4		20	12	23.6	0			12		13.9	2		28			64.1	0	56		
35.4	5	28			27.0	1		6			16.7	5	22				73.2	1	58		
38.1	0				28.9	3				20	19.2	1			36						

only $+\rightleftarrows-$ and $s\rightleftarrows s$ or $a\rightleftarrows a$. If the nuclear spin is zero, as is true for the carbon atom, only the symmetrical states exist. Under these conditions $^1\Sigma \rightarrow {}^1\Sigma$ transitions produce bands which have only lines with even J'' for $^1\Sigma_u^+ \rightarrow {}^1\Sigma_g^+$ and J'' odd for $^1\Sigma_g^+ \rightarrow {}^1\Sigma_u$.[4,6,7] The predicted structures for the case $B'=B''$ are shown in Fig. 2. The intensities of the lines near ν_0, where the Boltzmann factor may be disregarded, are given by the simple expression $I \propto (J'+J''+1)$.[8] This gives nearly equal intensity for the P and R branches.

In the present analysis of the λ2300 band, the first step was to arrange the lines in series, beginning with a strong series. This was facili-

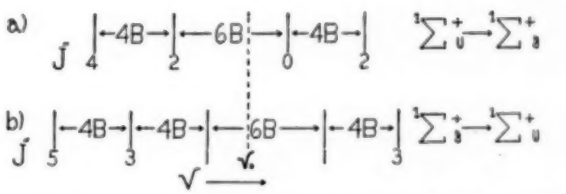

FIG. 2. Predicted structures for $^1\Sigma^+ \rightarrow {}^1\Sigma^+$ bands in C_2 for $B'=B''$.

[6] $^1\Sigma^+ \leftrightarrows {}^1\Sigma^-$ is theoretically impossible. $^1\Sigma_g^- \rightarrow {}^1\Sigma_u^-$ produces the same rotational structure as $^1\Sigma_u^+ \rightarrow {}^1\Sigma_g^+$ so that these two types cannot be distinguished by rotational analysis. $^1\Sigma^- \rightarrow {}^1\Sigma^-$ transitions are rare, however. Furthermore, if it is close to the normal state, as is probable here, the lower $^1\Sigma$ state is expected from configuration theory to be $^1\Sigma_g^+$. For a complete discussion of the possible states of C_2, see the accompanying article by R. S. Mulliken in this issue of the Review.

[7] Cf. R. S. Mulliken, Rev. Mod. Phys. **4**, 66 (1932).

[8] Cf. W. Jevens, *A Report on the Band Spectra of Diatomic Molecules* (London: The Physical Society, 1932), p. 134.

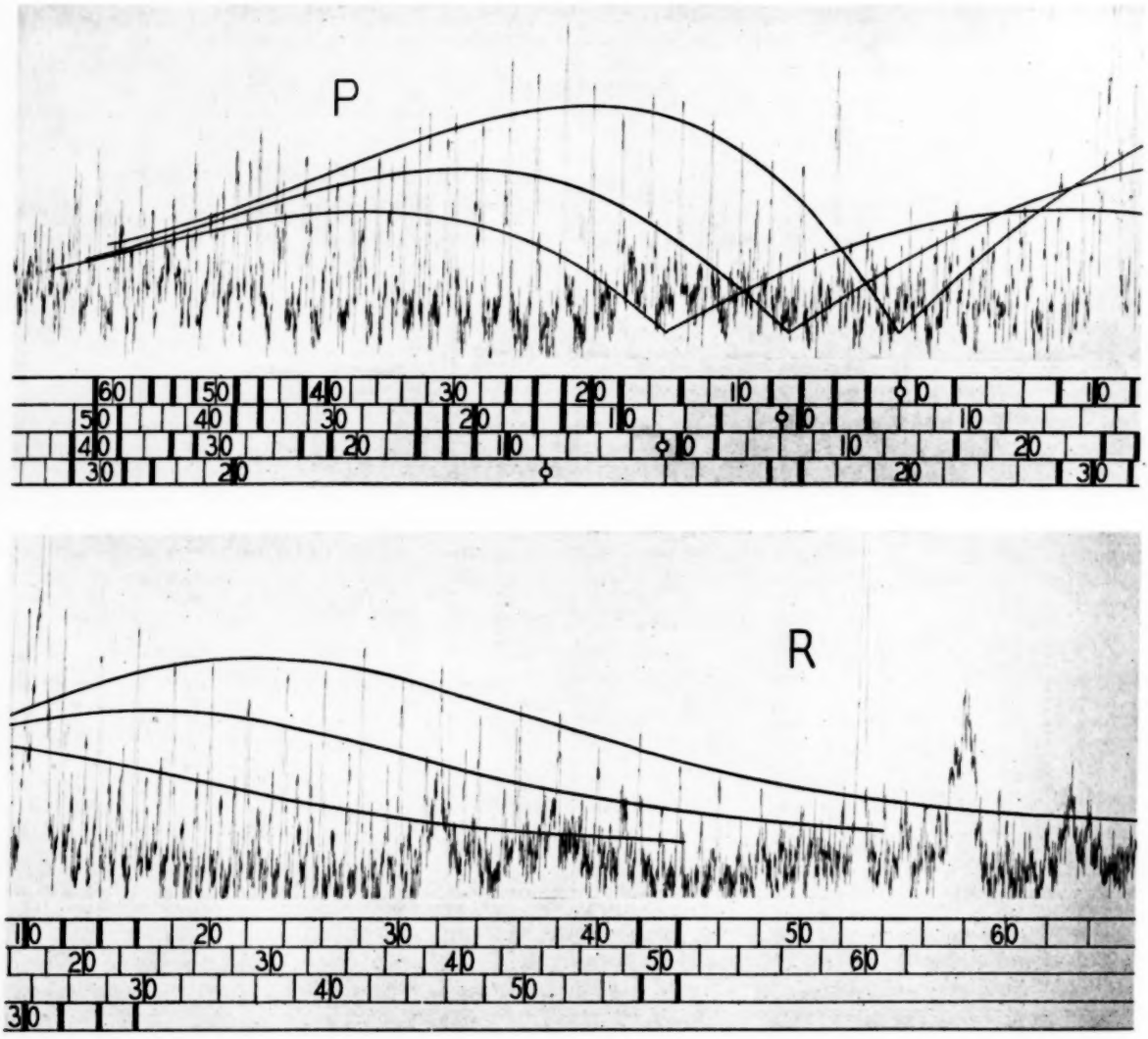

FIGS. 3a AND 3b. Microphotometer trace of the λ2300 band. The smooth curves are intensity curves drawn in each individual band through the peaks of the unblended lines. The diagram represents the lines of each individual band, with their J'' numbers. The heavy bars of the diagram indicate blended lines.

tated in the case of the (0,0) band by the use of a microphotometer trace of the band. Figs. 3*a* and 3*b* constitute a reproduction of such a trace; the lines are shown analyzed into four series attributed to the four bands (0,0), (1,1), (2,2), (3,3). The lines of each band with their J'' values are indicated in the diagram below the figure. It will be noted that there are many blends. Superposed on the microphotometer trace, three smooth intensity curves have been drawn, one for each of the three strongest bands. The curves are drawn through the peaks of those lines in each band that are not blended.

It is seen that a strong R branch and a strong P branch are joined to form what is interpreted as the (0,0) band. This band conforms to one of the $^1\Sigma \rightarrow {}^1\Sigma$ types discussed above. The lines are nearly uniformly spaced on both sides of a central intensity minimum, but at this point there occurs a gap which has just $\frac{3}{2}$ times the normal spacing. On the basis of intensities the position of this gap seems to be uniquely determined. In this space, to be sure, there are four weak lines, but these can be attributed to other bands.

We still have a choice of two positions for ν_0 of

the strongest band, each approximately occupied, as it happens, by a line of another band. This choice depends on whether we assume case *a* or case *b* of Fig. 2. If we assume case *a*, then ν_0 must be located as shown in the diagram of Fig. 3. This would require that intensities increase in the order $R(0)$, $P(2)$, $R(2)$, $P(4)$, and so on, proportionately to $J'+J''+1=2, 4, 6, 8,$ and so on. If we take account of the disturbances due to blended lines, it is seen that the intensities as judged from Fig. 3 agree well with the above ratios. This choice for ν_0 makes the transition $^1\Sigma_u^+ \rightarrow {}^1\Sigma_g^+$ (case *a*), which is the transition that seems most probable from configuration theory. It will, therefore, be assumed in the following analysis that the bands are of this type.

It should, however, be pointed out that the alternative choice of ν_0 (case *b*, $^1\Sigma_g^+ \rightarrow \Sigma_u^+$) is not entirely incompatible with the observed intensities, in view of the numerous blends. Case *b* would give slightly different values of the rotational constants. Theoretically a choice between the two cases could be made from a study of the Δ_2F's. Unfortunately, however, this would demand measurements of an accuracy which is not here realized and probably cannot be.

The ν_0's of the (1,1) and (2,2) bands were located in relation to $\nu_0^{0,0}$ by a study of first differences between successive lines in the bands. From Fig. 2 it is seen that these differences are all $4B$ if every other line is missing and $B'=B''$. When $B'>B''$, as is the case in the λ2300 bands, the first differences are greater than $4B''$ in the R branch, less than $4B''$ in the P branch and nearly exactly $4B''$ at ν_0. Now for the B's of bands in a sequence we may assume the usual relation $B_v=B_e-\alpha v$. Since $\nu_0^{0,0}$ is known, we can find the B_e's. If we tentatively assume reasonable values for the α's, then the B_1's and B_2's may be predicted. With the assumption of linear variation of the B's with the v's, it follows from a study of observed second differences in the series constituting the bands (0,0), (1,1), (2,2), that α' and α'' are very nearly equal.

The points in the (1,1) and (2,2) series of band lines at which the first differences equal four times the predicted B_1'' and B_2'' are then the predicted positions for $\nu_0^{1,1}$ and $\nu_0^{2,2}$, respectively. Assuming α'' to be in the neighborhood of 0.02 cm^{-1}, which is an average of the observed α's for other states of C_2 ($d\,^1\Pi_g$, 0.0255; $B\,^3\Pi_g$, 0.0173; $b\,^1\Pi_u$, 0.0174; $A\,^3\Pi_u$, 0.0149), the only possible choice of ν_0's is that given in Table III.

These ν_0's are found to give B's and D's that vary linearly with v, with $\alpha'=0.204$ cm^{-1}, $\alpha''=0.195$ cm^{-1}. Now considering other choices for the ν_0's, the smallest shifts that one can make from the above choice for $\nu_0^{1,1}$, namely, distances $+4B_1$ or $-4B_1$, give $\alpha\approx 0.04$ and 0.00 cm^{-1}, respectively. Either value appears unreasonable, and any other choice of $\nu_0^{1,1}$ is worse. Furthermore, any assumed shift in the positions of the several ν_0's must be of the form $\pm 4B_e v$ to preserve the linearity of the B's and D's with v. This indicates a minimum shift of $\pm 8B_2$ and $\pm 12B_3$, or two and three full line intervals, respectively, in the (2,2) and (3,3) bands. Such large shifts seem also to be excluded in the case of the (3,3) band on the basis of intensities (cf. Fig. 3).

The next step in the analysis is the evaluation of the molecular constants, making use of the

TABLE II. $\Delta_2F_v(J)$ *values.*

	$\Delta_2F''(J)$				$\Delta_2F'(J)$		
J	$v''=0$	$v''=1$	$v''=2$	J	$v'=0$	$v'=1$	$v'=2$
1	11.1	12.0	11.3				
3	25.5	26.0	24.7	2	18.5	18.0	18.0
5	39.9	39.6	39.0	4	32.9	33.0	31.7
7	54.4	53.5*	53.8	6	47.5	46.8	46.1
9	68.7	67.8	68.2	8	61.8	60.7*	61.5
11	83.2	82.8	82.3	10	76.5	75.9	75.9
13	97.5	96.9	95.9	12	91.0	90.6	89.6
15	112.2	110.8	109.3	14	105.6	104.4	103.2
17	126.7	125.2*	123.3	16	120.2	118.5	117.2
19	140.8	139.4	138.1*	18	134.6	133.0*	131.3*
21	155.2	153.7	152.6	20	148.9	147.4	146.0*
23	169.6	167.9	165.8	22	163.5	161.8	160.4
25	183.8	181.9*	179.8	24	177.9	175.8	173.7
27	198.0*	196.1*	193.9	26	192.2	190.3*	187.7
29	212.2*	210.2*	208.2*	28	206.2*	204.2*	202.2*
31	226.5*	224.5*	222.0	30	220.7*	218.6*	216.3*
33	240.4*	238.2*	235.5	32	235.0*	232.7*	230.1
35	254.7*	252.3	250.8*	34	249.2*	246.7*	243.8
37	268.5*	265.9	263.7	36	263.1*	260.7	258.9*
39	282.5	279.7*	277.6	38	277.3*	274.3	271.9
41	296.6	294.0*		40	291.2	288.4*	285.7
43	310.4	307.8*		42	305.3	302.3*	
45	324.4	321.3*		44	319.5	316.1*	
47	338.3			46	333.1	329.9*	
49	351.8*			48	347.1		
51	365.4			50	360.8*		
53	379.1			52	374.2		
55	392.4*			54	388.0		
57	405.5*			56	401.2		
59	418.8			58	414.6*		

* This symbol is to indicate differences between lines which are neither blended nor very weak. All the rest may be less accurate.

usual combination differences

$$\Delta_2F_v'(J)\equiv F_v'(J+1) - F_v'(J-1)=R(J)-P(J), \quad (1)$$

$$\Delta_2F_v''(J)\equiv F_v''(J+1) - F_v''(J-1)=R(J-1)-P(J+1). \quad (2)$$

The $\Delta_2F_v(J)$ values for the λ2300 bands are given in Table II, assuming J assignments as in Fig. 3, which is based on the preceding discussion.

Assuming the usual expression

$$F_v(J)=B_vJ(J+1)-D_vJ^2(J+1)^2+\cdots, \quad (3)$$

we have

$$\Delta_2F_v(J)/(J+\tfrac{1}{2})=4B_v-8D_v(J+\tfrac{1}{2})^2+\cdots. \quad (4)$$

If the expression on the left is plotted against $(J+\frac{1}{2})^2$, the graph should be a straight line, provided powers of $(J+\frac{1}{2})$ higher than the second are negligible in Eq. (4), as proved to be the case here. We can determine B_v and D_v, respectively, from the $J=0$ intercept and the slope of the graph.

A related method consists in plotting the left side of the equation

$$4B_v(J+\tfrac{1}{2})-\Delta_2F_v(J)=8D_v(J+\tfrac{1}{2})^3 \quad (5)$$

against J.[9] Using this method (cf. reference for details) the previously obtained B values were checked, and slightly different D values than before were obtained. These D's were averaged with those obtained by the first graphical method.

The best values for the ν_0's were obtained by use of the formula

$$\nu_M=\nu_0+(B'+B'')M+(B'-B''+D'-D'')M^2 +2(D'+D'')M^3+(D'-D'')M^4\cdots, \quad (6)$$

where M is the well-known serial number. After substituting the known B's and D's for a given band the ν_M's of its unblended lines were introduced and the equation solved for ν_0. The values so obtained were averaged for each band to give the final ν_0's. The B and D values obtained above and the ν_0's are collected in Table III together with estimates of their reliability.

The analysis assumes that the bands conform to case a of Fig. 2. This is probably correct, but, as discussed in the text, case b cannot be excluded with certainty. Case b would give slightly lower ν_0's and B's. Using

$$B_v=B_e-\alpha(v+\tfrac{1}{2}), \quad \text{and} \quad D_v=D_e-\beta(v+\tfrac{1}{2}) \quad (7)$$

in connection with Table III, we find values of α, β, B_e, and D_e for the upper and lower $^1\Sigma^+$ states. These are collected in Table IV. From the B_e's the internuclear distances r_e are also calculated in the usual manner. The ω_e's have also been determined approximately from the well-known relation $\omega_e=(4B_e^3/D_e)^{\frac{1}{4}}$, and are given in Table IV.

It will be noticed that the ω_e values just calculated using $\omega_e=(4B_e^3/D_e)^{\frac{1}{4}}$ obey the relation $\omega_e'>\omega_e''$, which is the usual relation when $B_e'>B_e''$, as is true here. Definite evidence will now be produced, however, showing that actually $\omega_e''>\omega_e'$, so that the relation $\omega_e'>\omega_e''$ just obtained must be attributed to small errors in the D_e's (about ±2 percent).

From the formulas for the positions of the ν_0's of the bands in a sequence, it is readily shown that, very nearly, the distance between zeros of two successive bands is

$$\nu_0^{v',\,v''}-\nu_0^{v'-1,\,v''-1}=(\omega_e'-\omega_e'') -2v'(\omega_e'x_e'-\omega_e''x_e''). \quad (8)$$

Now from Table III, $\nu_0^{1,1}-\nu_0^{0,0}$ is -25.84 cm^{-1} and $\nu_0^{2,2}-\nu_0^{1,1}$ is -25.62 cm^{-1}. Using Eq. (8), we then find $\omega_e'-\omega_e''=-26.06$ cm^{-1}, and $\omega_e'x_e'-\omega_e''x_e''=-0.11$ cm^{-1}. We note that the accurate value of $\omega_e'-\omega_e''$ thus obtained is opposite in sign to the rough value that was calculated above. The best way to combine the approximate values of ω_e' and ω_e'' obtained above

TABLE III. *Rotational constants and ν_0's from analysis of λ2300 band, all in cm^{-1}. The estimated probable errors in order of increasing v are: For ν_0's, ±0.02, ±0.03, ±0.05, and ±0.20 cm^{-1}; B's, ±0.0002, ±0.0005, ±0.0005, and ±0.005 cm^{-1}; D's, ±0.05, ±0.1, ±0.2×10^{-6} cm^{-1}.*

BAND	ν_0	B'	B''	$D'\times10^6$	$D''\times10^6$
0−0	43,227.23	1.8232	1.8125	7.54	7.39
1−1	43,201.39	1.8026	1.7927	6.87	6.47
2−2	43,175.77	1.7825	1.7735	6.15	5.50
*3−3	43,150.56	1.762	1.754		

[9] Cf. G. Herzberg, *Molekülspektren und Molekülstruktur* (Leipzig: Steinkopff, 1939), pp. 139–142.

* The range of measured and unblended lines in the (3,3) band is so restricted that accurate ν_0's and B's could not be had. $\nu_0^{3,3}$ by extrapolation from the values of the other ν_0's is 43,150.27 cm^{-1}.

TABLE IV. *Constants from analysis of λ2300 band (cm⁻¹).*

	B_e	D_e	α	β	ω_e	ω_e*	$r_e(A)$
Upper $^1\Sigma$	1.8334	7.89×10^{-6}	0.0204	7.0×10^{-7}	1767	1748	1.2382
Lower $^1\Sigma$	1.8223	7.86×10^{-6}	0.0195	9.4×10^{-7}	1755	1774	1.2419

* The ω_e* values are the best that could be had. See discussion in text.

with the accurate $\omega_e'-\omega_e''$ is to average the former and then add and subtract 13 cm^{-1}, so as to make $\omega_e'-\omega_e''$ correct. The results are $\omega_e'=1748$ cm^{-1} and $\omega_e''=1774$ cm^{-1} (the quantities ω_e* of Table IV).

There is an approximate relation given by Mecke and Birge which states that for all electronic states of a given diatomic molecule $B_e/\omega_e=$constant. It is found that for previously reported states of C_2[10] this ratio varies from 0.98×10^{-3} to 1.01×10^{-3}. In the present case these ratios become $B_e'/\omega_e'=1.04\times10^{-3}$ and $B_e''/\omega_e''=1.027\times10^{-3}$. The results are, therefore, in satisfactory agreement with the others.

It is interesting to calculate roughly where the $\Delta v=1$ and $\Delta v=-1$ sequences of the present $^1\Sigma\rightarrow{}^1\Sigma$ band system should occur. Substitution in the formulas for the ν_0 of electronic bands shows that[7]

$$\nu_0^{1,0}=\nu_0^{0,0}+\omega_e'-2x_e'\omega_e'+\cdots, \qquad (9)$$
$$\nu_0^{0,1}=\nu_0^{0,0}-\omega_e''+2x_e''\omega_e''-\cdots.$$

We have seen previously that $x_e'\omega_e'\approx x_e''\omega_e''$. We have also noted how various other coefficients for the $^1\Sigma\rightarrow{}^1\Sigma$ transition are roughly equal to the average of those for other states of C_2. If then we assume $x_e'\omega_e'\approx x_e''\omega_e''\approx20$ cm^{-1}, we shall probably not be in error by more than a few cm^{-1}. We then have $\nu_0^{1,0}\approx44{,}956$ and $\nu_0^{0,1}\approx41{,}473$. The (0,1) band ($B_0'-B_1''=+0.0305$ cm^{-1}) should degrade in the same direction as the (0,0) band ($B_0'-B_1''=+0.0107$) but much more strongly. M_{head} is calculated to be about -59. This corresponds to $\nu_{\text{head}}\approx41{,}366$, a distance of 107 cm^{-1} from $\nu_0^{0,1}$. A band with head at $\nu=41{,}284$ and degraded to the violet has been reported by Fox and Herzberg and may probably be interpreted as corresponding to the $\Delta v=-1$ sequence of the present system, as already suggested by Fox and Herzberg.[3] The $\Delta v=+1$ sequence of bands is expected to be of the headless type ($B_1'-B_0''=-0.0097$), as is the case in the $\Delta v=0$ sequence, but with a tendency to degrade to the red. Fox and Herzberg report two bands, with heads at 45,061 and 45,100, which may perhaps belong to the $\Delta v=+1$ sequence of the present system, although they are reported to degrade to the violet contrary to our prediction.

It is a pleasure to acknowledge gratefully the help and encouragement which have been received from Dr. R. S. Mulliken and Dr. H. G. Beutler in the solution of this problem.

[10] Cf. H. Sponer, *Molekülspektren*, Vol. I (Berlin: J. Springer, 1935), p. 14.

Note on Electronic States of Diatomic Carbon, and the Carbon-Carbon Bond

ROBERT S. MULLIKEN
University of Chicago, Chicago, Illinois

(Received August 29, 1939)

It is shown that the λ2300 carbon band analyzed by Landsverk belongs very probably to the transition $\sigma_g^2\sigma_u\pi_u^4\sigma_g$, $^1\Sigma_u^+ \rightarrow \sigma_g^2\sigma_u^2\pi_u^4$, $^1\Sigma_g^+$. The $^1\Sigma_g^+$ state should lie not far above the normal state of C_2, or possibly be the normal state. Approximate energies and internuclear distances (r_0) are predicted and tabulated for all low-energy states of C_2 and C_2^+; an equation for predicting r_0's is given. Carbon-carbon bond distances in polyatomic carbon compounds are compared with those in C_2. Apparently bonding to other atoms helps to shorten C−C and C=C bonds in polyatomic compounds as compared with C_2. The same effect is noted in nitrogen compounds.

I. Electronic States of Diatomic Carbon, and Interpretation of the λ2300 Carbon Band

LANDSVERK'S analysis of the λ2313 band of the carbon arc shows definitely[1] that this "band" is the zero sequence of a $\Sigma \rightarrow \Sigma$ transition[2] of the C_2 molecule. From the absence of any indication of fine structure in the band lines, and from the excitation conditions, $^2\Sigma \rightarrow ^2\Sigma$ of C_2^+ and $^3\Sigma \rightarrow ^3\Sigma$ of C_2 are very unlikely, and $^1\Sigma \rightarrow ^1\Sigma$ of neutral C_2 is altogether probable.[2]

Assuming $^1\Sigma^+ \rightarrow ^1\Sigma^+$, Landsverk's analysis still leaves $^1\Sigma_g^+ \rightarrow ^1\Sigma_u^+$ and $^1\Sigma_u^+ \rightarrow ^1\Sigma_g^+$ as possibilities, with evidence from intensities perhaps favoring the latter. The present paper attempts to decide between these alternatives and to determine the electron configurations and approximate energies of the two Σ states.

The low energy states of the C_2 molecule have been discussed in a previous article.[3] These and others of C_2 and C_2^+ are listed in Table I, together with rough estimates of their energies and of the internuclear separations r_0 for their respective lowest states of vibration.

Table I is obtained in the following way. For energies up to at least 10 ev above the normal state of C_2 or C_2^+, we can be sure that, besides the four K electrons, there are always two electrons in the $z\sigma_g$ MO (molecular orbital). This MO is a strongly bonding hybrid of $\sigma_g 2s$ and $\sigma_g 2p$, with $\sigma_g 2s$ somewhat preponderating in the mixture. There remain six electrons (or five in C_2^+) to be distributed among MO's of higher energy. The MO's $y\sigma_u$, $w\pi_u$, $x\sigma_g$, and $v\pi_g$, with energy increasing in the order named, here come into consideration. Of these four MO's the weakly antibonding $y\sigma_u$, a hybrid of $\sigma_u 2s$ and $\sigma_u 2p$ with the former somewhat preponderating, is definitely the most stable, as is known from a study of the N_2^+ spectrum.[2,3] Next in order are the strongly bonding degenerate MO $w\pi_u \equiv \pi_u 2p$ and the weakly bonding $x\sigma_g$, the latter a hybrid of $\sigma_g 2s$ and $\sigma_g 2p$ with the latter somewhat preponderating. Highest in energy is the strongly antibonding degenerate $v\pi_g \equiv \pi_g 2p$. (There is also the very strongly antibonding $u\sigma_u$, a hybrid of $\sigma_u 2s$ and $\sigma_u 2p$ with the latter preponderating, but its energy is higher than that of $\pi_g 2p$, and we need not consider it.)

As a rough approximation, we may assume $y\sigma_u$ to lie 3 ev deeper than $w\pi_u$ and $x\sigma_g$, and 9 ev deeper than $v\pi_g$, for internuclear distances in the neighborhood of 1.25A. These figures are justified by what is known of the energy levels of C_2, N_2 and N_2^+, and CN. For simplicity it may be assumed that $w\pi_u$ and $x\sigma_g$ lie equally deep for internuclear distances corresponding to the most stable states, as seems to be indicated to be approximately true by data for nitrogen.[3] The mean energies for various low energy electron configurations, relative to the lowest-energy configuration taken as zero, are then as given in Table I. In case there is more than one electronic state for a given configuration, the energies of the several states may be expected to be distributed about the tabulated mean value.

Next we need a system for estimating r_0

[1] O. G. Landsverk, Phys. Rev. **56**, 769 (1939).
[2] This identification was made tentatively some time ago by Dieke and by Mulliken (cf. R. S. Mulliken, Zeits. f. Elektrochemie **36**, 605 (1930).
[3] R. S. Mulliken, Rev. Mod. Phys. **4**, 66, 81 (1932).

TABLE I. *Approximate energy and r_0 values for low energy electron configurations of C_2 and C_2^+.*

$y\sigma_u$	$w\pi_u$	$x\sigma_g$	$v\pi_g$	Est. Mean Energy* (ev)	States	No. of C–C Bonds	r_0 Values (A) Calc.	Obs.
2	4			0	$^1\Sigma_g^+$	2	1.24	1.243
2	3	1		0	$^3\Pi_u$, $^1\Pi_u$	2	1.32	1.313, 1.318
2	2	2		0	$^3\Sigma_g^-$, $^1\Delta_g$, $^1\Sigma_g^+$	2	1.40	
1	4	1		3	$^3\Sigma_u^+$, $^1\Sigma_u^+$	3	1.18	1.240
1	3	2		3	$^3\Pi_g$, $^1\Pi_g$	3	1.26	1.266, 1.257
2	3	0	1	6	$^3, ^1\Sigma_u^+$, $^3, ^1\Delta_u$, $^3, ^1\Sigma_u^-$	1	1.46	
2	2	1	1	6	$^3, ^1\Phi_g$, $^3, ^3, ^3, ^3, ^3, ^1, ^1, ^1\Pi_g$	1	1.54	1.541
2	1	2	1	6	$^3, ^1\Sigma_u^+$, $^3, ^1\Delta_u$, $^3, ^1\Sigma_u^-$	1	1.62	
0	4	2		6	$^1\Sigma_g^+$	4	1.12	
0	4	2			$C\equiv C$	4	1.12	
(1)	4	(1)			$-C\equiv C-$	3	1.18	1.20
(1)	2+(1)	(1)	(1)		$>C=C<$	2	1.40	1.34
(1)	(2)	(1)	(2)		$\gtrless C-C\lessgtr$	1	1.62	1.54
2	3			0	$^2\Pi_u$	$1\frac{1}{2}$	1.35	
2	2	1		0	$^4, ^2\Sigma_g^-$, $^2\Delta_g$, $^2\Sigma_g^+$	$1\frac{1}{2}$	1.43	
2	1	2		0	$^2\Pi_u$	$1\frac{1}{2}$	1.51	
1	4			3	$^2\Sigma_u^+$	$2\frac{1}{2}$	1.21	
1	3	1		3	$^4, ^2, ^2\Pi_g$	$2\frac{1}{2}$	1.29	
1	2	2		3	$^4, ^2\Sigma_u^-$, $^2\Delta_u$, $^2\Sigma_u^+$	$2\frac{1}{2}$	1.37	
2	2	0	1	6	$^2\Phi_g$, $^4, ^2, ^2, ^2\Pi_g$	$\frac{1}{2}$	1.57	
2	1	1	1	6	$^4, ^2, ^2(\Sigma_u^-, \Delta_u, \Sigma_u^+)$	$\frac{1}{2}$	1.65	
2	0	2	1	6	$^2\Pi_g$	$\frac{1}{2}$	1.73	
0	4	1		6	$^2\Sigma_g^+$	$3\frac{1}{2}$	1.15	
0	3	2		6	$^2\Pi_u$	$3\frac{1}{2}$	1.23	

* The energy values are rough estimates made for internuclear distances near 1.25A. If r_0 differs much from 1.25A, the energy at r_0 is considerably lowered, as can be seen by drawing $U(r)$ curves. The above estimated energy values are based on the observed energy intervals of 2.39 ev ($^3\Pi_g - ^3\Pi_u$) and 3.20 ev ($^1\Pi_g - ^1\Pi_u$) between states of the configurations $\sigma_u^2\pi_u^2\sigma_g$ and $\sigma_u\pi_u^3\sigma_g^2$, and of 4.91 ev between $\sigma_u^2\pi_u^2\sigma_g$, $^3\Pi_u$ and $\sigma_u^2\pi_u^3\sigma_g\pi_g$, $^3\Pi_g$ (the latter found and identified by Fox and Herzberg, reference 4). The observed energy intervals just mentioned are those between the *minima* of potential curves; the required correction to constant r increases them, especially that for the Fox-Herzberg bands.

values. The simplest possibility is that the following equation is valid:

$$r_0 = P + yN_y - wN_w - xN_x + vN_v, \qquad (1)$$

where N_y, N_w, N_x, and N_v are the numbers of electrons in the respective MO's $y\sigma_u$, $w\pi_u$, $x\sigma_g$, and $v\pi_g$, and P, y, w, x, v are adjustable positive constants. Bonding electrons then make negative, antibonding electrons positive contributions to r_0 in Eq. (1). The several constants in Eq. (1) must be determined so as to give correctly the r_0 values of known states of C_2. Known states[1, 3, 4] are the $^3\Pi_u$ and $^1\Pi_u$ of $z\sigma^2y\sigma^2w\pi^3x\sigma$ with $r_0 = 1.3135$A and 1.318A, respectively (average 1.316A), the $^3\Pi_g$ and $^1\Pi_g$ states of $z\sigma^2y\sigma w\pi^3x\sigma^2$ with $r_e = 1.26$A and 1.25A, respectively (average r_0 1.261A), and the $^3\Pi_g$ state[4] of $z\sigma^2y\sigma^2w\pi^2x\sigma v\pi$ ($r_0 = 1.54$A); also the two probable $^1\Sigma^+$ states, with $r_0 = 1.243$A for the lower and 1.240A for the upper. From the data on the II states, we get $x+y = 0.058$A and $w+v = 0.224$A. Making the *assumptions* $x=y$ and $v=w$, which seem on the whole to be indicated as roughly true by available r_0 data[5] on N_2, N_2^+, and O_2, we then get $x=y=0.03$, $w=v=0.11$, and $P=1.62$. Hence, in A,

$$r_0 = 1.62 + 0.03(N_y - N_x) - 0.11(N_w - N_v). \qquad (2)$$

Eq. (2) has been used to obtain the "calculated" r_0 values in Table I.

Examination of r_0 data on various states of N_2 and O_2 indicates that such an equation as Eq. (2) is likely to hold fairly well only over a moderate range of r_0 values, but to give too small values when r_0 is unusually small or unusually large.

If, in the manner first proposed by Herzberg, we count the number of bonds between two atoms in a diatomic molecule as equal to half the number of bonding electrons minus half the number of antibonding electrons, the numbers of bonds for the various low-energy states of

[4] J. G. Fox and G. Herzberg, Phys. Rev. **52**, 638 (1937).

[5] Cf. H. Sponer, *Molekülspektren*, Vols. I, II (J. Springer, Berlin, 1935–36).

C_2 and C_2^+ are as given in the seventh column of Table I. It will be noted that for a given number of bonds, the r_0 values vary considerably. This is, of course, because different bonding (and antibonding) MO's differ considerably in their bonding (or antibonding) power.

Turning to the identification of the electronic states of the λ2300 band, we note that r_0 has the values 1.240A and 1.243A for the upper and lower states, respectively. Referring to Table I one finds only one $\Sigma\rightarrow\Sigma$ transition between low energy C_2 states both with predicted r_0 values near 1.24A. This is $\sigma_u\pi_u^4\sigma_g$, $^1\Sigma_u^+$ (predicted $r_0=1.18$A)$\rightarrow\sigma_u^2\pi_u^4$, $^1\Sigma_g^+$ (predicted $r_0=1.24$A). For the lower state the predicted and observed r_0's agree, for the upper there is a disagreement of 0.06A. For the energy change, the predicted value is 3 ev plus an amount equal to half the $^1\Sigma_u^+-{}^3\Sigma_u^+$ interval for $\sigma_u\pi_u^4\sigma_g$,—or say roughly about 4 ev. The observed value is 5.34 ev. Although there is a greater disagreement between observation and prediction than one can easily explain, every other $\Sigma\rightarrow\Sigma$ transition of C_2 or C_2^+ (including those between higher states than are listed in Table I) gives much worse agreement.[6]

By way of explaining the discrepancies between observed and predicted features, the following may perhaps help. In Table I two additional $^1\Sigma_u^+$ states, with r_0 values of 1.46A and 1.62A, are predicted to lie near 6 ev. It seems likely that the $U(r)$ curve of the lower of these, rising steeply near 1.24A since its minimum is near 1.5A, intersects that of the predicted $\sigma_u\pi_u^4\sigma_g$, $^1\Sigma_u^+$ not far from the latter's minimum near 1.2A. Interaction of the two curves might give rise to two new curves of which one (the upper) could have the characteristics of the upper level of the λ2300 band. It may here be noted also that a low $^1\Sigma_g^+$ state with r_0 about 1.40A is predicted which should lie near the $\sigma_u^2\pi_u^4$, $^1\Sigma_g^+$ state identified as the lower state of the λ2300 band; these two states may interact to some extent.

Accepting the foregoing interpretation of the λ2300 band as correct, we may ask, what is the lowest electronic level (normal state) of C_2? If the assumption made in Table I of equal energy for the configurations $\sigma_g^2\sigma_u^2\pi_u^4$, $\sigma_g^2\sigma_u^2\pi_u^3\sigma_g$, and $\sigma_g^2\sigma_u^2\pi_u^2\sigma_g^2$ is correct, then $^3\Pi_u$ of $\sigma^2\sigma^2\pi^3\sigma$ (lower state of the Swan bands) is probably lowest (as is now generally assumed), with $^3\Sigma_g^-$ of $\sigma^2\sigma^2\pi^2\sigma^2$ a close second, and with $^1\Sigma_g^+$ of $\sigma^2\sigma^2\pi^4$ and $^1\Delta_g$ of $\sigma^2\sigma^2\pi^2\sigma^2$ not very much higher.[7] If, however, the configuration $\sigma^2\sigma^2\pi^2\sigma^2$ is lowest of the three, the normal state of C_2 may be $^3\Sigma_g^-$ instead of $^3\Pi_u$. On the other hand, if $\sigma^2\sigma^2\pi^4$ is the lowest-energy configuration and is sufficiently low,[7] $^1\Sigma_g^+$ could be the normal state instead of $^3\Pi_u$. On the basis of present knowledge, none of the foregoing possibilities can be excluded, although $^3\Pi_u$ appears still to be the best guess for normal state. In any case, all the states mentioned may be expected to play a role for astrophysical problems where C_2 spectra are involved.

II. Carbon-Carbon Bond Distances in Carbon Compounds

In connection with Table I, it seemed of interest to attempt to use Eq. (2) to calculate carbon to carbon bond distances for single and multiple C−C bonds in carbon compounds. This can be done if we assume that the bonds formed with other atoms make use of C_2 MO's in the manner indicated by the assignments in parentheses in the middle section of the table.[8] In all cases a pair of $z\sigma_g$ electrons not given in the table is supposed to be present and to form one C−C bond. The calculated values are seen to agree roughly with average observed values as given by Pauling.[9] In the cases of double and single bonds the observed values are smaller than the calculated, suggesting that the C−C bonds are here strengthened by the process of sharing carbon electrons with other atoms instead of just between two carbons. However,

[6] The transition $\pi_u^4\sigma_g$, $^2\Sigma_g^+\rightarrow\sigma_u\pi_u^4$, $^2\Sigma_u^+$ is the most likely C_2^+ possibility, but the predicted r_0's are 1.15 and 1.21A and the predicted energy change only 3 ev; and the lines should be narrow doublets.

[7] These statements are based on estimated energies (relative to the mean energy for the given electron configuration) of −0.5, 0.0, and +0.5 ev for $^3\Sigma_g^-$, $^1\Delta_g$ and $^1\Sigma_g^+$ of $\sigma^2\sigma^2\pi^2\sigma^2$, −0.8 and +0.8 ev for $^3\Pi_u$ and $^1\Pi_u$ of $\sigma^2\sigma^2\pi^3\sigma$, and 0.0 for $^1\Sigma_g^+$ of $\sigma^2\sigma^2\pi^4$. These represent revisions of estimates given previously (reference 3).

[8] Cf. R. S. Mulliken, J. Chem. Phys. **3**, 517 (1935) for a description of the way in which the C_2 MO's are used to form bonds to other atoms.

[9] Cf. L. Pauling, *The Nature of the Chemical Bond* (Cornell University Press, 1939), p. 154.

the orbitals, particularly $z\sigma_g$, should be considerably modified (especially as regards extent of $s-p$ mixing) by the clustering of other atoms around the carbons, so that r_0 values calculated on the basis of a diatomic carbon molecule are no longer entirely appropriate.

When a table similar to Table I and an equation similar to Eq. (2) are written down for N_2 and N_2^+, one finds relations similar to those for carbon: bonding to other atoms seems to shorten the N=N and N−N bond distances as compared with those for N_2 itself. The equation for N_2 and N_2^+ is

$$r_0=1.49+0.03(N_y-N_x)-0.10(N_w-N_v). \quad (3)$$

OCTOBER 15, 1939 PHYSICAL REVIEW VOLUME 56

The Infra-Red Spectrum and Molecular Constants of Nitric Oxide

ALVIN H. NIELSEN* AND WALTER GORDY**
Mendenhall Laboratory of Physics, Ohio State University, Columbus, Ohio

(Received August 29, 1939)

The infra-red spectrum of nitric oxide has been remeasured under high dispersion with the result that the fundamental at 5.3μ has been almost completely resolved. The absorption in this region comprises two superposed bands arising from a $^2\Pi_{1/2,\,3/2}$ electronic ground state. In the P, and R branches a great many of the lines split up into doublets, the components of which belong to these two bands, respectively. The lines were found to fit the following two empirical formulas:

$\nu_{\Omega=1/2}=1877.36+3.34\,J-0.019\,J^2$ cm^{-1}
where $J=0, \pm 3/2, 5/2, \cdots,$

$\nu_{\Omega=3/2}=1877.00+3.42\,J-0.019\,J^2$ cm^{-1}
where $J=0, \pm 5/2, 7/2, \cdots.$

An experimental curve in percent absorption against frequency in cm^{-1} is compared with a theoretical intensity plot of the bands. From the new data some of the constants have been re-calculated, and compared with the results of the electronic band spectra. $I_0=1.63\times10^{-39}$ g cm^2, $r_0=1.15\times10^{-8}$ cm, $\nu_0=1891.3$ cm^{-1}.

I. INTRODUCTION

AMONG the diatomic molecules having infra-red spectra nitric oxide is of special interest. Because of its electronic configuration, which gives it a ground state of $^2\Pi_{\frac{1}{2}, \frac{1}{2}}$, the molecule has resultant angular momentum of $(1/2)\hbar$ and $(3/2)\hbar$ around its nuclear axis. It becomes, therefore, the only one of the diatomic molecules to exhibit a Q branch in the infra-red.

Warburg and Leithauser[1] in 1908, the first to investigate the spectrum, succeeded in showing that the contour of the fundamental at 5.3μ was a doublet. Later, in 1929–1930, Snow, Rawlins, and Rideal[2] resolved both the fundamental at 5.3μ and the first harmonic at 2.7μ into rotational structure by means of a grating spectrometer.

This spectrum has been re-investigated using an instrument of somewhat better resolving power. Several details of interest were observed and are reported here. Some of the constants are calculated from our data and compared with values given in the earlier work, and with those determined from the electronic band spectrum.[3]

II. APPARATUS

The nitric oxide was prepared according to the method outlined by Snow, Rawlins, and Rideal.[2] A large spherical bulb was filled to atmospheric pressure by passing gas through the bulb until all the air had been displaced by the gas. The nitric oxide was allowed to generate and flow until the colorlessness of the gas in the storage tank attested to its purity. For the 5.3μ region a cell 2 cm long fitted with rocksalt windows was used; for the 2.7μ region the cells used were from 10–30 cm long. Each cell was

* Department of Physics, University of Tennessee, Knoxville, Tennessee.
** Mary Hardin Baylor College, Belton, Texas.

[1] Warburg and Leithauser, Ber. D. Chem. Ges. **1**, 145 (1908).

[2] C. P. Snow, F. I. G. Rawlins and E. K. Rideal, Proc. Roy. Soc. **124**, 453 (1929); C. P. Snow, F. I. G. Rawlins and E. K. Rideal, Proc. Roy. Soc. **126**, 355 (1929).

[3] M. Guillery, Zeits. f. Physik **42**, 121 (1927); F. A. Jenkins, H. A. Barton and R. S. Mulliken, Phys. Rev. **30**, 150 (1927); R. S. Mulliken, Phys. Rev. **32**, 186 (1928).

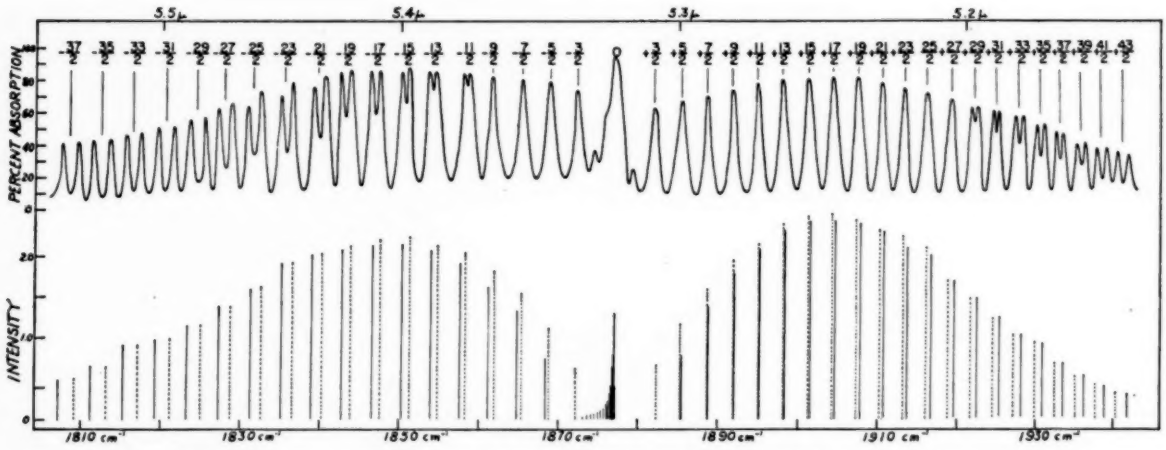

FIG. 1. The upper curve shows the observed absorption of NO at 5.3μ; the lower diagram gives theoretically predicted band spectrum of NO.

filled to atmospheric pressure from the storage tank.

Both regions in which absorption occurs—but more especially the harmonic region—overlap those of atmospheric absorption by water vapor. To make measurements in these regions it was found necessary to dry the spectrometer box thoroughly. This was accomplished by distributing P_2O_5 in photographic trays throughout the spectrometer box and sealing it securely. One such charge would last about a week indicating that the box was quite airtight. No falsification by water vapor was now apparent even in the middle of the 2.7μ water band.

The instrument with which these measurements were made was of the conventional prism-grating type and has been described in previous papers from this laboratory. The 5.3μ band was measured with the aid of the 3600 line-per-inch grating in the first order while the harmonic at 2.7μ was measured using the 4800 line-per-inch grating in first order. Both gratings were ruled by Professor R. W. Wood at Johns Hopkins University.

III. Experimental Results

The 5.3μ region

Figure 1 shows our observations on the fundamental vibration-rotation band of nitric oxide plotted with ordinates in percent absorption against abscissae of frequency in cm^{-1} and wave-length in μ. This curve differs from the one by Snow, Rawlins, and Rideal in several respects. The rotation lines are much more completely resolved, and the curve shows the existence of the two transitions $^2\Pi_{\frac{1}{2}}-{}^2\Pi_{\frac{1}{2}}'$, and $^2\Pi_{\frac{3}{2}}-{}^2\Pi_{\frac{1}{2}}'$ as two bands, whose Q branches are very nearly coincident. That two bands exist is evident from the fact that in both the P and the R branches the lines split up into pairs beginning a few lines from the center. The splitting appears to increase with the rotational quantum number. The lines in the P branch begin splitting up with the fifth line from the Q branch, while in the R branch the splitting does not occur until the fourteenth line. The closest pair which was resolved has a spacing of 0.6 cm^{-1}. The Q branch is much better resolved than in the earlier work and appears to be more intense. The slit widths used in this region included a spectral region of about 0.6 cm^{-1} and observations were made at intervals of 0.45 cm^{-1}.

The 2.7μ region

No curve for the harmonic is given in this paper. This region was very carefully measured and yields a band which appears to have a Q branch at 3740.2 cm^{-1}. The band has a very irregular structure and does not at all resemble the fundamental nor indeed a band due to a diatomic molecule. It does, however, in many respects corroborate the curve shown by Snow, Rawlins, and Rideal and the line spacing is about the same as that estimated from the curve given by them. This spacing is about

7.0 cm^{-1} and not at all in agreement with the spacing in the fundamental. It is hoped that this band may be measured again in the near future under better conditions.

IV. Discussion of Results

The energy of a diatomic molecule having angular momentum around the nuclear axis is given by Kronig[4] as

$$W_{v,J}=W^0-B_0\alpha+h\nu_0(v+\tfrac{1}{2})\{1-k(J+\tfrac{1}{2})^2+\Gamma\}+B_0[(J+\tfrac{1}{2})^2+\Gamma]\{1-\gamma^2[(J+\tfrac{1}{2})^2+\Gamma]\}-B_0\beta(v+\tfrac{1}{2})^2, \quad (1)$$

where $\alpha=(7/4)c_3+(7/8)c_3^2+(3/4)c_4$;
$k=(3/2)\gamma^2(1+2c_3)$;
$\Gamma=S(S+1)-2\Omega\Sigma$;
$\beta=(3+15c_3+15/c_3^2+3c_4)$.

The frequencies of the rotation lines in the bands may be obtained from this energy relation and are:

$$\nu_{\Omega=\frac{1}{2}}=[\nu_0-(3/2)\nu_0k-2B_0\beta/h]+[2B_0/h-2\nu_0k-6B_0\gamma^2/h]J-\nu_0kJ^2-4B_0\gamma^2J^3/h$$
where $J=0,\ \pm3/2,\ 5/2,\ 7/2,\ \cdots$, etc. (2)

arising from the transition $^2\Pi_{\frac{1}{2}}-{}^2\Pi_{\frac{1}{2}}'$ with $\Omega=\frac{1}{2}$, $\Sigma=-\frac{1}{2}$, $S=\frac{1}{2}$; and

$$\nu_{\Omega=\frac{3}{2}}=[\nu_0+(1/2)\nu_0k-2B_0\beta/h]+[2B_0/h-2\nu_0k+2B_0\gamma^2/h]J-\nu_0kJ^2-4B_0\gamma^2J^3/h$$
where $J=0,\ \pm5/2,\ 7/2,\ \cdots$, etc. (3)

arising from the transition $^2\Pi_{\frac{3}{2}}-{}^2\Pi_{\frac{1}{2}}'$ with $\Omega=\frac{3}{2}$, $\Sigma=\frac{1}{2}$, $S=\frac{1}{2}$.

These equations are of the form $\nu=a\pm bJ-cJ^2\pm dJ^3$. It has been found possible to fit the lines in the two bands to the following formulas:

$$\nu_{\Omega=\frac{1}{2}}=1877.36+3.34J-0.019J^2;$$
where $J=0,\ \pm3/2,\ 5/2,\ \cdots$, etc. (4)

and

$$\nu_{\Omega=\frac{3}{2}}=1877.00+3.42J-0.019J^2;$$
where $J=0,\ \pm5/2,\ 7/2,\ \cdots$, etc. (5)

The cube term in J was omitted because its value was known with too little accuracy to have any meaning. Table I shows the observed line positions in cm^{-1} and the line positions as computed from the empirical equations (4) and (5). In most cases the error between the observed and calculated positions is of the order of 0.3 cm^{-1}.

In Fig. 1, lower diagram, the rotation lines in the transitions $^2\Pi_{\frac{1}{2}}-{}^2\Pi_{\frac{1}{2}}'$ and $^2\Pi_{\frac{3}{2}}-{}^2\Pi_{\frac{1}{2}}'$ are plotted with calculated intensities as ordinates and as abscissa the same scale of frequency in cm^{-1} as was used in Fig. 1, upper curve. The intensities were computed from the relations given by Dennison.[5] The $^2\Pi_{\frac{1}{2}}-{}^2\Pi_{\frac{1}{2}}'$ transition is represented by the dotted lines, while the solid lines represent the $^2\Pi_{\frac{3}{2}}-{}^2\Pi_{\frac{1}{2}}'$ transition. The individual lines in the Q branch of the first transition and the Q branch of the latter transi-

Table I. *Observed and calculated frequencies (cm^{-1}) of the lines in the fundamental of* NO.

	$\Omega=\frac{1}{2}$			$\Omega=3/2$		
$2J$	ν(calc)	ν(obs)	$\Delta\nu$	ν(calc)	ν(obs)	$\Delta\nu$
+43	1940.4	1940.1	−0.3	1941.8	1942.1	+0.3
+41	1937.9	1938.2	+ .3	1939.1	1939.6	+ .5
+39	1935.7	1935.6	− .1	1936.5	1936.6	+ .1
+37	1933.1	1932.8	− .3	1933.8	1933.7	− .1
+35	1930.0	1930.2	+ .2	1931.0	1931.4	+ .4
+33	1927.3	1927.5	+ .2	1928.3	1928.6	+ .3
+31	1924.6	1924.6	.0	1925.5	1925.4	− .1
+29	1921.8	1922.0	+ .2	1922.6	1922.7	+ .1
+27	1919.0	1919.8	+ .8	1919.7	1919.8	+ .1
+25	1916.1	1916.3	+ .2	1916.8	1916.3	− .5
+23	1913.3	1913.4	+ .1	1913.8	1913.4	− .4
+21	1910.3	1910.6	+ .3	1910.8	1910.6	− .2
+19	1907.4	1907.6	+ .2	1907.8	1907.6	− .2
+17	1904.4	1904.5	+ .1	1904.7	1904.5	− .2
+15	1901.3	1901.5	+ .2	1901.6	1901.5	− .1
+13	1898.3	1898.2	− .1	1898.4	1898.2	− .2
+11	1895.2	1895.1	− .1	1895.3	1895.1	− .2
+ 9	1892.0	1891.7	− .3	1892.0	1891.7	− .3
+ 7	1888.8	1888.6	− .2	1888.7	1888.6	− .1
+ 5	1885.8	1885.5	− .3	1885.4	1885.5	+ .1
+ 3	1882.3	1882.1	− .2			
0	1877.36			1877.00		
− 3	1872.3	1872.2	− .1			
− 5	1868.9	1869.0	− .1	1868.3	1869.0	+ .7
− 7	1865.4	1865.4	.0	1864.8	1865.4	+ .6
− 9	1862.0	1861.6	− .4	1861.2	1861.6	+ .4
−11	1858.4	1858.7	+ .3	1857.7	1858.1	+ .4
−13	1854.9	1854.7	− .2	1854.0	1853.7	− .3
−15	1851.2	1851.2	.0	1850.3	1850.2	− .1
−17	1847.6	1847.4	− .2	1846.6	1846.1	− .5
−19	1843.9	1843.8	− .1	1842.8	1842.5	− .3
−21	1840.2	1840.4	+ .2	1839.0	1839.1	+ .1
−23	1836.4	1836.3	− .1	1835.2	1835.0	− .2
−25	1832.6	1832.3	− .3	1831.3	1830.8	− .5
−27	1828.8	1828.9	+ .1	1827.4	1827.2	− .2
−29	1824.9	1824.5	− .4	1823.4	1823.5	+ .1
−31	1821.0	1821.4	+ .4	1819.2	1819.4	+ .2
−33	1817.1	1817.2	+ .1	1815.4	1815.4	.0
−35	1813.1	1813.3	+ .2	1811.3	1811.2	− .1
−37	1809.1	1808.7	− .4	1807.2	1807.3	+ .1

[4] R. del Kronig, *Band Spectra* (Macmillan, Cambridge Series, 1930), p. 31.

[5] D. M. Dennison, Rev. Mod. Phys. **3**, 315 (1931).

tion are so nearly equal in position that on this scale it is impossible to distinguish them. The corresponding lines from each Q branch have therefore been added and the Q branch shown is the line for line sum of the two Q branches. The intensities in the experimental curve are only relative and can be compared with the lines in the theoretical curve only in general characteristics. The two curves agree very well except that in the experimental curve the Q branch appears to be too intense as compared with the lines of maximum intensity in the P and R branches. Also the resolution was not complete, as only about one-half of the lines could be separated into doublets.

From Eqs. (2) and (3) it is evident that the theory predicts that the constant term of $\nu_{\Omega=\frac{3}{2}}$ should be greater than the constant term of $\nu_{\Omega=\frac{1}{2}}$. It was not found possible to make the observed lines fit a set of equations in which this was the case but a very good fit was obtained by letting the reverse be true. A possible explanation of this inconsistency may be that ν_0 for the $^2\Pi_{\frac{1}{2}}$ state is greater than ν_0 for the $^2\Pi_{\frac{3}{2}}$ state by just this amount. It seems not unlikely that the two values may differ by small amounts. Some evidence of this is also presented by Jenkins, Barton, and Mulliken in their work.

The constants I_0, r_0, may be computed from Eqs. (2), (3), (4) and (5) by identifying the constant first term in (2) and (3) with the empirical constant of (4) and (5); and by identifying the theoretical coefficients of J and J^2 in (2) and (3) with the empirical coefficients of J and J^2 in (4) and (5).

The Q branch of the harmonic as obtained from our unpublished curve lies at 3740.2 cm^{-1}.

TABLE II. *Assembled values of some of the constants for* NO.

CONSTANT	NIELSEN-GORDY	JENKINS-BARTON-MULLIKEN	SNOW-RAWLINS-RIDEAL	JEVONS[1]
$I_0\times10^{-39}$ g cm^2	1.63	1.63	1.64	
$r_0\times10^{-8}$ cm	1.15	1.15	1.15	1.146
ν_0 cm^{-1}	1891.3	1892	1895.2	1906.5

[1] W. Jevons, *Report on Band Spectra of Diatomic Molecules* (Univ. Press Cambridge, 1932).

We may then set $[2\nu_0-6B_0\beta/h-3\nu_0k]=3740.2$ cm^{-1} and, using this together with the previously mentioned data, calculate ν_0. These values are compared with values for the same constants obtained by other investigators in Table II.

I_0 and r_0 agree very well in all cases because they are determined from the fundamental band only. ν_0 from our data agrees with the value given by Jenkins, Barton, and Mulliken rather than with the other values given in Table II. The reason for disagreement here is that ν_0 determined from the positions of both the fundamental and harmonic, depends on how these band centers are chosen. We believe the value 1877 cm^{-1} for the fundamental to be correct. It differs from Snow, Rawlins, and Rideal's value by 5.9 cm^{-1}. There is, however, some doubt about the position of the center of the harmonic. Therefore we feel that accurate values of such constants as ν_0, $x\nu_0$, c_3 and c_4 from infra-red data cannot be determined until the question of the position of the harmonic is settled.

We express our gratitude to Professor Alpheus W. Smith who graciously supplied the apparatus and materials for the experiment. We also thank Professor Harald H. Nielsen whose many suggestions and criticisms were of great aid to us in the work.

Emissive and Thermionic Characteristics of Uranium

W. L. HOLE* AND R. W. WRIGHT
University of Wisconsin, Madison, Wisconsin

(Received August 24, 1939)

Certain properties of clean uranium in vacuum have been investigated. The following values were found: for emissivity below the melting point ($\lambda=0.67\mu$), 0.51; for thermionic work function, 3.27 ± 0.05 volts, with a Richardson A of about 6; for melting point, 1700 ± 25°C; for average coefficient of linear expansion, 25°C to 1000°C, 4×10^{-6}.

INTRODUCTION

BY reason of its unique position in the periodic table of the elements, the physical properties of uranium are of peculiar interest. Enough of the element in metallic form was procured to permit observation of certain characteristics hitherto unreported.

A flat strip of uranium long enough to provide several filaments was obtained from A. D. Mackay. It was about 3 mm wide and 0.1 mm thick. These dimensions, however, were decidedly irregular. Another specimen, an oval rod about 16 cm long, was obtained through the kindness of Dr. H. C. Rentschler, of the Westinghouse Company. Its extreme diameters were 0.80 and 0.95 mm long, and its cross section was quite uniform. The degree of purity of neither sample is accurately known. The surfaces of both were initially covered with oxide, which readily forms when the metal is exposed to the atmosphere. Indeed, small pieces of uranium may be ignited by a match flame, burning brilliantly in air.

APPARATUS AND METHODS

Metallic uranium is rather hard and brittle at room temperature. Its high chemical activity precludes annealing in any of the common gases. Annealing in vacuum was found to improve its malleability only slightly. It was therefore necessary to make a blackbody for emissivity measurements of some other material. A hole 1/64-inch in diameter was drilled at the middle of a hollow columbium cylinder about 6 cm long and 3 mm in diameter. Above and below this opening patches of uranium about 1 mm square were spot-welded and filed thin. The cylinder, mounted in vacuum on a tungsten-Pyrex seal, was heated electrically. A Pyrex window for pyrometer observations was sealed in the tube. From the true temperature in the hole and the apparent temperature of the uranium patches the emissivity was calculated.

The thermionic tubes were of customary design. Filaments cut from the flat strip were hung by their ends as open loops. The oval rod, left straight, was mounted in a vertical position. Tungsten-Pyrex seals served as supports and heating current leads. Molybdenum collecting cylinders with insulated guard rings, outgassed before assembling the tubes, were afterward heated again by an induction furnace. Pyrometer windows in the cylinders were provided with magnetically operated shutters. Liquid-air traps were inserted between the tubes and any source of vapors. Outgassing periods up to 1000 hours gave final pressures of the order of 10^{-8} mm of Hg. Thermionic currents were measured with a high sensitivity Leeds and Northrup galvanometer.

In view of the uncertainties in published values[1] it was decided to make an approximate determination of the melting point. Curved segments were cut from the edges of a piece of the flat uranium strip so that the cross section at the thinnest point was about a third of its original value. In order to minimize gravitational effects a length of only 8 mm was supported horizontally on heavy vertical current leads. The strip was heated in vacuum until the thin portion melted. Its temperature was meanwhile followed continuously with a pyrometer.

The rough edges of one of the flat thermionic filaments were utilized for an approximate measurement of the coefficient of linear ex-

* Now at Elmhurst College, Elmhurst, Illinois.

[1] Cf. J. W. Mellor, *Treatise on Inorganic and Theoretical Chemistry* (Longmans, 1932), Vol. XII, p. 15.

pansion. Two notches were visible through the pyrometer window. The distance between them was measured with a comparator, at room temperature and at several temperatures in the pyrometer range. From these data the coefficient was calculated.

Discussion and Results

Clean uranium has a bright metallic luster similar to that of iron. This state was attained only when the vacuum system was thoroughly baked and flamed before the prolonged direct heating of the filament. The hot metal is reported to decompose water vapor. The presence of water from the flame used in sealing tubes together resulted in the appearance of a heavy oxide coating on samples initially bright, even at room temperature. Although no compound with hydrogen has been reported, uranium occludes considerable quantities of the gas. Heating in dry hydrogen was found to result in incomplete reduction of the oxide coating.

The non-uniformities of the flat specimens led at first to frequent hot spots and burning out of filaments. Rolling after annealing in vacuum improved the condition to some extent, although the edges cracked badly during rolling. It also became obvious that the melting point was somewhat lower than had been anticipated. Filaments always burned out near an end of the loop, appearing to soften at high temperatures and pull apart under their own weight. In many cases a sizable bead of metal formed on the lower lip of the melted aperture. No trace of vaporized metal was observable in any case.

Filaments warped, stretched and twisted in remarkable fashion during treatment, especially upon frequent heating and cooling. 12 cm of the oval rod stretched nearly 8 mm, or 6.5 percent, during thermionic study. The coefficient of linear expansion appears to have an abnormally high value (see below). The striking recalescence observed upon rapid heating or cooling has already been reported.[2] An x-ray study suggested by these phenomena is still in progress. It is hoped that a report may be published at a later date.

The temperature of the emissivity cylinder was increased, after preliminary outgassing, until one of the uranium patches softened and spread. This was done to insure good thermal contact and to minimize thermal gradient along the cylinder. To prevent further spread and possible alloying, readings were immediately taken on this patch at several lower temperatures. The average value found for the emissivity, at an effective wave-length of 0.67μ, was 0.51. This checks well with a value reported by Burgess and Waltenburg[3] for a similar method. Using a micro-sample fused on a Pt filament in hydrogen they obtained the value 0.55 at a wave-length of 0.65μ. They also indicate large changes with wave-length, and above the melting point.

Thermionic data were obtained from two flat filaments and from the oval rod. Currents of from 10^{-8} to 10^{-6} ampere were measured at temperatures between 950°K and 1300°K. During early stages of outgassing the curves of $\log I/T^2$ *vs.* $1/T$ often consisted of two portions with different slopes. This effect disappeared as heating was continued. Extreme values found for the work function during early stages were 3.15 and 3.60 volts. General progress with outgassing was from high to low values. The oval filament heated much more uniformly than the irregular flat filaments. It also exhibited satisfactory saturation at a much lower accelerating potential. Data from it have accordingly been more heavily weighted in arriving at the value, 3.27 ± 0.05 volts, for the thermionic work function of clean uranium. The value for the constant A of Richardson's equation also varied with the treatment of the specimen. Emitting areas were only roughly calculated. The final indicated value of about 6 is therefore only approximate.

In burning out the narrow strip for a melting point determination the final temperature rise, fuse-like, was uncontrollable and somewhat rapid. Fusion occurred just after the continuously variable pyrometer rheostat had reached the end of its range, and before a resetting could be made. Since the method is not one of precision, a repetition of the experiment was not considered worthwhile. However, our estimated value of 1700 ± 25°C for the melting point of uranium in

[2] W. L. Hole, R. Wright and H. B. Wahlin, Phys. Rev. **53**, 768 (1938).

[3] G. K. Burgess and R. G. Waltenburg, Bull. Nat. Bur. Stand. **11**, 591 (1915).

vacuum is considered more reliable than any value previously reported.

In measuring coefficient of linear expansion the total length observable with the comparator was only about 4 mm. Temperature measurements could be made only at room temperature and in the pyrometer range. Transition points, if they exist, lie between these limits. Repeated readings were not satisfactorily consistent. Doubtless the peculiar properties of uranium described at the beginning of this section partially account for the fact. The average value obtained for the coefficient of linear expansion over the range of 25°C to 1000°C is 4×10^{-5}, which is exceptionally large. No other value has appeared in the literature.

ACKNOWLEDGMENTS

Gladly is our indebtedness acknowledged to Dr. H. C. Rentschler, for providing one of the specimens; to the Wisconsin Alumni Research Foundation, for a grant in partial support of the project; and to Dr. H. B. Wahlin, for essential cooperation and assistance continued throughout the course of the experiments.

OCTOBER 15, 1939 PHYSICAL REVIEW VOLUME 56

Electronic Energy Bands in Metallic Tungsten[1]

MILLARD F. MANNING,* *University of Pittsburgh, Pittsburgh, Pennsylvania*

AND

MARVIN I. CHODOROW, *Massachusetts Institute of Technology, Cambridge, Massachusetts*

(Received June 21, 1939)

Calculations of the electronic energy bands in metallic tungsten are carried out by the Wigner-Seitz-Slater method. All numerical integrations were carried out on the M. I. T. differential analyzer. It is found that the *d* band is broken up into five sub-bands. Some of these *d* bands are found to be about fifteen electron volts in width. One is about two electron volts in width. The occupied energy range extends about five electron volts. The *s* band starts at a higher energy than the *d* bands and is occupied by much less than one electron per atom at the equilibrium interatomic distance. From the results of a previous paper, curves of E *vs.* k are plotted for the principal directions of propagation. From these, curves of the number of energy levels per unit energy range were determined by numerical and graphical methods which are described in an appendix. It is assumed that the $n(E)$ curve for tantalum is not greatly different from that for tungsten except that there is one less electron per atom. From the $n(E)$ curves the electronic contribution to the specific heat is calculated for the two metals and the results found to be in good agreement with the excess specific heat at high temperatures for both metals. The computed value does not agree with low temperature data on tantalum. There are no low temperature data for tungsten. Qualitative discussions of the differences in electrical resistance, temperature coefficient of resistance, and thermoelectric power of the two metals are given. The contribution of exchange effects to the paramagnetic susceptibility is treated by a rough model and it is shown that the assumption of the same value of the exchange integral for both metals gives satisfactory agreement with observed data.

CALCULATIONS of the electronic energy bands in solids have been carried out by either the Wigner-Seitz cellular method or by Slater's modification of that method for monovalent metals, for calcium, and for a number of insulators.[2, 3] No calculations by either of these methods have been reported for any transition metals, although some general characteristics have been discussed by Mott[4, 5, 6] in a series of

[1] A preliminary report of this work was presented at the Washington Meeting of the American Physical Society in April, 1938. Phys. Rev. **53**, 673 (1938).

* This work was started at M. I. T. and some of the senior author's part was done while he was at the University of Toledo, Toledo, Ohio.

[2] Na: E. Wigner and F. Seitz, Phys. Rev. **43**, 804 (1933); **46**, 509 (1934). Cu: H. M. Kritter, Phys. Rev. **48**, 664 (1935). Li: F. Seitz, Phys. Rev. **47**, 400 (1935); J. Millman, Phys. Rev. **47**, 286 (1935). Ca: M. F. Manning and H. M. Krutter, Phys. Rev. **51**, 761 (1937). C: G. E. Kimball, J. Chem. Phys. **3**, 560 (1935); F. Hund, Physik. Zeits. **36**, 888 (1935). C *et al.*: F. Hund and B. Mrowka, Ber. d. Sachs. Akad. d. Wiss. **87**, 185, 325 (1935). LiF: D. H. Ewing and F. Seitz, Phys. Rev. **50**, 760 (1936). NaCl: W. Shockley, Phys. Rev. **50**, 754 (1936).

[3] J. C. Slater, Phys. Rev. **45**, 794 (1934).

[4] N. F. Mott, Proc. Phys. Soc. **47**, 571 (1935).

[5] N. F. Mott, Proc. Roy. Soc. **A153**, 699 (1936).

[6] N. F. Mott, Proc. Roy. Soc. **A156**, 368 (1936).

papers and by Jones and Mott[7] in a recent paper which used a different approximation from that used here. In view of the great interest in the transition metals, it was believed that the detailed information obtained by the cellular method would justify the considerable amount of labor required to compute electronic energy bands for a transition element by Slater's method. Tungsten was chosen for this detailed study because of its practical importance and because for this metal there is a large amount of experimental material available. Necessary preliminaries to metallic calculations were self-consistent field calculations. These have been completed and reported in this journal.[8] Another necessary preliminary was the extension of Slater's discussion[3] of the electronic energy bands for the body-centered lattice. In his original paper, Slater used only eight atomic functions and satisfied boundary conditions at the centers of only eight faces of the atomic polyhedron. The difficulty in applying his results to a transition metal is that, in the eight functions, he included only three of the five d functions. Since the transition metals have a partly-filled d shell in the free atom, all of the d bands may be partly occupied in the metal, and hence if only three d functions are included, the band picture may be quite inaccurate. Slater's method has been extended to include boundary conditions at all fourteen faces of the atomic polyhedron. In setting up the wave function for a valence electron, the eight functions used by Slater and in addition the other two d functions, three more f functions, and a g function were included.[9] The details of this work are given in a previous paper to be referred to as I. In that paper relations were obtained between the energy of a valence electron and its momentum for important directions of propagation. The relations are transcendental equations in which the momentum k appears in certain tangent factors and the energy appears implicitly in the values of the radial wave functions and their derivatives at the radii corresponding to half the distance between nearest neighbors and at half the distance between next-nearest neighbors. The values of s_1, s_2, s_1', s_2',[10] etc. were found by numerical integration as in the Hartree method of calculating self-consistent fields. The potential used in this calculation was a modified form of that found by self-consistent field calculations for the tungsten atom. For all electrons inside of the $5p$ electron, the charge density used was the same as for the free atom. The results of the self-consistent field calculation for tungsten indicate that in the metal there will be a slight overlapping of the $5p$ wave functions. An attempt was made to allow for this, but it seems probable that it would have been as satisfactory to neglect this effect or allow for it by simply renormalizing the atomic charge density. The self-consistent field results show that nearly three-fourths of the charge density of the two $6s$ electrons in a tungsten atom lies *outside* the atomic sphere for metallic tungsten. This was taken as indicating that in the metal the s band would contain only a small fraction of an electron per atom. The self-consistent field results for the atom also show that about a third of the charge density of the four $5d$ electrons lies outside of the atomic sphere for the metal. Since in going from the atom to the metal a charge of over three electrons must be redistributed, the potential for a valence electron in metallic tungsten will be quite different from the potential of a valence electron in the atom and some correction must be made. As a first approximation to the potential for a valence electron in metallic tungsten, the potential due to the nucleus, inner electrons, and five $5d$ electrons was used. In finding the potential due to the $5d$ electrons, the atomic charge density normalized to the atomic sphere was used.

With this potential, integrations for the d and s functions were carried out. The results of the integration indicated the total width of the d bands to be about one and a half Bohr units,

[7] H. Jones and N. F. Mott, Proc. Roy. Soc. **A162**, 49 (1937).

[8] M. F. Manning and J. Millman, Phys. Rev. **49**, 848 (1936). M. F. Manning and L. Goldberg, Phys. Rev. **53**, 662 (1938).

[9] M. I. Chodorow and M. F. Manning, Phys. Rev. **52**, 731 (1934). Some errors appear in Table I of this paper. A corrected reprint may be obtained from one of the authors (M. F. M.) at the University of Pittsburgh.

[10] The notation is the same as in the previous paper—s_1 stands for the value of the s function of a given energy at the half-distance between nearest neighbors; s_2 is the value of the s function of a given energy at the half-distance between next nearest neighbors; and s_1' and s_2' are the derivatives with respect to r at the corresponding radii.

and that the bottom of the s band is at a considerably higher energy than the bottom of the d bands. Since the s band is very broad at this inter-atomic distance, the number of electrons per atom in the s band is small. Since there are spaces in the d bands for ten electrons per atom, these bands will be somewhat more than half-filled in tungsten.

For the next approximation, the same core potential was used as in the first approximation and the charge densities for the other five valence electrons were taken from the results of the first approximation. Since the first approximation shows that the two bottom d bands which can accommodate four electrons per atom are quite narrow, the charge distribution for two of the electrons was assumed to be the same as for a d function at the bottom of the d bands and the charge densities for the other three electrons were assumed to be those found for d functions with energies evenly spaced in the lower half of the d bands. With this new potential, integrations[11] were again carried out.

As a check on the consistency of the assumptions about the potential, the width of the d bands and curves of d' *vs.* E for the different approximations were compared. The discrepancies were so small as to indicate that little change would be produced by further stages of approximation. For the energy range considered, the d functions are the most sensitive to changes in the assumed field and hence the field is probably as near to being self-consistent as could be obtained without more elaborate methods of calculation. Furthermore, in the method used here, all exchange and correlation effects are neglected, and they would presumably have more effect than any departures from an exactly self-consistent field.

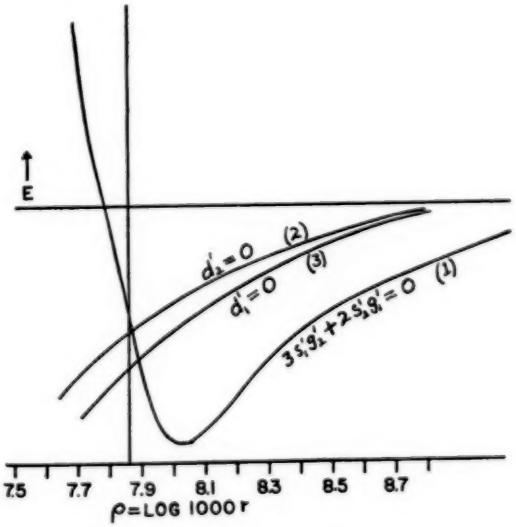

FIG. 1. E *vs.* log r. (E in Bohr units.)

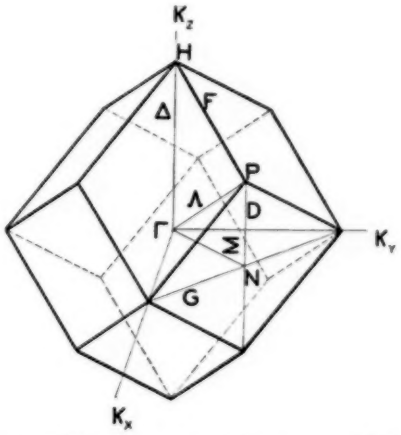

FIG. 2. Brillouin zone for body-centered lattice.

Rough calculations were also made of the way the positions of the bottoms of the various bands change with interatomic distance. Since the potential used in calculating these curves was either that of the free atom or that proper for the normal spacing, the curves of Fig. 1 are to be regarded as schematic. As shown in I, there will be three bands beginning at the energy for which $d_1'=0$, two bands beginning at the energy for which $d_2'=0$, and one band beginning at the energy for which $3s_1'g_2'+2s_2'g_1'=0$. There are other bands at higher energies, but they are not occupied under ordinary conditions and probably could not be accurately calculated by the method used here.

For a more detailed discussion of the electronic structure, it is necessary to determine the energy as a function of the momentum. As was discussed in I, for a general direction of propagation this would require the solution of a fourteenth-order secular determinant. This is too complicated for practical computation. However, for certain par-

[11] All of the integrations were carried out on the M. I. T. differential analyzer which was placed at the authors' disposal by Professor S. H. Caldwell of the Department of Electrical Engineering. The authors wish to thank Professor Caldwell and Mr. D. D. Terwilliger for their cooperation during the use of the differential analyzer.

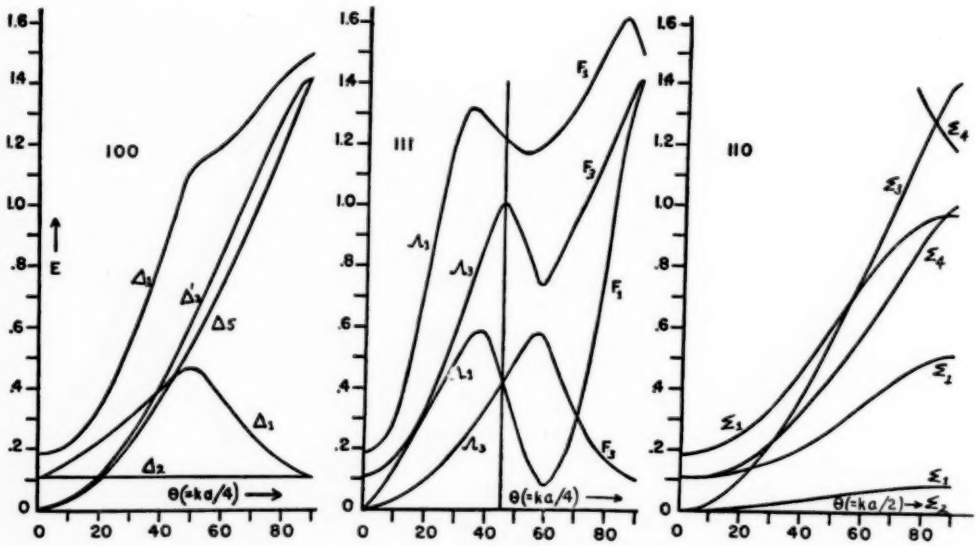

FIG. 3. E *vs.* k for the different directions of propagation.*

ticular directions of propagation, the fourteenth-order determinant can be factored into determinants of order not higher than the sixth. Expansion of such a determinant gives a transcendental equation, which usually has to be solved by numerical methods. The process is rather slow but once tables of the appropriate tangent factors have been made, it proceeds quite readily.

Figure 2 is the Brillouin zone for a body-centered lattice and on it the directions that have been investigated are indicated. Because of the symmetry of the body-centered cubic lattice, the polyhedron can be considered as consisting of forty-eight pyramids, each bounded by the 111, 110, and 100 lines and a quarter of one of the faces of the polyhedron. It is to be noted that for all the bounding edges of these pyramids, the energy as a function of k can be found by the solution of equations in I.

In Fig. 3 are the E *vs.* k curves for the directions of propagation, 111, 110, and 100. A certain amount of information can be obtained directly from these graphs, but for many properties it is more useful to have the density of states as a function of energy, $n(E)$. This requires a knowledge of E as a function of k throughout the Brillouin zone, i.e., the contours of constant energy in k space. Approximate contours can be obtained from our calculations by interpolation between the known directions. All the information obtained from the solutions for known directions can be represented on the developed surface of one of the pyramids, previously mentioned, which has one forty-eighth of the volume of the Brillouin zone. This developed surface is shown in Fig. 4. As can be seen, the known lines form a network on this surface. From the known lines and a knowledge of the manner in which the energy contours must intersect certain symmetry planes, plausible contours can be drawn. The details of determining these contours and also the method of calculating from them the density of energy states, $n(E)$, are discussed in the appendix. As an example, the contours of the band of lowest energy are shown in Fig. 5.

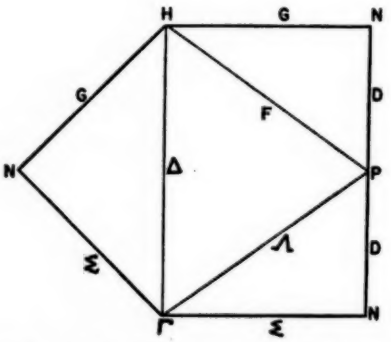

FIG. 4. Developed section of Brillouin zone.

* k in the scales for the abscissae refers to one of the components of the wave vector e.g. the wave vector along 111 is (k, k, k), along 110 it is $(k, k, 0)$ etc.

It is to be noticed that, when viewed in connection with the other contours in the same plane, the zero width E *vs.* k curves along various special directions, e.g. 100, 110, etc., are not as surprising as when only a particular direction is considered. The peculiar shape of the contours and in particular, the sharp corners, are a consequence of the intersection of two sets of contours, one set with wave functions odd with respect to reflection in the plane, and the other with wave functions even. This matter is discussed further in the appendix.

Graphs similar to Fig. 5 were also drawn for the other five bands, but they are not reproduced here. A comparison of the contours for the various bands show marked differences. The lowest band is narrow and, as can be seen, the contours are not at all like those for free electrons. The next two higher bands are wider, but do not have the characteristics of free electrons. The highest three bands are still wider and the contours resemble somewhat those for free electrons. The density of energy states, $n(E)$, was determined for each of the bands, the calculation being carried to energy levels several volts higher than those occupied in tungsten under normal conditions. The results for the separate bands are shown in the lower curves of Fig. 6 and the combined result for all the bands is shown in the upper curve.

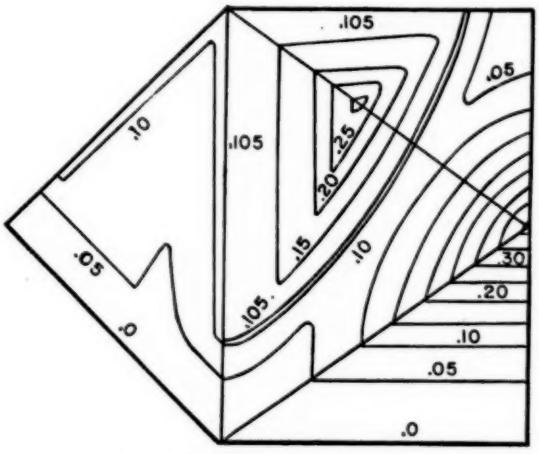

FIG. 5. Contours for band I.

Tungsten has six valence electrons per atom and the highest energy level which is occupied at the absolute zero of temperature is indicated by the right-hand vertical line in Fig. 6. Tantalum immediately precedes tungsten in the periodic table and has the same crystal structure. The calculations of $n(E)$ for tungsten should be roughly applicable to tantalum also. The left-hand vertical line in Fig. 6 corresponds to five valence electrons per atom.

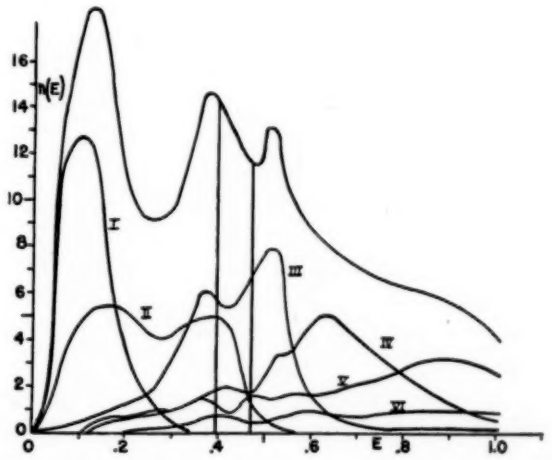

FIG. 6. $n(E)$ *vs.* E curves for the six lowest bands. The upper curve is the sum of the six lower curves. $n(E)$ = No. of states per unit energy range.

From the results expressed in Figs. 1 and 6, some general conclusions about the electronic structure of metallic tungsten and tantalum can be drawn. First, it is interesting to note the position and character of band VI which may be called the *s* band. It is seen that the number of electrons in this band is much less than one per atom and hence the neglect of *s* electrons in computing the potential is justified. More refined calculations might show an increase in the number in the *s* band, but the effect could hardly be appreciable. The position and nature of this band are of course in agreement with the very great "overlap" of the 6*s* atomic wave functions.

The lowest three bands and particularly band I probably contribute most of the binding energy which is known to be very large for these elements. Calculations of the binding energy[12] by the method used here are not practical, but rough calculations indicate that the zero of energy is about 0.5 or 0.6 of a Bohr unit below

[12] N. F. Mott and H. Jones, *Properties of Metals and Alloys* (Oxford Press, 1934), p. 146. This book will be referred to hereafter as M. & J. F. D. Rossini and F. R. Bichowsky, *Thermochemistry of Chemical Substances* (Reinhold, New York, 1936), p. 98.

the $5d$ and $6s$ eigenvalues. This is not inconsistent with the observed binding energies (about 225 kilocalories per mole or 9 ev per atom for tungsten).

The process of formation of the solid from the separate atoms may be visualized as follows: At large distances between atoms the configuration is d^4s^2 and the eigenvalues are about the same for the two types of electron. As the atoms are brought closer together, the s functions begin to overlap and the single level is broadened into a band of levels, while the d levels still maintain their atomic character. As the atoms are brought still closer together, the d levels become broadened into bands, and the s band becomes broadened so much that the upper levels in this band will have higher energies than the narrower d band, and hence there will be transitions from the s to the d band. This process will continue until the minimum of the s curve in Fig. 1 is reached. If the atoms are brought still further together the energy changes become more complicated. The binding energy of the electrons in the s band will now decrease. Since the d band is only about half filled, the binding energy of the electrons in this band will continue to increase.[13] For the first row of transition elements, evidence of various kinds indicates that these two effects balance each other at about the minimum of the s curve. For tungsten and tantalum the gain in binding energy due to the d band more than balances the decrease in binding in the s band and the interatomic distance will therefore be smaller than that corresponding to the minimum of the s curve. At smaller distances between atoms, the d band begins to broaden upward more than downward, corresponding to a repulsive force between atoms. At the actual interatomic distance there has been a considerable redistribution of charge—for tungsten, the self-consistent field calculations for the atom indicate nearly three electrons have been displaced from a position outside of the atomic sphere to a position inside of the atomic sphere. This large redistribution of charge and the change in shape of the d band are responsible for the repulsive force between the atoms and also for the comparatively low compressibility of tungsten and tantalum.

[13] For the noble metals and the elements immediately preceding them in the periodic table, the d band is full or nearly full, and this statement will no longer be true. For these elements the equilibrium distance will thus be determined to a considerable extent by the behavior of the s band.

Electronic Specific Heat

As was first shown by Sommerfeld,[14] the electrons in a metal contribute to the specific heat a term which is proportional to the absolute temperature, and which at ordinary temperatures is negligible compared with the contribution of the lattice vibrations. At low temperatures the lattice contributions are proportional to T^3, and hence at very low temperatures the electronic contribution will be appreciable and may even predominate. At temperatures above the Debye characteristic temperature the contribution from the lattice vibrations approaches the constant value of $3R$. However, Born and Brody have shown that if lattice vibrations have any anharmonicity, there will be, at high temperatures, a contribution to the specific heat which is proportional to the absolute temperature and may be positive or negative, depending upon the nature of the anharmonic terms in the potential energy of the lattice. It is difficult to estimate the sign of the anharmonic terms, as they will be positive for some directions of motion and negative for others.[15] It seems, however, to be reasonable to assume that at temperatures well below the melting point the anharmonic terms in the potential will make a negligible contribution to the specific heat.

The electronic contribution to the specific heat can be determined from a formula given by Stoner.[16] When higher powers of the temperature

Table I. *Electronic specific heat for tungsten and tantalum as determined by different methods.*

	Theoretical	Experimental (low temp.)	Experimental (high temp.)
Tungsten	$4.8\times10^{-4}T$		$5.1\times10^{-4}T$
Tantalum	$6.2\times10^{-4}T$	$27\times10^{-4}T$	$7\times10^{-4}T$

[14] Sommerfeld, Houston and Eckart, Zeits. f. Physik **47**, 1 (1928).

[15] One of the authors (M. F. M.) has discussed the material of this section with Professor N. F. Mott, Dr. Frederick Seitz and Dr. Lloyd A. Young. He wishes to thank them for their suggestions.

[16] E. C. Stoner, Proc. Roy. Soc. **154**, 656 (1936).

are neglected, this formula is:

$$(C_v)_e = (5.670/27.08) \times 10^{-4} n(E_0) RT, \quad (1)$$

where $(C_v)_e$ is the electronic contribution to the specific heat of a gram-atom, R is the universal gas constant, T is the absolute temperature, and $n(E_0)$ is the number of states of both spins per Rydberg unit of energy at the edge of the Fermi distribution. The value of $n(E_0)$ for tungsten found from Fig. 6 is 11.6 energy states per Rydberg unit of energy. For tantalum, the value is 14.7 energy states per Rydberg unit of energy.

Table I gives all of the pertinent data. The high temperature data are from measurements by Magnus and Holzmann.[17] The data for tantalum can be fitted quite well by an expression of the form $3R+AT$, where A has the value given. For tungsten the value given for A is that valid for temperatures above about 1000°K. The low temperature data for tantalum are from measurements by Daunt and Mendelssohn[18] upon the effect of a magnetic field upon the transition temperature of a super-conductor. As can be seen from Table I, the theoretical calculations for tungsten are in good agreement with the values for the excess specific heat at high temperatures. For tantalum, the theoretical calculations check the high temperature value which, however, is not at all in agreement with the low temperature value.

When the possibility of error in the measurements or in the reduction of the data is neglected, there are two possibilities of accounting for the discrepancy between the high and low temperature data for tantalum. One possibility is that the formula derived by Stoner is not applicable at low temperatures because it does not take exchange or correlation effects into account. A discussion of this point by Bardeen[19] and by Wigner[20] indicates that the effect of exchange is to spread out the levels near the top of the Fermi distribution and thus make the specific heat lower than is given by the Stoner formula, and thus increase the discrepancy. The correlation between electrons of the same spin tends to increase the specific heat, but no calculations have been made. The calculations of Wigner and Bardeen are based on a free electron model which is probably not applicable to a transition metal where the electrons retain much of their atomic character. Since tungsten has not been observed to be superconducting and since it has a high characteristic temperature, it should be possible to determine the electronic specific heat by direct measurements at liquid helium temperatures. The result of such a determination would help to clarify the points discussed here.

Another possibility for reconciling the high and low temperature data for tantalum is to assume that the difference is due to negative contributions to the specific heat from the anharmonic terms in the potential. The acceptance of this explanation would imply that the method used in this paper to calculate the energy levels in a metal is very inaccurate and that the numerical agreement with the high temperature data for *both* metals is highly fortuitous. It also implies a larger anharmonicity than seems reasonable.

It is difficult to obtain information about the anharmonic contributions to the specific heat because direct measurements of specific heats at liquid helium temperatures have been carried out for only a few metals. For nickel there are data available for both high and low temperature specific heats and a detailed analysis of these data by Stoner[21] seems to indicate that the anharmonic contribution to the specific heat is very small. Another line of evidence indicating that for nickel there is a large electronic contribution is the fact that for Ni-Cu alloys the excess specific heat decreases very rapidly with the addition of Cu.

Electrical and Related Properties

The detailed discussion of the resistance of a transition metal offers unsurmounted difficulties. Some general features of the problem have been discussed by Mott.[6] His discussion was based upon a model of two overlapping bands—an s band with approximately free electron characteristics and a d band with a high density of

[17] A. Magnus and H. Holzmann, Ann. d. Physik **3**, 602 (1929).
[18] J. G. Daunt and K. Mendelssohn, Proc. Roy. Soc. **A160**, 127 (1937).
[19] J. A. Bardeen, Phys. Rev. **50**, 1098 (1936).
[20] E. Wigner, Trans. Faraday Soc. **34**, 678 (1938).
[21] E. C. Stoner, Phil. Mag. **22**, 81 (1936).

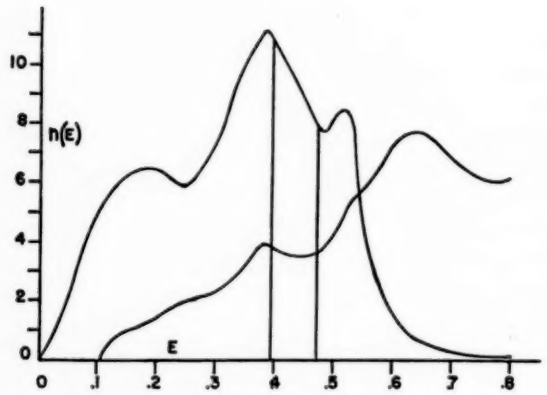

FIG. 7. $n(E)$ curves for bands II+III, and for bands IV+V+VI.

states and a high effective mass. His discussion can be carried over to our case, except that where he speaks of a d band we shall consider bands II and III which have a high density of vacant states and a low value for the effective number[22] of free electrons per atom. Where Mott refers to an s band we shall consider the highest three bands which have roughly free-electron characteristics and account for most of the conductivity. On the other hand, the vacant states in the lower bands contribute greatly to the scattering probability and hence make the mean free path much shorter. This is the essence of Mott's explanation of the low conductivity of the transition metals. In Fig. 7 are plotted the total number of states per unit energy range for bands II and III and the total number of states per unit energy range in the three higher bands. Since the lowest band is filled, it contributes to neither the conductivity nor the scattering and therefore is omitted from the graph. If Mott's explanation of the effect of the density of scattering states upon the resistance is correct, the different resistivities of tungsten and tantalum should be due in part to the greater density of scattering states for tantalum.

If the relation of the electrical conductivities of two different elements to their electronic structure is to be studied, it is necessary to make corrections for the different amplitudes of thermal vibration at a given temperature, for the different atomic volumes, and for the different scattering powers of the ions. Mott and Jones[23] have shown that the dependence upon the amplitude can be eliminated by comparing values of $\sigma/M\Theta^2$ where σ is the conductivity for a unit cube, M is the mass of the vibrating ion, and Θ is the Debye characteristic temperature. As Bridgman[24] and Hume-Rothery[25] have pointed out, the differing atomic volumes can be taken into account by considering not the conductivity of a unit volume, but the conductivity of a cube containing a constant number of atoms. This is equivalent to considering the quotient of σ/r where r is the atomic radius. For tantalum the value of $\sigma/Mr\Theta^2$ is 0.47 and for tungsten the value is 0.64. The ratio of these two values is 1.36. Neglecting the differing scattering powers of the two ions, this ratio should be very nearly equal to the ratio of the number of vacant states for tantalum to the number of vacant states for tungsten. The actual value as obtained from Fig. 7 is 1.27. The agreement between these values is an indication of the reasonableness of the explanation.

Variation of resistance of high temperatures

For temperatures above the characteristic temperature the change in resistance is caused chiefly by the increase in the amplitude of vibration of the scattering ions. There is also a change caused by the thermal expansion of the lattice. In addition, there may be an effect due to the change with temperature of the effective number of scattering states. A theory for the latter effect has been given by Mott.[26] The resistance at a high temperature can be written as

$$R/T=\text{const.}\ (1+BT)(1+AT^2), \qquad (2)$$

where R is the resistance, T the absolute temperature, B a constant determined from the thermal and mechanical properties, and A related to the shape of the $n(E)$ curve near the top of the filled states. If one assumes with Mott that the time of relaxation τ is proportional to

[22] The effective number of free electrons per unit volume is given by the formula:

$$N_{\text{eff}}=\frac{m}{4\pi^3\hbar^2}\int\left(\frac{\partial E}{\partial k_x}\right)^2\frac{dS_k}{|\text{grad}_k E|}.$$

See M. & J., p. 97.

[23] M. & J., p. 245.
[24] P. W. Bridgman, Proc. Am. Acad. **60**, 305 (1924).
[25] W. Hume-Rothery, *The Metallic State* (Oxford Press, 1931), p. 5.
[26] M. & J., p. 270; N. F. Mott, Proc. Roy. Soc. **153**, 699 (1936).

$1/n(E)$, A is proportional to $-[3(n')^2/n-n'']$, where the derivatives are taken at the top of the filled states. If the $n(E)$ curve for the scattering bands is concave toward the energy axis in the neighborhood of the highest occupied levels, then n'' is negative and hence A is negative. For this case it is to be expected that R/T would tend to decrease with increasing temperature. If the $n(E)$ curve is convex, the sign of A will depend on the comparative magnitude of the two terms comprising it. Reference to Fig. 7 indicates immediately that A should be negative for tantalum. Using analytic approximations to the $n(E)$ curve near the top of the filled states for both tantalum and tungsten, it was found that A was positive for tungsten and appreciably smaller in magnitude than for tantalum. Actually, the observed resistance[27] *vs.* temperature curve for tantalum is definitely concave toward the temperature axis and the curve for tungsten is slightly convex in agreement with the above considerations.

Thermoelectric power

Interpretations of the thermoelectric power have been given by Mott,[6] and by Jones and Mott.[7, 28] They point out that when the resistance is due to a high density of levels in a scattering band, the thermoelectric power will be negative if the density of scattering states decreases rapidly with E and positive if the density of scattering states increases rapidly with E. From this argument and Fig. 6, we conclude that tantalum should have a negative thermoelectric power. The observed values[29] are -5.0 microvolts/°C and -6.7 microvolts/°C at 100°C. As Mott[6] points out, the argument involving the density of states in the scattering bands is incomplete as it leaves out any discussion of the mechanism which produces the entire effect in a metal like copper or silver. Since these metals show a positive thermoelectric power of about 2 microvolts/°C, we might expect that when the density of scattering states changes only slightly with energy, the thermoelectric power would have about this value. Reference to Fig. 6 shows that for tungsten the slope of the $n(E)$ curve in the neighborhood of the highest occupied levels is small, so that we should expect a small, positive thermoelectric power. The observed values are +0.4 microvolt/°C at 0°C and +3.6 microvolts/°C at 100°C.

PARAMAGNETIC SUSCEPTIBILITY*

When exchange effects are neglected, the formula for the molar paramagnetic susceptibility is[30]

$$\chi_A = \mu^2 n(E_0) N, \tag{3}$$

where μ is the Bohr magneton, $n(E_0)$ is the number of energy states per atom per unit energy range, and N is Avogadro's number. When one takes the values of $n(E)$ as 11.6 for tungsten, and 14.7 for tantalum, the computed susceptibilities are 28 for tungsten and 35 for tantalum. The observed values are 45 for tungsten and 145 for tantalum.[31] The actual paramagnetic contribution from the electrons is greater than these amounts due to the diamagnetic contribution of the cores and of the valence electrons. The diamagnetic susceptibilities of the cores have been estimated by Stoner[31] and values of about 35 units found. We can thus say that the paramagnetic susceptibilities of the valence electrons must be at least 80 for tungsten and 180 for tantalum. These values are very much greater than those obtained from the simple formula. The difference has usually been believed due to exchange effects. There does not seem to have been any detailed analysis of the effect of exchange.

An approximate discussion can be carried out by the method suggested by Slater[32] for ferromagnetic substances. For each atom there are $n/2$ electrons per unit energy range for each direction of spin. Suppose that $\nu/2$ of them reverse their direction of spin, yielding a magnetic moment of $\nu\mu$ per atom. If this takes place in the presence of a magnetic field H, the changes in energy accompanying the process are: $H\nu\mu/2$,

[27] E. Gruneisen, *Handbuch der Physik* **10**, 16 (1928).
[28] M. & J., p. 310.
[29] G. Borelius, *Handbuch der Metall-Physik*, Vol. I, page 399.

* The authors wish to thank Dr. William Shockley for discussion about this section.
[30] M. & J., p. 185. The n used in this article is twice as large as that used in this reference.
[31] E. C. Stoner, *Magnetism and Matter* (Methuen, 1934), pp. 508, 271.
[32] J. C. Slater, Phys. Rev. **49**, 537 (1936).

due to reorientation, and $\nu^2/4J$, due to the fact that there are more exchange integrals between electrons of parallel spin than there were in the unmagnetized state. When the electrons reverse their spins, they must be lifted to higher energy levels and this requires an energy $\nu^2/2n$. Hence we have

$$\nu^2 J/4+H\mu\nu/2=\nu^2/2n \tag{4}$$

or

$$\nu\mu=\frac{\mu^2 n}{1-Jn/2}H \tag{5}$$

and the expression for the molar susceptibility becomes

$$\chi_A=\frac{\mu^2 n(E_0)N}{1-Jn(E_0)/2}. \tag{6}$$

It is noted that the correction factor is in the proper direction and has the correct dependence upon n to explain the fact that the discrepancy between the observed value and that calculated from the simple equation is greater for tantalum than for tungsten. If there were some satisfactory method of determining J, it would be possible to compute χ_A. Since there does not seem to be any method of computing J, we shall proceed differently and use the measured values of χ_A to solve for J. For tungsten this gives

$$1-5.8J=28/80;\quad J=.11 \text{ Rydberg units.} \tag{7}$$

For tantalum

$$1-7.3J=35/180;\quad J=.11 \text{ Rydberg units..} \tag{8}$$

The fact that the values of J for the two elements come out so nearly equal is evidence for the part that exchange forces play in determining the paramagnetic susceptibility. The value of J is rather large, but there does not seem to be any independent method of checking it.

Validity of the Method

There are a number of approximations involved in the method of calculation used and it is difficult to estimate the accuracy of the results. However, the authors believe that the agreement with experimental results, although usually only qualitative, indicates that the computations give a representative picture of the electronic structure of metallic tungsten and tantalum.

Perhaps the most serious approximation is the complete neglect of exchange and correlation effects. These effects are important in determining the binding energy and for this reason no attempt to calculate it has been made. Exchange effects might be expected to cause a contraction of the wave functions and hence a narrowing of the bands. For instance, Hartree[33] has found that exchange effects produce an appreciable change in the outer portions of the $3d$ wave functions for copper. There are, however, reasons for believing that this effect will be less pronounced in tungsten. For all of the electrons inside of the $4f$ electrons in tungsten the electrostatic contribution to the potential is so large that exchange effects will produce only a small effect. For the $4f$, $5s$, $5p$ electrons the solutions of Fock's equations will undoubtedly give an appreciable contraction. As far as the $5d$ electrons are concerned, this contraction acts to decrease the effective electrostatic potential. This decrease in the electrostatic potential has the opposite effect upon the $5d$ wave functions from the exchange effects, which furthermore are not as important in a partly-filled shell as in a filled shell. Another reason for discounting the effect of exchange on the $5d$ electrons in tungsten is the fact that throughout the self-consistent field calculations for the atom and the metal, these wave functions were not unduly sensitive to changes in the assumed field. For copper, Hartree found that the $3d$ wave functions were very sensitive to the assumed field.

Another point where errors may have entered was in the use of the differential analyzer. A problem as complicated as this could be handled even on the differential analyzer only by a compromise between the accuracy desired and the time required. None of the calculations for either the atom or the metal was checked by numerical integration, but certain cross-checks indicated that the errors introduced in the computation are not serious.

In general, it might be remarked that the entire computational process showed a considerable tendency toward cancellation of errors. For instance, the principal effect of a change in the assumed potential is to shift the entire band

[33] D. R. and W. Hartree, Proc. Roy. Soc. **157**, 490 (1936).

structure in energy without changing its shape. Slight changes in the curves of s, s', d, d', as a function of energy produced no appreciable changes in the E *vs.* k curves. In addition, it turned out that the final $n(E)$ curves were quite insensitive to changes in the contours in k space. (See Appendix A.)

The Slater method of computing metallic wave functions is, of course, only approximate. In an attempt to estimate the accuracy of the approximation, Shockley[34] has tested the cellular method by applying it to the case of a constant potential where the exact answer is available for comparison. He finds that when there is a single occupied band and a number of excited bands at higher energies, the lowest band will be determined with satisfactory accuracy, but the excited bands will be much less accurately determined. The argument is not as definite when there are a number of occupied bands, all having about the same energy, but it seems likely that for this case all of the bands will be determined with some intermediate accuracy. There is also the point that for metallic tungsten, the wave functions retain much of their atomic character, and therefore it might be expected that the results are better than Shockley's argument would indicate.

Jones and Mott[7] have carried out a discussion of the transition metals, using the approximation of tight binding. This approximation is more accurate than the cellular method when the overlap of the d functions is small and less accurate when the overlap is large. Using this criterion and the results of self-consistent field calculations, it seems that their method might be more accurate for the first row of transition elements, and the cellular method for the second and third rows.

The calculations of which this paper is a report were carried out under the general direction of Professor J. C. Slater. The authors wish to thank him for his helpful comments and suggestions.

Appendix A

We shall outline briefly here the method of obtaining approximate energy contours and $n(E)$ curves. To obtain the contours, we have available the E *vs.* k curves for the various special directions (Δ, Λ, Σ, D, G, F) and also the exact contours in the 100 and 110 planes for those states whose wave functions are odd with respect to reflection in those planes. From this information, all of which is obtained from the solution of equations in I, we must determine the contours throughout the Brillouin zone for each of the six bands. Mention must be made here that in classifying the energy levels in bands, all of one E *vs.* k curve, (obtained from one equation) does not necessarily belong to one band. The same applies to the exact contours in the special planes which we have mentioned above. In each band the energy is a continuous function of the reduced wave vector k and for two bands the energy level of one (for each k) is always higher than, or equal to, the corresponding level of the other. Thus, although the bands may touch at some values of k (degeneracy), they can never cross. For two E *vs.* k curves, on the other hand, this is not true. An E *vs.* k curve for a particular direction is determined by the property that all the energy states have wave functions of the same symmetry.[35] Thus there is nothing to prevent two E *vs.* k curves from crossing and if two curves for a given direction do cross, the two lower halves are taken as belonging to one band and the two upper halves to the other band. This procedure often gives the energy contours in a band queer shapes, including corners, where we have shifted from the lower (upper) half of one E *vs.* k curve to the lower (upper) half of another curve which intersects the first. In such a shift, the wave function in the band changes discontinuously with k, but the energy is continuous.

Our general procedure in finding the contours of a band was first to find the contours for the developed surface shown in Fig. 5. These contours were obtained by interpolation between the various lines on the surface, for which the energy as a function of k is known. The contours inside the pyramid bounded by the surface of Fig. 5 were obtained by interpolation from the contours on the surface. We have previously mentioned the possibility of the wave function in a band changing discontinuously at a point of degeneracy, with a corresponding peculiarity in the shape of the contour. This would seem to militate against results obtained by interpolation, if many of these points of contact occur distributed throughout the Brillouin zone. Actually, however, Herring[36] in a study of the types of contacts possible, has shown that two bands can touch only along symmetry axes and planes.[35] In terms of our basic pyramid, this means that corners, or any other irregularities due to band contacts, will be confined to the surface of the pyramid only, the surface being composed entirely of symmetry planes. If by some method we can get the contours on the surface, including any "contact" irregularities, fairly accurately, we can interpolate the interior contours with confidence since none of these "contact" irregularities can occur in the interior. In obtaining these surface contours, another property of the "contacts" found by Herring has been useful. He showed that in any symmetry axis or plane only E *vs.* k curves of

[34] W. Shockley, Phys. Rev. **52**, 866 (1937).

[35] In the language of group theory, all the states of one E *vs.* k curve for a particular direction belong to the same irreducible representation of the group which leaves a k vector in that direction invariant.

[36] C. Herring, Phys. Rev. **52**, 365 (1937).

different symmetries, belonging to different irreducible representations, can cross. For the symmetry planes constituting the surface of the pyramid, there are two symmetry types—contours with wave functions odd under reflection and contours with wave functions even. Applied to these contours, Herring's[37] result means that the only band contacts which can occur on the surface are due to the intersection of odd and even contours. (By even or odd contours we mean, of course, contours with wave functions having these symmetries.) Intersections between two sets of even contours or two sets of odd contours are forbidden. These statements about the nature of band contacts in symmetry planes, apply only to such portions of the symmetry planes as are not symmetry axes. For the latter, there are more than two symmetry types and we can no longer speak of odd and even contours. Two sets of contours which are odd (even) in a plane, may belong to different irreducible representations of an axis and may intersect *along the axis*. This actually does occur in our case, both Δ_1 and Δ_2' are even in the 110 plane, but these intersections offer no difficulty, as we know the energy exactly for all the axes. The fact that for all other portions of the symmetry planes, only odd and even contours can intersect, gives us a method of determining the contours in these regions quite accurately, even to the corners occurring at the intersections.

We can obtain all of the odd contours in the various planes from the solutions of equations given in I. For the even contours, similar equations could be found, but these would be so unwieldy that no attempt was made to use them. Instead, the even contours were interpolated from the known portions of these contours, that is, the E *vs.* k curves along the various axes. Since two sets of even contours cannot intersect, there is no problem of "contact" irregularities to vitiate interpolation methods. The lowest energy states along each axis belong to one set of contours, the next higher states to another set, etc. Having thus obtained both even and odd contours, we can determine the intersections of the two and apportion the various sections among the six bands according to their energy. With the contours on the surface of the basic pyramid known, the interior contours for each band can be found by interpolation.

From these contours, we determine the number of states per unit of energy, $n(E)$. In practice, it is easier to find first the number of states with energy less than a particular energy E. $n(E)$ is then determined by numerical differentiation. For any band the number of states with energy less than E is proportional to the volume of that portion of the Brillouin zone contained within the surface of energy E. This surface may consist of two or more sheets if the energy does not vary monotonically within the band. To obtain approximately the volume contained within an energy surface, we proceed as follows: The basic pyramid of the Brillouin zone is cut by ten evenly-spaced planes parallel to the 100 plane. In each of these planes the area enclosed by the cross section of the energy surface was measured by a planimeter. From these areas, plotted as a function of the height above the 100 plane, another integration gives the volume inside the energy surface.

In obtaining the contours, we have gone through the somewhat elaborate process of obtaining the odd and even contours in the symmetry planes separately, and then putting together pieces of each to obtain the contours of the individual bands. One could use the simpler, although theoretically less justifiable method of interpolating the contours of each band directly from the known energy states along the axis, that is, connect the lowest states along each axis by one set of contours for the lowest band, the next higher states by another set of contours for the next higher band, etc. As previously pointed out, such procedure tends to smooth out any irregularities in the bands. One cannot say *a priori* how important these irregularities will be and how seriously smoothing them out will affect the final results. Therefore, the more elaborate method which locates these contacts would seem to be preferable. We have also used the simpler method of interpolating each band directly. The resultant contours, of course, had no corners, but did resemble quite closely the contours found by the more accurate method. The change in the $n(E)$ curves would be even smaller than in the contours. In general, the entire process of determining the $n(E)$ curves turned out to be surprisingly insensitive to the assumed interpolations between known directions.

Note added in proof:—The value of $27\times10^{-4}T$ for the low temperature electronic specific heat of Ta was taken from a paper by Mott and Jones (reference 7). A closer examination of the data given by Daunt and Mendelssohn makes us believe that this value is higher than the data warrant and that for Ta the experimental uncertainties are considerably larger than for other elements measured by Daunt and Mendelssohn.

[37] One of the authors (M. I. C.) wishes to thank Dr. Herring for enlightening discussions about the results in his paper.

Spinor Equations for the Meson and Their Solution When No Field Is Present

A. H. TAUB
University of Washington, Seattle, Washington
(Received May 5, 1939)

The spinor equations equivalent to the Proca equations for the meson are found. They differ from those proposed by Dirac in three ways: (1) They contain two symmetric spinors A_{1AB}, A_{2AB} and a spinor $B^{A'}{}_{B}$, whereas the Dirac ones contain only one symmetric spinor and the spinor $B^{A'}{}_{B}$. (2) They are invariant under spin transformations corresponding to both proper and improper Lorentz transformations whereas the Dirac ones are invariant under the former alone. (3) When a field is present they contain terms which cannot be obtained from the equations for free particles by replacing the operator p_ν by $p_\nu - e\varphi_\nu/c$ as was proposed by Dirac. In case there is no field present the equations can be solved by introducing two pairs of simple spinors (ψ^A, φ^A) and (χ^A, η^A) each of which satisfies a Dirac equation for a free particle of spin one-half. It is proposed to interpet each pair of spinors as representing a free particle of mass m_1 and m_2, respectively. With this interpretation it follows that a free particle of mass m and spin one satisfying the Proca equations is equivalent to a pair of particles of masses m_1 and m_2 satisfying the Dirac equations in the following sense: If the three particles of masses m, m_1 and m_2 are in states determined by the energy momentum vectors p_ν, $p_{1\nu}$, and $p_{2\nu}$, respectively and if $m \neq 0$, then $p_{1\nu} = m_1/m p_\nu$ and $p_{2\nu} = m_2/m p_\nu$, $m = m_1 + m_2$; and the spin of the Proca particle is the vector sum of the spins of the two Dirac particles.

IN another paper,[1] the two component spinor formalism was used to obtain the tensor equations equivalent to the spinor equations proposed by Dirac[2] for a particle of spin one. These equations were shown to differ from those proposed by Proca.[3] In this paper we use the method and notation of T. E. and obtain the spinor equations equivalent to the Proca equations. In case there is no field present, the spinor equations are solved by using two pairs of simple spinors which satisfy Dirac equations for particles of spin one-half for particles of mass m_1 and m_2.

In the appendix we give a list of formulas taken from T. E. and used in this paper together with a brief summary of the notation. The numbering of the formulas given there is the same as that of T. E.

1. Spinor Equations Equivalent to the Proca Equations

The Proca equations for a meson, a particle of mass m, spin one and charge e in an electromagnetic field described by a vector potential ϕ_μ are

$$KG_{\mu\nu} = \left(\frac{\partial}{\partial x^\mu} - \frac{ie}{\hbar c}\varphi_\mu\right)U_\nu - \left(\frac{\partial}{\partial x^\nu} - \frac{ie}{\hbar c}\varphi_\nu\right)U_\mu, \quad (1.1)$$

$$\left(\frac{\partial}{\partial x^\nu} - \frac{ie}{\hbar c}\varphi_\nu\right)G^{\mu\nu} = KU^\mu (\mu, \nu = 1, 2, 3, 4), \quad (1.2)$$

where

$$K = mc/\hbar, \quad (1.3)$$

c is the velocity of light and $\hbar$ is Planck's constant divided by 2π and we have used the summation convention. We have used the tensor $g^{\mu\nu}$ to raise indices. In a preferred coordinate system $g^{\mu\nu} = 0$ unless $\mu = \nu$ and then $-g^{11} = -g^{22} = -g^{33} = g^{44} = 1$.

From Eqs. (1.2) it follows that

$$K\left(\frac{\partial}{\partial x^\mu} - \frac{ie}{\hbar c}\varphi_\mu\right)U^\mu = -\frac{ie}{2\hbar c}G^{\mu\nu}F_{\mu\nu}, \quad (1.4)$$

where

$$F_{\mu\nu} = \partial\varphi_\nu/\partial x^\mu - \partial\varphi_\mu/\partial x^\nu \quad (1.5)$$

and is the antisymmetric tensor describing the electromagnetic field.

We define the dual of an antisymmetric tensor by

$$G^{\dagger\mu\nu} = \tfrac{1}{2}g^{-\frac{1}{2}}\epsilon^{\mu\nu\sigma\tau}G_{\sigma\tau}, \quad (1.6)$$

where $g^{\frac{1}{2}}$ is the square root of the determinant of $g_{\mu\nu}$ and is $+(-1)^{\frac{1}{2}}$ in a preferred coordinate system and $\epsilon^{\mu\nu\sigma\tau}$ is zero unless all the indices are different. In that case it is $+1$ if $\mu\nu\sigma\tau$ is an even permutation of 1234 and -1 if $\mu\nu\sigma\tau$ is an odd permutation of 1234. It may be readily verified that the process of raising and lowering indices

[1] A. H. Taub, "Tensor Equations Equivalent to the Dirac Equations." (To appear in Ann. of Math.; referred to henceforth as T. E.)
[2] P. A. M. Dirac, Proc. Roy. Soc. **A155**, 447 (1936).
[3] A. Proca, J. de phys. et rad. **7**, 347 (1936).

by means of $g_{\mu\nu}$ and $g^{\mu\nu}$ commutes with the process of taking the dual. Under a transformation with positive determinant $G^{\dagger\mu\nu}$ transforms as an antisymmetric tensor whereas under a transformation with a negative determinant it transforms as follows:

$$G^{\dagger\mu\nu *}=-G^{\sigma\tau}\frac{\partial x^{\mu *}}{\partial x^{\sigma}}\frac{\partial x^{\nu *}}{\partial x^{\tau}}.$$

From Eq. (1.1) and (1.6) it follows that

$$\left(\frac{\partial}{\partial x^{\nu}}-\frac{ie}{\hbar c}\varphi_{\nu}\right)G^{\dagger\mu\nu}=-\frac{ie}{\hbar c}U_{\tau}F^{\dagger\mu\tau}. \tag{1.7}$$

In case there is no field present, this equation becomes

$$\partial G^{\dagger\mu\nu}/\partial x^{\nu}=0,$$

which is the same as

$$\frac{\partial G_{\mu\nu}}{\partial x^{\rho}}+\frac{\partial G_{\nu\rho}}{\partial x^{\mu}}+\frac{\partial G_{\rho\mu}}{\partial x^{\nu}}=0, \quad \rho\neq\mu\neq\nu.$$

This equation in turn is the necessary and sufficient condition that $G_{\mu\nu}$ be expressible in the form:

$$G_{\mu\nu}=\partial U_{\nu}/\partial x^{\mu}-\partial U_{\mu}/\partial x^{\nu}.$$

The one-to-one correspondence between four dimensional vectors and spinors of the form $B_{A'B}$ may be used to express the vector U_{τ} in spinor form. This is done by using the spinor $g^{\sigma}{}_{A'B}$.[4] Then it follows that

$$U_{\tau}=2g_{\tau A'B}B^{A'B} \tag{1.8}$$

and $B^{C'B}$ is uniquely determined by the equations

$$B^{A'B}=\tfrac{1}{4}U^{\tau}g_{\tau}{}^{A'B}. \tag{1.9}$$

The tensor $G_{\mu\nu}$ may be expressed in spinor form by using the one-to-one correspondence between self-dual antisymmetric tensors and symmetric second order spinors given by Laporte and Uhlenbeck.[5] This correspondence is readily expressed by means of the spinor $S^{\sigma\tau}{}_{AB}$ as follows[6]

$$\tfrac{1}{2}(G_{\mu\nu}+G^{\dagger}{}_{\mu\nu})=S_{\mu\nu AB}A_1{}^{AB}. \tag{1.10}$$

There is another self-dual tensor associated with the tensor $G_{\mu\nu}$, and it determines another symmetric spinor by the equations

$$\tfrac{1}{2}(\bar{G}_{\mu\nu}+(\bar{G}_{\mu\nu})^{\dagger})=S_{\mu\nu AB}A_2{}^{AB}.$$

It may be verified from Eq. (1.6) that

$$(\bar{G}_{\mu\nu})^{\dagger}=-\text{complex conjugate of } G^{\dagger}{}_{\mu\nu}.$$

Hence we have

$$\tfrac{1}{2}(G_{\mu\nu}-G^{\dagger}{}_{\mu\nu})=\bar{S}_{\mu\nu AB}\bar{A}_2{}^{AB}, \tag{1.11}$$

or

$$G_{\mu\nu}=S_{\mu\nu AB}A_1{}^{AB}+\bar{S}_{\mu\nu AB}\bar{A}_2{}^{AB}$$

and

$$G^{\dagger}{}_{\mu\nu}=S_{\mu\nu AB}A_1{}^{AB}-\bar{S}_{\mu\nu AB}\bar{A}_2{}^{AB}. \tag{1.12}$$

From Eq. (1.20) of T. E. it follows that the equations determining $A_1{}^{AB}$ and $A_2{}^{AB}$ are

$$A_1{}^{AB}=\tfrac{1}{16}(G_{\mu\nu}+G^{\dagger}{}_{\mu\nu})S^{\mu\nu AB}=\tfrac{1}{8}G_{\mu\nu}S^{\mu\nu AB}, \tag{1.13}$$

$$\bar{A}_2{}^{AB}=\tfrac{1}{16}(G_{\mu\nu}-G^{\dagger}{}_{\mu\nu})\bar{S}^{\mu\nu AB}=\tfrac{1}{8}G_{\mu\nu}\bar{S}^{\mu\nu AB}, \tag{1.14}$$

since $S^{\mu\nu AB}$ is self-dual.

We shall now obtain the spinor form of the Proca equations. Substituting Eqs. (1.10) into the sum of (1.2) and (1.7), multiplying by $g_{\mu}{}^{C'D}$ and using Eq. (1.22) of T. E., we obtain

$$g^{\nu A'}{}_{C}\left(\frac{\partial}{\partial x^{\nu}}-\frac{ie}{\hbar c}\varphi_{\nu}\right)A_1{}^{CB}=-KB^{A'B}+\frac{ie}{\hbar c}C^{A'B}, \tag{1.15}$$

where

$$C^{C'D}=\tfrac{1}{4}F^{\dagger\mu\tau}U_{\tau}g_{\mu}{}^{C'D}. \tag{1.16}$$

Similarly it follows that

$$\bar{g}^{\nu A'}{}_{C}\left(\frac{\partial}{\partial x^{\nu}}-\frac{ie}{\hbar c}\varphi_{\nu}\right)\bar{A}_2{}^{CB}=-KB^{B'C}-\frac{ie}{\hbar c}C^{B'C}. \tag{1.17}$$

By substituting from Eqs. (1.1) and (1.8) in Eq. (1.12) and again using T. E. (1.22) we obtain

$$\left(\frac{\partial}{\partial x^{\nu}}-\frac{ie}{\hbar c}\varphi_{\nu}\right)(g^{\nu A'}{}_{B}B_{A'C}+g^{\mu A'}{}_{C}B_{A'B})=2KA_{1CB}.$$

But

$$\left(\frac{\partial}{\partial x^{\nu}}-\frac{ie}{\hbar c}\varphi_{\nu}\right)(g^{\nu A'}{}_{C}B_{A'D}-g^{\nu A'}{}_{D}B_{A'C})=\rho\epsilon_{CD},$$

where $\epsilon_{12}=-\epsilon_{21}=1$ and all other components are zero, since the left member is antisymmetric in

[4] The one-to-one nature of the correspondence follows from Eqs. (1.15) and (1.16) of the appendix. We shall use the convention that Greek indices take on the values 1 to 4 and capital Latin indices the values 1 and 2.

[5] Laporte and Uhlenbeck, Phys. Rev. **37**, 1380 (1931).

[6] See appendix and §1 of T. E. The one-to-one nature of this correspondence follows from Eqs. (1.20) and (1.26) of the appendix.

C and D and there is only one antisymmetric second order spinor, namely ϵ_{CD}. Multiplying both sides by ϵ^{CD} and summing, we have

$$\rho=\left(\frac{\partial}{\partial x^\sigma}-\frac{ie}{\hbar c}\varphi_\sigma\right)g_\sigma{}^{A'D}B_{A'D}$$

$$=\tfrac{1}{2}\left(\frac{\partial}{\partial x^\sigma}-\frac{ie}{\hbar c}\varphi_\sigma\right)U^\sigma=-\frac{ie}{4K\hbar c}G^{\mu\nu}F_{\mu\nu}.$$

Hence

$$g^{\nu A'}{}_B\left(\frac{\partial}{\partial x^\nu}-\frac{ie}{\hbar c}\varphi_\nu\right)B_{A'C}$$

$$=KA_{1CB}-\frac{ie}{8K\hbar c}G^{\mu\nu}F_{\mu\nu}\epsilon_{BC}. \quad (1.18)$$

Similarly we may obtain

$$\bar{g}^{\nu B'}{}_D\left(\frac{\partial}{\partial x^\nu}-\frac{ie}{\hbar c}\varphi_\nu\right)B_{A'B}$$

$$=K\bar{A}_{2AD}-\frac{ie}{8K\hbar c}G^{\mu\nu}F_{\mu\nu}\bar{\epsilon}_{DA}. \quad (1.19)$$

Equations (1.15), (1.17), (1.18), and (1.19) are equivalent to (1.1) and (1.2) since the latter may be obtained from the former in the same manner as the tensor equations equivalent to the Dirac equations for a free particle of spin one, namely

$$g^{\nu A'}{}_B\frac{\partial}{\partial x^\nu}A^{BC}=-KB^{A'C}, \quad (1.20)$$

$$g^{\nu A'}{}_B\frac{\partial}{\partial x^\nu}B_{A'D}=KA_{BD}, \quad (1.21)$$

were obtained (see T. E. §4).

Kemmer[7] has stated that the tensor form of Eqs. (1.20) and (1.21) is not unique and has written two sets of tensor equations for the tensor form of Eqs. (1.20) and (1.21). One of these is the set of Proca equations. From the results given above we see that a unique set of spinor equations different from (1.20) and (1.21) are equivalent to the Proca equations. Moreover, in T. E. it has been shown that the tensor equations equivalent to (1.20) and (1.21) differ from the Proca equations unless U_ν is real. If, however, U_ν and $G_{\mu\nu}$ are real and no field is present then $A_1{}^{AB}=A_2{}^{AB}$, $B_{A'B}$ is Hermitian and Eqs. (1.15), (1.17), (1.18) and (1.19) become identical with Eqs. (1.20) and (1.21) and the complex conjugates of the latter two.

Kemmer ascribes the ambiguity of tensor forms for a set of spinor equations to the fact that "In the spinor notation no specification of the transformation of the wave functions for the reflexions of the coordinate system is implied." However, the isomorphism between Lorentz transformations on the variables x^σ and the group of linear and antilinear geometric transformations[8] in the spin space is such that linear transformations of the form

$$\varphi^A=P^A{}_B\psi^B \quad (1.22)$$

correspond to proper Lorentz transformations (those of determinant $+1$) and antilinear transformations of the form

$$\bar{\varphi}^A=P^{A'}{}_B\psi^B \quad (1.23)$$

correspond to improper Lorentz transformations (those of determinant -1). An example of a transformation of the type (1.23) is the transformation

$$\bar{\varphi}^A=\psi^A \quad (1.24)$$

and it corresponds to the improper Lorentz transformation

$$x^{1*}=x^1, \quad x^{2*}=x^2, \quad x^{3*}=-x^3$$

and

$$x^{4*}=x^4, \quad (1.25)$$

as may be verified from the values of the components of the spinor $g^{\sigma A'}{}_B$ in the particular coordinate system given in the appendix and the statement of the isormorphism theorem given there.

The numerical invariance of the coefficients $g^{\sigma A'}{}_B$ in Eqs. (1.15), (1.17), (1.18) and (1.19) under arbitrary Lorentz transformations on the

[7] Kemmer, Proc. Roy. Soc. **A166**, 134 (1937).

[8] A geometric transformation is a permutation of the points of a space in contrast to a coordinate transformation which is a renaming of the points. See §2 of T. E. and also B. L. Van der Waerden, *Die Gruppen Theoretischen Methode in der Quantenmechanik* (J. Springer, Berlin, 1932) p. 83.

variables x^σ, provided we replace A_{1AB}, A_{2AB} and $B^{A'}{}_B$ by suitable linear combinations, may be proved by the same method used in T. E. §2 for the Dirac equations for a particle of spin one half. We shall give a different proof here in detail so as to compare these equations to (1.20) and (1.21).

Since both sets of equations are spinor equations, they are invariant in form under arbitrary constant spin coordinate transformations. Furthermore, linear transformations of the form (1.22) behave formally as coordinate transformations. Hence both sets of equations retain their form if we perform a transformation of the type (1.22). If we now make a proper Lorentz transformation on the variables x^σ, this will induce a transformation on the $g^{\sigma A'}{}_B$, but this can be compensated for by a transformation of the type (1.22) which will leave the equations in the same form and they will have the same numerical coefficients $g^{\sigma A'}{}_B$.

In order to prove the numerical invariance of the coefficient $g^{\sigma A'}{}_B$ in Eqs. (1.15), (1.17), (1.18) and (1.19) under improper Lorentz transformations it is sufficient to prove it for the Lorentz transformation (1.25) since every other improper Lorentz transformation may be written as a product of (1.25) and a proper one. From the values given for the spinor $g^{\sigma A'}{}_B$ in the appendix it may be readily verified that

$$g^{\sigma A'}{}_B\left(\frac{\partial}{\partial x^\sigma}-\frac{ie}{\hbar c}\varphi_\sigma\right)=g^{\sigma A'}{}_B{}^*\left(\frac{\partial}{\partial x^{\sigma *}}-\frac{ie}{\hbar c}\varphi_\sigma{}^*\right)$$
$$=\bar{g}^{\sigma A'}{}_B\left(\frac{\partial}{\partial x^{\sigma *}}-\frac{ie}{\hbar c}\varphi_\sigma{}^*\right),$$

where $x^{\sigma *}$ and $\varphi_\sigma{}^*$ are obtained from x^σ and φ_σ by using the transformation (1.25).

If we perform the transformation (1.25) on the x^σ and follow this by the transformation

$$\begin{aligned} &A_1{}^{AB}\to A_1{}^{AB*}=\bar{A}_2{}^{AB},\\ &\bar{A}_2{}^{AB}\to\bar{A}_2{}^{AB*}=A_1{}^{AB},\\ &B^{A'B}\to B^{A'B*}=B^{B'A},\\ &C^{A'B}\to C^{A'B*}=-C^{B'A}, \end{aligned} \tag{1.26}$$

it may be readily verified that Eqs. (1.15), (1.17), (1.18) and (1.19) remain numerically invariant.

The spinors $A_1{}^{AB*}$, $A_2{}^{AB*}$, $B^{A'B*}$, and $C^{A'B*}$ are the same linear combinations of the quantities $G_{\mu\nu}{}^*$, $U_\tau{}^*$ and $F^{\dagger\mu\tau*}U_\tau{}^*$ as the original spinors were of the quantities $G_{\mu\nu}$, U_τ and $F^{\dagger\mu\tau}U_\tau$ as may be verified from Eqs. (1.9), (1.13) and (1.14) and the transformation law of the latter. It is in this sense that we say that the transformation (1.26) induced on the spinors by the transformation (1.25) or that (1.26) corresponds to (1.25) under the isomorphism between the Lorentz group and the anti-linear group in the spin space.

It is readily seen that if we perform the transformation (1.25) on the x^σ then Eqs. (1.20), (1.21) and their complex conjugates remain numerically invariant if we perform the transformation

$$\begin{aligned} &A^{BC}\to\bar{A}^{BC*}=A^{BC},\\ &B^{A'C}\to B^{A'C*}=\bar{B}^{A'C}. \end{aligned} \tag{1.27}$$

Under these transformations Eq. (1.20) goes into its complete conjugate as does (1.21). However, the transformation $B^{A'C}\to\bar{B}^{A'C}$ does not correspond to the transformation (1.25) unless $B^{A'B}$ is Hermitian, that is $\bar{B}^{A'B}=B^{B'A}$. Moreover, if one introduces an external field and modifies Eqs. (1.20) and (1.21) by replacing $\partial/\partial x^\nu$ by $(\partial/\partial x^\nu)-(ie/\hbar c)\varphi_\nu$ then the equations are not invariant for the sign of $(ie/\hbar c)\varphi_\nu$ changes on taking the complex conjugate.

The terms involving $C^{C'B}$ in Eqs. (1.15) and (1.17) and those involving $G_{\mu\nu}F^{\mu\nu}$ in Eqs. (1.17) and (1.18) show that it is not possible to obtain the spinor equations of the meson in a field from those of a free meson by replacing the operator $\partial/\partial x^\nu$ by the operator $(\partial/\partial x^\nu)-(ie/\hbar c)\varphi_\nu$, if this procedure is used for the tensor equations.

Moreover, it can be shown that the tensor equations equivalent to the spinor equations obtained from (1.15), (1.17), (1.18) and (1.19) by dropping the terms in $C^{C'}{}_B$ and $G_{\mu\nu}F^{\mu\nu}$ are (1.1) and (1.2) with the additional conditions that

$$G_{\mu\nu}F^{\mu\nu}=0,\quad F^{\dagger\mu\tau}U_\tau=0.$$

The second of these cannot be satisfied for arbitrary electromagnetic fields since we must have the determinant of $F^{\dagger\mu\tau}$ zero if U_τ is to be different from zero. This implies $F_{\mu\nu}F^{\dagger\mu\nu}=0$ or $E\cdot H=0$.

Fierz[9] in dealing with the equations for a free particle of arbitrary spin imposes certain linear and divergence conditions on the components of the wave functions describing the particle. These conditions would be violated if one went to the equations for a particle in a field from the equations of the free particle by replacing the operator $\partial/\partial x^\nu$ by the operator $(\partial/\partial x^\nu)-(ie/\hbar c)\varphi_\nu$ as was proposed by Dirac. We note that the terms $C^{B'C}$ and $G_{\mu\nu}F^{\mu\nu}$ which make this impossible for the meson are not zero because the divergence of U^ν and $G^{\dagger\mu\nu}$ are not zero.

The real antisymmetric tensor $F_{\mu\nu}$ determines a single symmetric spinor by the equations

$$F_{AB}=\tfrac{1}{8}S_{\mu\nu AB}F^{\mu\nu}.$$

The inverse of this equation is

$$F_{\sigma\tau}=F_{AB}S_{\sigma\tau}{}^{AB}+\bar{F}_{AB}\bar{S}_{\sigma\tau}{}^{AB}.$$

We may write $C^{C'}{}_B$ and $G_{\mu\nu}F^{\mu\nu}$ in terms of the spinor F_{AB} thus

$$C_{A'F}=2[\bar{F}_A{}^C B_{C'F}-B_{A'C}F^C{}_F] \quad (1.28)$$

and

$$G_{\mu\nu}F^{\mu\nu}=8[A_1{}^{AB}F_{AB}+\bar{A}_2{}^{AB}\bar{F}_{AB}]. \quad (1.29)$$

2. $\varphi_\nu=0$

In case there is no external field present, (i.e.) $\varphi_\nu=0$, Eqs. (1.14), (1.16), (1.17) and (1.18) become

$$g^{\nu A'B}A_{1BD,\nu}=KB^{A'}{}_D, \quad (2.1)$$

$$g^{\nu}{}_{A'D}B^{A'}{}_{C,\nu}=-KA_{1CD}, \quad (2.2)$$

$$g^{\nu A'B}A_{2BD,\nu}=K\bar{B}_{D'}{}^A, \quad (2.3)$$

$$g^{\nu}{}_{A'D}\bar{B}_{C'}{}^A{}_{,\nu}=-KA_{2CD}, \quad (2.4)$$

where

$$\lambda_{,\nu}=\partial\lambda/\partial x^\nu. \quad (2.5)$$

These equations admit solutions of the form

$$\begin{aligned} A_{1AB}&=A_{1AB}(p)\exp(ip_\sigma x^\sigma/\hbar),\\ A_{2AB}&=A_{2AB}(-p)\exp(-ip_\sigma x^\sigma/\hbar), \quad (2.6)\\ B^{A'}{}_B&=B^{A'}{}_B(p)\exp(ip_\sigma x^\sigma/\hbar), \end{aligned}$$

where $A_{1AB}(p)$, $A_{2AB}(-p)$ and $B^{A'}{}_B(p)$ are constants, if and only if

$$p_\sigma p^\sigma=m^2c^2. \quad (2.7)$$

[9] M. Fierz, Helv. Phys. Acta, **12**, 3–37 (1939).

We may choose $A_{1AB}(p)$ arbitrarily and then Eqs. (2.1) and (2.4) determine $B^{A'}{}_B(p)$ and $A_{2AB}(-p)$; these will satisfy (2.2) and (2.4) when (2.7) holds. Since $A_{1AB}(p)$ is symmetric, there are three possible linearly independent choices for it. Thus, for each set of p_σ which satisfy (2.7) there exist three linearly independent solutions which correspond to the three different orientations of spin.

From Eq. (2.2) and also from (2.4) we obtain by multiplying by ϵ^{CD} and summing

$$p_\nu g^{\nu}{}_{A'B}B^{A'B}(p)=0, \quad (2.8)$$

which corresponds to the equation

$$p_\nu U^\mu(p)=0,$$

where we have written

$$U_\nu=U_\nu(p)\exp(ip_\sigma x^\sigma/\hbar).$$

From Eqs. (2.2), (2.4), (2.7) and T. E. (1.14) we obtain

$$\begin{aligned} A_{1CD}(p)A_1{}^{CD}(p)&=\bar{A}_{2CD}(-p)\bar{A}_2{}^{CD}(-p)\\ &=-B_{C'D}(p)B^{C'D}(p). \quad (2.9) \end{aligned}$$

From Eqs. (1.8), (1.9), and T. E. (1.20), it follows that the first of these is equivalent to the statement that

$$G_{\mu\nu}(p)G^{\dagger\mu\nu}(p)=0.$$

This equation is satisfied for solutions of the type (2.6) since

$$G_{\mu\nu}(p)=(i/mc)(p_\mu U_\nu(p)-p_\nu U_\mu(p)).$$

The second of Eqs. (2.9) states

$$G_{\mu\nu}(p)G^{\mu\nu}(p)=-2U^\mu(p)U_\mu(p).$$

Since A_{1AB} is a symmetric second order matrix, it may be written in the form

$$A_{1AB}=\psi_A\chi_B+\chi_A\psi_B. \quad (2.10)$$

The spinors ψ_A and χ_B are determined up to a factor by the equations

$$A_{1AB}\psi^B=\rho\psi_A, \quad A_{1AB}\chi^B=-\rho\chi_A.$$

From Eq. (2.10) it follows that

$$2|A_{1AB}|=A_{1AB}A_1{}^{AB}=-2(\psi^A\chi_A)^2. \quad (2.11)$$

In what follows we shall require $|A_{1AB}| \neq 0$, then $(\psi^A \chi_A) \neq 0$ and hence ψ_A and χ_A are two linearly independent spinors.

We may now define two other spinors φ^A and η^A by the equation

$$B^{A'}{}_B = \bar{\varphi}^A \chi_B + \bar{\eta}^A \psi_B, \tag{2.12}$$

that is,

$$(\psi^A \chi_A)\bar{\varphi}^A = B^{A'}{}_B \psi^B, \quad -(\psi^A \chi_A)\bar{\eta}^A = B^{A'}{}_B \chi^B.$$

Eq. (2.4) may now be used to express A_{2AB} in terms of the four spinors ψ^A, χ^A, φ^A and η^A.

The set of Eqs. (2.1) to (2.4) may be used to determine equations for the four simple spinors; however, the equations thus obtained are not linear. We will now show that by taking ψ^A, φ^A and χ^A, η^A as plane wave solutions of the Dirac equation for a particle of spin one-half and of masses m_1 and m_2 respectively we can obtain a solution of Eqs. (2.1) to (2.4) of the form (2.6).

Let

$$\begin{aligned} \psi^A &= \psi^A(p_1) \exp(ip_{1\sigma}x^\sigma/\hbar), \\ \chi^A &= \chi^A(p_2) \exp(ip_{2\sigma}x^\sigma/\hbar), \\ \varphi^A &= \varphi^A(-p_1) \exp(-ip_{1\sigma}x^\sigma/\hbar), \\ \eta^A &= \eta^A(-p_2) \exp(-ip_{2\sigma}x^\sigma/\hbar). \end{aligned} \tag{2.13}$$

Then, if (ψ^A, φ^A) and (χ^A, η^A) are to represent free particles of spin one half and of masses m_1 and m_2, respectively, we must have the Dirac equations satisfied, that is

$$\begin{aligned} g^{\nu A'B} p_{1\nu} \psi_B(p_1) &= -im_1 c \bar{\varphi}^A(-p_1), \\ g^{\nu}{}_{A'D} p_{1\nu} \bar{\varphi}^A(-p_1) &= im_1 c \psi_D(p_1), \end{aligned} \tag{2.14}$$

$$\begin{aligned} g^{\nu A'B} p_{2\nu} \chi_B(p_2) &= -im_2 c \bar{\eta}^C(-p_2), \\ g^{\nu}{}_{A'D} p_{2\nu} \bar{\eta}^A(-p_2) &= im_2 c \chi_D(p_2), \end{aligned} \tag{2.15}$$

with

$$p_{1\nu}p_1{}^\nu = m_1{}^2c^2, \quad p_{2\nu}p_2{}^\nu = m_2{}^2c^2. \tag{2.16}$$

In order that $|A_{1AB}| \neq 0$, we must impose the condition

$$\psi^A(p_1)\chi_A(p_1) \neq 0. \tag{2.17}$$

Substituting Eqs. (2.13) in (2.10) and (2.12) and these in turn into (2.1) and (2.2) we obtain

$$\begin{aligned} &g^{\nu C'D} p_\nu (\psi_B(p_1)\chi_D(p_2) + \chi_B(p_2)\psi_D(p_1)) \\ &\quad = -imc(\bar{\varphi}^C(-p_1)\chi_D(p_2) + \bar{\eta}^C(-p_2)\psi_D(p_1)), \end{aligned}$$

$$\begin{aligned} &g^{\nu}{}_{A'D} p_\nu (\bar{\varphi}^A(-p_1)\chi_C(p_2) + \bar{\eta}^A(-p_2)\psi_C(p_1)) \\ &\quad = imc(\psi_D(p_1)\chi_C(p_2) + \chi_D(p_2)\psi_C(p_1)), \end{aligned}$$

where

$$p_\nu = p_{1\nu} + p_{2\nu}. \tag{2.18}$$

In virtue of (2.17) and the fact that $\psi_B\psi^B = \chi_B\chi^B = 0$, these equations may be written, in an equivalent form as

$$\begin{aligned} g^{\nu A'B} p_\nu \psi_B(p_1) &= -imc\bar{\varphi}^A(-p_1), \\ g^{\nu}{}_{A'D} p_\nu \bar{\varphi}^A(-p_1) &= imc\psi_D(p_1), \end{aligned} \tag{2.19}$$

and

$$\begin{aligned} g^{\nu A'B} p_\nu \chi_B(p_2) &= -imc\bar{\eta}^A(-p_2), \\ g^{\nu}{}_{A'D} p_\nu \bar{\eta}^A(-p_2) &= imc\chi_D(p_2). \end{aligned} \tag{2.20}$$

We may therefore obtain solutions of Eqs. (2.1) and (2.2) provided we can choose such solutions of (2.14) and (2.15) which satisfy (2.19) and (2.20). We must now determine under what conditions Eqs. (2.14) and (2.19) and (2.15) and (2.20) are consistent.

Multiplying the first of Eqs. (2.14) by m and the first of (2.19) by m_1 and subtracting we have as a necessary condition for consistency of these two equations

$$g^{\nu A'B}(mp_{1\nu} - m_1 p_\nu)\psi_B(p_1) = 0, \tag{2.21}$$

and similarly we obtain

$$g^{\nu A'B}(mp_{2\nu} - m_2 p_\nu)\chi_B(p_2) = 0. \tag{2.22}$$

as a necessary condition for the consistency of (2.15) and (2.20). In case m, m_1, and m_2 are different from zero, Eqs. (2.21) and (2.22) are sufficient conditions for the consistency of Eqs. (2.14) and (2.19) and (2.15) and (2.20), respectively. This follows from the fact that a general solution of (2.14) is obtained by choosing $\psi_B(p_1)$ arbitrarily and then determining $\bar{\varphi}^C(-p_1)$ by the first of Eqs. (2.14). Because of the first of Eqs. (2.16) this choice of $\bar{\varphi}^C(-p_1)$ will satisfy the second of (2.14). The same holds for Eqs. (2.19) provided $p^\sigma p_\sigma = m^2c^2$. If then we choose $\psi_A(p_1)$ so that it satisfies (2.21) then $\bar{\varphi}^C(-p_1)$ determined by the first of Eqs. (2.14) will be the same as the $\bar{\varphi}^C(-p_1)$ determined by the first of Eqs. (2.19).

Equations (2.21) will admit non-zero solutions if and only if the determinant of $g^{\nu C'B}(mp_{1\nu} - m_1 p_\nu)$

vanishes, that is,

$$(mp_{1\nu}-m_1p_\nu)(mp_1{}^\nu-m_1p^\nu)=0. \quad (2.23)$$

Similarly from Eq. (2.22) we must have

$$(mp_{2\nu}-m_2p_\nu)(mp_2{}^\nu-m_2p^\nu)=0. \quad (2.24)$$

From Eqs. (2.16) and (2.18), Eqs. (2.23) and (2.24) become

$$(m_1-m)^2m_1c^2+m_1m_2{}^2c^2+2(m_1-m)p_{1\nu}p_2{}^\nu=0$$

and

$$(m_2-m)^2m_2c^2+m_2m_1{}^2c^2+2(m_2-m)p_{1\nu}p_2{}^\nu=0.$$

On equating the two values of $p_{1\nu}p_2{}^\nu$ thus obtained we get the following relation between the three masses m, m_1, and m_2:

$$\frac{((m-m_2)^2+m_1{}^2)m_2}{m-m_2}=\frac{((m-m_1)^2+m_2{}^2)m_1}{m-m_1},$$

which is satisfied if

$$m=0, \quad m_1=m_2, \quad \text{or} \quad m=m_1+m_2. \quad (2.25)$$

Equation (2.17) cannot be satisfied in case $m=0$ for then Eqs. (2.19) and (2.20) admit only one independent solution when $p_\nu\neq 0$. In case $m_1=m_2$ the condition $p_\nu p^\nu=m^2c^2$ implies that $m=2m_1$. Hence this case is a special case of $m=m_1+m_2$.

We, therefore, discuss the case $m=m_1+m_2$. If m has this value, then

$$p_{1\nu}p_2{}^\nu=m_1m_2c^2$$

and hence

$$p_\nu p^\nu=(m_1+m_2)^2c^2=m^2c^2.$$

In this case Eqs. (2.21) and (2.22) become

$$g^{\nu A'B}(m_2p_{1\nu}-m_1p_{2\nu})\psi_B(p_1)=0,$$

$$g^{\nu A'B}(m_2p_{1\nu}-m_1p_{2\nu})\chi_B(p_2)=0.$$

But these equations do not admit two linearly independent solutions which we must have in view of Eqs. (2.17), unless the coefficients are identically zero. That is, as a consequence of (2.17) we must have

$$m_2p_{1\nu}=m_1p_{2\nu}$$

hence

$$p_{1\nu}=m_1/mp_\nu \quad \text{and} \quad p_{2\nu}=m_2/mp_\nu. \quad (2.26)$$

If we now substitute Eqs. (2.13) in (2.12) and the latter in (2.4) we obtain

$$A_{2CD}=(\varphi_C(-p_1)\eta_D(-p_2)+\varphi_D(-p_1)\eta_D(-p_2))\exp(-ip_\nu x^\nu/\hbar), \quad (2.27)$$

and using this value of A_{2CD} we find that Eq. (2.3) is satisfied. Hence, we see that we may obtain solutions of Eqs. (2.1), to (2.4) of the form of (2.6) where

$$\begin{aligned} A_{1AB}(p)&=\psi_A(p_1)\chi_B(p_2)+\chi_A(p_2)\psi_B(p_1),\\ B_{A'B}(p)&=\bar{\varphi}_A(-p_1)\chi_B(p_2)+\bar{\eta}_A(-p_2)\psi_B(p_1), \quad (2.28)\\ A_{2AB}(-p)&=\varphi_A(-p_1)\eta_B(-p_2)+\varphi_B(-p_1)\eta_A(-p_2), \end{aligned}$$

the spinors $(\psi_A(p_1),\ \varphi_A(-p_1))$ represent a particle of spin one-half and mass m_1 and the spinors $(\chi_A(p_2),\ \eta_A(-p_2))$ represent a particle of spin one half and mass m_2, and Eqs. (2.18) and (2.26) hold between the momentum energy vectors of the three particles. Conversely, any solution of Eqs. (2.1) to (2.4) of the form (2.6) can be written in the form (2.28) and if we define m_1 and m_2 by Eqs. (2.26) then the spinors $(\psi_A,\ \varphi_A)$ and $(\chi_A,\ \eta_A)$ represent particles of spin one-half, masses m_1 and m_2 which satisfy the Dirac equation.

The spin of the Proca particle is determined by the values assigned to the constant spinor $A_{1AB}(p)$ whereas the spins of the two Dirac particles are determined by the values assigned to the two constant spinors $\psi_A(p_1)$ and $\chi_A(p_2)$. The first of Eqs. (2.28) then relates the spin of the Proca particle to the spins of the two Dirac particles. It states that the spin of the Proca particle is the vector sum of the spins of the two Dirac particles. This may be seen as follows:

Let

$$b_1=a_1=\left\|\begin{matrix}1\\0\end{matrix}\right\|, \quad a_2=b_2=\left\|\begin{matrix}0\\1\end{matrix}\right\|.$$

Then a_1 and b_1 are the values taken on by $\|\psi_A\|$ and $\|\chi_A\|$, respectively, when in the rest coordinate system (where $p_i=p_{1i}=p_{2i}=0\ (i=1,2,3)$) the x component of the spins of both Dirac particles are positive and a_2 and b_2 are the values of these quantities when the x component of the

spins of both Dirac particles are negative. The general state of spin for the Dirac particle of mass m_1 is given when

$$\|\psi_A\| = \psi_1 a_1 + \psi_2 a_2$$

and the general state of spin for the Dirac particle of mass m_2 is given when

$$\|\chi_A\| = \chi_1 b_1 + \chi_2 b_2.$$

If the spins of these two particles are to be compounded to give a spin one, we must take the symmetric product of these two spin functions. Let $A_1 = \|A_{1AB}\|$ represent the spin function of the state with spin one, then we must have

$$A_1 = (\psi_1 a_1 + \psi_2 a_2)(\chi_1 b_1 + \chi_2 b_2) + (\chi_1 a_1 + \chi_2 a_2)(\psi_1 b_1 + \psi_2 b_2)$$

or

$$A_1 = 2\psi_1\psi_1 V_1 + (\psi_2\chi_2 + \chi_1\psi_2) V_0 + 2\psi_2\chi_2 V_{-1},$$

where

$$V_1 = a_1 b_1, \quad V_0 = a_1 b_2 + a_2 b_1, \quad V_{-1} = a_2 b_2.$$

But any symmetric matrix may be written as

$$A_1 = A_{11}\left\|\begin{matrix}1 & 0\\ 0 & 0\end{matrix}\right\| + A_{12}\left\|\begin{matrix}0 & 1\\ 1 & 0\end{matrix}\right\| + A_{22}\left\|\begin{matrix}0 & 0\\ 0 & 1\end{matrix}\right\|.$$

The two expressions for the matrix A_1 become identical by setting

$$V_1 = \left\|\begin{matrix}1 & 0\\ 0 & 0\end{matrix}\right\| = a_1 b_1, \quad V_0 = \left\|\begin{matrix}0 & 1\\ 1 & 0\end{matrix}\right\| = a_1 b_2 + a_2 b_1,$$

$$V_{-1} = \left\|\begin{matrix}0 & 0\\ 0 & 1\end{matrix}\right\| = a_2 b_2$$

and making use of the first of Eqs. (2.28). Hence it follows that the spin of the Proca particle is the vector sum of the spins of the two Dirac particles and that if

$$\|A_{1AB}\| = \left\|\begin{matrix}1 & 0\\ 0 & 0\end{matrix}\right\|, \quad \|A_{1AB}\| = \left\|\begin{matrix}0 & 1\\ 1 & 0\end{matrix}\right\|$$

or

$$\|A_{1AB}\| = \left\|\begin{matrix}0 & 0\\ 0 & 1\end{matrix}\right\|,$$

then in the rest coordinate system the x component of the spin of the Proca particle is positive, zero or negative, respectively.

The use of the spinor formalism will be illustrated by seeing how it is possible to form three linear combinations of the components of the wave functions for the state of spin one which under space rotations transform as a vector. That this is possible is well known. From the values given for the components of the spinor $\|S_{\sigma\tau}{}^{AB}\|$ it follows that

$$\tfrac{1}{2}(G_{14} + G^\dagger{}_{14}) = -(i/2)(G_{23} + G^\dagger{}_{23}) = A_{1AB} S_{14}{}^{AB} = -2(\psi_1\chi_2 + \psi_2\chi_1) = -2A_{12},$$

$$\tfrac{1}{2}(G_{24} + G^\dagger{}_{24}) = -(i/2)(G_{13} + G^\dagger{}_{13}) = A_{1AB} S_{24}{}^{AB} = 2(\psi_2\chi_2 - \psi_1\chi_1) = A_{22} - A_{11},$$

$$\tfrac{1}{2}(G_{34} + G^\dagger{}_{34}) = (i/2)(G_{12} + G^\dagger{}_{12}) = A_{1AB} S_{34}{}^{AB} = -2i(\psi_2\chi_2 + \psi_1\chi_1) = -i(A_{11} + A_{12}).$$

Since $G_{\mu\nu}$ is an antisymmetric tensor it follows that the left members of these equations transform as vectors under space rotations and hence the right members do.

The wave function components for a free particle of rest mass m which satisfies Proca's equations and is in a state described by the energy-momentum vector p_ν have been expressed as products of wave functions of two particles of spin one half of rest masses m_1 and m_2, satisfying Dirac's equations for such particles and having definite energy momentum vectors $p_{1\nu}$ and $p_{2\nu}$, respectively. The correlation between the wave functions is such that (*a*) $p_\nu = p_{2\nu} + p_{1\nu}$; (*b*) $m = m_1 + m_2$; (*c*) the spin of the Proca particle is the sum of the spins of the Dirac particles. In the above sense of additivity of rest masses, energy momentum vectors and spins, the Proca particle is seen to be equivalent to the two Dirac particles correlated to it.

If the Proca particle is charged one of the Dirac particles must be charged and it may be interpreted as the electron. In this case the other Dirac particle is neutral and of rest mass equal to the difference between the rest mass of the Proca particle and the rest mass of the electron.

The argument given here holds in case m_1 or m_2 is zero. In this case Eqs. (2.26) hold. It follows then that if a Proca particle is equivalent to a pair of particles of spin one-half, one of which is a neutrino, then the rest mass of the other particle is equal to the rest mass of the Proca particle.

3. The Four-Component Formalism

The results given above may be formulated in terms of four component spinors. In order to do this we go from the two component spinor formalism to the four component formalism in the manner given in the notes of a seminar or spinors conducted by O. Veblen.[10] A four component spinor which satisfies the equation

$$\gamma^\sigma p_\sigma \Phi = mc\Phi \tag{3.1}$$

may be constructed from two two component spinors ψ_A, φ_A which satisfy equations of the type (2.14) as follows:

$$\Phi = \|\Phi^a\| = \left\| \begin{matrix} \Phi^1 \\ \Phi^2 \\ \Phi^3 \\ \Phi^4 \end{matrix} \right\| = \left\| \begin{matrix} \psi_1 \\ \psi_2 \\ \bar{\varphi}^1 \\ \bar{\varphi}^2 \end{matrix} \right\}, \quad (a=1, 2, 3, 4). \tag{3.2}$$

It may be readily verified that Eqs. (3.1) are another equivalent form of (2.14) with

$$\gamma^\sigma = \left\| \begin{matrix} 0 & -i\|\bar{g}^\sigma{}_{A'B}\| \\ i\|g^{\sigma A'B}\| & 0 \end{matrix} \right\|. \tag{3.3}$$

From Eq. (1.3) of the appendix it follows that

$$\tfrac{1}{2}(\gamma^\sigma\gamma^\tau + \gamma^\tau\gamma^\sigma) = g^{\sigma\tau}\cdot 1, \tag{3.4}$$

where 1 is the four dimensional identity matrix.

From Eq. (3.3) and (1.17) of the appendix we see that

$$\gamma^{\sigma\tau} = \tfrac{1}{2}(\gamma^\sigma\gamma^\tau - \gamma^\tau\gamma^\sigma) = \left\| \begin{matrix} -\|S^{\sigma\tau A}{}_C\| & 0 \\ 0 & \|\bar{S}^{\sigma\tau A}{}_C\| \end{matrix} \right\|. \tag{3.5}$$

Let

$$\gamma_5 = -i\gamma^1\gamma^2\gamma^3\gamma^4, \tag{3.6}$$

then in the coordinate system used here we have

$$\gamma_5 = \left\| \begin{matrix} 1 & 0 \\ 0 & -1 \end{matrix} \right\| \tag{3.7}$$

and hence in this coordinate system

$$\gamma_5\gamma^\sigma = \left\| \begin{matrix} 0 & -i\|\bar{g}^\sigma{}_{A'B}\| \\ -i\|g^{\sigma A'B}\| & 0 \end{matrix} \right\|. \tag{3.8}$$

The sixteen matrices γ^σ, $\gamma^{\sigma\tau}$, $\gamma_5\gamma^\sigma$, γ_5, and 1 are linearly independent and form a bais for all four rowed matrices as is well known. The antisymmetric matrix B which may be used to raise and lower four component spin indices is in this coordinate system[11]

$$B = \left\| \begin{matrix} 0 & i & 0 & 0 \\ -i & 0 & 0 & 0 \\ 0 & 0 & 0 & -i \\ 0 & 0 & i & 0 \end{matrix} \right\| = \left\| \begin{matrix} i\|\epsilon^{AB}\| & 0 \\ 0 & -i\|\epsilon_{A'B'}\| \end{matrix} \right\|. \tag{3.9}$$

From the above we have

$$B\gamma_5\gamma^{\sigma\tau} = \left\| \begin{matrix} i\|S^{\sigma\tau AB}\| & 0 \\ 0 & i\|\bar{S}^{\sigma\tau}{}_{AB}\| \end{matrix} \right\| \tag{3.10}$$

and

$$B\gamma_5\gamma^\sigma = \left\| \begin{matrix} 0 & -\|\bar{g}^{\sigma A'}{}_B\| \\ -\|g^\sigma{}_{A'}{}^B\| & 0 \end{matrix} \right\| = \left\| \begin{matrix} 0 & -\|\bar{g}^{\sigma A'}{}_B\| \\ -\|\bar{g}^{\sigma A'}{}_B\| & 0 \end{matrix} \right\|. \tag{3.11}$$

Consider now the symmetric second-order spinor where

$$A^{ab} = \Phi^a\Psi^b + \Psi^a\Phi^b, \quad (a, b=1, 2, 3, 4), \tag{3.12}$$

where Φ^a is given by Eqs. (3.2) and Ψ^a is the four component spinor formed from χ_A, η_A in a similar manner. Then if Eqs. (2.28) hold we have

$$A = \|A^{ab}\| = \left\| \begin{matrix} \|A_{1AB}\| & \|B^{A'}{}_B\|' \\ \|B^{A'}{}_B\| & \|\bar{A}_2{}^{AB}\| \end{matrix} \right\| \quad (a, b=1, 2, 3, 4, \quad A, B=1, 2), \tag{3.13}$$

where the prime denotes the transposed matrix. Hence

$$-i \text{ trace } (B\gamma_5\gamma^{\sigma\tau}A) = (S^{\sigma\tau AB}A_{1AB} + \bar{S}^{\sigma\tau}{}_{AB}\bar{A}_2{}^{AB}) = G^{\sigma\tau}$$

in virtue of Eqs. (1.12). This may be written as

$$G^{\sigma\tau} = -i(B\gamma_5\gamma^{\sigma\tau})_{ab}A^{ab} = -2i(B\gamma_5\gamma^{\sigma\tau})_{ab}\Phi^a\Psi^b. \tag{3.14}$$

[10] O. Veblen and J. V. Neumann, "Geometry of Complex Domains," Princeton mimeographed notes (1935–36), p. 2–28.

[11] See W. Pauli, *Zeeman Verhandlingen* (Nijhoff, 1935), p. 41, and also O. Veblen, Proc. Nat. Acad. Sci. **19**, 979–989 (1933).

Similarly it follows that

$$-\text{trace}\,(B\gamma_5\gamma^\sigma A)=2\bar{g}^{\sigma A'}{}_{B}B^{B'}{}_{A}$$
$$=-2g^{\sigma B'A}B_{B'A}=-U^\sigma$$

in virtue of Eqs. (1.8). This may be written as

$$U^\sigma=(B\gamma_5\gamma^\sigma)_{ab}A^{ab}=2(B\gamma_5\gamma^\sigma)_{ab}\Phi^a\Psi^b. \quad (3.15)$$

Eqs. (3.14) and (3.15) then express the wave functions of the Proca particle in terms of the two four-component spinors Φ^a and Ψ^a which represent each of the Dirac particles. These equations hold in any coordinate system.

4. Associated Tensor Quantities in Terms of Spinors

In this section we will use the identities given in T. E. to express tensors involving $G_{\mu\nu}$ and U_ν in terms of the spinors A_{1AB}, A_{2AB}, and $B_{A'B}$.

From Eqs. (1.8), (1.9), T. E. (1.20) and T. E. (1.21) it follows that

$$\begin{aligned}
G_{\mu\nu}G^{\mu\nu}&=8(A_{1AB}A_1{}^{AB}+\bar{A}_2{}^{AB}\bar{A}_{2AB}),\\
G_{\mu\nu}\bar{G}^{\mu\nu}&=8(A_1{}^{AB}A_{2AB}+\bar{A}_1{}^{AB}\bar{A}_{2AB}),\\
G_{\mu\nu}G^{\dagger\mu\nu}&=8(A_1{}^{AB}A_{1AB}-\bar{A}_2{}^{AB}\bar{A}_{2AB}),\\
\bar{G}_{\mu\nu}G^{\dagger\mu\nu}&=8(A_1{}^{AB}A_{2AB}-\bar{A}_1{}^{AB}\bar{A}_{2AB}).
\end{aligned} \quad (4.1)$$

Where Eqs. (2.6) and (2.26) hold, we have

$$\begin{aligned}
A_{1AB}(p)A_1{}^{AB}(p)&=-2(\psi^A(p_1)\chi_A(p_2))^2\\
&\equiv-2T_1{}^2,\\
B_{A'B}(p)B^{A'B}(p)&=-2(\bar{\varphi}^A(-p_1)\bar{\eta}_A(-p_2))\\
&\quad\times(\psi^A(p_1)\chi_A(p_2))\equiv-2T_1{}'\bar{T}_2,\\
A_{2AB}(p)A_2{}^{AB}(p)&=-2(\varphi^A(-p_1)\eta_A(-p_2))^2\\
&\equiv-2T_2{}^2.
\end{aligned} \quad (4.2)$$

Eq. (2.9) is

$$T_1=-\bar{T}_2. \quad (4.3)$$

This result could have been obtained directly from Eqs. (2.19) and (2.20). Eqs. (4.1) may be written as

$$\begin{aligned}
G_{\mu\nu}(p)G^{\mu\nu}(p)&=-32T_1{}^2,\\
G_{\mu\nu}(p)\bar{G}^{\mu\nu}(p)&=-8(T_3T_4+\bar{T}_3\bar{T}_4),\\
G_{\mu\nu}(p)G^{\dagger\mu\nu}(p)&=0,\\
\bar{G}_{\mu\nu}(p)G^{\dagger\mu\nu}(p)&=-8(T_3T_4-\bar{T}_3\bar{T}_4),
\end{aligned} \quad (4.4)$$

where

$$\begin{aligned}
T_3&=\varphi_A(-p_1)\psi^A(p_1),\\
T_4&=\eta_A(-p_2)\chi^A(p_2).
\end{aligned} \quad (4.5)$$

The current vector associated with the Proca equations is

$$S_\mu=\frac{eci}{\hbar}(\bar{G}_{\mu\sigma}U^\sigma-G_{\mu\sigma}\bar{U}^\sigma). \quad (4.6)$$

Because of Eqs. (1.8), (1.12) and T. E. (1.22) this becomes

$$S_\mu=\frac{4eci}{h}g_\mu{}^{A'B}(\bar{B}_{B'C}\bar{A}_2{}^C{}_A-B_{A'C}A_2{}^C{}_B$$
$$+A_{1B}{}^C\bar{B}_{C'A}-\bar{A}_{1A}{}^CB_{C'B}). \quad (4.7)$$

Where Eqs. (2.6) and (2.26) hold this becomes

$$S_\mu=\frac{4eci}{h}\{(T_4-\bar{T}_4)J_{1\mu}+(T_3-\bar{T}_3)J_{2\mu}$$
$$+[2(\psi^D\eta_D)g_\mu{}^{A'B}(\bar{\eta}_A\varphi_B+\bar{\psi}_A\chi_B)-\text{C.C.}]\}, \quad (4.8)$$

where

$$\begin{aligned}
J_{1\mu}&=g_\mu{}^{C'B}(\bar{\psi}_C\psi_B+\bar{\varphi}_C\varphi_B),\\
J_{2\mu}&=g_\mu{}^{C'B}(\bar{\chi}_C\chi_B+\bar{\eta}_C\eta_B)
\end{aligned}$$

and $J_{1\mu}$ and $J_{2\mu}$ are the velocity vectors corresponding to the particles of masses m_1 and m_2, respectively. In obtaining Eq. (4.8) we used the result

$$\chi_C\varphi^C=\bar{\psi}^C\bar{\eta}_C,$$

which follows from Eqs. (2.19) and (2.20).

The Lagrangian function used by Proca is

$$L=h^2c^2(\tfrac{1}{2}G_{\mu\nu}\bar{G}^{\mu\nu}+\bar{U}^\rho U_\rho) \quad (4.9)$$

and it may be expressed as

$$L=-4h^2c^2[4(\bar{\psi}^C\bar{\eta}_C)(\psi^D\eta_D)+T_3T_4$$
$$+\bar{T}_3\bar{T}_4+2(\bar{T}_3T_4+T_3\bar{T}_4)]. \quad (4.10)$$

The stress energy tensor derived by Proca is

$$T_{\mu\rho}=h^2c^2(G_{\nu\mu}\bar{G}^\nu{}_\rho+G_{\nu\rho}\bar{G}^\nu{}_\mu$$
$$+\bar{U}_\mu U_\rho+\bar{U}_\rho\bar{U}_\mu)-g_{\mu\rho}L. \quad (4.11)$$

By using Eqs. (1.8), (2.6), (2.26), and T. E. (1.23) and (1.23a) we may write Eq. (4.11) as

$$T_{\mu\rho}=h^2c^2(8g_{\mu\rho}\{(\psi^A\eta_A)(\bar{\psi}^A\bar{\eta}_A)$$
$$+(T_3+\bar{T}_3)(T_4+\bar{T}_4)\}+\bar{U}_\mu U_\rho$$
$$+\bar{U}_\rho U_\mu-4\{2(g_\mu{}^{C'A}\bar{\psi}_C\psi_A)(g_\rho{}^{C'A}\bar{\chi}_C\chi_A)$$
$$+(g_\mu{}^{C'A}\bar{\chi}_C\psi_A)(g_\rho{}^{C'A}\bar{\psi}_C\chi_A)$$
$$+(g_\mu{}^{C'A}\bar{\psi}_C\chi_A)(g_\rho{}^{C'A}\bar{\chi}_C\psi_A)$$
$$+\text{terms obtained by replacing } \psi_A$$
$$\text{by } \varphi_A \text{ and } \chi_A \text{ by } \eta_A\}). \quad (4.12)$$

Appendix

We denote by $g^\sigma=\|g^{\sigma A'}{}_B\|$ an element of a set of four matrices which satisfy

$$\tfrac{1}{2}(\bar{g}^\sigma g^\tau+\bar{g}^\tau g^\sigma)=-g^{\sigma\tau}\cdot 1. \quad (1.3)$$

A solution of these equations is given by the matrices

$$-g^1=g_1=\left\|\begin{matrix}0 & 1\\ 1 & 0\end{matrix}\right\|, \quad -g^2=g_2=\left\|\begin{matrix}1 & 0\\ 0 & -1\end{matrix}\right\|,$$

$$-g^3=g_3=\left\|\begin{matrix}-i & 0\\ 0 & -i\end{matrix}\right\|$$

and

$$g_4=g^4=\left\|\begin{matrix}0 & -1\\ 1 & 0\end{matrix}\right\|. \quad (1.4)$$

Spin indices are manipulated by the spinors ϵ_{AB} and ϵ^{AB} where

$$\|\epsilon_{AB}\|=\|\epsilon^{AB}\|=\left\|\begin{matrix}0 & 1\\ -1 & 0\end{matrix}\right\|, \quad (1.6)$$

as follows:

$$\psi_A=\epsilon_{AB}\psi^B \quad (1.7)$$

and

$$\psi^A=\epsilon^{BA}\psi_B. \quad (1.9)$$

The following identities are satisfied by $g_\sigma{}^{A'B}$:

$$g^{\sigma A'B}g_{\tau A'B}=2\delta_\tau{}^\sigma, \quad (1.15)$$

$$g^{\sigma A'B}g_{\sigma C'D}=2\delta_{C'}{}^{A'}\delta_D{}^B. \quad (1.16)$$

Let

$$S_{\sigma\tau}{}^A{}_C=\tfrac{1}{2}(g_\sigma{}^{B'A}g_{\tau B'C}-g_\tau{}^{B'A}g_{\sigma B'C}), \quad (1.17)$$

then

$$S_{\sigma\tau}{}^A{}_A=0 \quad \text{or} \quad S_{\sigma\tau AB}=S_{\sigma\tau BA}. \quad (1.18)$$

In the coordinate system in which Eqs. (1.4) hold we have

$$\|S_{14}{}^{AB}\|=\left\|\begin{matrix}0 & -1\\ -1 & 0\end{matrix}\right\|, \quad \|S_{12}{}^{AB}\|=\left\|\begin{matrix}-1 & 0\\ 0 & -1\end{matrix}\right\|,$$

$$\|S_{24}{}^{AB}\|=\left\|\begin{matrix}-1 & 0\\ 0 & 1\end{matrix}\right\|, \quad \|S_{13}{}^{AB}\|=\left\|\begin{matrix}-i & 0\\ 0 & i\end{matrix}\right\|,$$

$$\|S_{34}{}^{AB}\|=\left\|\begin{matrix}-i & 0\\ 0 & -i\end{matrix}\right\|, \quad \|S_{23}{}^{AB}\|=\left\|\begin{matrix}0 & i\\ i & 0\end{matrix}\right\|.$$

The following identities hold:

$$S^{\sigma\tau AB}S_{\sigma\tau CD}=4(\delta_C{}^A\delta_D{}^B+\delta_D{}^A\delta_C{}^B), \quad (1.20)$$

$$\bar{S}^{\sigma\tau AB}S_{\sigma\tau CD}=0, \quad (1.21)$$

$$g^{\sigma C'D}S_{\sigma\tau AB}=-\delta_A{}^Dg_\tau{}^{C'}{}_B-\delta_B{}^Dg_\tau{}^{C'}{}_A, \quad (1.22)$$

$$S^{\sigma\tau}{}_{AB}\bar{S}_{\tau\rho}{}^{CD}=\tfrac{1}{2}[g_\sigma{}^{C'}{}_Ag_\rho{}^{D'}{}_B+g^{\sigma C'}{}_Ag_\rho{}^{D'}{}_B$$
$$+g^{\sigma C'}{}_Bg_\rho{}^{D'}{}_A+g^{\sigma D'}{}_Bg_\rho{}^{C'}{}_A], \quad (1.23)$$

$$S^\sigma{}_\rho{}^{DE}S_{\sigma\tau AB}=-\tfrac{1}{2}[\delta_B{}^DS_{\tau\rho A}{}^E+\delta_B{}^ES_{\tau\rho A}{}^D$$
$$+\delta_A{}^DS_{\tau\rho B}{}^E+\delta^{E'}{}_AS_{\tau\rho B}{}^D]$$
$$+g_{\tau\rho}[\delta_B{}^D\delta_A{}^E+\delta_A{}^D\delta_B{}^E], \quad (1.23a)$$

$$S^{\mu\nu A}{}_BS_{\sigma\tau}{}^B{}_A=-2\eta^{\mu\nu}{}_{\sigma\tau}=$$
$$-2(\delta^{\mu\nu}{}_{\sigma\tau}+(1/g^1)\epsilon^{\mu\nu\rho\lambda}g_{\rho\sigma}g_{\lambda\tau}), \quad (1.26)$$

$$S^{\mu\nu A}{}_B\bar{g}^{\rho B'}{}_C=-\eta_{\rho\tau}{}^{\mu\nu}g^{\tau A'}{}_C \quad (1.27)$$

and

$$g_\rho{}^{A'}{}_BS^{\mu\nu B}{}_C=\eta_{\rho\tau}{}^{\mu\nu}g^{\tau A'}{}_C. \quad (1.28)$$

The isomorphism theorem between the Lorentz group on the variables x^σ and the anti-linear group in the spin space may be stated as follows:

For every proper Lorentz transformation on the variables x^σ there are exactly two unimodular matrices $P=\|P^A{}_B\|$ and $-P$ which satisfy

$$g^\sigma=\bar{P}g^\tau P^{-1}L^\sigma{}_\tau \quad (2.1)$$

and for every improper Lorentz transformation

there are exactly two unimodular matrices $P=\|P^{A'}{}_{B}\|$ and $-P$ which satisfy

$$g^{\sigma}=P\bar{g}^{\tau}\bar{P}^{-1}L^{\sigma}{}_{\tau}=Pg'^{\tau}\bar{P}^{-1}L^{\sigma}{}_{\tau}, \qquad (2.2)$$

where the prime denotes the transposed matrix. The last of these equations follows from the fact that

$$\bar{g}^{\sigma A'B}=g^{\sigma B'A}$$

and hence

$$\bar{g}^{\sigma A'}{}_{B}=g^{\sigma}{}_{B'}{}^{A}.$$

When dealing with complex vectors in the space of the x^{σ} the last form of Eq. (2.2) should be used.

OCTOBER 15, 1939 PHYSICAL REVIEW VOLUME 56

An Improved Method of Making Permanent Electrets and Factors Which Affect Their Behavior

WILFRED M. GOOD AND J. D. STRANATHAN
Department of Physics, University of Kansas, Lawrence, Kansas

(Received July 24, 1939)

A method is described for making strong, smooth, and uniform electrets. The study concerns both the mixing of the carnauba wax and rosin of which the electret is made, and the manner of cooling in the electric field. The electret was cooled in a heavy iron cylinder placed in an oil bath whose rate of cooling was controlled automatically. Electrets were made for which the time of cooling ranged from 30 minutes to 10 days. Observations made on some 35 electrets seem to justify the following conclusions: (1) Electret behavior depends markedly upon details of preparation of the carnauba wax-rosin mixture. The time required for reversal of the electret's charge is increased by mechanical mixing of the components, by heating to a high temperature for a short time, or by heating to a somewhat lower temperature for a longer time. (2) Extending the cooling time in the electric field beyond a day produces little effect. Below this there exists a range of cooling times vital to the behavior of the electret. Those cooled in the open air in the customary manner reverse sign in a shorter time than do those cooled within the cylinder. X-ray photographs show a structural difference between these. (3) Alignment of crystals, as judged from x-ray studies, has little to do with the final charge density attained by the electret. Many samples which are electrets show no alignment. (4) The behavior of the carnauba wax-rosin electret is that of carnauba wax physically modified by the presence of the rosin.

PERMANENT electrets composed of carnauba wax and rosin acquire a final charge which is of sign opposite to that which one expects on the basis of an ionic or polar hypothesis; that is, the face of the electret adjacent to the positive electrode during the manufacturing process finally assumes a positive rather than a negative charge. Crumrine[1] and Gemant[2] have suggested that such behavior might be expected if one of the constituents of these electrets were piezoelectric. Some force mechanism would have to exist to produce the observed charge. This force might arise because of strains set up in the wax during cooling. If we accept this concept, then we might expect these strains, and hence the electret charge, to be affected by the rate at which the wax is cooled during manufacture of the electret.

Preliminary to investigating how the charge on the electret is related to the manner in which the wax mixture is allowed to cool during manufacture, some effort has been directed towards a method of securing smoother, more uniform samples. Our experience has shown that the details of preparation have a greater effect upon the subsequent behavior of an electret than the literature would lead one to believe.[3] Therefore, the purposes of this investigation were: (1) to devise a method of making smooth, uniform electrets; (2) to obtain information as to what effect the details of preparation have upon the behavior and structure of the electret; (3) to observe how the final charge on the electret

[1] K. Crumrine, Master's Thesis, University of Kansas (1933).
[2] A. Gemant, Phil. Mag. **20**, 929 (1935).
[3] J. V. Eguchi, Phil. Mag. **49**, 181 (1925).

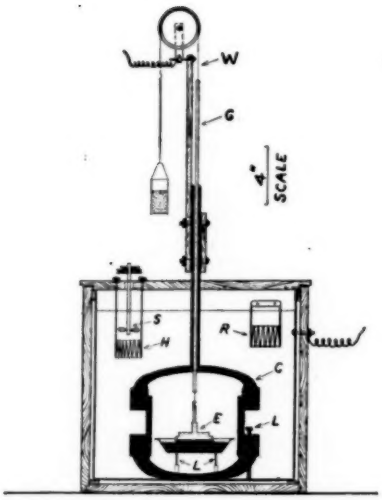

FIG. 1. *C*, heavy iron cylinder immersed in an oil bath; *H*, heater; *S*, stirrer; *R*, resistance thermometer; *L*, leveling screws; *E*, upper electrode; *G*, glass tube; *W*, flexible wire supporting and making electrical contact with the upper electrode.

and the rate at which this charge is acquired, depend upon the manner of cooling in the electric field.

THE METHOD OF MANUFACTURE

The behavior of permanent electrets has been shown to depend upon the kinds and relative amounts of materials in their composition.[2] The strength of the electric field in which they are cooled has also been shown to be significant.[1, 2] All electrets in the present study were composed of equal weights of rosin and carnauba wax, and were made with a field strength of approximately 8000 volts per centimeter. To control the rate at which cooling took place in the electric field, an oil bath as shown in Fig. 1 was used. A resistance thermometer, bridge with continuously variable galvanometer contact, photo-cell, and relay system, made it possible to extend the time required for cooling to 24 days.

Tin seems most satisfactory as an electrode material; it showed less evidence of electrochemical activity than other metals which were tried. The bottom electrode was a tinned pan; the top electrode was a solid tin disk, turned on a lathe, and polished with carbon tetrachloride and rouge. A new pan was used and the top electrode repolished, for each electret made. Since the melted wax wets the tin, it is possible, by counterbalancing the top electrode slightly in excess of its weight, to cause that part of the electret in contact with the electrode to be elevated. (See Fig. 1.) In this way the electret is left free to contract when it cools, without the inevitable cracking that occurs when the electrode is imbedded. The temperature of the oil bath was not allowed to exceed 90°C; at higher temperatures the tin showed evidence of chemical action. For the same reason the mixture was not poured into the tinned pans at temperatures above 90°.

The oil bath was kept at 90° for twelve hours after lowering the top electrode onto the surface of the melted wax. This prolonged heating at 90° seemed to have no significant influence upon the behavior of the electret; it was found necessary to produce electrets having no air pockets in the surface next to the top electrode. The bath was allowed to cool to 75°C at a rate determined by surrounding temperatures. Below 75° the cooling time was controlled automatically; it could be made as long as 24 days. The electric field was applied automatically when the temperature dropped to 75°; if it were applied at 90° the resulting electret inevitably cracked at the periphery of the top electrode.[4] The electret was removed from the cylinder at or below 24°C. If it were removed at a temperature much higher, the top electrode would stick. The electrets were kept in the pans in which they were made. These pans were provided with lids of such design that the top face of the electret was shorted to the bottom face when the lid was closed. Avoiding the use of tin foil as an electrode leads to much smoother electret surfaces; avoiding its use as a wrapper minimizes effects introduced by handling. An air-tight cabinet with dryer was used for storage.

RESULTS AND CONCLUSIONS

A series of electrets was made in which successive samples of the series were heated to successively higher temperatures during melting. As the carnauba wax and rosin going into a particular electret were melted together, the

[4] This cracking was peculiar in that it appeared to follow the fringing lines of electric force as they leave the edge of the upper electrode. It is not clear just what causes this.

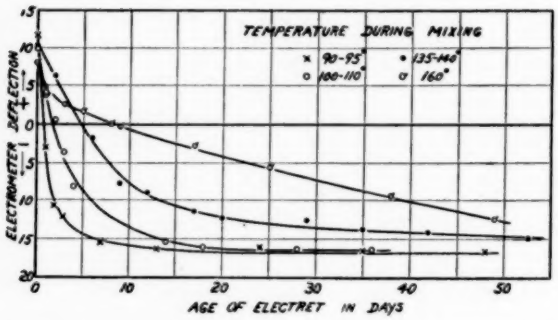

FIG. 2. Showing the effect of the temperature maintained during mixing upon the subsequent behavior of the electret. The cooling time for each of these electrets was one day. A positive electrometer deflection indicates that the face of the electret bears a charge opposite in sign to that on the electrode adjacent it during manufacture. Although these observations were made without the use of a guard ring, further measurements with a guard ring showed the same relative behavior. The final charge density attained by these electrets is essentially the same as that attained by electrets made in the usual way.

temperature of the melted portion was held at that temperature characterizing this given electret until the last bit of solid carnauba wax or rosin had melted. The curves in Fig. 2 illustrate the effect of the temperature maintained during melting upon the subsequent behavior. There are two conclusions that can be drawn from these curves. First, all samples attain approximately the same final surface density of charge; and second, the time required for reversal[5] in sign of charge becomes less and less as the temperature maintained during melting is lowered. Further investigation has revealed that the reversal time approaches a lower limit which is that characteristic of an electret of pure carnauba wax. There is evidence that either prolonged heating or vigorous stirring of the wax at lower temperatures accomplishes to a lesser degree what is here accomplished by higher temperatures during the initial melting. These facts suggest that the subsequent behavior of the electret depends upon the thoroughness with which the components are mixed, and that heating contributes to this mixing. Chemical action may play a part, but x-ray evidence to be presented indicates that the effect is mainly one of physical mixing.

[5] It appears that this time of reversal depends also upon the rosin, since electrets made from another batch had reversal times, when well mixed, of about 4 weeks instead of the 8 days shown in Fig. 2.

In order to study the way in which the characteristics of the electret depend upon the rate at which it is cooled in the electric field, it was necessary to adopt a standard method of preparing the wax which could be duplicated with sufficient accuracy to insure otherwise identical electrets. The wax was prepared by heating it at 135° for two hours. Constant moderate stirring assisted in establishing a uniform temperature throughout. Results having to do with the effect of the manner of cooling in the electric field will, for convenience, be classified as follows: (a) those for electrets cooled in the iron cylinder, and, (b) those for electrets cooled in the open air. When cooled inside the iron cylinder the electrets are smooth, uniform, and strong. The two parallel faces are as smooth as the electrodes with which they were in contact. Samples of such electrets have been made for which the cooling times ranged from 30 minutes to 10 days. The shortest cooling time attainable by allowing the oil bath to cool normally was a little over a day. Electrets were made in 10 days, 4 days, and 1 day without having to resort to rapid cooling schemes. These electrets yield rather consistent evidence that the time for reversal of charge becomes longer, and the final density of charge becomes smaller, as the time of cooling in the electric field is increased. The differences are so small, however, that they can scarcely be considered significant. A more perceptible trend of this character was evidenced by electrets which were cooled by cold oil added immediately after the hot oil had been drawn off at 75°C. These more rapidly cooled[6] electrets reversed in a shorter time, acquiring essentially the same final charge in a shorter time. If, on the other hand, one adds ice water instead of the cold oil, thereby reducing the total cooling time to 30 minutes, the samples do not become electrets at all. This was the only manner of cooling which did not yield an electret of some character. The three samples so made did not reverse during a 3½-month period after manufacture; and they gave no indication that a reversal would ever take place. Finally, electrets cooled inside the iron cylinder require a much

[6] These electrets cooled from 75° to 37° in one hour. They remained in the cylinder approximately a day, until the oil bath had reached room temperature.

longer time to reverse their sign of charge than those cooled in the open air, using the same electrode system without the inclosing iron cylinder. Those cooled in the cylinder were free from cracks and strong; those cooled in air were full of cracks and easily broken. The authors see no reason why cooling in the cylinder and cooling in the open air should produce results so radically different, or why cooling the cylinder with ice water produces no permanent electret. The phenomena are no doubt connected with the temperature gradient within the cooling electret. Information regarding this might be obtained through use of thermocouples imbedded in the cooling wax.

In addition to investigating the behavior of the charge on the electret, a simultaneous x-ray study was made by removing a small core from each one and examining the diffraction rings immediately after the electret's manufacture and again after the reversal of charge had taken place. For the electrets composed of rosin and carnauba wax and cooled in the open air, results were obtained corroborating the work of Ewing.[7] The present work, however, shows a diffuse ring inside those described by Ewing.[8] By securing the diffraction patterns for pure carnauba wax and for pure rosin, it was ascertained that the three sharp rings described previously belonged to carnauba wax, while the inner diffuse ring had a contribution from both rosin and carnauba wax. The fact that the diffraction patterns for the two component materials are not modified by thoroughly mixing the components, indicates the absence of a predominant chemical combination. A notable difference exists for all electrets cooled inside the cylinder in that they all show entirely uniform diffraction rings. This is true even for electrets of pure carnauba wax. Both types, the one showing uniform diffraction rings, the other showing marked variations in intensity, make equally good electrets. Crystalline orientation seems to have no effect upon the final strength of an electret. Significant is the fact that when pure carnauba wax is cooled in the open air, the diffraction pattern indicates a more nearly complete alignment of crystals than does that of any other type of electret. (See Fig. 3.) The intensity distribution in the diffraction rings of one pure carnauba wax electret was found to change noticeably during a 5-month period; there was no observable change in electret behavior.

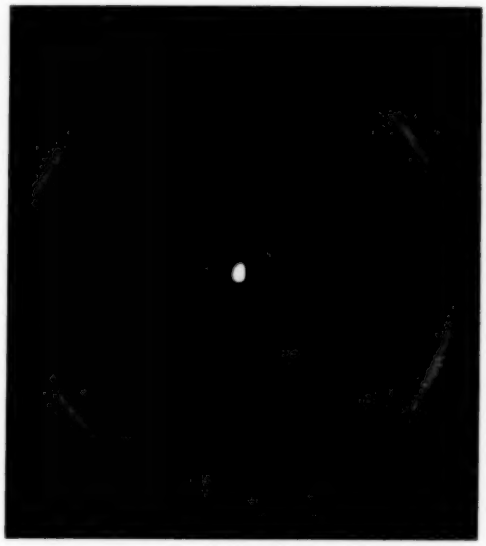

FIG. 3. X-ray diffraction photograph of an electret of pure carnauba wax cooled in the open air. The x-ray beam was perpendicular to the previously applied electric field. This field was directed horizontally across the photograph.

The authors wish to express their appreciation of suggestions and criticisms offered by various members of the Department. Particularly, they wish to thank Professor C. V. Kent for his interest and aid in the x-ray study, and to acknowledge the benefit of some earlier unpublished work done jointly by Dr. R. L. Dolecek and one of the authors.

[7] M. Ewing, Phys. Rev. **36**, 378 (1930).

[8] Ewing found three sharp rings, and found that for electrets all these rings varied in intensity in a simple symmetrical manner.

A Note on the Hole Theory of Diffusion

R. P. JOHNSON
Research Laboratory, General Electric Company, Schenectady, New York
(Received August 14, 1939)

The activation energy Q_x for diffusion in a dilute metallic solution cannot be less than the activation energy Q_0 for self-diffusion, if the solute atoms can move only through the medium of "holes" which diffuse to them from the solvent lattice, displace them, and leave in another direction. Since the experiments show that generally $Q_x<Q_0$ an alternative mechanism is required. Solute atoms which are not so firmly bound in the lattice as are solvent atoms will tend to trap holes to form solute-hole molecules. These molecules can move as units through the dense solvent lattice by cycles of inversion and re-orientation. This mechanism yields for the diffusion constant the value

$$D=A^* \exp\left[-(W+S)/RT\right],$$

where W is the energy required to form a hole adjacent to a solute atom, and S is the activation energy for re-orientation or inversion of a solute-hole molecule. $Q_x(\equiv W+S)$ may be much smaller than either Q_0 or the binding energy of the solvent. A^* should be significantly less than the corresponding A for self-diffusion. Both these predictions are in accord with the data. The same considerations should apply also to diffusion in liquids.

1. The Problem and the Proposed Mechanism

Stiegman, Shockley and Nix[1] (SSN) decide from energy considerations that diffusion in dilute solid metallic solutions probably occurs through the medium of vacant lattice sites ("holes") rather than by simple interchange of position between pairs of atoms or by a process involving interstitial atoms. According to the hole theory the diffusion constant, they say, is

$$D_x=\nu\delta^2 \exp\left[-(H_0+J_x)/RT\right] \equiv A \exp\left[-Q_x/RT\right], \quad (1)$$

where ν is the frequency of the atomic vibrations and δ is the lattice spacing; H_0, the energy required for forming a hole in the solvent lattice, is of the order of the binding energy and J_x, the activation energy for passage of a solute atom into an adjacent hole, is presumably considerably smaller. The data accumulated in Table II of SSN show that for a given solvent Q_x has its greatest value (Q_0) for self-diffusion and may be as low as $Q_0/2$ for other solute elements. They conclude: "If hole diffusion is the dominant process, the energy H_0 should be the same for a given solvent (the concentration of the solute in all cases is small) and therefore all changes in Q should come from J_x. We are, therefore, forced to assume either that J_x is at least as large as H_0 and is very sensitive to the nature of the solute or that another process of diffusion is involved."

Actually the matter is more desperate than SSN indicate. Eq. (1) gives correctly the diffusion constant for self-diffusion and for the diffusion of solutes for which $J_x>J_0$, J_0 being the activation energy for passage of a solvent atom into an adjacent hole. But to the cases of practical interest, where $Q_x<Q_0$, Eq. (1) does not apply. Briefly, the diffusion of the solute atoms is finally limited by the rate at which holes diffuse to them from the hinterland of the solvent. Even if $J_x=0$, D_x should exceed D_0 only by a numerical factor of the order of the coordination number, and Q_x should be identical with Q_0. This conclusion seems to be inevitable so long as diffusion of solute atoms is supposed to occur by means of holes which approach from the reaches of the solvent lattice, pass through solute atoms and displace them, and retreat in another direction.

There is another mechanism of diffusion, involving holes, which avoids this impasse. If the binding between a solute atom and its neighboring solvent atoms is less tight than the binding between neighboring solvent atoms, holes will appear preferentially in sites adjacent to solute atoms. Statistically the lattice will contain a certain concentration of solute-hole molecules; the fraction of the solute atoms instantaneously associated with holes to form diatomic molecules will be

$$z \exp\left[-W/RT\right],$$

where z is the coordination number and W is the

[1] J. Stiegman, W. Shockley and F. C. Nix, Phys. Rev. **56**, 13 (1939).

energy required for removing a solvent atom from a site adjacent to a solute atom. A solute-hole molecule can proceed amoeba-like through the lattice by cyclic changes in its orientation—that is, by cyclic rearrangements of the surrounding solvent atoms—without having to wait for an additional hole to diffuse to it from the solvent lattice. It is this random drift of solute-hole molecules which is proposed as the dominant process in the diffusion of solute atoms, in the cases where $Q_x < Q_0$. This mechanism yields for the value of the diffusion constant

$$D_x = A^* \exp\left[-(W+S)/RT\right] \equiv A^* \exp\left[-Q_x/RT\right],$$

where S is the activation energy for passage of a solvent atom into an adjacent hole, when both the solvent atom and the hole are near neighbors of a solute atom. Neither of the two terms now composing Q_x is directly related to H_0, J_0, or J_x defined above. It appears that Q_x need not be restricted to a narrow range of values; it may be considerably smaller than either Q_0 or the binding energy of the solvent. A^* should be smaller than the corresponding A_a for self-diffusion by a factor which decreases exponentially with the number of moves a trapped hole must make to complete a cycle displacing the solute-hole molecule by one lattice-spacing. Some such trend appears in the A values in Table II of SSN: for Cu, $A_a/A^* > 100$; for *Pb*, $A_a/A^* \leqq 12$. The serious uncertainty of measured or calculated A values limits, of course, the worth of this apparent agreement.

The arguments basic to these statements are presented in the following sections.

2. Diffusion Constant for Holes

Consider a crystal containing N_a normal atoms a and N_0 holes 0. In equilibrium, when the free energy is a minimum,

$$N_0/N_a = f = \exp\left[-H_0/RT\right].$$

Each hole occasionally moves a distance of one lattice-spacing p. Each such move is assumed independent of all preceding moves—this is true if the frequency n of moves by a particular hole is small in comparison with the frequency ν of the atomic vibrations. If J_0 is the activation energy for passage of a hole to an adjacent lattice site,

$$n = \nu \exp\left[-J_0/RT\right].$$

After n moves of a particular hole (which will on the average require unit time) the vector displacement[2] of the hole from its original position will be

$$\boldsymbol{S}_0 = \sum_n \boldsymbol{p}_i,$$

each vector $\boldsymbol{p}_i$ having one of the several possible directions. Forming the scalar product of each side by itself, and averaging over many holes each of which has made n moves:

$$\langle S_0^2 \rangle_{Av} = \langle \sum_n \boldsymbol{p}_i \cdot \boldsymbol{p}_i \rangle_{Av} + \langle \sum\sum_{i \neq j} \boldsymbol{p}_i \cdot \boldsymbol{p}_j \rangle_{Av} = np^2,$$

the products $\boldsymbol{p}_i \cdot \boldsymbol{p}_j$ being as often positive as negative. The expression np^2 is clearly identical, except for a numerical factor determined by the geometry, with the diffusion constant D_0 for holes in the diffusion equation

$$\dot{N}_0 = D_0 \nabla^2 N_0;$$

that is,

$$D_0 = np^2 = \nu p^2 \exp\left[-J_0/RT\right].$$

This same device will be generally used hereafter: an $\langle S^2 \rangle_{Av}$ will be calculated and set identical with the corresponding diffusion constant D.

3. Constant of Self-Diffusion

A move by a hole is obviously identical with a move (in the opposite sense) by an atom. Let a few of the a atoms be marked (for example, be made radioactive). The probability that a single move by a particular hole will also be a move of a particular marked atom is $1/N_a$. The total displacement S_a of a particular marked atom from its original position, after the N_0 holes in the crystal have made an average of n moves each, will be given by

$$\langle S_a^2 \rangle_{Av} = n \frac{N_0}{N_a} p^2.$$

It follows that

$$D_a = fD_0 = D_0 \exp\left[-H_0/RT\right] = \nu p^2 \exp\left[-(H_0+J_0)/RT\right].$$

[2] This method was suggested by M. J. Polissar, J. Chem. Phys. **6**, 833 (1938).

That is, the diffusion constant for self-diffusion is smaller than the constant for hole-diffusion by a factor which is just the fractional concentration of holes. The division of Q_0 into two terms, one the energy H_0 required to form a hole and the other the energy of activation J_0 for an atom to move into an adjacent hole, is patently justified.

4. Constant for Diffusion of Impurity Atoms

Let the few marked a atoms be replaced by chemically-different atoms x. If an x atom requires an energy of activation $J_x > J_0$ for moving into an adjacent hole, the probability that it will so move is only $\exp[-(J_x-J_0)/RT]$ times the probability that a marked a atom in the same position would move into the hole. It follows that

$$\begin{aligned} D_x &= D_a \exp[-(J_x-J_0)/RT] \\ &= \nu p^2 \exp[-(H_0+J_x)/RT] \\ &\equiv A_0 \exp[-Q_x/RT]. \end{aligned} \tag{2}$$

This case of $J_x > J_0$ appears, however, to be without practical interest, for Table II of SSN shows that $Q_x < Q_0$ for all the dilute metallic solutions listed there. It is clear on reflection that Eq. (2) is not applicable when $J_x < J_0$—that is, when an x atom is more likely than an a atom to move into an adjacent hole. The successive moves of an x atom are then not generally independent, for the x atom will interchange positions with an adjacent hole a number of times before the hole can escape by capturing one of the a atoms; it is certainly not legitimate to count these to-and-fro moves as contributing to the mean square displacement of the x atom from its original position. An *upper bound* for D_x, if only this mechanism of hole-capture-hole-release is operative, can be calculated as follows: Consider the case most favorable for x atom diffusion, in which J_x has the extreme value zero. Imagine each x atom surrounded by a "sphere of influence" containing several a atoms, and assume that whenever a hole reaches the boundary of this sphere it inevitably and immediately gravitates in to the x atom and displaces it by one lattice-spacing, passing out of the sphere in another direction. The probability that a single move of a particular hole will place it on the boundary of a particular sphere of influence is b/N_a, where b is the number of a atoms on this boundary and is of the order of magnitude of the coordination number. This by assumption is also the probability that a single move by a particular hole will result in a move of the particular x atom in this sphere. The total displacement S_x of the particular x atom after each of the N_0 holes present has made an average of n moves will be given by

$$\langle S_x^2 \rangle_N = bnp^2 N_0/N_a,$$

and it follows that

$$D_x = bD_a.$$

The diffusion constant, even for $J_x=0$, is seen to exceed the constant for self-diffusion only by a factor of the order of 10, and the Q values for the two are the same except for a possible temperature dependence (presumably negligible) of the size of the sphere of influence.

This mechanism, in which the holes diffuse to the impurity atoms, displace them, and move on, is clearly in disagreement with the values of Q_x in Table II of SSN, not essentially because those values are *markedly* smaller than Q_0, but because they are *at all* smaller than Q_0. The alternative mechanism of molecule-motion, which avoids this limitation, is developed in the next section.

5. Formation and Drift of Solute-Hole Molecules

The holes in their equilibrium distribution (which they will attain relatively rapidly, since they diffuse rapidly) will not be scattered at random in the lattice, but will tend (1) to cluster around x atoms if these are not so tightly bound to their neighboring a atoms as a atoms are bound to one another, and will tend (2) to avoid contiguity with x atoms if the $x-a$ binding is more firm than $a-a$ binding. This is readily seen either by considering the probable moves of a hole in the vicinity of an x atom or by using the Boltzmann theorem to find the average local equilibrium concentration of the holes. Case (2), in which the holes detour around x atoms, yields a slower diffusion for x than for a atoms and hence is without practical interest. In case (1), where x atoms are more likely than a atoms to have holes associated with them, it is convenient and legitimate to speak of xo molecules as

statistically present in the lattice. In the simplest situation, where the disturbing influence of an x atom extends not far beyond its nearest neighbors, the fraction of the sites adjacent to x atoms which will in equilibrium be vacant is

$$\exp\,[-W/RT],$$

where W is the energy necessary for removing an a atom from one of these sites. The fraction of the x atoms instantaneously associated with holes to form a diatomic xo molecules is therefore approximately

$$z\exp\,[-W/RT],$$

where z as before is the number of nearest neighbors.

It remains only to notice that an xo molecule can travel, unassisted by additional holes, through the a lattice. A typical cycle which restores the molecule to its original configuration and orientation but leaves it displaced by one lattice-spacing is shown in Fig. 1, the lattice being approximated by a plane square array. The diagonal orientation of the molecule in this simple array (Fig. 1 (3) and (5)) is a sort of excited state—in a more complicated lattice so wide a separation between x and o might never have to occur in the course of a cycle (for example, it would not occur in a plane hexagonal array).

The rate of diffusion by this mechanism can be estimated very roughly as follows: Consider first the case in which inversion of the molecule requires less energy of activation than does re-orientation—that is, the x atom is more likely than an a atom to move into the trapped hole. Suppose that m moves of the hole are necessary for completing a displacement-cycle, and that each move can occur in q directions only one of which contributes to completion of the cycle. The probability that a given sequence of m moves will complete a cycle and so advance the molecule by one lattice-spacing is $1/q^m$. In the time required for n moves of a trapped hole ($n\gg m$) the molecule will have moved a distance S_d given by

$$\langle S_d^2\rangle_{Av}=np^2/mq^m,$$

where p as before is the lattice-spacing. The diffusion constant for xo molecules is therefore

$$D_d=\nu p^2/mq^m\exp\,[-S/RT],$$

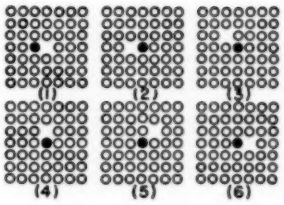

FIG. 1. A cycle of inversion (1–2) and reorientation (2–6) which moves a solute-hole molecule one lattice-spacing.

where S is the activation energy for moving an a atom into an adjacent hole, both the a atom and the hole being in the immediate neighborhood of an x atom. Correspondingly, the diffusion constant for x atoms generally, whether associated with holes or not, is

$$D_x=z\nu p^2/mq^m\exp\,[-(W+S)/RT]$$
$$=A^*\exp\,[-Q_x/RT].$$

With this mechanism Q_x again appears as the sum of two interpretable terms, but neither of these is directly related to the work necessary for forming a hole in the a lattice, nor to the activation energy for moving a hole about in the a lattice, nor to the activation energy for moving an x atom into an adjacent hole. It is plausible (though not essential) to suppose that if $W<H_0$, then also $S<J_0$. At any rate, Q_x is left largely unrestricted, and it is entirely reasonable that Q should generally be larger for self-diffusion than for the diffusion of any solute whose solubility increases with increasing temperature. Since z, q and m are all of the same order, evidently A^*, with this mechanism, should be significantly less than the corresponding A for self-diffusion, calculated on the basis of the other mechanism.

In the second possible case, where the activation energy for passage of the x atom into the trapped hole exceeds that for passage of an a atom into the hole, the rate of diffusion would be limited by the rate of inversion of molecules rather than by the rate of re-orientation. S as defined above would then be replaced by the activation energy for inversion, and A would be larger than A^* estimated above. This case seems less likely to occur than does the alternative discussed in detail in the two preceding paragraphs.

6. Range of Application of the Mechanism

None of the discussion has involved the ratio of the concentration of holes to that of x atoms. Either of these may far outnumber the other. In particular, the concentration of impurity atoms may increase from zero up to the point where interactions among the impurity atoms become appreciable. The arguments, in short, apply to the same range as do the usual "infinite dilution" theories.

No use has been made of the periodicity of the lattice. For this reason it seems that the foregoing considerations ought to apply without change to dilute liquid solutions, wherever the hole theory of diffusion is at all applicable. It is uncertain from the data[3] whether the solute-hole molecule mechanism is commonly suitable for accounting for diffusion in liquids—that is, whether Q_0 commonly exceeds Q_x.

I am indebted to Dr. C. W. Hewlett, Mr. C. G. Found and Dr. W. Shockley for several discussions on this subject.

[3] H. S. Taylor, J. Chem. Phys. **6**, 331 (1938).

OCTOBER 15, 1939 PHYSICAL REVIEW VOLUME 56

Transport Phenomena in Mixtures of Gases

E. J. Hellund and E. A. Uehling
University of Washington, Seattle, Washington

(Received April 17, 1939)

The theory of transport in gases taking into account the full effect of quantum statistics is extended to include mixtures as well as one-component gases. The method of Lorentz, Hilbert, and Enskog, which was used previously in the development of the quantum theory of transport in a single component gas, is used again in this more general case. As is to be expected, all transport equations have formally the same dependence on velocity, temperature, and pressure gradients as in the classical statistics, the effects of diffraction and interference introduced by the quantum statistics appearing only in the coefficients themselves. Expressions for the viscosity, heat conductivity, pressure diffusion, and thermal diffusion coefficients into which assumptions with regard to the interaction laws may be introduced have been obtained. It is expected that these expressions may form the basis for calculation based on plausible assumptions as to the interaction that will provide a relatively good test of these laws as well as of the theory itself.

Introduction

THE study of transport phenomena in gases has been recognized as a most promising field of investigation having as its objective the determination of intermolecular forces. The study of viscosity, heat conductivity and diffusion by numerous early investigators together with the rigorous analytical treatments of the subject given by Enskog and Chapman have demonstrated fully the sensitivity of the method and the practicality of the calculations which lead to the possibility of detailed comparisons between theoretical results and experimental observations.

With the introduction of the quantum statistics, the study of transport phenomena in gases took on a further significance, which was to be found in the possibility of an experimental test of these statistics. Certain discrepancies between observational data and the results of calculations based on the classical theory of Chapman and Enskog had already appeared. These discrepancies, which were observed for all transport coefficients, were at first attributed to the assumption of incorrect interaction laws on the basis of which the theoretical results were obtained. That this interpretation of the discrepancies was inadequate was demonstrated by Massey and Mohr[1] for the case of viscosity and heat conductivity in single component gases. The considerable improvement in the theoretical results obtained by these authors when quantum-

[1] H. S. W. Massey and C. B. O. Mohr, Proc. Roy. Soc. **A141**, 434 (1933): **A144**, 188 (1934).

theoretical cross sections were substituted for the classical cross sections in the expressions for the gas coefficients derived by Chapman was an indication of the importance of having a complete quantum-statistical treatment of transport.

Such a theory of transport in single component gases was given by Uehling and Uhlenbeck,[2] and calculations based on the theory applicable to the gases H_2 and He under the assumption of elastic sphere interaction were given by one of the present authors.[3] The theory shows that the modifications due to the quantum statistics are of two kinds: (a) a diffraction effect, which for light gases of moderate density is appreciable even at room temperatures; and, (b) an interference effect due to modifications in the "Stoszzahlansatz," which is inappreciable even for the case of H_2 and He^4 except at temperatures in the neighborhood of the critical values. The experiments of Itterbeek and Keesom[5] on the viscosity of helium at low temperatures together with the results of previous experiments at higher temperatures demonstrate the importance of the diffraction effect. What discrepancies still remain in the temperature dependence of the viscosity coefficient are presumably attributable to the simplifying assumptions used with respect to the interaction laws. Numerical calculations of Massey and Mohr, Massey and Buckingham, and the authors[6] based on Van der Waals types of interaction substantiate this conclusion.

The second of the two quantum-mechanical effects appears to be more difficult to detect. The theory shows a density dependence for the viscosity coefficient of He which is large compared with the nonideality correction in the neighborhood of 5°K.[3] According to the experiments of Itterbeek and Keesom, this effect appears, however, to be too small for detection within the range of density variations in which the theory may be presumed to be valid, and the temperature dependence of the density effect is difficult to separate from the temperature dependence of the diffraction effect.

For these reasons the development of a quantum theory of gas mixtures is undertaken. In addition to the phenomena of viscosity and heat conductivity, one now has also the phenomena of diffusion to consider. The introduction of diffusion processes into the problem leads to the following interesting considerations. There exist in general two types of diffusion; a pressure diffusion, and a thermal diffusion. As is the case with all transport coefficients, the diffusion coefficients will exhibit temperature and density variations which are characteristic of the diffraction effect and of the interference effect. Under certain conditions, however, only the ratio of these diffusion coefficients is important. This is true for any experimental arrangement in which a definite quantity of a mixture of gases is allowed to come to equilibrium under the influence of an impressed temperature gradient. Equilibrium is established under these conditions with variations in density of each component along the direction of the temperature gradient such that the processes of pressure diffusion in one direction are just balanced by the processes of thermal diffusion in the opposite direction. This equilibrium situation is described by the ratio of the pressure and thermal diffusion coefficients. Unlike all other transport coefficients this ratio does not depend on any single integral over transport cross sections, but only on the ratio of such integrals. One would expect, therefore, that in this particular case the importance of the diffraction effect is minimized, and that the interference effect in the quantum statistics is, in consequence, of relatively greater importance.

A test of this expectation seems to be of considerable importance from a theoretical point of view. As a test of interaction laws the transport process under consideration may be of considerable sensitivity, since the thermal diffusion process vanishes altogether in the classical statistics for a particular interaction law.[7] Also, the temperature dependence of the ratio of thermal and pressure diffusion coefficients is of

[2] E. A. Uehling and G. E. Uhlenbeck, Phys. Rev. **43**, 552 (1933).
[3] E. A. Uehling, Phys. Rev. **46**, 917 (1934).
[4] Reference 3, Tables VII and VIII.
[5] A. v. Itterbeek and W. H. Keesom, Physica **5**, 257 (1938).
[6] H. S. W. Massey and C. B. O. Mohr, Proc. Roy. Soc, **A144**, 188 (1934). H. S. W. Massey and R. A. Buckingham. Proc. Roy. Soc. **A168**, 378 (1938). E. A. Uehling and E. J. Hellund, Phys. Rev. **54**, 479 (1938).

[7] The inverse fifth-power law. See Sir James Jeans, *The Dynamical Theory of Gases* (Cambridge University Press, 1925), 4th ed., p. 324.

importance for any process of isotope separation which depends upon the establishment of an equilibrium state under the influence of a temperature gradient. In spite of the appearance of only ratios of cross section integrals in the description of this process, and the resulting complete lack of temperature dependence in the classical statistics for elastic sphere interaction, there is no *a priori* reason to believe that the temperature dependence in the quantum statistics is negligible for any interaction law.

From the point of view of isotope separation there is still another consideration which may be of importance. The ratios of cross sections which appear must involve, necessarily, similar and dissimilar molecules, and in a few cases, also, molecules of opposite statistics. The large effect arising from considerations of identity in the theory of collisions is, therefore, of importance in any consideration of separation of molecular species of approximately equal mass.

No numerical results are included in this paper, though preliminary calculations based on the elastic sphere model have been made in order to test the temperature sensitivity of the ratio of the thermal and pressure diffusion coefficients. In view of the known inadequacy of the elastic sphere model to even approximately describe the process of thermal diffusion these calculations are not included in this paper, though the results may be stated here. With this type of interaction the ratio of thermal and pressure diffusion coefficients shows a temperature dependence for the case of a mixture of helium and neon of approximately 20 percent between the temperatures of 10°K and 273°K as compared with a variation of approximately 30 percent in addition to the $T^{\frac{1}{2}}$ for each gas coefficient separately.

The formal theory of gas mixtures considered here is developed in three sections. The general theory of transport with a determination of the fundamental transport equations valid for a gas consisting of an arbitrary number of components is given in Section I. In Section II the differential integral equations for a gas of two components is solved according to usual methods valid for the case of infinitesimal deviations from the equilibrium state. In Section III an application of the variation method is made in order to obtain explicit forms for the gas coefficients.

Numerical calculations based on the theory and on the assumption of a five-parameter type of interaction are in progress. These results will be obtained for cases of particular interest and published in a succeeding paper.

I. The Transport Equations

The state of a gas consisting of N components is completely described by the distribution functions $f_i(x_\alpha, r_\alpha, t)$ which are solutions of the following differential integral equation:[8]

$$\frac{\partial f_i}{\partial t}+D_i(f_i)=\sum_{j=1}^{N}\int d\phi_j\int g_{ij}w_{ij}(\vartheta\varphi)d\Omega \times\{f_i'f_j'(1+\theta_i f_i)(1+\theta_j f_j) -f_i f_j(1+\theta_i f_i')(1+\theta_j f_j')\} \quad i=1,2,\cdots N, \quad (1)$$

where

$$D_i=r_{i\alpha}\partial/\partial x_\alpha+\mathfrak{x}_{i\alpha}\partial/\partial r_{i\alpha},$$

$$d\phi j=G_j(m_j/h)^3 dr_{j1}dr_{j2}dr_{j3}.$$

The distribution function f_i of these equations represents the number of particles of component i per cell of phase space of which the space part is taken to have the value unity. The notation adopted here is to use Latin letters as subscripts to designate the gas components, and to use Greek letters as subscripts to designate the components of vectors, with the repetition of a Greek letter as a subscript in the product of two quantities indicating a summation over the vector components. The meaning of the remaining quantities is as follows: $r_{i\alpha}$, the components of velocity of particles belonging to the ith specie; $\mathfrak{x}_{i\alpha}$, the force components per unit mass; G_i, a weight factor; g_{ij}, the relative velocity of two particles belonging to the ith and jth species; $w_{ij}(\vartheta\varphi)d\Omega$ where $d\Omega=\sin\vartheta d\vartheta d\phi$, the differential cross section for scattering in which the direction of the relative velocity is changed through an angle ϑ and falls into an element of solid angle $d\Omega$ after collision; m_i, the particle mass; and h, Planck's constant representing the volume of a cell in phase space. The statistics are determined

[8] Reference 3. See also R. H. Fowler, *Statistical Mechanics*, 2nd Ed. (Camb. Univ. Press, 1936), Chapter XVII.

by the value of θ_i, being Einstein-Bose if $\theta_i=1$ and Fermi-Dirac if $\theta_i=-1$. In this equation as in all succeeding equations in which collision integrals appear, primes are attached to functions of the velocity variables when the values of the variables after a collision are meant.

The general transport equations for the gas are obtained in the usual manner by multiplying Eq. (1) by a function $F_i(x_\alpha, r_\alpha, t)$, representing any additive property of the individual molecules, and integrating over all velocity space. Performing this operation, introducing new velocity variables $v_{i\alpha}=r_{i\alpha}-u_\alpha$, where u_α is any function of x_α, t possessing derivatives with respect to these variables, and defining

$$d/dt=\partial/\partial t+u_\alpha\partial/\partial x_\alpha$$

the general transport equation becomes

$$\frac{d}{dt}(n_i\langle F_i\rangle_{Av})+n_i\langle F_i\rangle_{Av}\frac{\partial u_\alpha}{\partial x_\alpha}+\frac{\partial}{\partial x_\alpha}(n_i\langle v_{i\alpha}F_i\rangle_{Av})$$
$$=n_i\left\{\left\langle\frac{dF_i}{dt}\right\rangle_{Av}+\left\langle v_{i\alpha}\frac{\partial F_i}{\partial x_\alpha}\right\rangle_{Av}+\left(\mathfrak{X}_{i\alpha}-\frac{du_\alpha}{dt}\right)\left\langle\frac{\partial F_i}{\partial v_{i\alpha}}\right\rangle_{Av}-\left\langle v_{i\alpha}\frac{\partial F_i}{\partial v_{i\beta}}\right\rangle_{Av}\frac{\partial u_\beta}{\partial x_\alpha}\right\}+\sum_{j=1}^{N}\Delta_{ij}(F_i),\quad(2)$$

where

$$\Delta_{ij}(F_i)=\int d\phi_i\int d\phi_j\int g_{ij}w_{ij}(\vartheta\varphi)d\Omega F_i\times\{f_i'f_j'(1+\theta_if_i)(1+\theta_jf_j)-f_if_j(1+\theta_if_i')(1+\theta_jf_j')\}.\quad(3)$$

Average values are taken with the distribution function, and n_i denotes the total number of particles per unit volume of component i. Symmetry considerations lead to the following properties for $\Delta_{ij}(F_i)$

$$\Delta_{ij}(F_i)=\tfrac{1}{2}\int d\phi_i\int d\phi_j\int g_{ij}w_{ij}d\Omega\times\{F_i-F_i'\}\{f_i'f_j'(1+\theta_if_i)(1+\theta_jf_j)-f_if_j(1+\theta_if_i')(1+\theta_jf_j')\}\quad\text{for } i\neq j,\quad(3a)$$

$$\Delta_{ii}(F_i)=\tfrac{1}{4}\int d\phi_i\int d\phi_{i1}\int g_{ii}w_{ii}d\Omega\times\{F_i-F_i'+F_{i1}-F_{i1}'\}\times\{f_i'f_{i1}'(1+\theta_if_i)(1+\theta_if_{i1})-f_if_{i1}(1+\theta_if_i')(1+\theta_if_{i1}')\},\quad(3b)$$

where for the case of $i=j$ a subscript 1 is attached to certain functions to distinguish the two velocity classes over which integration occurs.

The hydrodynamical equations are obtained from Eq. (2) by allowing the function F_i to assume in turn the character of mass, momentum, and kinetic energy. The function u_α is specialized to denote the components of mass velocity of the entire gas, and a variable $u_{i\alpha}=\langle r_{i\alpha}\rangle_{Av}$ is introduced to represent the same property for each of the gas components. The hydrodynamical equations then become

$$\frac{d\rho_i}{dt}+\rho_i\frac{\partial u_{i\alpha}}{\partial x_\alpha}+(u_{i\alpha}-u_\alpha)\frac{\partial\rho_i}{\partial x_\alpha}=0,\quad(4a)$$

$$\frac{dj_{i\alpha}}{dt}+j_{i\alpha}\frac{\partial u_\beta}{\partial x_\beta}+\frac{\partial p_{i\alpha\beta}}{\partial x_\beta}=\rho_i\left(\mathfrak{X}_{i\alpha}-\frac{du_\alpha}{dt}\right)-j_{i\beta}\frac{\partial u_\alpha}{\partial x_\beta}+\sum_{j=1}^{N}\Delta_{ij}(m_iv_{i\alpha}),\quad\alpha=1,2,3\quad(4b)$$

$$\rho_i\frac{d(Q_i/\rho_i)}{dt}+\frac{\partial q_{i\alpha}}{\partial x_\alpha}=\frac{Q_i}{\rho_i}\frac{\partial j_{i\alpha}}{\partial x_\alpha}+j_{i\alpha}\left(\mathfrak{X}_{i\alpha}-\frac{du_\alpha}{dt}\right)-p_{i\alpha\beta}S_{\alpha\beta}+\sum_{j=1}^{N}\Delta_{ij}\left(\frac{1}{2}m_iv_{i\alpha}v_{i\alpha}\right),\quad(4c)$$

where

$$\rho_i=n_im_i,\quad\rho=\sum_{i=1}^{N}\rho_i,\quad\rho u_\alpha=\sum_{i=1}^{N}\rho_iu_{i\alpha},$$

$$j_{i\alpha}=\rho_i(u_{i\alpha}-u_\alpha)=\frac{\rho_i}{\rho}\sum_{i=1}^{N}\rho_j(u_{i\alpha}-u_{j\alpha}),\quad\sum_{j=1}^{N}j_{j\alpha}=0,$$

$$p_{i\alpha\beta}=\rho_i\langle v_{i\alpha}v_{i\beta}\rangle_{Av},\qquad p_{\alpha\beta}=\sum_{i=1}^{N}p_{i\alpha\beta},$$

$$p_i=\tfrac{1}{3}\sum_{\alpha=1}^{3}p_{i\alpha\alpha},\qquad p=\sum_{i=1}^{N}p_i,\quad(5)$$

$$Q_i=\tfrac{1}{2}\rho_i\langle v_{i\alpha}v_{i\alpha}\rangle_{Av}=\tfrac{1}{2}\sum_{\alpha=1}^{3}p_{i\alpha\alpha}=\tfrac{3}{2}p_i,\quad Q=\sum_{i=1}^{N}Q_i,$$

$$q_{i\alpha}=\tfrac{1}{2}\rho_i\langle v_{i\alpha}v_{i\beta}v_{i\beta}\rangle_{Av},\qquad q_\alpha=\sum_{i=1}^{N}q_{i\alpha},$$

$$S_{\alpha\beta}=\tfrac{1}{2}\left(\frac{\partial u_\alpha}{\partial x_\beta}+\frac{\partial u_\beta}{\partial x_\alpha}\right).$$

Eqs. (4a, b and c) are, respectively, the continuity, hydrodynamical, and energy equations for the individual components of the gas mixture. The quantities $j_{i\alpha}$, $q_{i\alpha}$ and Q_i are, respectively, the mass current, heat current and kinetic energy density of the ith component in the gas, and $p_{\alpha\beta}$ and $S_{\alpha\beta}$ are, respectively, the stress and strain tensors for the gas as a whole.

The hydrodynamical equations for the gas mixture are now obtained by summing Eqs. (4) over all components. Using Eqs. (5) and the relations

$$\sum_{i,j}^{N}\Delta_{ij}(m_i v_{i\alpha})=0, \quad \sum_{i,j}^{N}\Delta_{ij}(\tfrac{1}{2}m_i v_{i\alpha}v_{i\alpha})=0,$$

which follow from (3a and b), one obtains for the entire mixture

$$\frac{d\rho}{dt}+\rho\frac{\partial u_\alpha}{\partial x_\alpha}=0, \tag{6a}$$

$$\frac{\partial p_{\alpha\beta}}{\partial x_\beta}=-\rho\frac{du_\alpha}{dt}+\sum_{i=1}^{N}\rho_i \mathfrak{X}_{i\alpha}, \ \alpha=1, 2, 3 \tag{6b}$$

$$\rho\frac{d(Q/\rho)}{dt}+\frac{\partial q_\alpha}{\partial x_\alpha}=-p_{\alpha\beta}S_{\alpha\beta}+\sum_{i=1}^{N}j_{i\alpha}\mathfrak{X}_{i\alpha}. \tag{6c}$$

In the summation over i in Eq. (4c) two of the terms are conveniently grouped, and with the use of Eq. (4a) put in the form

$$\rho_i\frac{d(Q_i/\rho_i)}{dt}-\frac{Q_i}{\rho_i}\frac{\partial j_{i\alpha}}{\partial x_\alpha}=\frac{dQ_i}{dt}+Q_i\frac{\partial u_\alpha}{\partial x_\alpha}.$$

Equations (4) and (6) are exact. The form of these equations in zeroth approximation is of some interest. In this approximation all mean values quantities are evaluated for an equilibrium state of the gas. Since there are $N+4$ gas parameters, ρ_i, u_α and T ($i=1, 2, \cdots N$; $\alpha=1, 2, 3$), describing the equilibrium state of an N component gas, there must be just $N+4$ zero-order hydrodynamical equations. These equations may be obtained from (4a, 6b and 6c) by introducing the conditions of spherical symmetry into the evaluation of $p_{i\alpha\beta}$, $q_{i\alpha}$ and $j_{i\alpha}$. The form of the equations will be given in the next section in connection with the determination of the first approximation to the nonequilibrium distribution function.

II. Solution of the Boltzmann Equation

§ 1. Principle of solution

Applying the method of Lorentz, Hilbert and Enskog to Eq. (1) we seek an approximate solution of the form

$$f_i=f_i^{(0)}(1+\varphi_i), \tag{7}$$

where $f_i^{(0)}$ is the equilibrium distribution function, and φ_i is a function of the velocity, temperature, and pressure gradients within the gas, and expresses in first approximation the departure of the actual distribution function from that corresponding to the equilibrium state. The equilibrium distribution function is determined by the vanishing of the collision integral in Eq. (1). Multiplying this integral by $\ln f_i/(1+\theta_i f_i)d\phi_i$, integrating, and using Eqs. (3a and b) one obtains in the manner familiar from the development of the H theorem

$$f_i^{(0)}=[A_i^{-1}\exp\{m_i(r_{i\alpha}-u_\alpha)\times(r_{i\alpha}-u_\alpha)/2kT\}-\theta_i]^{-1}, \tag{8}$$

where the constants u_α are necessarily the same for all gas components.

Proceeding to the next approximation in the determination of f_i, its form given by (7) is substituted into Eq. (1), and second-order quantities are neglected. This corresponds to the introduction of $f_i^{(0)}$ into the left member and the neglect of products of the φ_i in the right member of Eq. (1). Defining

$$\chi_j=\varphi_i/(1+\theta_i f_i^{(0)}), \tag{9}$$

one then obtains an integral equation for φ_i which is

$$\frac{\partial f_i^{(0)}}{\partial t}+D_i(f_i^{(0)})=-\sum_{j=1}^{N}I_{ij}(\chi), \tag{10}$$

where

$$I_{ij}(\chi)=\int d\phi_j\int g_{ij}w_{ij}(\vartheta\varphi)d\Omega f_i^{(0)\prime}f_j^{(0)\prime}\times(1+\theta_i f_i^{(0)})(1+\theta_j f_j^{(0)})[\chi_i+\chi_j\to\chi_i'-\chi_j']. \tag{11}$$

Considering now the homogeneous part of Eq. (10), multiplying it by $\chi_i d\phi_i$ and integrating, one obtains

$$\sum_{j=1}^{N}[\chi,\chi]_{ij}=0, \tag{12}$$

where for functions F and G of the velocity components

$$[F, G]_{ij}=\int d\phi_i F_i I_{ij}(G)$$
$$=\int d\phi_i \int d\phi_j \int g_{ij} w_{ij}(\vartheta\varphi) d\Omega \times f_i^{(0)\prime} f_j^{(0)\prime}(1+\theta_i f_i^{(0)})(1+\theta_j f_j^{(0)}) \times F_i[G_i+G_j-G_i'-G_j']. \quad (13)$$

As in the derivation of Eqs. (3a and b) one may write

$$[F, G]_{ij}=\tfrac{1}{2}\int d\phi_i \int d\phi_j \int g_{ij} w_{ij}(\vartheta\varphi) f_i^{(0)\prime} \times f_j^{(0)\prime}(1+\theta_i f_i^{(0)})(1+\theta_j f_j^{(0)}) \times (F_i-F_i')(G_i+G_j-G_i'-G_j') \quad \text{for } i\neq j, \quad (14a)$$

$$[F, G]_{ii}=\tfrac{1}{4}\int d\phi_i \int d\phi_{i1} \int g_{ii} w_{ii}(\vartheta\varphi) f_i^{(0)\prime} \times f_{i1}^{(0)\prime}(1+\theta_i f_i^{(0)})(1+\theta_i f_{i1}^{(0)}) \times (F_i+F_{i1}-F_i'-F_{i1}') \times (G_i+G_{i1}-G_i'-G_{i1}'). \quad (14b)$$

Then

$$[F, F]_{ij}+[F, F]_{ji}\geq 0. \quad (15)$$

The solutions $\chi_i^{(0)}$ of Eq. (12) are null solutions of Eq. (10). In order that such solutions exist it follows necessarily from (12) that

$$\sum_{i,j}[\chi^{(0)}, \chi^{(0)}]_{ij}=\sum_i [\chi^{(0)}, \chi^{(0)}]_{ii} + \sum_{i<j}\{[\chi^{(0)}, \chi^{(0)}]_{ij}+[\chi^{(0)}, \chi^{(0)}]_{ji}\}=0. \quad (16)$$

Since, by Eq. (15), every term in this sum is positive definite, null solutions are those which fulfill the relation

$$\chi_i^{(0)}+\chi_j^{(0)}-\chi_i^{(0)\prime}-\chi_j^{(0)\prime}=0, \quad i, j=1, 2, \cdots N, \quad (17)$$

or

$$\chi_i^{(0)}=a_i+c_0 m_i r_{i\alpha} r_{i\alpha}+m_i c_\alpha r_{i\alpha}, \quad (18)$$

containing five arbitrary constants which are functions of x_α and t, and of which only one may be different for the different components. The form (18) of $\chi_i^{(0)}$ follows strictly from (17) for spherically symmetric molecules without internal degrees of freedom to which the theory is restricted. The existence of null solutions of Eq. (10) permits the imposition of auxiliary conditions on the solution χ_i which are taken to be of the following form

$$\int f_i^{(0)}\varphi_i d\phi_i=\int f_i^{(0)}(1+\theta_i f_i^{(0)})\chi_i d\phi_i=0, \quad (19a)$$

$$\sum_{i=1}^N m_i \int (r_{i\alpha}-u_\alpha) f_i^{(0)}\varphi_i d\phi_i = \sum_{i=1}^N m_i \int (r_{i\alpha}-u_\alpha) f_i^{(0)}(1+\theta_i f_i^{(0)})\chi_i d\phi_i=0, \quad \alpha=1, 2, 3, \quad (19b)$$

$$\sum_{i=1}^N m_i \int (r_{i\alpha}-u_\alpha)(r_{i\alpha}-u_\alpha) f_i^{(0)}\varphi_i d\phi_i = \sum_{i=1}^N m_i \int (r_{i\alpha}-u_\alpha)(r_{i\alpha}-u_\alpha) f_i^{(0)} \times (1+\theta_i f_i^{(0)})\chi_i d\phi_i=0. \quad (19c)$$

The physical interpretation of these conditions is that the macroscopic description of the gas in terms of the $N+4$ parameters ρ_i, u_α and T is unaltered by the perturbation. Thus, from Eqs. (7) and (19)

$$\rho_i=m_i\int f_i d\phi_i=m_i\int f_i^{(0)} d\phi_i, \quad (20a)$$

$$\rho u_\alpha=\sum_{i=1}^N \rho_i u_{i\alpha}=\sum_{i=1}^N m_i \int r_{i\alpha} f_i d\phi_i = \sum_{i=1}^N m_i \int r_{i\alpha} f_i^{(0)} d\phi_i, \quad (20b)$$

$$\rho\epsilon=\sum_{i=1}^N \rho_i \epsilon_i=\tfrac{1}{2}\sum_{i=1}^N m_i \int (r_{i\alpha}-u_\alpha)(r_{i\alpha}-u_\alpha) f_i d\phi_i = \tfrac{1}{2}\sum_{i=1}^N m_i \int (r_{i\alpha}-u_\alpha)(r_{i\alpha}-u_\alpha) f_i^{(0)} d\phi_i = \tfrac{3}{2}\sum_{i=1}^N p_i=\tfrac{3}{2}\sum_{i=1}^N \frac{RT}{M_i}\rho_i W_i(T\rho_i^{-1}), \quad (20c)$$

where ϵ_i and ϵ are the kinetic energies per unit mass in component i and in the entire gas, respectively. The last two forms given in Eq. (20c) follow from the definitions given in Eqs. (5) and the well-known form of the equation of state for ideal gases.[9]

[9] G. E. Uhlenbeck and E. A. Uehling, Phys. Rev. **39**, 1014 (1932).

If Eq. (10) is multiplied by $\chi_i^{(0)}d\phi_i$, integrated and summed over i, the right member vanishes by (14a and b and 17). Setting successively all but one of the $N+4$ arbitrary constants in $\chi_i^{(0)}$ equal to zero, one thus obtains $N+4$ equations representing the orthogonality conditions which must be fulfilled in order that Eq. (10) possess a solution. These conditions may be written in the form

$$\int m_i\left[\frac{\partial f_i^{(0)}}{\partial t}+D_i(f_i^{(0)})\right]d\phi_i=0, \quad i=1, 2, \cdots N, \quad (21a)$$

$$\sum_i\int m_i r_{i\alpha}\left[\frac{\partial f_i^{(0)}}{\partial t}+D_i(f_i^{(0)})\right]d\phi_i=0, \quad \alpha=1, 2, 3, \quad (21b)$$

$$\sum_i\int m_i r_{i\alpha}r_{i\alpha}\left[\frac{\partial f_i^{(0)}}{\partial t}+D_i(f_i^{(0)})\right]d\phi_i=0. \quad (21c)$$

One may readily show[10] that these conditions are equivalent to the requirement that the parameters ρ_i, u_α and T of the equilibrium distribution function satisfy the hydrodynamical equations in zeroth approximation. Since this approximation is obtained by introducing the conditions for an equilibrium state, one evaluates the various mean value quantities of the transport equations under the assumption of a spherically symmetric velocity distribution. Thus, one has in this approximation

$$u_{i\alpha}=u_\alpha, \quad j_{i\alpha}=0, \quad q_{i\alpha}=0,$$
$$p_{i\alpha\beta}=p_i\delta_{\alpha\beta}, \quad p_{\alpha\beta}=p\delta_{\alpha\beta}.$$

Then from Eqs. (4a, 6b and c) the zeroth approximation to the hydrodynamical equations equivalent to the orthogonality conditions (21) are

$$\frac{d\rho_i}{dt}+\rho_i\frac{\partial u_\alpha}{\partial x_\alpha}=0, \quad i=1, 2, \cdots N, \quad (22a)$$

$$\frac{\partial p}{\partial x_\alpha}=-\rho\frac{du_\alpha}{dt}+\sum_{i=1}^{N}\rho_i\mathfrak{X}_{i\alpha}, \quad \alpha=1, 2, 3, \quad (22b)$$

$$\rho\frac{d(Q/\rho)}{dt}=-p\frac{\partial u_\alpha}{\partial x_\alpha}. \quad (22c)$$

As in the classical theory of the one component gas[11] one can now show that if a general solution χ of Eq. (10) is decomposed into a term satisfying the auxiliary conditions (19) and a term which is a null solution of the form (18) with constants a_i, c_0 and c_α ($i=1, 2, \cdots N$; $\alpha=1, 2, 3$), the constants can without loss of generality be chosen equal to zero at $t=t_0$, and they then remain equal to zero for all values of t. If a solution of Eq. (10) is obtained, then, subject to the condition that the gas parameters satisfy Eqs. (22), the auxiliary conditions (19) may be imposed and remain valid for all values of the time.

§ 2. Decomposition of the integral equation

Returning now to Eq. (10) the left member is transformed by the introduction of $f_i^{(0)}$ from Eq. (8) and the substitution of new velocity variables $\xi_{i\alpha}$ for $r_{i\alpha}$ according to the definition

$$\xi_{i\alpha}=(r_{i\alpha}-u_\alpha)c_i^{\frac{1}{2}}, \quad \tau_i^2=\xi_{i\alpha}\xi_{i\alpha}, \quad (23)$$

where $c_i=m_i/2kT$. Then Eq. (10) becomes

$$\frac{f_i^{(0)2}}{A_i e^{-\tau_i^2}}\left[\frac{d\ln A_i}{dt}+\frac{\tau_i^2}{T}\frac{dT}{dt}+\frac{\xi_{i\alpha}}{c_i^{\frac{1}{2}}}\left\{\frac{\partial\ln A_i}{\partial x_\alpha}-2c_i\left(\mathfrak{X}_{i\alpha}-\frac{du_\alpha}{dt}\right)+\frac{\tau_i^2}{T}\frac{\partial T}{\partial x_\alpha}\right\}+2\xi_{i\alpha}\xi_{i\beta}\frac{\partial u_\alpha}{\partial x_\beta}\right]=-\sum_{j=1}^{N}I_{ij}(\chi). \quad (24)$$

The time derivatives in the left member of this equation may be eliminated by making use of the following relations:[12]

$$\frac{d\ln A_i}{dt}=\frac{dW_i}{dt}+W_i\left(\frac{1}{\rho_i}\frac{d\rho_i}{dt}-\frac{3}{2}\frac{1}{T}\frac{dT}{dt}\right), \quad (25a)$$

$$\frac{\partial\ln A_i}{\partial x_\alpha}=\frac{p_i}{n_i kT}\left(\frac{1}{p_i}\frac{\partial p_i}{\partial x_\alpha}-\frac{5}{2}\frac{1}{T}\frac{\partial T}{\partial x_\alpha}\right), \quad (25b)$$

with $W_i(Tp_i^{-\frac{2}{3}})$, the function defined in (20c), an adiabatic invariant. In accordance with the discussion of §1 all time derivatives of the gas parameters must fulfill the hydrodynamical equations in zeroth approximation. Then (25a) and (25b) must be evaluated subject to the conditions

[10] Reference 2, note 2.

[11] D. Enskog, *Kinetische Theorie der Vorgänge in mässig verdünnten Gasen, Dissertation* (Upsala, 1917).

[12] Reference 2, note 3; Phys. Rev. **39**, 1014 (1932).

given by Eqs. (22) and the vanishing of the total time derivative of W_i. For this purpose, Eq. (22c) is expressed in the form

$$dT/dt = -\tfrac{2}{3}T\partial u_\alpha/\partial x_\alpha, \tag{26}$$

which is obtained in the following manner:

$$Q = \tfrac{3}{2}p = \tfrac{3}{2}RT\sum_{i=1}^{N}\frac{\rho_i}{M_i}W_i(T\rho_i^{-1}),$$

$$\frac{d}{dt}\left(\frac{p}{\rho}\right) = \frac{p}{\rho T}\frac{dT}{dt} - \frac{p}{\rho^2}\frac{d\rho}{dt} + \frac{RT}{\rho}\sum_{i=1}^{N}\frac{W_i}{M_i}\frac{d\rho_i}{dt} + \frac{RT}{\rho}\sum_{i=1}^{N}\frac{\rho_i}{M_i}\frac{dW_i}{dt}.$$

The second and third terms of this equation vanish as a consequence of (22a) and the fourth as a consequence of the adiabatic invariance of W_i. Introducing Eqs. (22a, b and 26) into Eqs. (25a and b) one obtains

$$\frac{d\ln A_i}{dt} = 0, \tag{27a}$$

$$\frac{\partial \ln A_i}{\partial x_\alpha} - 2c_i\left(\mathfrak{x}_{i\alpha} - \frac{du_\alpha}{dt}\right) = \frac{1}{n_i kT}\left[-\frac{5}{2}\frac{p_i}{T}\frac{\partial T}{\partial x_\alpha} + \frac{\partial p_i}{\partial x_\alpha} - \rho_i\mathfrak{x}_{i\alpha} - \frac{\rho_i}{\rho}\sum_{j=1}^{N}\left(\frac{\partial p_j}{\partial x_\alpha} - \rho_j\mathfrak{x}_{j\alpha}\right)\right]. \tag{27b}$$

Then the integral Eq. (24) becomes

$$\frac{f_i^{(0)2}}{A_i e^{-\tau_i^2}}\left[\frac{1}{c_i^{\frac{1}{2}}}\frac{1}{T}\xi_{i\alpha}\frac{\partial T}{\partial x_\alpha}\left(\tau_i^2 - \frac{5}{2}\frac{p_i}{n_i kT}\right) + \left(\xi_{i\alpha}\xi_{i\beta} - \frac{\tau_i^2}{3}\delta_{\alpha\beta}\right)\left(\frac{\partial u_\alpha}{\partial x_\beta} + \frac{\partial u_\beta}{\partial x_\alpha}\right) + \frac{2c_i^{\frac{1}{2}}}{\rho_i}\xi_{i\alpha}\left\{\left(\frac{\partial p_i}{\partial x_\alpha} - \rho_i\mathfrak{x}_{i\alpha}\right) - \frac{\rho_i}{\rho}\sum_{j=1}^{N}\left(\frac{\partial p_j}{\partial x_\alpha} - \rho_j\mathfrak{x}_{j\alpha}\right)\right\}\right] = -\sum_{j=1}^{N}I_{ij}(\chi). \tag{28}$$

In the collision integrals $I_{ij}(\chi)$ it is convenient to introduce in addition to the variables $\xi_{i\alpha}$ a new relative velocity variable γ_{ij} for the g_{ij} defined by

$$g_{ij} = \gamma_{ij}\left(\frac{c_i + c_j}{c_i c_j}\right)^{\frac{1}{2}}.$$

Denoting $d\omega_i = d\xi_{i1}d\xi_{i2}d\xi_{i3}$, so that

$$d\phi_i = G_i\left(\frac{m_i}{h}\right)^3 c_i^{-\frac{1}{2}}d\omega_i,$$

the collision integral written out in full becomes

$$I_{ij}(\chi) = G_j\left(\frac{m_j}{h}\right)^3\left(\frac{c_i + c_j}{c_i c_j}\right)^{\frac{1}{2}}c_j^{-\frac{1}{2}} \times F_{\frac{1}{2}}(A_i)F_{\frac{1}{2}}(A_j)J_{ij}(\chi), \tag{29}$$

where

$$J_{ij}(\chi) = F_{\frac{1}{2}}^{-1}(A_i)F_{\frac{1}{2}}^{-1}(A_j)\int d\omega_j\int\gamma_{ij}w_{ij}(\vartheta\varphi)d\Omega \times f_i^{(0)\prime}f_j^{(0)\prime}(1+\theta_i f_i^{(0)}) \times(1+\theta_j f_j^{(0)})(\chi_i + \chi_j - \chi_i' - \chi_j') \tag{30}$$

and

$$F_S(A_i) = \frac{1}{\Gamma(S+1)}\int_0^\infty\frac{u^S du}{(1/A_i)\exp u - \theta_i} \tag{30a}$$

is the Sommerfeld integral.

Equation (28) with I_{ij} defined by Eqs. (29) and (30) must be solved now for χ_i in order to determine the distribution function to the first order of approximation. We consider here only a two-component gas and restrict all further considerations to this case. Writing out Eq. (28) in full one has then

$$\frac{f_1^{(0)2}}{A_1 e^{-\tau_1^2}}\left[\frac{1}{c_1^{\frac{1}{2}}}\frac{1}{T}\xi_{1\alpha}\frac{\partial T}{\partial x_\alpha}\left(\tau_1^2 - \frac{5}{2}\frac{p_1}{n_1 kT}\right) + \left(\xi_{1\alpha}\xi_{1\beta} - \frac{\tau_1^2}{3}\delta_{\alpha\beta}\right)\left(\frac{\partial u_\alpha}{\partial x_\beta} + \frac{\partial u_\beta}{\partial x_\alpha}\right) + \frac{2c_1^{\frac{1}{2}}}{\rho_1}\xi_{1\alpha}\left\{\frac{\rho_2}{\rho}\frac{\partial p_1}{\partial x_\alpha} - \frac{\rho_1}{\rho}\frac{\partial p_2}{\partial x_\alpha} - \frac{\rho_1\rho_2}{\rho}(\mathfrak{x}_{1\alpha} - \mathfrak{x}_{2\alpha})\right\}\right] = -G_1\left(\frac{m_1}{h}\right)^3\frac{2^{\frac{1}{2}}}{c_1^2}F_{\frac{1}{2}}^2(A_1)J_{11}(\chi) - G_2\left(\frac{m_2}{h}\right)^3\left(\frac{c_1 + c_2}{c_1 c_2}\right)^{\frac{1}{2}}c_2^{-\frac{1}{2}}F_{\frac{1}{2}}(A_1)F_{\frac{1}{2}}(A_2)J_{12}(\chi), \tag{31a}$$

$$\frac{f_2^{(0)2}}{A_2 e^{-\tau_2^2}}\left[\frac{1}{c_2^{\frac{1}{2}}}\frac{1}{T}\xi_{2\alpha}\frac{\partial T}{\partial x_\alpha}\left(\tau_2^2 - \frac{5}{2}\frac{p_2}{n_2 kT}\right) + \left(\xi_{2\alpha}\xi_{2\beta} - \frac{\tau_2^2}{3}\delta_{\alpha\beta}\right)\left(\frac{\partial u_\alpha}{\partial x_\beta} + \frac{\partial u_\beta}{\partial x_\alpha}\right) + \frac{2c_2^{\frac{1}{2}}}{\rho_2}\xi_{2\alpha}\left\{\frac{\rho_1}{\rho}\frac{\partial p_2}{\partial x_\alpha} - \frac{\rho_2}{\rho}\frac{\partial p_1}{\partial x_\alpha} - \frac{\rho_2\rho_1}{\rho}(\mathfrak{x}_{2\alpha} - \mathfrak{x}_{1\alpha})\right\}\right]$$

$$= -G_1\left(\frac{m_1}{h}\right)^3\left(\frac{c_1+c_2}{c_1c_2}\right)^{\frac{1}{2}}c_1^{-\frac{1}{2}}F_{\frac{1}{2}}(A_1)F_{\frac{1}{2}}(A_2)J_{21}(\chi)$$

$$-G_2\left(\frac{m_2}{h}\right)^3\frac{2^{\frac{1}{2}}}{c_2^2}F_{\frac{1}{2}}^2(A_2)J_{22}(\chi). \quad (31b)$$

The solution of these equations is to be obtained subject to the auxiliary conditions (19) which now take the form

$$\int f_i^{(0)}(1+\theta_i f_i^{(0)})\chi_i d\omega_i = 0, \qquad i=1, 2, \quad (32a)$$

$$G_1 m_1^2\int \xi_{1\alpha}f_1^{(0)}(1+\theta_1 f_1^{(0)})\chi_1 d\omega_1$$

$$+G_2 m_2^2\int \xi_{2\alpha}f_2^{(0)}(1+\theta_2 f_2^{(0)})\chi_2 d\omega_2 = 0,$$

$$\alpha=1, 2, 3. \quad (32b)$$

$$G_1 m_1^{\frac{1}{2}}\int \xi_{1\alpha}\xi_{1\alpha}f_1^{(0)}(1+\theta_1 f_1^{(0)})\chi_1 d\omega_1$$

$$+G_2 m_2^{\frac{1}{2}}\int \xi_{2\alpha}\xi_{2\alpha}f_2^{(0)}(1+\theta_2 f_2^{(0)})\chi_2 d\omega_2 = 0. \quad (32c)$$

Since Eqs. (31) are linear, and all temperature, velocity and pressure gradients and the external forces are arbitrary, the solution χ_i may be decomposed into a linear combination of twelve functions $\mathrm{X}_{i\alpha}$, $\Psi_{i\alpha}$ and $\Pi_{i\alpha\beta}$ ($\alpha, \beta=1, 2, 3$; $\Pi_{i\alpha\beta}=\Pi_{i\beta\alpha}$) with coefficients depending on the gas constants and parameters together with their gradients. Thus, we may express

$$\chi_i = -\frac{\pi^{\frac{1}{2}}}{n_1n_2}\left(\frac{m_1m_2}{m_1+m_2}\right)^{\frac{1}{2}}\left[\frac{\mathrm{X}_{i\alpha}}{kT}\left\{\frac{\rho_2}{\rho}\frac{\partial p_1}{\partial x_\alpha}\right.\right.$$

$$\left.\left.-\frac{\rho_1}{\rho}\frac{\partial p_2}{\partial x_\alpha}+\frac{\rho_1\rho_2}{\rho}(\mathfrak{X}_{2\alpha}-\mathfrak{X}_{1\alpha})\right\}+\frac{\Psi_{i\alpha}}{T}\frac{\partial T}{\partial x_\alpha}\right.$$

$$\left.+\frac{\Pi_{i\alpha\beta}}{(2kT)^{\frac{1}{2}}}\left(\frac{\partial u_\alpha}{\partial x_\beta}+\frac{\partial u_\beta}{\partial x_\alpha}\right)\right], \quad i=1, 2. \quad (33)$$

Introducing this form of χ_i into Eqs. (31) and using the relation

$$\rho_i = n_i m_i = m_i G_i\left(\frac{2\pi m_i kT}{h^2}\right)^{\frac{1}{2}}F_{\frac{1}{2}}(A_i),$$

which follows directly from (8) and (20a), one obtains the following component equations for the individual functions

$$\frac{\xi_{1\alpha}}{m_1^{\frac{1}{2}}}\frac{f_1^{(0)2}e^{\tau_1^2}}{A_1F_{\frac{1}{2}}(A_1)} = \frac{n_1}{n_2}\left(\frac{2m_2}{m_1+m_2}\right)^{\frac{1}{2}}J_{11}(\mathrm{X}_\alpha)$$

$$+J_{12}(\mathrm{X}_\alpha), \quad (34a)$$

$$-\frac{\xi_{2\alpha}}{m_2^{\frac{1}{2}}}\frac{f_2^{(0)2}e^{\tau_2^2}}{A_2F_{\frac{1}{2}}(A_2)} = J_{21}(\mathrm{X}_\alpha)$$

$$+\frac{n_2}{n_1}\left(\frac{2m_1}{m_1+m_2}\right)^{\frac{1}{2}}J_{22}(\mathrm{X}_\alpha), \quad (34b)$$

$$\frac{n_1}{m_1^{\frac{1}{2}}}\xi_{1\alpha}\left(\tau_1^2-\frac{5}{2}\frac{p_1}{n_1kT}\right)\frac{f_1^{(0)2}e^{\tau_1^2}}{A_1F_{\frac{1}{2}}(A_1)}$$

$$=\frac{n_1}{n_2}\left(\frac{2m_2}{m_1+m_2}\right)^{\frac{1}{2}}J_{11}(\Psi_\alpha)+J_{12}(\Psi_\alpha), \quad (34c)$$

$$\frac{n_2}{m_2^{\frac{1}{2}}}\xi_{2\alpha}\left(\tau_2^2-\frac{5}{2}\frac{p_2}{n_2kT}\right)\frac{f_2^{(0)2}e^{\tau_2^2}}{A_2F_{\frac{1}{2}}(A_2)}$$

$$=J_{21}(\Psi_\alpha)+\frac{n_2}{n_1}\left(\frac{2m_1}{m_1+m_2}\right)^{\frac{1}{2}}J_{22}(\Psi_\alpha), \quad (34d)$$

$$n_1\left(\xi_{1\alpha}\xi_{1\beta}-\frac{\tau_1^2}{3}\delta_{\alpha\beta}\right)\frac{f_1^{(0)2}e^{\tau_1^2}}{A_1F_{\frac{1}{2}}(A_1)}$$

$$=\frac{n_1}{n_2}\left(\frac{2m_2}{m_1+m_2}\right)^{\frac{1}{2}}J_{11}(\Pi_{\alpha\beta})+J_{12}(\Pi_{\alpha\beta}), \quad (34e)$$

$$n_2\left(\xi_{2\alpha}\xi_{2\beta}-\frac{\tau_2^2}{3}\delta_{\alpha\beta}\right)\frac{f_2^{(0)2}e^{\tau_2^2}}{A_2F_{\frac{1}{2}}(A_2)}$$

$$=J_{21}(\Pi_{\alpha\beta})+\frac{n_2}{n_1}\left(\frac{2m_1}{m_1+m_2}\right)^{\frac{1}{2}}J_{22}(\Pi_{\alpha\beta}). \quad (34f)$$

As in the simple gas theory[13] one can show from the form of these equations as linear integral equations of the second kind that the functions $\mathrm{X}_{i\alpha}$, $\Psi_{i\alpha}$ and $\Pi_{i\alpha\beta}$ are necessarily of the form

$$\mathrm{X}_{i\alpha} = \xi_{i\alpha}\chi_i(\tau^2), \quad (35a)$$

$$\Psi_{i\alpha} = \xi_{i\alpha}\psi_i(\tau^2), \quad (35b)$$

$$\Pi_{i\alpha\beta} = (\xi_{i\alpha}\xi_{i\beta}-\tfrac{1}{3}\tau_i^2\delta_{\alpha\beta})\pi_i(\tau^2). \quad (35c)$$

In terms of the solutions of Eqs. (34) a formal expression for the distribution function may now

[13] D. Enskog, reference 11, p. 37.

be given. Using Eqs. (7), (8), (9), (33) and (35) one obtains

$$f_i=f_i^{(0)}\Big[1-\frac{\pi^{\frac{1}{2}}}{n_1n_2}\Big(\frac{m_1m_2}{m_1+m_2}\Big)^{\frac{1}{2}}\frac{f_i^{(0)}e^{\tau_i^2}}{A_i}$$
$$\times\Big\{\frac{\xi_{i\alpha}\chi_i}{kT}\Big[\frac{\rho_2}{\rho}\frac{\partial p_1}{\partial x_\alpha}-\frac{\rho_1}{\rho}\frac{\partial p_2}{\partial x_\alpha}$$
$$+\frac{\rho_1\rho_2}{\rho}(\mathfrak{X}_{2\alpha}-\mathfrak{X}_{1\alpha})\Big]+\frac{\xi_{i\alpha}\psi_i}{T}\frac{\partial T}{\partial x_\alpha}$$
$$+\Big(\xi_{i\alpha}\xi_{i\beta}-\frac{\tau_i^2}{3}\delta_{\alpha\beta}\Big)\frac{\pi_i}{(2kT)^{\frac{1}{2}}}\Big(\frac{\partial u_\alpha}{\partial x_\beta}+\frac{\partial u_\beta}{\partial x_\alpha}\Big)\Big\}\Big],$$
$$i=1,\ 2, \quad (36)$$

giving the distribution function in a form containing unknown functions which depend only on τ_i^2. Using this form of the function all phenomena of transport may be considered, and the transport coefficients may be evaluated. The numerical values of these coefficients, in which we are particularly interested, may then be obtained by a variation method which will be discussed in succeeding sections.

§ 3. The diffusion coefficients

The gas coefficients which we now seek to evaluate are found as constants in the evaluation of the mean value quantities of the hydrodynamical equations. Referring to Eqs. (5) the quantities to be evaluated are

$$j_{1\alpha}=-j_{2\alpha}=(\rho_1\rho_2/\rho)(u_{1\alpha}-u_{2\alpha}),$$
$$p_{i\alpha\beta}=\rho_i\langle v_{i\alpha}v_{i\beta}\rangle_{Av},$$
$$q_{i\alpha}=\tfrac{1}{2}\rho_i\langle v_{i\alpha}v_{i\beta}v_{i\beta}\rangle_{Av},$$

the remaining quantities ρ_i, u_α and

$$Q_i=\tfrac{3}{2}p_i=\tfrac{1}{2}\sum_{\alpha=1}^{3}p_{i\alpha\alpha}$$

remaining unchanged from their values as given by the equilibrium distribution function by virtue of the auxiliary conditions (20). Considering first the case of diffusion we evaluate the quantity $(u_{1\alpha}-u_{2\alpha})$ given by the equation

$$u_{1\alpha}-u_{2\alpha}=\frac{1}{n_1}\int f_1r_{1\alpha}d\phi_1-\frac{1}{n_2}\int f_2r_{2\alpha}d\phi_2$$
$$=\frac{G_1}{n_1c_1^2}\Big(\frac{m_1}{h}\Big)^3\int f_1\xi_{1\alpha}d\omega_1$$
$$-\frac{G_2}{n_2c_2^2}\Big(\frac{m_2}{h}\Big)^3\int f_2\xi_{2\alpha}d\omega_2.$$

Introducing f_1 and f_2 as given by Eq. (36) one obtains

$$u_{1\alpha}-u_{2\alpha}=-\kappa\Big[\frac{\rho_2}{\rho}\frac{\partial p_1}{\partial x_\alpha}-\frac{\rho_1}{\rho}\frac{\partial p_2}{\partial x_\alpha}$$
$$+\frac{\rho_1\rho_2}{\rho}(\mathfrak{X}_{2\alpha}-\mathfrak{X}_{1\alpha})+\nu\frac{\partial T}{\partial x_\alpha}\Big], \quad (37)$$

where

$$\kappa=2\frac{(2kT)}{h^3}\frac{\pi^{\frac{1}{2}}}{n_1n_2}\Big(\frac{m_1m_2}{m_1+m_2}\Big)^{\frac{1}{2}}\Big[\frac{G_1m_1}{n_1A_1}\int f_1^{(0)^2}e^{\tau_1^2}$$
$$\times\xi_1^2\chi_1d\omega_1-\frac{G_2m_2}{n_2A_2}\int f_2^{(0)^2}e^{\tau_2^2}\xi_2^2\chi_2d\omega_2\Big], \quad (38a)$$

$$\kappa\nu=2k\frac{(2kT)}{h^3}\frac{\pi^{\frac{1}{2}}}{n_1n_2}\Big(\frac{m_1m_2}{m_1+m_2}\Big)^{\frac{1}{2}}\Big[\frac{G_1m_1}{n_1A_1}\int f_1^{(0)^2}e^{\tau_1^2}$$
$$\times\xi_1^2\psi_1d\omega_1-\frac{G_2m_2}{n_2A_2}\int f_2^{(0)^2}e^{\tau_2^2}\xi_2^2\psi_2d\omega_2\Big]. \quad (38b)$$

In these integrals, which contain the square of a single vector component $\xi_{1\alpha}^2$, the distinguishing subscript α has been dropped. If we now multiply Eqs. (34a and b) by $\xi_1\chi_1d\omega_1=\mathrm{X}_1d\omega_1$ and $\xi_2\chi_2d\omega_2=\mathrm{X}_2d\omega_2$, respectively, and integrate, and then substitute the left member into Eqs. (38a) one obtains

$$\kappa=\frac{2}{(2kT)^{\frac{1}{2}}}\frac{1}{n_1n_2}\Big(\frac{m_1m_2}{m_1+m_2}\Big)^{\frac{1}{2}}$$
$$\times\Big[\frac{n_1}{n_2}\Big(\frac{2m_2}{m_1+m_2}\Big)^{\frac{1}{2}}\int\mathrm{X}_1J_{11}(\mathrm{X})d\omega_1$$
$$+\int\mathrm{X}_1J_{12}(\mathrm{X})d\omega_1+\int\mathrm{X}_2J_{21}(\chi)d\omega_2$$
$$+\frac{n_2}{n_1}\Big(\frac{2m_1}{m_1+m_2}\Big)^{\frac{1}{2}}\int\mathrm{X}_2J_{22}(\mathrm{X})d\omega_2\Big]. \quad (39a)$$

Similarly, multiplying Eqs. (34a and b) by $\xi_1\psi_1 d\omega_1=\Psi_1 d\omega_1$ and $\xi_2\psi_2 d\omega_2=\Psi_2 d\omega_2$, respectively, one obtains

$$\kappa\nu=\frac{2k}{(2kT)^{\frac{1}{2}}}\frac{1}{n_1n_2}\left(\frac{m_1m_2}{m_1+m_2}\right)^{\frac{1}{2}}\times\left[\frac{n_1}{n_2}\left(\frac{2m_2}{m_1+m_2}\right)^{\frac{1}{2}}\int\Psi_1J_{11}(\mathrm{X})d\omega_1+\int\Psi_1J_{12}(\mathrm{X})d\omega_1+\int\Psi_2J_{21}(\mathrm{X})d\omega_2+\frac{n_2}{n_1}\left(\frac{2m_1}{m_1+m_2}\right)^{\frac{1}{2}}\int\Psi_2J_{22}(\mathrm{X})d\omega_2\right]. \quad (39b)$$

In a manner analogous to the definition of the operator $[F, G]_{ij}$ on functions F and G of the velocity variables $r_{i\alpha}$ and $r_{j\alpha}$ given by Eq. (13) we now define new operators on functions of the velocity variables $\xi_{i\alpha}$. With F_i and G_i functions of the variables $\xi_{i\alpha}$, F_j and G_j functions of $\xi_{j\alpha}$, we define

$$[F, G]_{ij}=\int F_iJ_{ij}(G)d\omega_i, \quad (40)$$

where the operator $J_{ij}(G)$ is defined by Eq. (30). Since only operators on functions of the $\xi_{i\alpha}$ will now appear, no confusion with the operator previously defined by Eq. (13) will arise. Also, we define the operator

$$\{F, G\}=\frac{n_1}{n_2}\left(\frac{2m_2}{m_1+m_2}\right)^{\frac{1}{2}}[F, G]_{11}+[F, G]_{12}+[F, G]_{21}+\frac{n_2}{n_1}\left(\frac{2m_1}{m_1+m_2}\right)^{\frac{1}{2}}[F, G]_{22}. \quad (41)$$

These operators have obviously the properties

$$[F, G]_{ii}=[G, F]_{ii}, \quad (42a)$$

$$[F, G+H]_{ij}=[F, G]_{ij}+[F, H]_{ij}, \quad (42b)$$

$$[F, cG]_{ij}=c[F, G]_{ij}, \quad (42c)$$

$$[F, F]_{ii}\geq 0, \quad (42d)$$

$$[F, G]_{12}+[F, G]_{21}=[G, F]_{12}+[G, F]_{21}, \quad (42e)$$

$$[F, F]_{12}+[F, F]_{21}\geq 0, \quad (42f)$$

where c is a constant. Also

$$\{F, G\}=\{G, F\}, \quad (43a)$$

$$\{F, G+H\}=\{F, G\}+\{F, H\}, \quad (43b)$$

$$\{F, cG\}=c\{F, G\}, \quad (43c)$$

$$\{F, F\}\geq 0. \quad (43d)$$

Other properties of this operator which will be required are the following. The equation

$$\{\chi, \chi\}=0$$

can have only the solutions

$$\chi_i=a_i+c_0\xi_{i\alpha}\xi_{i\alpha}+m_i^{\frac{1}{2}}c_\alpha\xi_{i\alpha}, \quad (44a)$$

where a_1, a_2, c_0, c_1, c_2 and c_3 are six arbitrary constants. But solutions of this form must vanish identically if they are to satisfy the auxiliary conditions (32). Secondly,

$$\{F, F\}\{G, G\}\geq\{F, G\}^2. \quad (44b)$$

The existence of this property may be shown as follows. Form a function H out of functions F and G in the manner

$$H=G\{F, F\}-F\{F, G\}.$$

Then

$$\{H, H\}=\{F, F\}[\{F, F\}\{G, G\}-\{F, G\}^2]\geq 0.$$

According to the above properties the result then follows immediately. Finally, if

$$\{F, F\}\{G, G\}-\{F, G\}^2=0,$$

where F and G are two functions satisfying the auxiliary conditions, it is necessarily true that

$$F=cG, \quad (44c)$$

where c is a constant. This result follows as a consequence of the property that if $\{H, H\}=0$, H is of the form (44a). But G and F cannot be of this form and simultaneously satisfy the auxiliary conditions.

Returning now to the expressions for κ and $\kappa\nu$ one may express these coefficients in terms of the operators defined. Thus

$$\kappa=\frac{2}{(2kT)^{\frac{1}{2}}}\frac{1}{n_1n_2}\left(\frac{m_1m_2}{m_1+m_2}\right)^{\frac{1}{2}}\{\mathrm{X}, \mathrm{X}\}, \quad (45a)$$

$$\kappa\nu=\frac{2k}{(2kT)^{\frac{1}{2}}}\frac{1}{n_1n_2}\left(\frac{m_1m_2}{m_1+m_2}\right)^{\frac{1}{2}}\{\Psi, \mathrm{X}\}, \quad (45b)$$

$$\nu=k\frac{\{\Psi, \mathrm{X}\}}{\{\mathrm{X}, \mathrm{X}\}}. \quad (45c)$$

The method of evaluation of these coefficients and the determination of the unknown functions X, Ψ and Π may now be discussed. For the case of the function X let us define functions L which satisfy the auxiliary conditions (32) and which belong to a class defined by the equation

$$\{L, L\} = \frac{1}{m_1^{\frac{1}{2}}} \int \frac{\xi_1 f_1^{(0)2} e^{\tau_1^2}}{A_1 F_1(A_1)} L_1 d\omega_1 - \frac{1}{m_2^{\frac{1}{2}}} \int \frac{\xi_2 f_2^{(0)2} e^{\tau_2^2}}{A_2 F_1(A_2)} L_2 d\omega_2.$$

Using the integral Eqs. (34a and b) this condition is found to be equivalent to the equation

$$\{L, L\} = \{L, \mathrm{X}\}. \tag{46}$$

Since the properties of this operator yield

$$\{\mathrm{X}-L, \mathrm{X}-L\} \geq 0,$$

it follows that

$$\{\mathrm{X}, \mathrm{X}\} - \{L, L\} \geq 0. \tag{47}$$

But, according to the discussion following Eq. (44a), there exists none but vanishing solutions of the equation $\{\mathrm{X}-L, \mathrm{X}-L\}=0$, and, therefore, the equality sign of Eq. (47) is valid only for $L=\mathrm{X}$. Then X may be determined as that function L satisfying the auxiliary conditions which maximizes $\{L, L\}$, and which gives, therefore, to the coefficient κ the largest possible value.

§ 4. The heat conductivity coefficient

In order to determine the heat conductivity coefficient one evaluates the heat current density. For each gas component

$$q_{ia} = \tfrac{1}{2}\rho_i \langle v_{ia} v_{i\beta} v_{i\beta} \rangle_M = \tfrac{1}{2} m_i \int f_i v_{ia} v_{i\beta} v_{i\beta} d\phi_i = \frac{m_i G_i}{2 c_i^3} \left(\frac{m_i}{h}\right)^3 \int f_i \xi_{ia} \tau_i^2 d\omega_i.$$

For the purpose of calculation it is convenient to consider the difference between this quantity and the quantity

$$\frac{5}{2} p_i \langle v_{ia} \rangle_M = \frac{5}{2} p_i (u_{ia} - u_a) = \frac{5}{2} \frac{p_i}{n_i} \int f_i v_{ia} d\phi_i = \frac{5}{2} \frac{p_i}{n_i} \frac{G_i}{c_i^2} \left(\frac{m_i}{h}\right)^3 \int f_i \xi_{ia} d\omega_i.$$

Taking this difference and summing over the two components one obtains

$$q_a - \frac{5}{2}[p_1(u_{1a}-u_a) + p_2(u_{2a}-u_a)] = \frac{1}{2}\left(\frac{2kT}{h}\right)^3 \left[m_1 G_1 \int f_1 \xi_{1a} \left(\tau_1^2 - \frac{5}{2} \frac{p_1}{n_1 kT} \right) d\omega_1 + m_2 G_2 \int f_2 \xi_{2a} \left(\tau_2^2 - \frac{5}{2} \frac{p_2}{n_2 kT} \right) d\omega_2 \right].$$

The distribution function (36) is now introduced into this expression giving the result

$$q_a = \frac{5}{2}[p_1(u_{1a}-u_a) + p_2(u_{2a}-u_a)] - \nu_1 \left[\frac{\rho_2}{\rho} \frac{\partial p_1}{\partial x_a} - \frac{\rho_1}{\rho} \frac{\partial p_2}{\partial x_a} + \frac{\rho_1 \rho_2}{\rho} (\mathfrak{X}_{2a} - \mathfrak{X}_{1a}) \right] - \lambda_1 \frac{\partial T}{\partial x_a}, \tag{48}$$

where

$$\nu_1 = \frac{(2kT)^2}{h^3} \frac{\pi^{\frac{1}{2}}}{n_1 n_2} \left(\frac{m_1 m_2}{m_1 + m_2}\right)^{\frac{1}{2}} \times \left[\frac{m_1 G_1}{A_1} \int f_1^{(0)2} e^{\tau_1^2} \xi_1^2 \left(\tau_1^2 - \frac{5}{2} \frac{p_1}{n_1 kT} \right) \chi_1 d\omega_1 + \frac{m_2 G_2}{A_2} \int f_2^{(0)2} e^{\tau_2^2} \xi_2^2 \left(\tau_2^2 - \frac{5}{2} \frac{p_2}{n_2 kT} \right) \chi_2 d\omega_2 \right], \tag{49a}$$

$$\lambda_1 = k \frac{(2kT)^2}{h^3} \frac{\pi^{\frac{1}{2}}}{n_1 n_2} \left(\frac{m_1 m_2}{m_1 + m_2}\right)^{\frac{1}{2}} \times \left[\frac{m_1 G_1}{A_1} \int f_1^{(0)2} e^{\tau_1^2} \xi_1^2 \left(\tau_1^2 - \frac{5}{2} \frac{p_1}{n_1 kT} \right) \psi_1 d\omega_1 + \frac{m_2 G_2}{A_2} \int f_2^{(0)2} e^{\tau_2^2} \xi_2^2 \left(\tau_2^2 - \frac{5}{2} \frac{p_2}{n_2 kT} \right) \psi_2 d\omega_2 \right]. \tag{49b}$$

Multiplying Eqs. (34c and d) by $\xi_1 \chi_1 d\omega_1 = \mathrm{X}_1 d\omega_1$ and $\xi_2 \chi_2 d\omega_2 = \mathrm{X}_2 d\omega_2$ respectively, integrating and

substituting into Eq. (49a) one obtains

$$\nu_1=\frac{(2kT)^{\frac{1}{2}}}{n_1n_2}\left(\frac{m_1m_2}{m_1+m_2}\right)^{\frac{1}{2}}\left[\frac{n_1}{n_2}\left(\frac{2m_2}{m_1+m_2}\right)^{\frac{1}{2}}\right.$$
$$\times\int X_1J_{11}(\Psi)d\omega_1+\int X_1J_{12}(\Psi)d\omega_1$$
$$+\int X_2J_{21}(\Psi)d\omega_2$$
$$\left.+\frac{n_2}{n_1}\left(\frac{2m_1}{m_1+m_2}\right)^{\frac{1}{2}}\int X_2J_{22}(\Psi)d\omega_2\right]$$
$$=\frac{(2kT)^{\frac{1}{2}}}{n_1n_2}\left(\frac{m_1m_2}{m_1+m_2}\right)^{\frac{1}{2}}\{X,\Psi\}=\kappa\nu T. \tag{50a}$$

Similarly, multiplying Eqs. (34c and d) by $\xi_1\psi_1d\omega_1=\Psi_1d\omega_1$ and $\xi_2\psi_2d\omega_2=\Psi_2d\omega_2$, integrating and substituting into Eq. (49b) one obtains

$$\lambda_1=\frac{(2kT)^{\frac{1}{2}}}{2n_1n_2T}\left(\frac{m_1m_2}{m_1+m_2}\right)^{\frac{1}{2}}\{\Psi,\Psi\}. \tag{50b}$$

Combining (37), (48) and (50a) one obtains finally

$$q_\alpha=\frac{5}{2}[p_1(u_{1\alpha}-u_\alpha)+p_2(u_{2\alpha}-u_\alpha)]$$
$$+\nu T(u_{1\alpha}-u_{2\alpha})-\lambda\frac{\partial T}{\partial x_\alpha}, \tag{51}$$

where

$$\lambda=\lambda_1-\kappa\nu^2T. \tag{52a}$$

According to the property expressed in Eq. (43d), the coefficients κ and λ_1 are positive definite quantities. Also, evaluating $\kappa\lambda_1$ and $\kappa^2\nu^2T$ from (45a and b and 50b) and using (44b) one finds that the quantity $\lambda_1-\kappa\nu^2T$ is positive definite. The latter may never vanish, however, for according to (44c) the expression

$$\kappa\lambda_1-\kappa^2\nu^2T=\frac{2k}{(n_1n_2)^2}\left(\frac{m_1m_2}{m_1+m_2}\right)$$
$$\times[\{X,X\}\{\Psi,\Psi\}-\{\Psi,X\}^2]$$

can vanish only if $\Psi=cX$ where c is a constant. But such a relation cannot be fulfilled since Ψ and X must simultaneously satisfy Eqs. (34a, b, c and d). Then

$$\left.\begin{aligned}&\lambda_1>\kappa\nu^2T,\\&\lambda>0,\\&\lambda<\lambda_1 \text{ unless } \nu=0.\end{aligned}\right\} \tag{52b}$$

Like X, the function Ψ may be determined by a variation process. Consider a class of functions M fulfilling the auxiliary conditions and defined by the equation

$$\{M,M\}=\frac{n_1}{m_1^{\frac{1}{2}}}\int\xi_1\left(\tau_1^2-\frac{5}{2}\frac{p_1}{n_1kT}\right)\frac{f_1^{(0)2}e^{\tau_1^2}}{A_1F_{\frac{1}{2}}(A_1)}M_1d\omega_1$$
$$+\frac{n_2}{m_2^{\frac{1}{2}}}\int\xi_2\left(\tau_2^2-\frac{5}{2}\frac{p_2}{n_2kT}\right)\frac{f_2^{(0)2}e^{\tau_2^2}}{A_2F_{\frac{1}{2}}(A_2)}M_2d\omega_2.$$

According to Eqs. (34c and d) this condition is equivalent to

$$\{M,M\}=\{M,\Psi\}.$$

Since

$$\{\Psi-M,\Psi-M\}\geq0,$$

it follows that

$$\{\Psi,\Psi\}-\{M,M\}\geq0.$$

Thus, Ψ may be determined as that function M satisfying the above conditions which maximizes the coefficient λ_1.

§ 5. The viscosity coefficient

We consider now the stress tensor and evaluate the quantities $p_{\alpha\beta}$ and $p_{\alpha\alpha}-p$. Since

$$p_{i\alpha\beta}=\rho_i\langle v_{i\alpha}v_{i\beta}\rangle_{Av}=m_i\int f_iv_{i\alpha}v_{i\beta}d\phi_i$$
$$=G_im_i\left(\frac{m_i}{h}\right)^3c_i^{-5/2}\int f_i\xi_{i\alpha}\xi_{i\beta}d\omega_i,$$

one obtains

$$p_{xy}=\frac{(2kT)^{5/2}}{h^3}\left[G_1m_1^{\frac{1}{2}}\int f_1\xi_{1x}\xi_{1y}d\omega_1\right.$$
$$\left.+G_2m_2^{\frac{1}{2}}\int f_2\xi_{2x}\xi_{2y}d\omega_2\right],$$

$$p_{xx}-p=\frac{(2kT)^{5/2}}{h^3}\left[G_1m_1^{\frac{1}{2}}\int f_1\left(\xi_{1x}^2-\frac{\tau_1^2}{3}\right)d\omega_1\right.$$
$$\left.+G_2m_2^{\frac{1}{2}}\int f_2\left(\xi_{2x}^2-\frac{\tau_2^2}{3}\right)d\omega_2\right].$$

Introducing (36)

$$p_{xy}=-\mu\left(\frac{\partial u_x}{\partial y}+\frac{\partial u_y}{\partial x}\right), \tag{53a}$$

$$p_{xx}=p-\frac{2}{3}\mu\left[2\frac{\partial u_x}{\partial x}-\frac{\partial u_y}{\partial y}-\frac{\partial u_z}{\partial z}\right], \tag{53b}$$

where

$$\mu=2\frac{(2kT)^2}{h^3}\frac{\pi^{\frac{1}{2}}}{n_1n_2}\left(\frac{m_1m_2}{m_1+m_2}\right)^{\frac{1}{2}}\times\left[\frac{G_1m_1^{\frac{1}{2}}}{A_1}\int f_1^{(0)2}e^{\tau_1^2}\xi_{1x}^2\xi_{1y}^2\pi_1d\omega_1+\frac{G_2m_2^{\frac{1}{2}}}{A_2}\int f_2^{(0)2}e^{\tau_2^2}\xi_{2x}^2\xi_{2y}^2\pi_2d\omega_2\right],$$

$$=\frac{3}{2}\frac{(2kT)^2}{h^3}\frac{\pi^{\frac{1}{2}}}{n_1n_2}\left(\frac{m_1m_2}{m_1+m_2}\right)^{\frac{1}{2}}\times\left[\frac{G_1m_1^{\frac{1}{2}}}{A_1}\int f_1^{(0)2}e^{\tau_1^2}\left(\xi_{1x}^2-\frac{\tau_1^2}{3}\right)\pi_1d\omega_1+\frac{G_2m_2^{\frac{1}{2}}}{A_2}\int f_2^{(0)2}e^{\tau_2^2}\left(\xi_{2x}^2-\frac{\tau_2^2}{3}\right)\pi_2d\omega_2\right].$$

In the evaluation of this coefficient it will be sufficient to consider only the second form, and to restrict our considerations to the functions

$$\Pi_{iaa}=\left(\xi_{ia}^2-\frac{\tau_i^2}{3}\right)\pi_i.$$

Proceeding then as before with Eqs. (34e and f) one obtains finally

$$\mu=\frac{3}{2}\frac{(2kT)^{\frac{1}{2}}}{n_1n_2}\left(\frac{m_1m_2}{m_1+m_2}\right)^{\frac{1}{2}}\{\Pi,\Pi\}. \tag{54}$$

As is the case with the other two functions, Π has a maximal property, such that of all functions N defined by the condition

$$\{N,N\}=\{N,\Pi\}$$

and satisfying the auxiliary conditions, Π is that one which maximizes the coefficient μ. All of the gas coefficients may be evaluated, therefore, with the help of a variation method. Explicit expressions for the gas coefficients in terms of known functions will be found in this manner, and discussed in the succeeding section.

III. Derivation of Expressions for the Gas Coefficients in Terms of Known Functions

§ 1. Method of solution

For the purpose of this section it is convenient to consider a slight change in notation. Hitherto, all functions of velocity variables have been regarded as defined in their respective spaces ξ_{1a} and ξ_{2a}. We shall now regard each function as defined over the combined velocity space of two particles, and introduce a new operator on functions H and K defined in this six-dimensional space as follows:

$$[H,K]=\tfrac{1}{2}F_1^{-1}(A_1)F_1^{-1}(A_2)\int d\omega_1\int d\omega_2\times\int\gamma_{12}w_{12}(\vartheta\varphi)d\Omega(H-H')(K-K')\times f_1^{(0)\prime}f_2^{(0)\prime}(1+\theta_1f_1^{(0)})(1+\theta_2f_2^{(0)}). \tag{55}$$

Then for two functions $H=F_1+F_2$ and $K=G_1+G_2$ where F_1 and G_1 are defined so as to vanish in the subspace 2, and F_2 and G_2 to vanish in the subspace 1, the operator defined by Eq. (41) becomes

$$\{H,K\}=\frac{n_1}{n_2}\left(\frac{2m_2}{m_1+m_2}\right)^{\frac{1}{2}}[F_1,G_1]_{11}+[F_1+F_2,G_1+G_2]+\frac{n_2}{n_1}\left(\frac{2m_1}{m_1+m_2}\right)^{\frac{1}{2}}[F_2,G_2]_{22}, \tag{56}$$

since, obviously, from a comparison of Eqs. (55) and (40)

$$[F_1+F_2,G_1+G_2]=[F,G]_{12}+[F,G]_{21}, \tag{56a}$$

where, in the left member each function appearing is regarded as defined over the combined space, and in the right member all functions are defined separately in both component spaces. The purpose of this change of notation is that we have now a notation for a portion of the operator $\{H,K\}$ which occurs when one term of H or K or both vanish over the entire space.

Conforming with this notation the solutions of the integral equations, X, Ψ and Π, must be regarded as functions of six variables; e.g.,

$$X = X_1 + X_2,$$

where X_1 vanishes in region 2 and X_2 vanishes in region 1. The quantities $\{F, G\}$ appearing in the expressions for the transport coefficients derived in the last section may be taken, then, as of the form given by Eq. (56) without altering their meaning.

The procedure now, as indicated in the previous discussion of the maximal properties of the solutions of the integral equations, is to choose complete sets of linearly independent functions which individually fulfill the auxiliary conditions (32), and from which linear combinations may be formed which belong to the proper functional class as defined, for example, in the case of the function X, by Eq. (46). The constants of this linear combination are then to be varied in order to satisfy the maximal property.[14]

Since both X and Ψ are proportional to ξ and depend otherwise only on τ^2 one set of $(2n+1)$ functions, $h^{(0)}$, $h_1^{(r)}$, $h_2^{(r)}$ $(r=1, 2, \cdots n)$, may be used in the determination of these solutions. Similarly, we determine that solution Π which is proportional to $(\xi^2-\frac{1}{3}\tau^2)$, and in terms of which the viscosity coefficient may be evaluated, by choosing a set of $2n$ functions, $k_1^{(r)}$, $k_2^{(r)}$ $(r=1, 2, \cdots n)$, each of which is of this form. Sets of functions of this character, which satisfy also the auxiliary conditions may be chosen, then, as follows:

$$h^{(0)} = \frac{\rho_1\rho_2}{\rho}\frac{\xi_1}{n_1(m_1)^{\frac{1}{2}}} \text{ in region 1;}$$

$$= -\frac{\rho_1\rho_2}{\rho}\frac{\xi_2}{n_2(m_2)^{\frac{1}{2}}} \text{ in region 2;}$$

$$h_1^{(r)} = \xi_1\left[\tau_1^{2r} - \frac{\Gamma(r+5/2)}{\Gamma(5/2)}\frac{F_{r+\frac{1}{2}}(A_1)}{F_{\frac{1}{2}}(A_1)}\right] \text{ in region 1;}$$

$$= 0 \text{ in region 2;}$$

$$h_2^{(r)} = 0 \text{ in region 1;}$$

$$= \xi_2\left[\tau_2^{2r} - \frac{\Gamma(r+5/2)}{\Gamma(5/2)}\frac{F_{r+\frac{1}{2}}(A_2)}{F_{\frac{1}{2}}(A_2)}\right] \text{ in region 2}$$

for the first set, and

$$k_1^{(r)} = (\xi_1^2 - \tfrac{1}{3}\tau_1^2)\tau_1^{2r-2} \text{ in region 1;}$$

$$= 0 \text{ in region 2;}$$

$$k_2^{(r)} = 0 \text{ in region 1;}$$

$$= (\xi_2^2 - \tfrac{1}{3}\tau_2^2)\tau_2^{2r-2} \text{ in region 2}$$

for the second set. Since these functions satisfy the auxiliary conditions, any linear combination of them also satisfies these conditions.

§ 2. Series developments for the gas coefficients

In order to determine X we consider the function $X^{(n)}$ given by

$$X^{(n)} = \beta^{(0)}h^{(0)} + \sum_{r=1}^{n}(\beta_1^{(r)}h_1^{(r)} + \beta_2^{(r)}h_2^{(r)}) \quad (57)$$

and determine the coefficients β so as to minimize the quantity

$$H_n = \{X - X^{(n)}, X - X^{(n)}\}.$$

Differentiating H_n with respect to each of the β's one obtains the following set of algebraic equations

$$\{h^{(0)}, X^{(n)}\} = \{h^{(0)}, X\},$$

$$(r=1, 2, \cdots n; s=1, 2). \quad (58)$$

$$\{h_s^{(r)}, X^{(n)}\} = \{h_s^{(r)}, X\}$$

It follows from (57) and (58) that

$$\{X^{(n)}, X^{(n)}\} = \{X^{(n)}, X\} \quad (58a)$$

and that

$$H_n = \{X, X\} - \{X^{(n)}, X^{(n)}\} \geq 0.$$

Solving Eqs. (58) for the β's and introducing the results into Eq. (57) one obtains

$$X^{(n)} = -\frac{A^{(2n+2)}}{D^{(2n+1)}}, \quad (59)$$

where

[14] For a complete discussion of this procedure together with questions of convergence see Enskog, reference 11, pp. 71–87.

$$A^{(2j+2)}=\begin{vmatrix} \{h^{(0)},h^{(0)}\} & \cdots & \{h^{(0)},h_1^{(j)}\} & \{h^{(0)},h_2^{(j)}\} & \{h^{(0)},\mathbf{X}\} \\ \vdots & \cdots & \vdots & \vdots & \vdots \\ \{h_1^{(j)},h^{(0)}\} & \cdots & \{h_1^{(j)},h_1^{(j)}\} & \{h_1^{(j)},h_2^{(j)}\} & \{h_1^{(j)},\mathbf{X}\} \\ \{h_2^{(j)},h^{(0)}\} & \cdots & \{h_2^{(j)},h_1^{(j)}\} & \{h_2^{(j)},h_2^{(j)}\} & \{h_2^{(j)},\mathbf{X}\} \\ h^{(0)} & \cdots & h_1^{(j)} & h_2^{(j)} & 0 \end{vmatrix},$$

$$D^{(2j+1)}=\begin{vmatrix} \{h^{(0)},h^{(0)}\} & \cdots & \{h^{(0)},h_1^{(j)}\} & \{h^{(0)},h_2^{(j)}\} \\ \vdots & \cdots & \vdots & \vdots \\ \{h_1^{(j)},h^{(0)}\} & \cdots & \{h_1^{(j)},h_1^{(j)}\} & \{h_1^{(j)},h_2^{(j)}\} \\ \{h_2^{(j)},h^{(0)}\} & \cdots & \{h_2^{(j)},h_1^{(j)}\} & \{h_2^{(j)},h_2^{(j)}\} \end{vmatrix}.$$

The ratio of determinants occurring in Eq. (59) may be rewritten as a series, and takes the form

$$\mathbf{X}^{(n)}=\frac{\{h^{(0)},\mathbf{X}\}h^{(0)}}{\{h^{(0)},h^{(0)}\}}+\sum_{r=1}^{n}P^{(r)}, \tag{60}$$

where

$$P^{(r)}=\frac{A^{(2r+2)}_{2r+2,\,2r+1}A^{(2r+2)}_{\left\{\begin{smallmatrix}2r,&2r\\2r+1,&2r+2\end{smallmatrix}\right\}}-A^{(2r+2)}_{2r+2,\,2r}A^{(2r+2)}_{\left\{\begin{smallmatrix}2r,&2r+1\\2r+1,&2r+2\end{smallmatrix}\right\}}}{D^{(2r-1)}D^{(2r+1)}}$$

and $A_{k,\,l}^{(2j+2)}$ is the cofactor of the element in the kth row and lth column of $A^{(2j+2)}$. We now form the quantity $\{\mathbf{X}^{(n)},\mathbf{X}^{(n)}\}$. In order to obtain this expression, we observe that if h is any of the functions $h^{(0)},\cdots h_1^{(r-1)}, h_2^{(r-1)}$, then both of the quantities

$$\left\{h, A^{(2r+2)}_{\left\{\begin{smallmatrix}2r,&2r\\2r+1,&2r+2\end{smallmatrix}\right\}}\right\} \quad \text{and} \quad \left\{h, A^{(2r+2)}_{\left\{\begin{smallmatrix}2r,&2r+1\\2r+1,&2r+2\end{smallmatrix}\right\}}\right\}$$

vanish, since in both cases one obtains a determinant with two equal rows. Then

$$\{P^{(r)},h^{(0)}\}=\{P^{(r)},P^{(s)}\}=0, \quad (r\neq s). \tag{61}$$

Using Eqs. (58), (60) and (61) one then obtains

$$\{P^{(s)},\mathbf{X}^{(n)}\}=\{P^{(s)},P^{(s)}\}=\{P^{(s)},\mathbf{X}\}. \tag{62}$$

Now using Eqs. (58a) and (62) the result

$$\{\mathbf{X}^{(n)},\mathbf{X}^{(n)}\}=\frac{\{h^{(0)},\mathbf{X}\}^2}{\{h^{(0)},h^{(0)}\}}+\sum_{r=1}^{n}\{P^{(r)},P^{(r)}\}$$

follows. The expression $\{P^{(r)},P^{(r)}\}$ may be rewritten. From Eq. (62) it follows that $\{P^{(r)},P^{(r)}\}$ is given by $P^{(r)}$ if each element $h^{(0)}, h_1^{(1)}, h_2^{(1)}, \cdots h_2^{(r)}$ in $P^{(r)}$ is replaced, respectively, by $\{h^{(0)},\mathbf{X}\}, \{h_1^{(1)},\mathbf{X}\}, \cdots, \{h_2^{(r)},\mathbf{X}\}$. Then

$$\{P^{(r)},P^{(r)}\}=\frac{B^{(2r+2)}_{2r+2,\,2r+1}B^{(2r+2)}_{\left\{\begin{smallmatrix}2r,&2r\\2r+1,&2r+2\end{smallmatrix}\right\}}-B^{(2r+2)}_{2r+2,\,2r}B^{(2r+2)}_{\left\{\begin{smallmatrix}2r,&2r+1\\2r+1,&2r+2\end{smallmatrix}\right\}}}{D^{(2r-1)}D^{(2r+1)}},$$

where $B^{(2r+2)}$ is the determinant $A^{(2r+2)}$ in which this replacement has been made. But all of the elements $\{h_1^{(j)},\mathbf{X}\}$ and $\{h_2^{(j)},\mathbf{X}\}$ in $B^{(2r+2)}$ vanish. This may be shown as follows using Eqs. (56) and (56a)

$$\{h_1^{(j)},\mathbf{X}\}=\frac{n_1}{n_2}\left(\frac{2m_2}{m_1+m_2}\right)^{\frac{1}{2}}[h^{(j)},\mathbf{X}]_{11} +[h_1^{(j)},\mathbf{X}_1+\mathbf{X}_2]$$
$$=\frac{n_1}{n_2}\left(\frac{2m_2}{m_1+m_2}\right)^{\frac{1}{2}}[h^{(j)},\mathbf{X}]_{11}+[h^{(j)},\mathbf{X}]_{12}.$$

Using Eq. (34a) and the definition of $F_s(A_1)$ given by Eq. (30a)

$$\{h_1^{(j)},\mathbf{X}\}=\frac{1}{m_1^{\frac{1}{2}}A_1F_{\frac{1}{2}}(A_1)}\int\xi_1 f_1^{(0)2}e^{r_1^2}h_1^{(j)}d\omega_1$$
$$=\frac{2\pi}{3m_1^{\frac{1}{2}}F_{\frac{1}{2}}(A_1)}\left[\frac{3}{2}\int_0^\infty\frac{z^{\frac{1}{2}}}{(1/A_1)e^z-\theta_1}\times\left\{z^j-\frac{\Gamma(j+5/2)}{\Gamma(5/2)}\frac{F_{j+\frac{1}{2}}(A_1)}{F_{\frac{1}{2}}(A_1)}\right\}dz +j\int_0^\infty\frac{z^{j+\frac{1}{2}}}{(1/A_1)e^z-\theta_1}dz\right]=0.$$

The determinant $B^{(2r+2)}$ is now conveniently expressed in terms of the determinant $D^{(2r+1)}$.

One then obtains

$$\{P^{(r)}, P^{(r)}\} = \{h^{(0)}, \mathrm{X}\}^2 \times \frac{D_{1,2r}^{(2r+1)} D_{\left\{\substack{2r,\\2r+1}\ \substack{1\\2r+1}\right\}}^{(2r+1)} - D_{1,2r+1}^{(2r+1)} D_{\left\{\substack{2r,\\2r+1}\ \substack{1\\2r}\right\}}^{(2r+1)}}{D^{(2r-1)} D^{(2r+1)}}. \quad (63)$$

As in the one component gas theory one can show that if the integral equations (34a and b) possess finite and continuous solutions, the limit as n approaches infinity of $\{\mathrm{X}^{(n)}, \mathrm{X}^{(n)}\}$ is $\{\mathrm{X}, \mathrm{X}\}$. Therefore, from Eq. (45a) one obtains for the gas coefficient κ

$$\kappa = \frac{22}{(2kT)^{\frac{1}{2}}} \frac{1}{n_1 n_2} \left(\frac{m_1 m_2}{m_1+m_2}\right)^{\frac{1}{2}} \times \left[\frac{\{h^{(0)}, \mathrm{X}\}^2}{\{h^{(0)}, h^{(0)}\}} + \sum_{r=1}^{\infty} \{P^{(r)}, P^{(r)}\}\right] \quad (64)$$

with $\{P^{(r)}, P^{(r)}\}$ given by (63). This coefficient is thus expressed completely in terms of known functions since the quantity $\{h^{(0)}, \mathrm{X}\}$ may be evaluated by integration of Eqs. (34a and b).

In order to determine Ψ and the thermal conductivity coefficient associated with it one considers as before a function $\Psi^{(n)}$ formed as a linear combination from the set $h^{(0)}, h_1^{(1)}, \cdots h_2^{(n)}$. One obtains then as in the case of $\mathrm{X}^{(n)}$ the result

$$\Psi^{(n)} = -\frac{C^{(2n+2)}}{D^{(2n+1)}} = \frac{\{h^{(0)}, \Psi\} h^{(0)}}{\{h^{(0)}, h^{(0)}\}} + \sum_{r=1}^{n} Q^{(r)},$$

where $C^{(2n+2)}$ is the same determinant as $A^{(2n+2)}$ with Ψ replacing X and $Q^{(r)}$ is the same as $P^{(r)}$ with the same replacement. The quantity $\{h^{(0)}, \Psi\}$ unlike $\{h^{(0)}, \mathrm{X}\}$ vanishes, as may be shown in a manner analogous to that used above to prove the vanishing of $\{h_s^{(j)}, \mathrm{X}\}$, and using finally the relation $p/nkT = F_{3/2}(A)/F_{1/2}(A)$. Then

$$\Psi^{(n)} = \sum_{r=1}^{n} Q^{(r)}.$$

Of the two thermal conductivity coefficients, the coefficient λ given by Eq. (52a) is of the greater interest. In order to determine it the expressions $\{\Psi^{(n)}, \Psi\}$ and $\{\Psi^{(n)}, \mathrm{X}\}$ must be evaluated in addition to $\{\mathrm{X}^{(n)}, \mathrm{X}\}$ already obtained. Denoting

$$F^{(2r+1)} = \begin{vmatrix} \{h_1^{(1)}, h_1^{(1)}\} & \cdots & \{h_1^{(1)}, h_2^{(r)}\} & \{h_1^{(1)}, \Psi\} \\ \cdots & \cdots & \cdots & \cdots \\ \{h_2^{(r)}, h_1^{(1)}\} & \cdots & \{h_2^{(r)}, h_2^{(r)}\} & \{h_2^{(r)}, \Psi\} \\ \{h_1^{(1)}, \Psi\} & \cdots & \{h_2^{(r)}, \Psi\} & 0 \end{vmatrix}, \quad (66a)$$

$$G^{(2r)} = F_{2r+1,\,2r+1}^{(2r+1)}, \quad (66b)$$

one finds

$$\{\Psi^{(n)}, \Psi\} - \frac{\{\mathrm{X}, \Psi^{(n)}\}^2}{\{\mathrm{X}^{(n)}, \mathrm{X}\}} = -\frac{F^{(2n+1)}}{G^{(2n)}} = \sum_{r=1}^{n} \frac{F_{2r+1,\,2r}^{(2r+1)} F_{\left\{\substack{2r-1,\\2r}\ \substack{2r-1\\2r+1}\right\}}^{(2r+1)} - F_{2r+1,\,2r-1}^{(2r+1)} F_{\left\{\substack{2r-1,\\2r}\ \substack{2r\\2r+1}\right\}}^{(2r+1)}}{G^{(2r-2)} G^{(2r)}},$$

where $G^{(0)}$ is to be set equal to unity. Taking the limit of this expression as n approaches infinity, and using Eqs. (52a), (50b), (45b and c) one obtains

$$\lambda = \frac{(2kT)^{\frac{1}{2}}}{2n_1 n_2 T} \left(\frac{m_1 m_2}{m_1+m_2}\right)^{\frac{1}{2}} \sum_{r=1}^{\infty} \frac{F_{2r+1,\,2r}^{(2r+1)} F_{\left\{\substack{2r-1,\\2r}\ \substack{2r-1\\2r+1}\right\}}^{(2r+1)} - F_{2r+1,\,2r-1}^{(2r+1)} F_{\left\{\substack{2r-1,\\2r}\ \substack{2r\\2r+1}\right\}}^{(2r+1)}}{G^{(2r-2)}\ G^{(2r)}}. \quad (67)$$

Similarly, the function Π and the viscosity coefficient associated with it are evaluated by introducing a function $\Pi^{(n)}$ expressed as a linear combination of the functions $k_1^{(1)}, k_2^{(1)}, \cdots, k_2^{(n)}$.

Proceeding as before and denoting

$$L^{(2r+1)}=\begin{vmatrix} \{k_1^{(1)}, k_1^{(1)}\} & \cdots & \{k_1^{(1)}, k_2^{(r)}\} & \{k_1^{(1)}, \Pi\} \\ \vdots & & \vdots & \vdots \\ \{k_2^{(r)}, k_1^{(1)}\} & \cdots & \{k_2^{(r)}, k_2^{(r)}\} & \{k_2^{(r)}, \Pi\} \\ \{k_1^{(1)}, \Pi\} & \cdots & \{k_2^{(r)}, \Pi\} & 0 \end{vmatrix}, \tag{68a}$$

$$K^{(2r)}=L^{(2r+1)}_{2r+1,\,2r+1}, \tag{68b}$$

one obtains from Eq. (54)

$$\mu=\frac{3}{2}\frac{(2kT)^{\frac{1}{2}}}{n_1n_2}\left(\frac{m_1m_2}{m_1+m_2}\right)^{\frac{1}{2}}\sum_{r=1}^{\infty}\frac{L^{(2r+1)}_{2r+1,\,2r}L^{(2r+1)}_{\{2r-1,\,2r-1\}_{2r,\,2r+1}}-L^{(2r+1)}_{2r+1,\,2r-1}L^{(2r+1)}_{\{2r-1,\,2r\}_{2r,\,2r+1}}}{K^{(2r-2)}K^{(2r)}}. \tag{69}$$

Finally, the thermal diffusion coefficient may be developed from the relations already obtained. Referring to Eq. (45b) one finds that it is the limit of the expression $\{X^{(n)}, \Psi^{(n)}\}$ which is required for this purpose. This may be obtained from Eq. (60) for $X^{(n)}$ or from the corresponding equation for $\Psi^{(n)}$ to give

$$\{X^{(n)}, \Psi^{(n)}\}=\sum_{r=1}^{n}\{P^{(r)}, \Psi^{(n)}\}=\sum_{r=1}^{n}\{Q^{(r)}, X^{(n)}\}$$

$$=\sum_{r=1}^{n}\{P^{(r)}, \Psi\}=\sum_{r=1}^{n}\{Q^{(r)}, X\}.$$

Passing to the limit in the summation over n and introducing the result into Eq. (45b) one obtains

$$\kappa\nu=\frac{2k}{(2kT)^{\frac{1}{2}}}\frac{1}{n_1n_2}\left(\frac{m_1m_2}{m_1+m_2}\right)^{\frac{1}{2}}\sum_{r=1}^{\infty}\frac{M^{(2r+2)}_{2r+2,\,2r+1}M^{(2r+2)}_{\{2r,\,2r\}_{2r+1,\,2r+2}}-M^{(2r+2)}_{2r+2,\,2r}M^{(2r+2)}_{\{2r,\,2r+1\}_{2r+1,\,2r+2}}}{D^{(2r-1)}D^{(2r+1)}}, \tag{70}$$

where

$$M^{(2r+2)}=\begin{vmatrix} \{h^{(0)}, h^{(0)}\} & \{h^{(0)}, h_1^{(1)}\} & \cdots & \{h^{(0)}, h_2^{(r)}\} & 0 \\ \{h_1^{(1)}, h^{(0)}\} & \{h_1^{(1)}, h_1^{(1)}\} & \cdots & \{h_1^{(1)}, h_2^{(r)}\} & \{h_1^{(1)}, \Psi\} \\ \vdots & \vdots & & \vdots & \vdots \\ \{h_2^{(r)}, h^{(0)}\} & \{h_2^{(r)}, h_1^{(1)}\} & \cdots & \{h_2^{(r)}, h_2^{(r)}\} & \{h_2^{(r)}, \Psi\} \\ \{h^{(0)}, X\} & 0 & \cdots & 0 & 0 \end{vmatrix}. \tag{71}$$

The coefficients characterizing a mixture of two gases are thus completely determined and expressed in terms of known functions. The diffusion process depends on κ and ν, the heat conduction on λ and ν, and the viscosity on μ. In order to obtain numerical values of the coefficients there remains the evaluation of integrals of the type $\{h_i^{(r)}, h_j^{(s)}\}$, $\{h_i^{(r)}, X\}$ and $\{k_i^{(r)}, \Pi\}$. Integrals involving the unknown functions are evaluated by direct substitution from the integral equations. These calculations with reference to particular gas coefficients will be given in a succeeding paper.

LETTERS TO THE EDITOR

Prompt publication of brief reports of important discoveries in physics may be secured by addressing them to this department. Closing dates for this department are, for the first issue of the month, the eighteenth of the preceding month, for the second issue, the third of the month. Because of the late closing dates for the section no proof can be shown to authors. The Board of Editors does not hold itself responsible for the opinions expressed by the correspondents.

Communications should not in general exceed 600 words in length.

A Modified Arc Source for the Cyclotron

Encouraged by the success of Livingston *et al.*[1] and particularly of Allen[2] with arc ion sources in cyclotrons, we have tried a similar source in the 60-inch cyclotron here. The design is a modification of those recommended in the references given, but we believe that it is sufficiently different and simpler to merit a brief description. Fig. 1 shows a cross section of our source. The cone is turned from a solid block of copper; it has a $\frac{1}{4}$-inch hole in the top and is beveled at about 45°. The filament is a coil of 50-mil tungsten, with vertical leads that bend horizontally at the bottom, and are clamped in water-cooled blocks. Below the filament is a tungsten plate at the filament potential, to prevent the arc from striking downward. The arc runs with 1.5–2 amperes at about 100 volts drop, in a deuterium pressure estimated at about 10^{-2} mm Hg.

The performance of this source may be illustrated by some results of trials. These figures were collected from the data of operation over several weeks and may not be strictly comparable. In all cases the beam consisted of 16-Mev deuterons, and the oscillators were fed with single phase full wave rectified power. The peak voltage between dees was about 200 kv. Old filament source 14μA; arc source, $\frac{3}{16}$" hole, not beveled, no feelers 5μA; arc source, $\frac{3}{16}$" hole, beveled, no feelers 25μA; arc source, $\frac{1}{4}$" hole, beveled, no feelers 52μA; arc source, $\frac{1}{4}$" hole, beveled, feelers on 90μA. The introduction of the feelers reduced the amount of power needed to maintain the dee voltage, even though it increased the beam. This would seem to indicate that their function, in this case at least, is to give the ions from the source a better start rather than to pull more ions from the source.

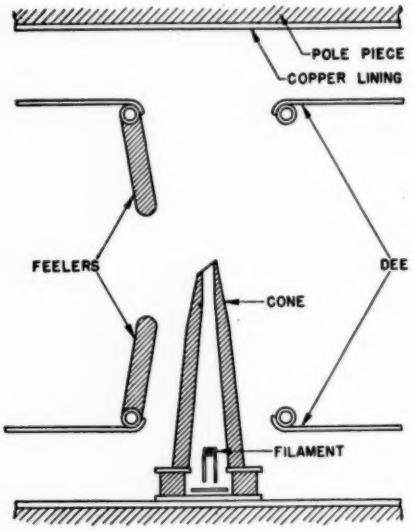

FIG. 1. Cross section of ion source in place in 60-inch cyclotron. The feelers are 2 inches wide in the direction along the dee gap. The pole pieces are 10 inches apart.

By operating the oscillators on three-phase power, an ion current increase of 2–3 times should be obtained, with the same maximum dee voltage and arc conditions.

The operating life of the 50-mil filament is found to be about 24 hours. We have now put in a 60-mil filament; since a 40-mil filament lasted about 4 hours, this should give a great increase in life.

EDWIN MCMILLAN
W. W. SALISBURY

William H. Crocker Radiation Laboratory,
University of California,
Berkeley, California,
October 2, 1939.

[1] M. Stanley Livingston, M. G. Holloway and C. P. Baker, Rev. Sci. Inst. **10**, 63 (1939).
[2] Alexander Allen, J. Frank. Inst. Oct., 1939, and private communications.

The High Frequency Perpendicular Fundamental Vibration of the Ammonia Molecule

For some time it has been recognized that the high frequency perpendicular fundamental of ammonia (conventionally denoted as ν_2) has a value around 3400 cm^{-1}, but the exact location has proved difficult. In a recent paper[1] Barker has suggested the value 3415 cm^{-1} from a very careful investigation of certain combination bands, but particularly from a band at 4μ, which he interprets as $\nu_2-\nu_3$. The purpose of the present note is to point out that the interpretation of this combination band offered by Barker is open to question. The value it yields for ν_2 seems to be too low if we are to interpret the band at 2.2μ as $\nu_2+\nu_3$. The center of the latter band appears to be at 4450 cm^{-1} whereas Barker's value of ν_2 would make it fall at 4365 cm^{-1} or even lower. Again in the plot of the 3μ region, where a part of the ν_2 fundamental can be picked out, the maximum of intensity would appear to be much closer to 3450 cm^{-1} than to 3415 cm^{-1}. Further, a comparison of the values of ν_2 and ν_4 in the isotopic molecules NH_3 and ND_3 indicates that the value for ν_2 in NH_3 should be considerably nearer 3450 cm^{-1} than 3400 cm^{-1}. Since these three separate lines of evidence suggest a value for ν_2 near 3450 cm^{-1} we must find another inter-

pretation of the band at 4μ, and there seems to be no reason why it should not be interpreted as $\nu_3+\nu_4$. An examination of the behavior of this band at low temperatures would perhaps be the best method of checking its assignment as a sum, rather than a difference, of two fundamentals.

The writer wishes to acknowledge the benefit of discussing this matter with Professor Barker.

G. B. B. M. SUTHERLAND*

Pembroke College,
Cambridge, England,
September 15, 1939.
* At present Leverhulme Research Fellow.

[1] E. F. Barker, Phys. Rev. **55**, 657 (1939).

Magnetic Anisotropy of Nickel at 20°K

The only experiments on ferromagnetic anisotropy that have been carried out below the temperature of liquid nitrogen are those of Honda, Masumoto and Shirakawa[1] on nickel in liquid hydrogen. Their results indicate a large increase in the anisotropy as the temperature is lowered from 77° to 20°K, the constant K_1 changing by a factor of about 5. On the other hand, Brukhatov and Kirensky[2] have found that in the temperature range from 77° to 350°K, the constant is given by the relation

$$K_1 = K_0 e^{-\alpha T^2} \qquad (1)$$

which predicts an increase of but 20 percent in going from 77° to 20°K. Accordingly we have undertaken, with the kind cooperation of Drs. H. A. Boorse and S. L. Quimby of Columbia University, to measure again the anisotropy constants at 77° and 20°K, using this time the more accurate method of torques.

The ratio of the constants was found to be about 1.2 (accuracy about 10 percent), as compared with the ratio 5 derived from the data of Honda, Masumoto and Shirakawa and 1.21 from the equation of Brukhatov and Kirensky. Our absolute values at 77°K and above are very close to those of Brukhatov and Kirensky. Thus our work extends the validity of this equation to lower temperatures (see Fig. 1) and shows that there is no unusual behavior in the ferromagnetic anisotropy at these low temperatures. This clarifies the theoretical situation since Van Vleck[3] in his discussion of the wave-mechanical theory of anisotropy, has not been able to find any basis for a difference in variation with temperature of the constants for iron and for nickel.

The crystal of nickel used was grown[4] in pure hydrogen from high purity nickel kindly supplied by Mr. E. Wise of the International Nickel Company. It was cut in the form of a disk with planes parallel to (100) and edges rounded to a semi-circle. The thickness was 0.29 cm, the largest diameter 1.38 cm. The liquid hydrogen was introduced into the Dewar flask surrounding the crystal through a straight Dewar tube of stainless steel connected directly to the bottom of the liquefier. The flask and crystal and torsion-measuring apparatus[5] were then removed to the electromagnet for measurement of the torque when the field was inclined at various angles to [011], the direction of easiest magnetization in the (100) plane. The highest field used was about 4000 oersteds. This was not sufficient

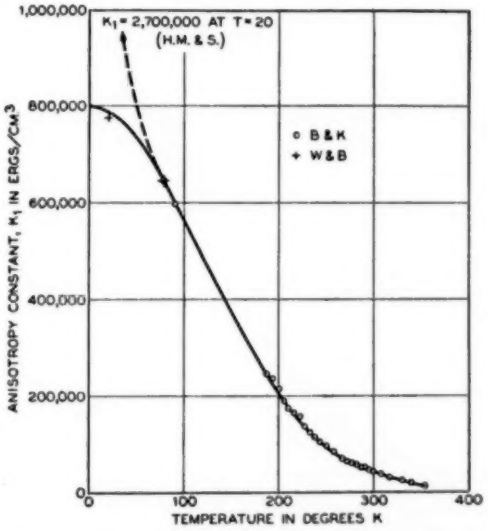

FIG. 1. Anisotropy constant of nickel as dependent on temperature. Data from 77° to 350°K, inclusive, by Brukhatov and Kirensky. Data at 77° and 20°K by the authors, adjusted slightly to fit the former data at 77°K. Curve calculated from Eq. (1) using $K = 800{,}000$, $\alpha = 0.000034$.

to permit observation of the torque at saturation, but was so near this point that the ratio of the constants at 77° and 20°K could be determined with some accuracy. Saturation was later observed at 77°K in a field of about 5000 oersteds.

We wish to express our appreciation to Dr. Boorse and Dr. Quimby and others of the Cryogenic Laboratory of Columbia University, for supplying the liquid hydrogen.

H. J. WILLIAMS
R. M. BOZORTH

Bell Telephone Laboratories,
New York, New York,
September 25, 1939.

[1] K. Honda, H. Masumoto and Y. Shirakawa, Sci. Rep. Tohoku Imp. Univ. **24**, 391 (1935). The anisotropy constant was derived by one of us (R. M. B., J. App. Phys. **8**, 575 (1937)) from their magnetization curves for the [100] and [110] directions. A similar calculation by L. W. McKeehan (Phys. Rev. **52**, 18 (1937)) yielded an even higher value of K_1. Its value is somewhat uncertain on account of the extrapolation of the magnetization curves to saturation.
[2] N. L. Brukhatov and L. V. Kirensky, Soviet Phys. **12**, 602 (1937).
[3] J. H. Van Vleck, Phys. Rev. **52**, 1178 (1937).
[4] By Mr. O. L. Boothby, using the method described by P. P. Cioffi and O. L. Boothby, Phys. Rev. **55**, 673 (1939).
[5] Similar in design to that described by H. J. Williams, Rev. Sci. Inst. **8**, 56 (1937).

The Disintegration of Mesotrons

In order to test the hypothesis of the spontaneous decay of mesotrons we have compared the absorption of the mesotron component of cosmic radiation in air and in carbon.

The mesotrons were detected by the coincidences of three Geiger-Müller tubes arranged in a vertical plane. The counters were shielded with 10 cm of lead on each side to prevent coincidences from the air showers. Also, 12.7 cm of lead was placed between the counters in order to cut off the soft component.

The absorption in air was measured by counting coincidences at different heights from Chicago up to the top of Mt. Evans, Colorado, (4300 m). The absorption in carbon

was measured by putting layers of graphite above the counters.

It was consistently found that the mass absorption in air was considerably larger than that in carbon. One set of measurements, for instance, gave the following results: Mt. Evans (4300 m, atmospheric pressure 618 g/cm²) without graphite: 11.9±0.07 coinc./min. *Ibid.*, under 84 g/cm² graphite: 11.0±0.057 coinc./min. Echo Lake (3240 m, atmospheric pressure 700 g/cm²) without graphite: 9.7±0.046 coinc./min.

Thus the additional air layer of 82 g/cm² between Mt. Evans and Echo Lake reduced the intensity of the mesotrons by more than twice as much as did the graphite screen of 84 g/cm². It is obvious that this large difference cannot be ascribed to the difference in stopping power of air and carbon. We see, therefore, definite evidence for the disintegration of the mesotrons.

The above results show that 1.3 mesotrons out of 11 disintegrate while traveling a distance of $4.30\times10^5-3.24\times10^5=1.06\times10^5$ cm. Their mean-free-path for the distintegration is, therefore, $L=1.06\times10^5/\log(11/9.7)=8.5\times10^5$ cm.

L is connected with the lifetime τ_0 by the formula: $c\tau_0=\mu cL/p$ where μ is the mass and p the momentum of the mesotrons. At sea level the average value of $\mu c/p$ was estimated to be about 0.07.[1] Assuming tentatively the same value in our case, one finds $\tau_0=2\times10^{-6}$ sec.

A fuller account of these experiments will be published later. The writers acknowledge with thanks the helpful discussions and support given to this work by Professor A. H. Compton. They also wish to express their appreciation for the facilities made available in Colorado by Dr. Joyce Stearns, as well as for the assistance of Mr. O. E. Polk and Mr. W. Bostick.

BRUNO ROSSI
H. VAN NORMAN HILBERRY
J. BARTON HOAG

Ryerson Physical Laboratory,
University of Chicago,
Chicago, Illinois,
September 30, 1939.

[1] B. Rossi, Cosmic Ray Symposium, Chicago, June, 1939; Rev. Mod. Phys. July–October (1939).

Magnetic Spectrograph Investigation of N^{13} Gamma-Radiation

Richardson[1] has reported that the decay of N^{13} is accompanied by a gamma-ray of 280±30 kev in addition to the well-known positron annihilation radiation. This gamma-ray is estimated to occur in 40 percent of all N^{13} disintegrations which take place.

The same radiation has been reported by Lyman[2] who estimates it to occur in 20±15 percent of all disintegrations; and by Watase and Itoh[3] who estimate it to occur in 20 percent of all disintegrations. The estimates of Richardson and of Watase and Itoh are uncertain by a factor of two. In view of the general interest in N^{13}, it has seemed desirable to make further observations on this radiation, using a method which is free from statistical errors.

The N^{13} gamma-ray spectrum was explored by measuring the energy and intensity of the secondary electrons ejected from lead and aluminum foils of equivalent thickness. The magnetic spectrograph used was of the usual semi-circular focusing type, constructed largely of lead. The slit jaws and other parts nearest the radioactive source were faced with graphite in order to minimize the background. The radioactive sources were produced by bombarding 0.5 mm thick graphite plates with 4.3-Mev deuterons. Eastman "No Screen" x-ray film was used, and was developed for eight minutes in D19 developer at 66°F.

The Pb and Al foils were placed in contact with the radioactive sources. A particular gamma-ray will eject both photoelectrons and recoil electrons from lead, but only recoil electrons from aluminum because of the different Z dependence of the two effects. The photoelectrons from a particular gamma-ray, having an initially homogeneous velocity, will appear on the spectrogram as a group with a sharp upper energy limit followed by a gradual decrease in intensity toward lower energies because of a straggling in the emitting foil. The recoil electrons ejected by the same gamma-ray under these conditions will have a much less homogeneous energy distribution because their energies depend greatly upon their directions of emission with respect to those of the quanta.

In this experiment the photoelectron spectrum of lead irradiated by N^{13} gamma-radiation was isolated from the recoil spectrum as well as from the instrumental background. This was done by successive exposures with lead and aluminum secondary emitters, the latter distribution being subtracted from the former. The relative photoelectron intensities due to any gamma-rays present may thus be directly compared without making any estimates of the contribution of recoil electrons as was necessary in the experiments of Watase and Itoh.

The data are shown in Fig. 1, which gives the film opacity as a function of $H\rho$. Because of differences in source intensities it was necessary to multiply the aluminum ordi-

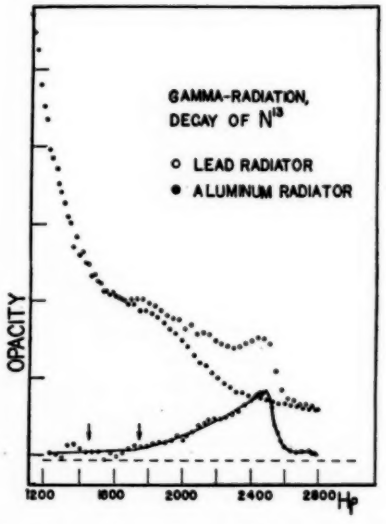

FIG. 1. Photometric measurements of films exposed to secondary electron spectra from lead and aluminum irradiated by N^{13} gamma-radiation. The lowermost curve is the difference between the Pb and Al data. The vertical arrows indicate the $H\rho$ region corresponding to lead K photoelectrons from a gamma-ray of 280±30 kev.

nates by 1.26 in order to bring them into coincidence with those for the lead at the point of lowest $H\rho$ shown. The zero line of the difference curve was drawn through its lowermost points. The large maximum in the difference curve is due to K photoelectrons from annihilation radiation; the L photoelectron edge does not fall on the film for the field intensity used. There is no evidence for a photoelectron line in the region of 280 ± 30 kev (indicated by arrows).

In order to obtain the relative gamma-ray sensitivity of the spectrograph for annihilation and 280-kev radiation, it is necessary to correct, for the variation of the photoelectric effect with gamma-ray energy,[4] the variation of film sensitivity with electron energy[5] and the instrumental effect due to the different radii of curvature of the two distributions.[6] Taking all these into account the spectrograph is estimated to be *at least* four times as sensitive to 280-kev radiation as to 512-kev radiation. From Fig. 1 it is necessary to conclude that in the region corresponding to 280 ± 30 kev there is not more than 0.05 gamma-rays per disintegration. At no point in the range from 1200 to 1800 gauss cm (gamma-ray energy 200 to 325 kev) could there be more than 0.11 gamma-ray per disintegration.

The author wishes to thank Professor L. A. DuBridge and Dr. S. N. Van Voorhis for their interest in this problem.

G. E. VALLEY*

Department of Physics,
University of Rochester,
Rochester, New York,
September 29, 1939.

* Now at Harvard University, Cambridge, Massachusetts.

[1] J. R. Richardson, Phys. Rev. **53**, 610 (1938); **55**, 609 (1939).
[2] E. M. Lyman, Phys. Rev. **55**, 1123(A) (1939).
[3] Y. Watase and J. Itoh, Proc. Phys. Math. Soc., Japan **21**, 289 (1939).
[4] L. H. Gray, Proc. Camb. Phil. Soc. **27**, 103 (1931).
[5] C. D. Ellis and G. H. Aston, Proc. Roy. Soc. **A119**, 645 (1928).
[6] K. T. Li, Proc. Camb. Phil. Soc. **33**, 164 (1937).

Search for β- and Delayed γ-Radiation from the Deuteron-Deuteron Reaction

The evidence[1-3] for the existence of a group of low energy neutrons resulting from the reaction $H^2(d, n)He^3$ has been strengthened by recent experiments of Bonner.[4] The low energy group is found to have an energy of 1.1 Mev ($Q=1.48$ Mev) and to comprise 10 percent of the total neutron yield. Since the well-known 2.4-Mev group of neutrons corresponds to a Q of 3.32 Mev it follows that there should exist an excited state of He^3 having excitation energy of 1.84 Mev, and that the decay of this excited nucleus should give rise to observable radiation. There are several possible decay processes

(1) $He^{3*}\rightarrow He^3+\gamma$,
(2) $He^{3*}\rightarrow He^3+\gamma$ (largely internally converted),
(3) $He^{3*}\rightarrow H^3+e^+$ (upper limit of spectrum 0.8 Mev).

Attempts[5-7] to observe instantaneous γ-radiation from the d-d reaction have failed to show its presence in amount greater than one γ-ray per hundred neutrons, a value too small by a factor of ten to account for the low energy neutron group.

We have attempted to observe radiation from other possible processes indicated above. The apparatus used is shown in Fig. 1. The heavy ice target was bombarded by a

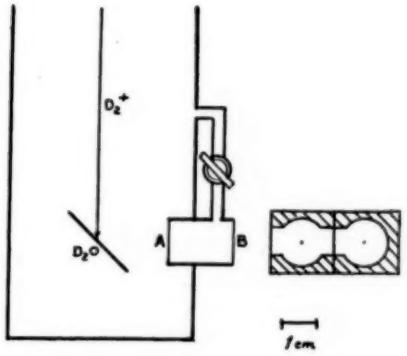

FIG. 1.

beam of deuterons from the 400-kv transformer-rectifier set in this laboratory. In the first set of experiments, designed to detect internal-conversion electrons, or positrons from the decay of a short-lived He^{3*}, only the foil B, of 0.02 mm Al, was used. Observations were made with a double counter of the Trost type which was used in a coincidence circuit[8] having a resolving time of 2×10^{-6} sec. The total thickness of window B and both counter windows was such that electrons having energy greater than 0.23 Mev would have been counted. Numbers of counts were recorded with and without a 6-mm Al absorber between the window B and the counter. With 20μa of 135-kev deuterons incident on the target a count of 900/min. was recorded. This was due to the neutrons, as it was unchanged within the limits of error (75/min.) by the interposition of the Al absorber and also of a Pb absorber. We calculate from the known yield of the d-d reaction[9] and the geometry of the apparatus that an electron-emitting process in equilibrium with the deuteron beam should give about 2×10^6 counts/min., assuming that the reaction leading to He^{3*} is 10 percent of the whole. This seems definitely to eliminate any possibility of internal conversion or short-lived positron radioactivity.

In order to investigate the possibility that the He^{3*} might be a long-lived positron or γ-ray emitter the foil A, which consisted of a collodion film of 0.5 mm air equivalent covered with an Al foil of 0.7 mm air equivalent, was introduced. The introduction of this foil made it possible, by closing the stopcock shown in the figure, to collect in a separate vacuum-tight chamber the He^{3*} recoils (range 4 mm) from the target, and to investigate their activity. Experiments were made by bombarding the target for ten minutes with 20μa of 135-kev deuterons and then making measurements with the beam shut off. Check measurements were made after identical bombardments with the stopcock open, in order to take into account the effect of induced radioactivity in the metal of the target chamber. We used the coincidence arrangement for observing electrons and a sensitive copper-walled counter for the detection of γ-radiation. The results were as follows: With the coincidence counter we obtained 4 counts/min. after bombardment with the stopcock in either position. With the γ-ray counter we obtained about 10 counts/min. over the counter background (75/min.) after bombardment

with the stopcock in either position. We should have been able to detect very unambiguously a difference of 3 electron counts/min. due to the changed position of the stopcock, and similarly a difference of 20 counts per min. in the γ-ray case. No such differences were observed. We calculate that with the stopcock closed there would be 2×10^7 He^{3*} caught in the side chamber after a ten-minute bombardment. From the geometry used and from the counter sensitivities we find that if there exists an excited He^3, its lifetime for positron emission is greater than 10 days and its lifetime for γ-ray emission is greater than 45 min. The high voltage apparatus used was built with the aid of a grant to Professor Ladenburg from the Rockefeller foundation.

M. H. KANNER
W. T. HARRIS*

Palmer Physical Laboratory,
Princeton University,
Princeton, New Jersey,
September 17, 1939.

[1] T. W. Bonner, Phys. Rev. **52**, 685 (1937); 53, 711 (1938).
[2] Baldinger, Huber and Staub, Helv. Phys. Acta **11**, 245 (1938).
[3] E. Hudspeth and H. Dunlap, Phys. Rev. **55**, 587 (1939).
[4] T. W. Bonner, Nature **143**, 681 (1939).
[5] Kallmann and Kuhn, Naturwiss. **25**, 231 (1937).
[6] A. J. Ruhlig, Phys. Rev. **54**, 308 (1938).
[7] S. Kikuchi and H. Aoki, Proc. Phys. Math. Soc. Japan **21**, 20 (1939).
[8] L. A. Turner, Phys. Rev. **55**, 1134 (1939).
[9] R. Ladenburg and M. H. Kanner, Phys. Rev. **52**, 911 (1939).
* Now with the United States Rubber Company, Providence, Rhode Island.

Pair Emission from Fluorine Bombarded with Protons

When fluorine is bombarded by protons of suitable energies gamma-rays with 6.3 ± 0.1 Mev quantum energy are emitted. Measurements of the gamma-ray yield as function of proton energy were first made by Hafstad and Tube[1] and later with higher resolution and over a greater range by Bernet, Herb and Parkinson.[2]

These measurements were made with ionization chambers and the radiation was filtered through $\frac{1}{8}$ in. or more of lead. They show that the penetrating gamma-radiation is produced at several sharply defined energies. Dee, Curran and Strothers[3] have shown that the resonance levels at 330, 670 and 860 kev all give rise to the same gamma-radiation. We[4] have confirmed this and in addition have found that the same is true for the prominent resonances at 0.920 and 1.36 Mev. It has also been shown in this laboratory[5] that at the 330-kev resonance the gamma-rays are accompanied by alpha-particles, with a range of 8 mm in air. It seemed safe, therefore, to conclude that the 6.3-Mev gamma-radiation originates from the reaction

$$F^{19}+H^1\rightarrow(Ne^{20})\rightarrow{}^*O^{16}+He^4$$

and represents a transition in oxygen from an excited state to the ground state. The alpha-particle group at 330 kev has also been found by Burcham and Smith[6] and we have recently been informed that Burcham and his collaborators have found the corresponding alpha-particles at the 860- and 920-kev resonances.[7]

In order to investigate the possible existence of radiation of low penetrating power from fluorine bombarded by protons we have made yield measurements by simultaneous observations with two ionization chambers, to which we shall refer as No. I and No. II. The two chambers were as similar as practicable but No. II was arranged so that suitable filters could be interposed between target and chamber. To reach the chambers the radiation passed through the 0.13-mm German silver wall of the target tube and the 0.40-mm aluminum ionization chamber wall. This filtration was desirable in order to exclude the x-rays produced by protons in the target, which consisted of a copper disk on which a thin layer of CaF_2 was deposited.

The filter chosen for the yield measurements with chamber No. II was 3.3 mm of lead. This is sufficient to absorb gamma-radiation up to several hundred kv or electrons up to 10 Mev.

Curves 1 and 2 (Fig. 1) represent the readings obtained with chambers I and II, respectively, as function of bombarding voltage, and curve 3 represents the difference between 1 and 2.

On the assumption that curve 2 is a measure of 6.3-Mev radiation only, and that chamber No. I is equally affected by this radiation, we can conclude that curve 3 represents a kind of radiation which is completely absorbed in 3 mm of lead. These assumptions are not entirely correct and for this reason we cannot exclude the existence of a few percent of absorbable radiation, even where curves 1 and 2 coincide, but this does not in any way invalidate the conclusions to be drawn from the difference between them.

Measurements of the absorption in lead and in aluminum made at 820 and 1130 kv proved that the radiation represented by curve 3 did not consist of soft gamma-radiation and that it probably consisted of fast electrons with a maximum range of approximately 1.5 mm in lead and 7.5 mm in aluminum. From 500 cloud-chamber photographs, taken at 820 kv, we obtained 166 positive and 173 negative electrons and 29 pairs could be identified with some certainty.

We conclude from this that curve 3 represents the ionization produced by pairs. The observed energy is 5.9 ± 0.5

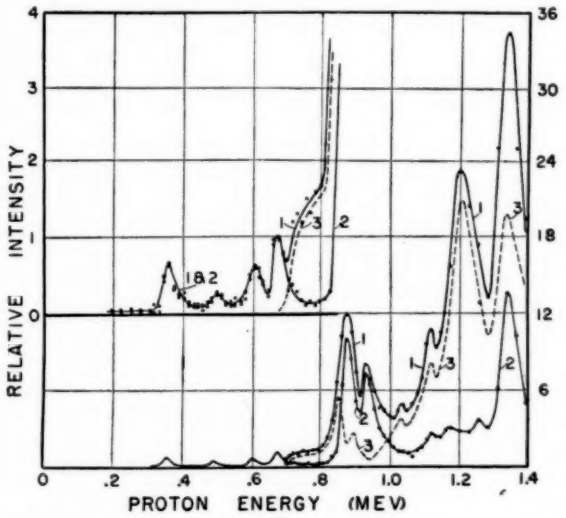

FIG. 1. Relative intensity of ionization *vs.* bombarding proton energy. Curve 1—radiation filtered by 0.5 mm aluminum. Curve 2—radiation filtered by an additional 3.3 mm lead. Curve 3—difference between 1 and 2.

Mev. In comparing the relative transition probabilities it must be remembered that the pairs are approximately twenty times as effective in producing ionization as are the gamma-rays, hence the latter are in all cases much more numerous.

It is interesting that although these pairs occur at definite resonance energies they do not coincide with the gamma-ray resonances. For example, at 920 kv the ionization due to gamma-radiation is nearly ten times as intense as that produced by pairs, while at 840 and 1190 kv the reverse is true. Clearly, therefore, the pairs are not produced by internal conversion of gamma-rays in the usual sense, but are emitted directly from a nucleus in an excited state. Presumably this is a state in O^{16} with $j=0$ and the transition is to the ground state which is known to have $j=0$. It is, however, possible that some or all of the pairs observed originate from a transition in Ne^{20}. If so, gamma-rays of approximately 7.5 Mev energy should accompany the pairs and we cannot exclude this possibility from our experiments so far. If the transition is in O^{16} alpha-particles should be observable at the pair resonances. Since no single quantum transition is allowed from such a state, the lifetime must be very long. Professor Oppenheimer has made a tentative estimate of 10^{-4} second for the half-life.

It seems probable that the pairs observed by Crane and Halpern[8] at 600 kv—11 pairs per thousand quanta—are to be attributed to this process rather than to internal conversion.

W. A. Fowler
C. C. Lauritsen

California Institute of Technology,
Pasadena, California,
September 27, 1939.

[1] L. R. Hafstad and M. A. Tuve, Phys. Rev. **48**, 306 (1935).
[2] Bernet, Herb and Parkinson, Phys. Rev. **54**, 398 (1938).
[3] Dee, Curran and Strothers, Nature **143**, 759 (1939).
[4] Fowler, Lauritsen and Lauritsen, Bulletin Phys. Soc. Stanford Meeting, June (1939).
[5] McLean, Becker, Fowler and Lauritsen, Phys. Rev. **55**, 796 (1939).
[6] W. E. Burcham and C. L. Smith, Nature **143**, 795 (1939).
[7] We are indebted to Dr. Burcham for communicating these results to us before publication.
[8] H. R. Crane and J. Halpern, Phys. Rev. **55**, 260 (1939).

Low Energy Gamma-Radiation from Lithium Bombarded with Protons

By means of the method described in the preceding letter we have investigated the radiation from Li^7+H^1 as function of proton energy. The target used consisted of separated Li^7 with a stopping power of approximately 30 kev.[1]

The filter used in front of ionization chamber No. II was 1.33 cm of lead. The readings of chambers Nos. I and II are shown in curves 1 and 2, respectively, and curve 3 is the difference between 1 and 2 (Fig. 1).

The resonance at 440 kev appears to be due entirely to the well-known 17.5 Mev gamma-radiation, while the radiation above 800 kev is strongly absorbed in lead.

We have measured the attenuation of the radiation at 1080 and 1290 kev and find an apparent absorption coefficient $\mu=1.50\pm0.10$ cm^{-1} in lead and $\mu=0.12\pm0.01$ cm^{-1} in aluminum. For annihilation radiation from N^{13} we find,

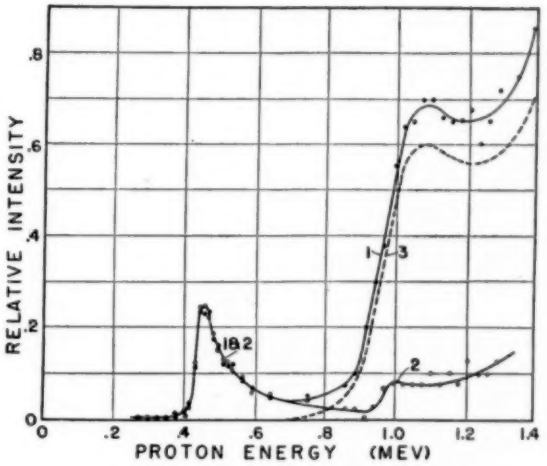

FIG. 1. Relative intensity of ionization *vs.* bombarding energy. Curve 1—radiation filtered by 0.15 mm lead. Curve 2—radiation filtered by an additional 1.33 cm lead. Curve 3—difference between 1 and 2.

with the same arrangement, $\mu=1.43\pm0.05$ cm^{-1} in lead. This gives the value 495 ± 25 kev for the gamma-rays at 1080 and 1290 kev bombarding energy.

From this and from the character of the yield curve above 800 kev it seems reasonable to assume that this radiation originates from excitation of Li^7 without capture of the proton in analogy with the well-known excitation of Li^7 by He^4. Rumbaugh, Roberts and Hafstad[2] have observed the same state in the following reactions:

$$\begin{aligned} Li^6+H^2 &\rightarrow (Be^8)\rightarrow Li^7+H^1 \\ &\rightarrow {}^*Li^7+H^1 \\ &\rightarrow Be^7+n^1 \\ Be^7 &\rightarrow {}^*Li^7-e^-. \end{aligned}$$

From the difference in proton ranges they find the separation of the states in Li^7 to be 455 ± 15 kev, and from the attenuation of the radiation following the decay of Be^7, 425 ± 25 kev.

Although our value 495 ± 25 kev is somewhat higher there can be little doubt that the same state in Li^7 is involved.

W. A. Fowler
C. C. Lauritsen

California Institute of Technology,
Pasadena, California,
September 27, 1939.

[1] We are indebted to Professor Rumbaugh and the Bartol Foundation for their kindness in supplying us with this target.
[2] Rumbaugh, Roberts and Hafstad, Phys. Rev. **54**, 657 (1938).

On the Equality of the Proton-Proton and Proton-Neutron Interactions

A comparison of the ^1S proton-proton interaction and the ^1S proton-neutron interaction has been made recently by Breit, Hoisington, Share and Thaxton.[1] It is the purpose of this letter to add a remark to this subject. With the meson type of potential, $Ce^{-\lambda r}/r\lambda$, a variational calculation has been made of the binding energy of H^3 of high accuracy (error <0.1 percent).[2] This calculation together with the value of the binding energy of H^2 and the scattering of

thermal neutrons by protons gives the following values for the constants in the meson potential for the ^3S neutron-proton interaction:

$$C(^3S) = -62.75\ mc^2; \quad \lambda(^3S) = 1.536\ (mc^2/e^2). \tag{1}$$

Any change within reasonable limits of the ^1S proton-neutron interaction affects this determination of the ^3S interaction very little. If one assumes the range, $\lambda(^1S)$, of the ^1S interaction between neutron and proton is the same as $\lambda(^3S)$, one gets the following constants:

$$C(^1S) = -36.32\ mc^2; \quad \lambda(^1S) = \lambda(^3S). \tag{2}$$

This calculation uses the experimental value for the scattering of thermal neutrons by protons of 18.3×10^{-24} cm^2. It may be noted that a 35 percent change in the value of the scattering cross section gives only 1.5 percent change in $C(^1S)$ for fixed $\lambda(^1S)$.

The proton-proton interaction as deduced from scattering experiments leads to the following interaction constants as determined by Share, Hoisington and Breit:[3]

$$C = -89.1\ mc^2; \quad \lambda = 2.38\ (mc^2/e^2). \tag{3}$$

The constants in (3) are considerably different from those in (2) where it was assumed that the proton-neutron ^1S range was the same as the proton-neutron ^3S range. If one assumes that the ^1S proton-proton interaction constants (3) also holds for the ^1S proton-neutron interaction, one may also fit the experimental data on the scattering of thermal neutrons by protons.[1]

If the fitting of the proton-proton scattering data is unambiguous, then either of two conclusions is indicated: that $\lambda(^3S) \neq \lambda(^1S)$; or that the ^1S proton-proton interaction does not equal the ^1S proton-neutron interaction. These conclusions will not be appreciably affected by the introduction of spherically symmetric spin-spin forces, but may be affected by other spin-spin forces such as give rise to the quadripole moment of H^2.

FREDERICK W BROWN
MILTON S. PLESSET

Norman Bridge Laboratory of Physics,
California Institute of Technology,
Pasadena, California,
September 19, 1939.

[1] G. Breit, L. E. Hoisington, S. S. Share and H. M. Thaxton, Phys. Rev. **55**, 1103 (1939).
[2] Frederick W. Brown, to be submitted shortly to the *Physical Review*.
[3] S. S. Share, L. E. Hoisington and G. Breit, Phys. Rev. **55**, 1130 (1939).

Proceedings of the Southeastern Section of the American Physical Society

Minutes of the University of Georgia Meeting, March 31 and April 1, 1939

THE fifth annual meeting of the Southeastern Section of the American Physical Society was held at the University of Georgia, Athens, Georgia, on March 31 and April 1, 1939. Local arrangements for the meeting were in charge of a committee consisting of: L. L. Hendren, chairman, E. H. Dixon, R. G. Henry, and R. H. Snyder. Approximately 150 members and guests were registered. The following officers were elected for the year 1939–40:

Chairman,	B. A. Wooten
Vice-chairman,	R. C. Williamson
Secretary,	P. Rudnick
Treasurer,	W. S. Nelms

Charleston, S. C., was selected as the place for the annual meeting in 1940, at the invitation of The Citadel.

Dr. Detlev W. Bronk, Director of the Johnson Foundation for Medical Physics at the University of Pennsylvania, was the guest of the Section and principal speaker in a symposium on biophysics, for which the program is printed below, together with abstracts of research papers presented at the meeting. The total number of papers on the program was 52; abstracts of those related to the teaching of physics are published in the August issue of the American Physics Teacher.

Philip Rudnick
Secretary, Southeastern Section

Program of Symposium on Biophysics

The Physical Basis of Biological Organization.—Detlev W. Bronk, *Johnson Foundation for Medical Physics.*

Applications of Nuclear Physics to Biology.—J. B. Fisk, *University of North Carolina.*

The Present Status of the Electron Microscope.—Otto Stuhlman, Jr., *University of North Carolina.*

Applications of Photography to Medical and Biophysical Problems.—G. G. Quarles, *University of Alabama.*

Purification of Biological Materials by Centrifuging.—J. W. Beams, *University of Virginia.*

A Recording Sensitive Differential Manometer.—William Hurst, *Duke University.* (See abstract 18)

The Lethal Effect of 2537A Radiation on Bacteria.—D. Gordon Sharp, *Duke University.* (See abstract 19)

Abstracts

1. A Method of Measuring Electrolytic Conductivity at High Frequencies. Gordon Stipe, Jr., and J. H. Purks, Jr., *Emory University.*—The rate of energy absorption by different solutions of hydrochloric acid in a cylindrical glass cell placed in a coil carrying several amperes at frequencies of the order of ten magacycles has been measured. This rate of energy absorption was found to be a function of the specific electrical conductivity σ, the volume v of the solution, the area a of the solution normal to the field, the frequency f of the current i in the coil, and a factor k which depends only on the dimensions of the coil and is defined by $H=ki$. An empirical relation was found which is expressed by the equation $\Delta u/\Delta t=\rho vs\Delta T/\Delta t=[1.449\times10^{-16}]av\sigma k^2i^2f^2$, where $\Delta u/\Delta t$ is the rate of energy absorption. A theoretical equation for the rate of energy absorption was derived. This equation is $\varphi u/\varphi t=[\pi/2\times10^{-16}]av\sigma k^2i^2f^2$ which agrees closely with the empirical equation. Since all factors in this equation other than the conductivity may be measured independently, the above relation may be used to determine the high

frequency electrical conductivity of electrolytic solutions from the rate of energy absorption by the solution in a high frequency magnetic field.

2. The Determination of Melting Points by Transmitted Light. DUDLEY WILLIAMS AND BENJAMIN HINTON, *University of Florida.*—An arrangement for the determination of melting points is described. A sample of the compound being studied is placed on a thin glass plate mounted inside a temperature-control bath. Light from a linear filament passes through the sample and is focused on a narrow slit behind which is mounted a photo-cell. At the melting point the intensity of the transmitted radiation increases and causes a rapid rise in the photo-current. Temperatures are determined by means of a thermocouple mounted in the control bath close to the sample. Typical photo-current *vs.* temperature plots are shown. Results obtained by the present method are compared with those obtained by visual observation and cooling-curve measurements.

3. An Apparatus for the Excitation of Raman Spectra of Gases. J. S. KIRBY-SMITH, *Duke University.*—An apparatus designed primarily for the excitation of Raman spectra of gases at low pressures has been constructed and put into operation. The light source consists of 16 low voltage direct-current Pyrex mercury arc lamps. Each lamp is 60 cm long and dissipates, normally, about 500 watts. A specially designed lamp housing, cooled with compressed air, permits reflectors, arcs, and scattering tube to be mounted in close contact without overheating. Appropriate filter solutions for isolating the various exciting lines, usually either Hg4047 or Hg4358, are circulated through a jacket surrounding the Raman tube. The entire apparatus operates in a vertical position, and the scattered light is reflected, by means of a right angle prism, into a Zeiss 3-prism spectrograph with an effective camera aperture of f: 2.3. Initial measurements have been made on a series of gaseous amines at about two atmospheres pressure. Good Raman plates have been obtained after exposures of from 3 to 6 hours.

4. Spectrographic Differentiation of Thallium Toxicity and Frenching of Tobacco Plants. G. M. SHEAR AND H. D. USSERY, *Virginia Polytechnic Institute.*—It is known that certain elements in minute amounts produce marked results on the growth of plants, some producing toxic effects, and the absence of certain others causing deficiency diseases. Frenching, one of the most important tobacco diseases, has remained confused with thallium toxicity, primarily because it has not been possible by ordinary chemical analysis to detect and measure the very small amounts of thallium required to produce toxic effects. In this investigation, ashed samples of leaves from tobacco plants grown in water cultures, and on frenching and nonfrenching soils were arced on copper electrodes, the spectrum from $\lambda = 2200$A to $\lambda = 4400$A being photographed with a grating spectrograph. Estimations of the thallium content for certain samples was made by comparing the intensity of the thallium line $\lambda = 3775.73$A in these samples with the intensity of the same line in samples of ash to which known amounts of thallium were added. The results of this work show that thallium toxicity and frenching are not the same, because no thallium was detected in the ash of the frenched tobacco, whereas thallium was found in measurable amounts in the ash of plants receiving thallium in amounts too small to produce thallium toxicity.

5. The Physical Factors Involved in Blood Volume Determination. JOHN C. BURCH, E. T. ELLISON AND N. UNDERWOOD, *Vanderbilt University.*—A brief outline of the method of measurement is presented. Measurements of the index of refraction, the density, and the hematocrit are made at the same time the blood volume is measured. Thus the changes in the quality of the blood that accompany changes in volume are indicated in these experiments.

6. Skin Temperature Measurements. M. A. PITTMAN, *Madison College.*—A study of the skin temperatures of various types of individuals was made using very simple apparatus. Radiation leaving the subjects passed through a hole in the end of a box housing a vacuum thermocouple with rocksalt window. The thermocouple was connected to a 10-ohm galvanometer and temperatures were measured by comparing deflections of the mirror with those produced by a blackbody of known temperature.

7. Dental Fluoroscope and Shield. C. R. FOUNTAIN, *George Peabody College for Teachers.*—The present form of dental fluoroscope, consisting of a small fluorescent screen clipped at an angle of about 30° to a regular dental mirror, is very similar to that designed by the author several years ago. The original design was not as satisfactory as desired and was not made public because the fluorescent screens available at the time did not show quite enough contrast when exposed to the type of x-rays regularly used for photographic work. The new fluorescent screens (Type B) are much more sensitive and give ample contrast, especially when exposed to the softer x-rays available with modern x-ray machines. The x-ray image on the screen, within the mouth, is viewed in the mirror by an observer entirely outside the path of the small beam of x-rays. When used with a lead shield designed to limit the direct beam and concentrate most of the secondary radiations upon the same small area, the operator of this dental fluorescope is not exposed to harmful radiations. The screen is protected from action upon it by saliva and sterilizing agents.

8. Graphical Evaluation of the Statistical Significance of Rate Differences. F. T. HOLMES, *University of Virginia.*—Workers in the general field of biology frequently must interpret rate differences. This is often done qualitatively rather than on a sound quantitative statistical basis. The work presented here was begun in the belief that the above-described condition was caused and fixed as a habit in many individuals by fear of the square root sign. It has been found possible to exhibit graphically on log-log scales certain curves which are sufficient to determine the presence or absence of a statistically significant difference between two rates. The graphs cover explicitly a wide

range of these four parameters: 2σ, p_2, N_2, and N_1/N_2 where $2\sigma = p_1 - p_2$ = twice the standard error for the numerical data given by p_1 and the remaining parameters, the p's and N's representing, respectively, the rates to be compared and the totals of the numbers of events from which the rates were computed. It is believed that the use of these graphs will occasionally save time for persons who are mathematically skilled and both time and effort for those who are not.

9. A Statistical Treatment of the Ultracentrifugation of a Bacteriophage. THOMAS DAVIS, *Virginia Polytechnic Institute.*—The formulae for the statistical treatment of the errors of sedimentation constants and their influence upon subsequent calculations are set forth. Emphasis is placed upon the special advantage of statistical methods to biological data. The sedimentation constant, density, diameter and apparent "molecular weight" of an anti-colibacteriophage are given along with their mean errors, based on many independent determinations.

10. Mileage of Gasoline at Different Speeds, and of Different Grades. J. B. DERIEUX, *North Carolina State College.*—The miles per gallon of gasoline were determined at speeds from five to sixty miles per hour, and the grades tested were "high-test," "regular," and "traffic." Graphs of mileage against speed were smooth curves rising rapidly as speed increased to twenty-five miles per hour, where the maximum was reached, then falling away more slowly beyond. Data on different cars were obtained and they all had approximately the same values. There was very little difference in the mileage of different grades. Gasolines of different companies all gave approximately the same value. The tests were made without adjusting the octane selector for the different grades, just as the average motorist usually does in trying out the different grades. In the apparatus arrangement, the fuel pump was disconnected from the pipe leading to the car's gasoline tank, and connected to a tube leading to a two-way stopcock, one of the ways of the cock was connected by a tube into a graduate where the volume used was measured, the other way of the cock was connected into a large bottle of the gasoline under test, and was switched to it while initiating a run.

11. Remarks on the Study of Structural Viscosity and an Example of the Technique for a Cellulosic "Solution." FRANCIS BREAZEALE, *American Enka Corporation.*—The problem of determining the flow properties of imperfect viscous fluids, is discussed. It is shown how the data from capillary and Couette viscometers may be correlated with that from other experimental procedures to give good information about the fluid in regard to: (1) the existence (and magnitude) of yield value; (2) the existence (and extent) of creep; (3) the form of the viscosity rate of shear function. The differences between, and factors governing Ostwald and Bingham systems are emphasized. It is indicated how the expressions for the flux of such fluids through a cylindrical pipe may be derived. As an example, photographs of the movement of a cellulosic solution through a tube are shown. They indicate: no creep; no yield value; but structural viscosity. Measurement of this liquid in capillary and Couette viscometers confirm this. An approximate expression for the flux of the fluid is derived *in extenso.*

12. Infra-Red Absorption of Mixtures Containing D_2O. P. E. SHEARIN AND E. K. PLYLER, *University of North Carolina.*—The purpose of the present study was to determine if the nature of the solvent affected the association of D_2O molecules. The investigation included mixtures of heavy water and acetone, isopropyl ether, ethyl alcohol, and isoamyl alcohol. One absorption band of heavy liquid water is at 4μ and the corresponding band of heavy water vapor occurs at 3.6μ. Mixtures of heavy water with the two alcohols showed the water absorption band at 4μ. Practically no change was observed in this band as concentrations were varied from 2 percent to 20 percent. This indicated that the association between D_2O and the alcohols produces about the same effect as the association of D_2O with itself. In the case of a 5-percent solution of D_2O in isopropyl ether a broad band was observed with a minimum at approximately 3.95μ. This showed that the binding between the ether molecules and the water molecules is different from the association of D_2O and alcohol. The acetone-water mixtures showed a further shift in the D_2O band to 3.8μ. The concentrations varied from 5 percent to 20 percent of D_2O. The D_2O molecules are nearer to the vapor state in the acetone-water mixtures than in the other mixtures.

13. Near Infra-Red Absorption Spectra of Some Sugars. E. S. BARR AND C. H. CHRISMAN, *Tulane University.*—By use of a fluorite prism spectrometer, infra-red spectra have been observed in the region between 1.7μ and 5.0μ for nine monosaccharides (*d*-arabinose, *l*-arabinose, *d*-xylose, *l*-rhamnose, *d*-mannose, *d*-galactose, *d*-levulose, *d*-glucose, and β-*d*-glucose) and four disaccharides (sucrose, maltose, *d*-lactose and β-*d*-lactose). Saturated solutions in water were used for some of these materials, but for most of them it was found that slow evaporation made it possible to prepare cells with the water content highly reduced, without crystallization setting in. This procedure reduces the error involved in correcting for the absorption of the solvent. Characteristic absorptions were observed at 2.16μ and 2.35μ. The strong general absorption in the region of 3.3μ was partially resolved into the component bands.

14. The Influence of Discharge Chamber Geometry upon the Striking Potential of the H.F. Discharge. SHERWOOD GITHENS, JR., *University of North Carolina and Wake Forest College.*—In a paper on the striking potential of the h.f. discharge in hydrogen given at an earlier meeting (February 20, 1937), the relations of striking potential to pressure at 6 frequencies between 5 and 10.5 megacycles were shown. These curves possessed three minima instead of the usual Paschen law single minimum. A corresponding set of curves, obtained with the latest of a series of specially-designed discharge chambers, will be presented. A comparison of curves and discharge chambers verifies that the

lowest-pressure minimum in the older chamber is produced by a discharge initiating between either electrode and the walls of the chamber; and leads to the conclusion that at most frequencies, there are two modes, rather than one, in which a discharge may initiate between the electrodes.

15. The Effect of Humidity and Sphere Material on the Sparkover Voltage of the 2-Centimeter Sphere Gap. ARTHUR B. LEWIS, *University of Mississippi.*—Data are presented showing that: (1) The effect of humidity on the irridiated 2-centimeter sphere gap, set at a gap of 4 mm, is to increase the sparkover voltage by +0.13 percent per mm (of mercury) increase in vapor pressure of the water in the atmosphere. This effect is apparently independent of the sphere material for the metals aluminum, brass, chromium, nickel and steel. (2) There seems to be no choice between these metals so far as the repetition of the results is concerned, the probable error of a day's results averaging ±0.28 percent. This error can be largely if not wholly accounted for in terms of known sources of uncertainty. (3) Even when corrected for all known variables, including humidity, the final sparkover voltages for the spheres of various metals differ from each other by far more than can be accounted for by any definitely recognized source of uncertainty.

16. Apparatus for Nuclear Physics. J. C. MOUZON, *Duke University.*—A description of an inexpensive half-million volt a.c. transformer set made up of discarded x-ray transformers, its associated equipment, and its application to specific nuclear problems will be given.

17. Emission of Electrons from "Cold" Metallic Targets under High Energy Positive Ion Bombardment.* J. B. FISK, *University of North Carolina.*—A small electrostatic generator at the Massachusetts Institute of Technology has been used to accelerate protons, (hydrogen molecular ions, and singly charged helium ions), to energies between 50 and 450 kv. The ions then struck a cold metallic target. The number of electrons emitted per incident ion was measured as a function of incident energy for a number of different metals. For protons, the "yield" of electrons varied smoothly from about 4 at low energies to about 2 at high energies, nearly independent of target material. The yield for hydrogen molecular ions was about seven; for helium ions about 13, there being little variation with energy. For targets of Mo, Cu, Pb, Al prepared in a given manner the yield was very nearly proportional to the mass of the bombarding particle. However, the yield depends very markedly on the condition of the surface of the target.

* Hill, Buechner, Clark and Fisk, Phys. Rev., in press.

18. A Recording Sensitive Differential Manometer. WILLIAM HURST, *Duke University.*—A modification of the differential manometer recently described in the literature[1] has been made which possesses several advantages over the former instrument. A drum with light weight rubber stretched over it actuates a mirror which pivots on a glass shaft. The manometer is sensitive to pressure changes equivalent to 0.00005 cm of mercury and responds to pressure variations occurring as rapidly as 25 per second. Pressure variations are recorded on moving sensitized paper. While the instrument has been developed for use in clinical medicine, it has already been applied to problems in zoology, such as the study of the respiration of small insects.

[1] William Hurst, "A Sensitive Differential Manometer," Rev. Sci. Inst. **10**, 27 (1939).

19. The Lethal Effect of 2537A Radiation on Bacteria. D. GORDON SHARP, *Duke University.*—In order to measure the lethal effect of 2537A radiation on bacteria an apparatus[1] was used in which the organisms were carried in a stream of compressed air through a region of high intensity rays. Measurements made on intensity of radiation and speed of the air stream were used to calculate the energy incident per unit area of each bacterium. By taking samples of the air beyond the exposure chamber and counting the number of survivors, quantitative data were obtained on several species. *Bacillus subtilis* was killed with an incident energy of 62,225±7.2 percent ergs/cm² while *Pseudomonas aeruginosa* required 16,100±5.4 percent for complete killing. All other organisms tested were in this region. In the case of *Escherischia coli* the survivor curve was plotted. It was found that this curve showed considerable deviation from the one predicted by existing theory. This deviation was especially apparent for survival ratios less than one percent. These low survival ratios have not been examined by the plate method because of its physical limitations not inherent in the present method. The explanation of these results necessitates an alteration in the proposed theories of lethal action of ultraviolet rays, and it is suggested that more weight be given to the variation in individual cell resistance.

[1] D. Gordon Sharp, J. Bacteriol. **35**, 589 (1938).

20. Surface Effects in Testing for Ferromagnetic Impurities. F. W. CONSTANT AND J. M. FORMWALT, *Duke University.*—As described in previous papers, a method has been developed whereby a permanent magnetic moment as small as 10^{-7} per cc may be measured in any small solid specimen—less than 10^{-7} percent of that found for Armco iron. For the various metals tested, magnetic moments per cc of 2×10^{-7} to 8×10^{-3} were found. In such measurements the elimination of surface impurities is of prime importance. The effectiveness of various methods of cleaning has been investigated with several metals. In most cases the cleaning fluid used made little difference, and a series of tests on the same specimen would show a linear relationship between the total magnetic moment and the volume, or a constant magnetic moment per cc. In testing aluminum, however, it was found that some solvents appear to leave the ferromagnetic impurity in the form of a film adhering to the surface, so that the magnetic moment per cc increases with successive cleanings.

21. Linearity of Wide Range Galvanometer Response in a Photoelectric Spectrophotometer Utilizing a Balanced Amplifier Circuit. WALTER C. BOSCH AND BARREMORE B. BROWN, *Tulane University.*—Photo-cell conductances, *C*, for a large range of spectral intensities in the visible and

ultraviolet are measured by a null method and for each intensity the deflection, d, of the plate galvanometer in a DuBridge-Brown amplifier is read. An equation, $d=AEC/(1+CR)k$ is experimentally investigated. E, the potential across the photo-cell and series resistance, R, is kept constant at 90 v. A 3.5-meter mirror to scale distance reduces the galvanometer constant, k, and increases the voltage sensitivity of the amplifier. The factor $(1+CR)$ equals 1.005 for the greatest deflection used. The current amplification factor, A, quickly deviates from constancy unless proper bias conditions are established and a method for determining correct bias is given. Experimental data and curves for $R=10^9$ and 10^{10} ohms show that, with correct bias, conductance/cm for any given value of R is a constant within ± 1 percent of a mean value for deflections up to 1500 cm. The incident light flux in this deflection range, both values of R considered, is estimated to vary between 10^{-6} and 10^{-8} lumen.

22. Effective Rotation Temperatures of CO in the Electrodeless Discharge. MYRON S. MCCAY, *Virginia Polytechnic Institute*, AND HAROLD P. KNAUSS AND BRUCE ARCHDEACON, *Ohio State University*.—The effective rotation temperatures of carbon monoxide in the electrodeless discharge heated by an electric furnace have been determined by the method of band intensity maxima, and from the intersection of the intensity envelopes of the branches composing the band.[1] The temperatures were found from the line intensities of the (0,1), (0,2), and (0,3) bands of the Angstrom system of CO for furnace temperatures ranging from 300°K to 600°K. Comparison with readings of an air thermometer placed within the discharge indicates a consistently higher spectroscopic temperature, in contrast with the observed convergence of furnace temperature and rotation temperature at high values for the low-voltage arc.[2]

[1] Phys. Rev. **52**, 1143 (1937).
[2] Proc. Phys. Soc. **47**, 413 (1935).

23. The 7.5μ Fundamental Vibration of CH_3Cl. ALVIN H. NIELSEN* AND HARALD H. NIELSEN, *Ohio State University*.—Because of the small separation of the rotation lines in the parallel bands of CH_3Cl they were not at first[1] resolved. Somewhat later Barker and Plyler[2] partially resolved the band ν_5 at 13.7μ giving the spacing as 1.1 cm^{-1} and computing the moment of inertia A to be 50×10^{-40} g cm^2. Nielsen and Barker[3] remeasured ν_3 at 7.5μ and with poor resolution found $\Delta\nu_r$ to be 1.3 cm^{-1}. The writers have made a new attempt to resolve ν_3 with fair success. The spectrometer used was of prism-grating design equipped with a 2000-line-per-inch grating. The slits included a spectral interval of 0.6 cm^{-1} and galvanometer readings were taken at intervals of 0.2 cm^{-1}. The lines in the P branch are resolved much better than the lines in the R branch because of the isotope shift, but on averaging the best line spacings over the whole band, the value appears to be about 0.96 cm^{-1} which gives a value of A equal to 57.9×10^{-40} g cm^2.

* University of Tennessee, Department of Physics.
[1] W. H. Bennett and C. F. Meyer, Phys. Rev. **32**, 888 (1928).
[2] E. F. Barker and E. K. Plyler, J. Chem. Phys. **3**, 367 (1935).
[3] A. H. Nielsen and E. F. Barker, Phys. Rev. **46**, 970 (1934).

24. Force Constants of NO_2 Groups. DUDLEY WILLIAMS AND LORAINE DECHERD, *University of Florida*.—The infrared spectra of inorganic nitrite solutions have been studied. From the fundamental frequencies it was possible to determine the force constants and angles involved in the group. The values obtained for the angles are in fair agreement with x-ray data. The force constants of the nitrite group are compared with those of the nitro groups in organic compounds and with those of nitrogen dioxide.

25. Change of the Viscosity of Liquids Produced by an Electric Field. A. A. DIXON, *North Carolina State College*.—The work of Alcock[1] showed that for polar liquids, the viscosity was changed by an electric field but for nonpolar liquids the effect was zero. A rotating cylinder type of viscosimeter has been used during the past year to measure the effect of an electric field on the viscosity of several liquids. A potential difference which could be varied, was applied between the two cylinders. Some of the liquids tested were the same as those reported by Alcock and the results were similar to those contained in his report. Measurements on a few additional liquids have been made. In all the polar liquids tested the viscosity was found to increase with the electric field strength.

[1] E. D. Alcock, Physics **7**, 126 (1936).

26. The Unit Cell and Space Group of Potassium Bicarbonate. RICHARD C. KEEN, *Louisiana State University*.—Small needle-shaped crystals of potassium bicarbonate were prepared by passing carbon dioxide gas through a solution of potassium carbonate. X-ray rotation photographs about all three coordinate axes were taken. The planes producing the diffraction spots were indexed using the Benal reciprocal lattice method. According to data given by Groth the crystal should have axial ratios of $a:b:c=2.677:1:1.311$. This was found to be incorrect and axial ratios are actually $a:b:c=2.667:1:0.655$. The length of a unit cell along Z axis is only one-half of the value given by crystallographic measurements. Planes having indices hOO and OkO were missing when h and k were odd. Calculations from density, molecular weight of potassium bicarbonate and the dimensions of unit cell, obtained from measurements of photographs, show that there are four molecules of this compound in each unit cell. These measurements and missing planes would suggest the compound should belong to space group C_{2h}^4. Characteristics of this space group together with preliminary calculations show this to be an impossible arrangement. A space group, retaining the glide plane along X axis and having much lower symmetry, C_s^2, is suggested. This space group accounts for absence of hOO planes when h is odd. There is also no physical reason why the computed intensity of OkO planes should not be zero when k is odd. Then this space group, C_s^2, having only two molecules per unit cell enables one to apply its parameters twice to obtain the four molecules and to overcome the impossible difficulty of concentrating atoms at one-fourth, one-half, and three-fourths the distance along X axis, which led to the impossible atomic distances inherent in the C_{2h}^4 space group arrangement.

27. An Analytical Centrifuge.* J. W. BEAMS AND R. E. FOX, *University of Virginia.*—A new design of a vacuum type analytical centrifuge is described which requires no optical system. The driving and supporting mechanism has been previously described,[1] the only changes being in the large rotor or "centrifuge." The centrifuge contains a number of identical sector-shaped cells spaced symmetrically with respect to the axis of rotation and equidistant from it. These cells are connected by small channels near their periphery so that each is filled to the same radial distance when the centrifuge is spinning. If the cells "overflow," the material is collected in a chamber situated above them. The centrifuge is first accelerated to the desired speed and the material to be centrifuged is injected through the hollow supporting shaft into the cells. The centrifuge is maintained at constant angular speed until the desired separation has taken place. A sufficient amount of heavy nonmiscible liquid is then injected into the cells at their periphery, to force about half of the solution (by volume) being centrifuged into the upper chamber. The machine is then stopped. From a determination of the cencentration of the material in the upper chamber and of the original material, the dimensions of the centrifuge, time of centrifuging, and angular speed, molecular weights and sizes can be found. This apparatus may be used either for sedimentation equilibrium measurements or rate of sedimentation measurements.

* Supported by a grant from the Research Corporation.
[1] Beams, J. App. Phys. **8**, 795 (1937).

28. Measurement of Radiation of the Sky. C. M. HECK, *North Carolina State College.*—The radiation of the sky toward the earth has been recorded throughout 1938 by means of thermometers and thermocouples placed in the bottom of a small hemispherical aluminum mirror, which mirror was placed confocally within an enclosing mirror of double the diameter. In turn, the larger mirror was enclosed by a still larger mirror and this by one still larger, making a confocal nest of four mirrors, the function of each being: (a) to protect the mirror enclosed from the radiation of the earth and convectional currents of the air; (b) to direct radiation to the enclosed mirror only from the sky. With such devices the radiation has been continuously studied at Raleigh and for a short time from the top of Mount Mitchell and from the top of the Empire State Building. Curves of the variation in radiation show: (a) a sudden fall in radiated heat around sunset that allows the temperature within the radiometer to fall as much as 35° below that of the surrounding atmosphere, which great differential tends to remain constant thereafter throughout the night. (b) the differential appears dependent on the absolute humidity and its relative distribution in the atmosphere whereby upper gulf air masses or passing invisible clouds of higher absolute humidity are recorded with precision. (c) the average point of thermic control of such insulated and radiation environed points at the earth's surface can thus be carried to heights of two or more miles.

29. The Light Plane Hypothesis. J. L. TALLEY, *Junior College of Augusta.*

30. Displacements of Raman Frequencies of Some Aliphatic Molecules in Water Solution. R. C. WILLIAMSON, *University of Florida.*—The substances studied were methanol, ethanol, acetone, dioxane, formic, and acetic acids. Curves are presented showing the displacements (plus or minus) of the following Raman frequencies as functions of the ratio of the number of molecules of water to one of the solute: $C-H^{(\nu)}$ (+methanol, +dioxane); C−O (−methanol, −ethanol, −dioxane); C=O (−acetone); C−C (−ethanol, +acetone, −dioxane). The curves indicate approximate saturation, the greater part of the shift being attained below a molar ratio of four of water to one of solute. The frequencies are usually displaced with no broadening of the lines. Except that in the case of formic and acetic acids (as noted by previous observers), the C=O line at 1666 cm^{-1} gradually fades and a new one develops with a frequency increase of 52 cm^{-1} (formic) and 42 cm^{-1} (acetic). Microphotometer records show that the original line and the new one are about equal intensity at a molar ratio of approximately one of water to two or three of acid. The shifts observed for dioxane in water agreed to within approximately 2 cm^{-1} with those reported by Simon and Feher. Dioxane shows well marked $C-H^{(\nu)}$ shifts, reaching +14 cm^{-1} at ratios of six to one. No measurable shifts were observed for the flexural $C-H^{(\delta)}$ frequencies. The C=O acetone line at 1712 cm^{-1} was decreased by 11 cm^{-1} at a molar ratio of 6 to 1, contrary to Edsall who reported no observable shift.

31. A Study of Dielectric Absorption. J. W. SIMMONS, *Virginia Polytechnic Institute.*—An extensive study of absorption in waxed paper used as a dielectric has been made to determine empirical equations expressing the relation of absorbed current to times of change, discharge, and recovery after discharge. High capacity and low direct-current potential were used to avoid leakage and other losses. Results have been as expected, residual charge increasing rapidly with time of charge, for fixed times of discharge and recovery after discharge, until maximum charge is approached, then increasing very slowly. The inverse effect is true for variation of residual charge with discharge time, charge time and time of recovery being fixed. Curves of residual charge plotted against time of recovery after discharge show a marked increase in slope for the higher values of charge time, but are almost flat for small charge times. Increase in time of discharge tends to flatten the curves, even those of large charge time values. It is hoped that a connection between the curve equations and alternating-current dielectric losses may be shown.

Proceedings of the American Physical Society

MINUTES OF THE STANFORD, CALIFORNIA MEETING, JUNE 28–JULY 1, 1939

THE 229th regular meeting of the American Physical Society was held at Stanford University, California, on Wednesday, Thursday, Friday, and Saturday, June 28, 29, 30, and July 1, 1939.

Morning sessions were held on Thursday, Friday, and Saturday for the presentation of the 57 contributed papers abstracted below. The symposium on Wednesday afternoon, held jointly with the Astronomical Society of the Pacific, was concerned principally with the problem of limb darkening, and was addressed by C. D. Shane, Edison Pettit, A. B. Wyse, and E. M. McMillan. On Thursday afternoon a demonstration symposium on "Some New Ultra-High Frequency Radio Apparatus" was addressed by D. L. Webster, W. W. Hansen, and S. F. Varian. On Friday afternoon a symposium on "Methods and Results of X-Ray Structure Determination" was held, the speakers being M. L. Huggins, J. D. Bernal, and O. L. Sponsler.

Attendances ranged from about 50 to 230 persons.

PAUL KIRKPATRICK,
Local Secretary for the Pacific Coast

ABSTRACTS

1. Initial Recombination. N. E. BRADBURY, *Stanford University.*—In an attempt to determine the fraction of ions lost by recombination in an x-ray ionization chamber, a theory has been developed for the processes involved in preferential and initial ionic and electronic recombination. The theory considers the change of the energy distribution of the electrons as they diffuse away from the parent atom. From this together with a knowledge of the electron capture process, the space distribution of negative ions formed may be obtained. The probability of the initial electron recombining preferentially with the parent positive ion is considered as well as the preferential process for the negative ion. Knowing the initial spacing of the ions, it is possible to calculate the recombination occurring during the diffusion process until random distribution is reached. The final volume recombination may then be calculated in the usual manner. The theory may be employed in both electronegative and free electron gases and to ions formed in the presence or absence of an electric field.

2. Experiments on the Multiple Scattering of Electrons and Positrons. C. W. SHEPPARD AND W. A. FOWLER, *California Institute of Technology.*—Measurements on multiple scattering[1] have been continued in lead, aluminum and carbon foils of various thicknesses. The distribution in energy times scattering angle has been found to be Gaussian as predicted by the theory of E. J. Williams but with a smaller arithmetic mean angle than given by the theory. No difference in the scattering of positrons from that of electrons could be found within the experimental error. The results are contained in the following table:

SCATTERER	THICKNESS	NO. OF TRACKS	OBS. $\overline{Wa}$	THEO. $\overline{Wa}$
Lead	0.015 cm	362	45	106.0
Lead	.033	415	89	173.5
Aluminum	.102	423	46	64.0
Carbon	.114	401	38	42.7
Carbon	.330	252	57	75.7

W. A. Fowler, Phys. Rev. **54**, 773 (1938).

3. Energy Fluctuations in the Electromagnetic Field. P. MORRISON, *University of California.*—There is a well-known analogy between the quantized electromagnetic field and a system of Bose particles. This analogy is strict in the case of the total energy and momentum; the infinite zero-point energy of the field can be removed by introducing a term independent of the occupation numbers. But the energy localized in a small volume fluctuates even for a field containing no quanta in a way to which there is no particle analogue. These zero-point fluctuations arise from terms corresponding to the emission and absorption of two quanta. The zero-point energy fluctuations actually diverge for instantaneous measurements of energy. The effects of time averaging and of smearing the space-time boundaries of the defining region are examined. Various methods of measuring energy density are compared.

4. Conduction and Mobility of Thin Lead Films. M. G. FOSTER AND A. GOETZ, *California Institute of Technology.*—From measurements of electric conductivity made on thin films of Pb obtained by condensing the metal on cooled glass surfaces at rates from 5×10^{12} to 100×10^{12} atoms

sec.$^{-1}$ cm^{-2} under high vacuum conditions designed to eliminate contamination, the following results are obtained: The critical film thickness at which the (specific) conductivity of the metal begins changing rapidly from its low value (10^{-6} mho-cm^{-1}) in the thinnest films to that of the bulk metal (10^{+6} mho-cm^{-1}) is in the neighborhood of 60A for room temperature films and of 30A for films cooled with liquid air. The mutual configuration of the condensed Pb atoms changes with time as is shown by a decrease observed in the conductivity when the film was isolated from external influences, and by the eventual appearance of a granular structure visible under the ultramicroscope. In some cases a reproducible dependence of the conductivity on the applied potential was observed. These effects prove to be in harmony with the thermodynamic expectancy for the stability of such films (tendency toward aggregation) resulting in the removal of mobile atoms into crystallization centers, and thus in gaps which obstruct the conduction electrons. Certain deficiencies in quantitative reproducibility are ascribed to variations in the physical surface conditions on the glass plate.

5. Concentration of C^{13} and Measurement of its Nuclear Spin. CHARLES H. TOWNES, *California Institute of Technology.*—Heavy carbon was concentrated with a Hertz diffusion apparatus of 34 members to a maximum of 50 percent, and enough carbon at 30 to 40 percent concentration was obtained to make possible spectroscopic and nuclear disintegration work. The concentration was in two processes. Ordinary methane was let continuously through the light reservoir of a Hertz apparatus for the collection of a large quantity of gas containing 6 or 7 percent heavy methane, then this gas reintroduced into the system for a final concentration. From measurements on the $C^{13}-C^{13}$ band spectrum, the C^{13} nucleus obeys Fermi-Dirac statistics and apparently has a spin of 1/2. A 21-ft. grating and Lummer-Gehrke plate combined were used to resolve some of the close Λ-type doublets of the (O−O) band of the $C^{13}-C^{13}$ Swan system. Resolution was not complete, but was enough to determine the nuclear statistics and allow a good estimate of the spin from preliminary measurements. It is hoped that a microphotometric analysis will allow a conclusive measurement of the spin.

6. The Generation of Square-Wave Voltages at High Frequencies. W. H. FENN, *University of California* (*Introduced by L. C. Marshall*).—Two methods are described for the generation of high frequency alternating voltages having a square wave shape. The first method is based on a previously developed system utilizing an overloaded direct-coupled amplifier. The second method makes use of a special pulse generator followed by a vacuum-tube trigger circuit. Square waves are obtained with both methods at frequencies above 200 kilocycles per second. The applications of such square waves are considered, as well as the importance of the circuits for other purposes. Of special interest are the suggested improvements in conventional "scale-of-two" counting circuits and the description of the high-frequency pulsing circuit.

7. A Question in General Relativity. L. I. SCHIFF, *University of California.*—Professor J. R. Oppenheimer has suggested the following question: Consider two concentric spheres with equal and opposite total charges uniformly distributed over their surfaces. When the spheres are at rest, the electric and magnetic fields outside the spheres vanish. When the spheres are in uniform rotation about an axis through their center, the electric field outside vanishes, while the magnetic field does not. Suppose that the spheres are stationary; then an observer traveling in a circular orbit around the spheres should find no field, for since all of the components of the electromagnetic field tensor vanish in one coordinate system, they must vanish in all coordinate systems. On the other hand, the spheres are rotating with respect to this observer, and so he should experience a magnetic field. The resolution of this apparent paradox shows in an interesting manner how the warping of the metric caused by the rotation in the observer's coordinate system of the distant masses that determine our inertial frame introduces current-like terms into Maxwell's equations at the surfaces of the spheres. These just cancel the currents caused by the rotation of the spheres in this system.

8. The Contact Difference of Potential Between Silver Films on Glass and on Rocksalt. PAUL A. ANDERSON, *State College of Washington.*—Study of the structural dependence of the work function has been hampered by the experimental difficulties involved in preparing monocrystalline metal surfaces of known orientation which are free from mechanical deformation and atmospheric contamination. A new method of attack, suggested by Brück's observation[1] that certain metals when condensed on rocksalt cleavages form mosaics of crystals all oriented with their (100) planes parallel to NaCl (100), has been tested for silver films formed on rocksalt at 200°C in the measuring tube. Using methods of measurement previously described[2] and a tube which was intensively outgassed and gettered with barium, the contact P.D. between these films and polycrystalline silver surfaces of known work function,[2] formed on glass at room temperature, is found to be $0.12 \pm .01$ v. Referred to a work function of 4.46 ev for Ag (glass), the work function of Ag (rocksalt) is then 4.58 ev. Since deviation of the Ag (rocksalt) films from the ideal structure would lower the contact P.D., 4.58 ev is to be regarded as a minimum value for the work function of Ag (100).

[1] Brück, Ann. d. Physik **26**, 233 (1936).
[2] P. A. Anderson, Phys. Rev. **49**, 320 (1936); **54**, 753 (1938).

9. About the Physical Nature of the Graininess of Photographic Emulsions. W. O. GOULD AND A. GOETZ (in collaboration with F. W. Brown, III), *California Institute of Technology.*—Measurements concerning the cause and nature of the graininess of photographic emulsions are described. They are obtained with the use of the graininess meter previously reported,[1] with particular reference to the definition of the graininess coefficient (G) as parameter of the Gaussian integral.

$$\left(\frac{.2}{\sqrt{\pi}\cdot G}\int_0^x e^{-(x/G)^2}dx;\ x=\Delta T/T_m.\right)$$

The G values vary for commercial emulsions between 30 and 150. The G density function $G(D)$ has a maximum for $D \leq 1.0$, which is in qualitative agreement with subjective graininess measurements (Lowry).[2] For a given emulsion the position of the maximum as well as dG/dD depends upon the aperture with which the emulsion is observed as the optical scattering power of the emulsion (Caillier coefficient) causes a dependence of the objective graininess upon the optics of the illuminating and observing system. The scattering power of different emulsions depends only upon the grain size (granularity). It increases nearly linear with $D(\leq 1)$ and is almost independent of the graininess. Effects of the superposition of the graininess of two different emulsions upon another are studied as they appear in the printing process. The printing factor $P = G_P/G_N$ has been determined for a number of emulsions and has been found to be smaller than 1 for small densities of the print and for closely identical gamma.

[1] A. Goetz and W. O. Gould, J. Soc. Mot. Pic. Eng. **24**, 510 (1937); W. O. Gould, A. Goetz and A. Dember, Phys. Rev. **54**, 240 (1938).
[2] E. M. Lowry, J. Opt. Soc. Am. **26**, 65 (1936).

10. A Note on the Wave Functions of the Relativistic Hydrogenic Atom. LEVERETT DAVIS, JR., *California Institute of Technology*.—It does not appear to have been noticed that the radial functions of Dirac's relativistic hydrogenic atom can be expressed in terms of generalized Laguerre polynomials. By using the known properties of these polynomials, it is easy to evaluate the normalization constants and to calculate the average value of r^q. The expressions for r^q involve the sum of three generalized hypergeometric functions of the type ${}_3F_2$ with unit argument. All results are obtained in closed form since the series terminate. It should be noted that while the properties of the generalized Laguerre polynomials[1] are well known to mathematicians, these functions are slightly different from the associated Laguerre polynomials ordinarily used in quantum mechanics.

[1] E. T. Copson, *Functions of a Complex Variable* (Oxford University Press, 1935), pp. 269–270.

11. A Low-Background Electron Counter. ROBERT R. WILSON AND DALE R. CORSON, *University of California*.—We have successfully applied Winkler's[1] arrangement to count weak beta-radioactive samples. The counter consists of a wire surrounded by a cylindrical electrode in which is a small hole that permits electrons to pass to a collecting plate. The radioactive wire is maintained at a negative potential with respect to the cylinder which is negative with respect to the plate, the voltages being just below corona onset. The whole arrangement is maintained at a pressure of one or two cm. The secondary electrons ejected from the surface of the wire by the beta-particles are multiplied by collision in the intense field near the wire. The electrons passing through the hole are further multiplied by collision in the field between the cylinder and plate. The total multiplication is of the order of 10^5 and the impulses are easily amplified to register on an oscillograph or mechanical counter. The background counting rate is low because of the small volume of the high field region around the wire. By using many holes in the cylinder the effective solid angle can be made to approach 4π. The method is applicable to substances which can be deposited on a wire, or which can be bombarded in wire form.

[1] Winkler, Zeits. f. Physik **107**, 235 (1937).

12. Growth of Droplets in an Expansion Chamber. R. M. LANGER, *California Institute of Technology*.—The temperature of the drop in a Wilson chamber at all times is essentially the temperature at which the drop has a vapor pressure equal to the partial pressure of the vapor in the chamber. This physical condition permits an approximate solution for the radius r of a drop in a fog of moderate density as a function of time t after expansion. The gas in the chamber is supposed to warm up to room temperature T after expansion x as $(1-e^{-\alpha t})$ and the fractional volume increase on expansion is supposed small compared with unity. Then if r_0 is the drop radius before expansion

$$r^2 - r_0^2 = (6K/\lambda\rho\alpha\mu^2)\{1 - e^{-\mu\alpha t}\},$$

where

$$\mu = 1/[(1+\sigma)\kappa - 1]xT$$

and λ = latent heat of evaporation of the drop liquid, ρ = density of the liquid, $\sigma = RT/\lambda$, K = thermal conductivity of the gas and κ = the ratio of specific heats of the expanding gas. For alcohol vapor in air at about room temperature and pressure and with $\alpha = 2$ which is about right the formula leads to

t (in seconds)	0.01	0.1	0.2	0.3	0.4	0.5	1
r (in microns)	4	18	28	32	37	41	60

Slight corrections from more detailed theory have been made for the early stages. These values are in approximate agreement with qualitative observations of Anderson, Neddermeyer and Bøggild who, in studying distortions, took motion pictures at 40 frames per second during the first $\frac{1}{3}$-second after expansion in various chambers.

13. Effect of Cloud Chamber Expansion Ratio on Drop Count Determination of Specific Ionization of Cosmic Rays. DALE BAGLEY, *University of California* (*Introduced by Robert B. Brode*).—The variation with expansion ratio of the number of positive and negative ions on which condensation takes place in cosmic-ray cloud-chamber tracks has been studied. The tracks were separated into columns of positive and negative ions by an electric field applied in the plane of focus of the camera. In order to count the number of drops in each track, it was necessary to allow the tracks to broaden by diffusion. This was accomplished by means of a cam mechanism which delayed the expansion of the chamber 0.2 second. The delay circuit was set in operation by the passage of an ionizing particle through Geiger counters placed above and below the chamber. Nitrogen, oxygen, or argon at 1.5 atmospheres pressure containing alcohol, water, or a mixture of two parts ethyl alcohol and one part water was used in the chamber.

14. Transport Phenomena in a Mixture of Gases. E. J. HELLUND AND E. A. UEHLING, *University of Washington*.—The theory of transport in gases obeying the quantum statistics is extended to include mixtures as well as one component gases. Expressions for the coefficients, into

which assumptions with regard to the interaction laws may be introduced, have been obtained. From the point of view of separating the two effects of quantum mechanics, the problem of thermal diffusion seemed to be of particular interest since the ratio of the thermal to pressure diffusion coefficients depends only on the ratio of integrals involving the molecular cross sections. As contrasted with all other transport coefficients the phenomenon of thermal diffusion might be expected, therefore, to depend less sensitively on the diffraction effect in collision in comparison with the interference effect than the other coefficients do. A preliminary caclulation based on the elastic sphere model for helium and neon bears out this presumption only slightly, however, the temperature effect between 10°K and 273°K amounting to 20 percent as compared with temperature effects of the order of 30 percent for the pressure diffusion coefficient itself in this range of temperatures. However, it is just for the case of thermal diffusion that the elastic sphere model is particularly inadequate. Calculations based on a five-parameter potential are now in progress.

15. A Quantitative Study of the Clean-Up of Hydrogen by Barium. G. W. JOHNSON, W. A. HANE AND P. A. ANDERSON, *State College of Washington.*—A known mass of barium, thermally vaporized to form a film of uniform thickness on a spherical surface of known area, was exposed to a succession of measured, approximately equal "doses" of pure hydrogen. After each admission of hydrogen, pressure-time curves were taken with an ionization gauge operating automatically at constant grid current. The clean-up time (time required to reduce the hydrogen pressure from 10^{-2} to 10^{-6} mm) decreased progressively (from 8 min. to <2 min.) during the admission of a quantity of hydrogen equal to *ca.* 25 percent of that required for saturation, then remained constant until the absorption of hydrogen ceased abruptly with saturation. The initial increase in the rate of clean-up with the amount of hydrogen absorbed is probably due to break-up of the original mirror smooth barium surface under the corrosive attack of the first doses of hydrogen, with consequent increase in the effective surface area. Analysis of the pressure-time curves, taken after the initial break-up, shows the diffusion of hydrogen into the barium-hydrogen mass to be the limiting factor determining the rate of removal of gaseous hydrogen. At saturation, and within an experimental error estimated as <10 percent, one molecule of hydrogen was absorbed per atom of barium, pointing to BaH_2 as the end product in the gettering of hydrogen by barium.

16. Adsorbed Films on Interferometer Mirrors. W. V. HOUSTON AND S. RUBIN, *California Institute of Technology.*—One of the methods of measuring the index of refraction of air involves the measurement of the order of interference in a Fabry-Perot interferometer, in air, and with the air removed. The calculations are usually based on the assumption that the phase change upon reflection is independent of the presence of the air. A series of observations has shown that the order of interference changes steadily after the air has been removed or admitted, and the equilibrium is not reached for some eight days. This is presumably due to the breaking down and building up of an adsorbed layer on the reflecting surfaces. The total observed change has amounted to about 0.06 fringe, and probably considerably more before the first observation could be made. This effect must be taken into account in measurements of the index of refraction, and its neglect may be a cause of some of the existing discrepancies.

17. Virtual Level of He^5 and Meson Forces. S. M. DANCOFF, *University of California.*—Resonance neutron scattering in helium observed by Staub indicates a virtual level of He^5 near ground. If this is the lowest level of He^5 the added neutron is probably in a P state, forming either a $P_{1/2}$ or a $P_{3/2}$ doublet. Splitting of these two states by the spin-orbit forces of the type $(\boldsymbol{\sigma}_i \cdot \mathbf{r})(\boldsymbol{\sigma}_j \cdot \mathbf{r}) V(r)$ resulting from meson theory might be expected to be considerable, since the above type of force seems to be present in nuclei in large amounts. However, a first-order perturbation calculation yields no splitting for the above two states. Higher order splitting should be reduced by the fact that the only states combining with these involve excitation of the alpha-particle core.

18. Normal Modes of Vibration of a Body-Centered Cubic Lattice. PAUL FINE,* *California Institute of Technology.*—An atomic model has been set up for the purpose of finding the frequencies of vibration of a crystal lattice. The potential energy was assumed to be a quadratic function of the displacements of the atoms from their equilibrium positions, and actual solutions of the secular equation were found by selecting suitable atomic force constants for tungsten, a body-centered cubic crystal whose elastic constants satisfy the isotropy condition. Numerical methods yield a frequency distribution which is characterized by two rather steep maxima. The result has been used in evaluating the specific heat of tungsten as a function of temperature, and a better fit with observed values is obtained by this method than by the particular Debye distribution with which it agrees at low frequencies. Discrepancies at low temperatures are partly due to the necessity of using experimental elastic constants determined at room temperature. Calculations have also been carried out for the thermal variation of the intensity of reflection of x-rays. Deviations from the Debye theory are apparent at absolute zero and become more pronounced at higher temperatures. However, there are no experimental data available for tungsten to compare with the theoretical values in this case.

* Now at the University of Oregon.

19. Streamline Flow of Water from an Artesian Basin into Horizontal Drains: Theory Compared with Experiment. DON KIRKHAM, *Utah State Agricultural College.*—Farr and Gardner[1] and Muskat[2] have obtained theoretical expressions for the pressure distribution in artificially drained homogeneous soil overlying an artesian basin. The tile drains are circular and are laid horizontally with equal spacing and at equal depths. In order to simulate an actual field case and to test the theory a small model[3] with a plate glass front is constructed. Theoretical equations for the streamlines corresponding to various boundary conditions

are obtained and are plotted on photographs of the experimentally obtained streamlines. Theory agrees well with experiment.

[1] Doris Farr and Willard Gardner, Agricultural Eng. **14**, 349 (1933).
[2] M. Muskat, *The Flow of Homogeneous Fluids Through Porous Media* (McGraw-Hill, 1937), p. 356.
[3] D. Kirkham, Trans. Am. Geophys. Union. (Now in press.)

20. The Validity of the Field Current Equations. FRANK R. ABBOTT AND JOSEPH E. HENDERSON, *University of Washington.*—Under good experimental conditions, field currents become practically as steady as thermionic currents. It is thus possible to test the form of the equation relating the current to the generating potential. A series of six precise point to plane field current curves was taken. Both the applied voltage and the emission current were measured, using type K potentiometers. A consistent deviation from linearity was apparent when the log of the total emission current was plotted against the reciprocal voltage. The field currents within the accuracy of the experimental work are described by the equation

$$I=\alpha V^4 e^{-\beta/V},$$

in which I is the *total* emission current, V is the applied voltage, while α and β are numerical constants. This differs from the Millikan-Lauritzen experimental equation only in the dependence of the coefficient of the exponential on V^4. Although this is in disagreement with the equation for the *specific* emission as given by the Fowler-Nordheim theory of field emission it is shown that it is not necessarily in disagreement with the basis of that theory. The effect of Nordheim's modification of the theoretical equation through consideration of an image force is indistinguishable from that given by a simple barrier.

21. The Quenched Primary Spark of an Induction Coil. W. P. BOYNTON, *Whittier, Calif.*—The author extends his previous study of circuits containing a spark gap to the case of the circuit breaker of an induction coil. The behavior of the primary current is described through three stages: the period of "make," the duration of the primary spark, and the oscillatory discharge of the condenser. The condenser potential is also described through the two later periods. A plausible approximate formula for the secondary e.m.f. is also deduced.

22. Spinor Equations for the Meson and Their Solution When No Field is Present. A. H. TAUB, *University of Washington.*—The spinor equations equivalent to the Proca equations for the meson are found. They differ from those proposed by Dirac in three ways: (1) They contain two symmetric spinors A_{1AB}, A_{2AB} and a spinor $B^A{}_B$, whereas the Dirac ones contain only one symmetric spinor and the spinor $B^A{}_B$. (2) They are invariant under spin transformations corresponding to both proper and improper Lorentz transformations whereas the Dirac ones are invariant under the former alone. (3) When a field is present they contain terms which cannot be obtained from the equations for free particles by replacing the operator p_ν by $p_\nu - e\varphi_\nu/c$ as was proposed by Dirac. In case there is no field present the equations can be solved by introducing two pairs of simple spinors (ψ^A, φ^A) and (χ^A, η^A) each of which satisfies a Dirac equation for a free particle of spin one-half. It is proposed to interpret each pair of spinors as representing a free particle of mass m_1 and m_2, respectively. With this interpretation it follows that a free particle of mass m and spin one satisfying the Proca equations is equivalent to a pair of particles of masses m_1 and m_2 satisfying the Dirac equations. If the three particles of masses m, m_1 and m_2 are in states determined by the energy momentum vectors p_ν, $p_{1\nu}$, and $p_{2\nu}$, respectively, and if $m \neq 0$, then $p_{1\nu}=m_1 p_\nu/m$ and $p_{2\nu}=m_2 p_\nu/m$, and $m=m_1+m_2$.

23. Contact Electric Phenomena in the Flow of Oil. S. KYROPOULOS, *California Institute of Technology (Introduced by A. Goetz).*—Phenomena of contact electricity associated with the flow of gasoline through pipes are well known for their disastrous effects. It is also known that they can be suppressed by imparting electrical conductivity to the gasoline. A simple model bearing permitted to detect the same effect with lubricating oils. It can be demonstrated by means of the oscillograph and its cleaning effect on the oil. The potentials appear high enough to result in "field currents." The phenomenon is particularly easy to understand in the case of lubricating oils with their highly dissymmetrical molecules as a consequence of the interaction of molecular surface- and flow-orientation. This means contact of molecules approximately with their maximum and minimum polarizabilities respectively and separation of charges according to Coehn's law. In the technical process of lubrication this electrical effect results in increased wear due to its clean-up effect with respect to dispersed solid particles. Addition of polar molecules tends to suppress the effect, resulting in lower friction and improved apparent "film strength" of the oil.

24. A Thermoelectric Method for the Determination of Work Functions. G. M. FLEMING AND JOSEPH E. HENDERSON, *University of Washington.*—During the process of investigating the temperature effects accompanying field current emission it was found feasible to measure the corresponding effect for thermionic emission. This was done calorimetrically using essentially the same method as for field currents, in which a tantalum-tungsten thermocouple junction was incorporated in the cathode to measure changes of temperature. This method gives experimental values for the average net energy loss per electron emitted. The value given by theory for this energy loss is $\phi+3kT$, where ϕ is the work function of the emitting metal. With the use of this relation the work function of tungsten has been computed to be 4.46 ± 0.09 ev. This method was originally applied to thermionic emission, where a cooling effect was known to exist, in order to test the sensitivity of the apparatus. It is believed that the measurements are capable of considerable refinement.

25. Absorption Spectrum of CN. JOHN U. WHITE, *University of California.*—Free CN radicals in the gaseous state are formed in the electric discharge through cyanogen. By using a very intense low pressure spark as a background the 0,0 and 1,1 bands of the $^2\Sigma \leftarrow {}^2\Sigma$ transition of CN have been observed in absorption at short intervals of time

after the end of this discharge. The intensities of the lines were measured by calibration of the plates and corrected for the imperfect resolving power of the spectrograph. Relative concentrations of CN were calculated. By diluting the cyanogen in the discharge tube with argon until the CN bands were no longer visible an upper limit to the partial pressure of CN was calculated on the assumption that near this point all the cyanogen present was dissociated. From this a lower limit to the f value of the 0,0 band was calculated to be $f=0.04$. The rate of disappearance of CN after the end of the discharge was studied and found to be exponential. It is unaffected by pressure or by dilution with argon. Possible mechanisms of the disappearance are discussed. Using data from the thermal dissociation of cyanogen a lower limit to the heat of reaction is calculated.

26. Transition Probabilities of Forbidden Lines. SIMON PASTERNACK, *California Institute of Technology.*—Recent work on forbidden lines has made it desirable to reexamine and extend the calculations made by E. U. Condon[1] on the theoretical transition probabilities of these lines. The method used is essentially that developed by Condon, with a few modifications. Formulae are derived for the magnetic dipole and electric quadrupole contributions to the transition probabilities for the p^2, p^3, p^4 and d^2 configurations. A few errors are found in Condon's calculations for the p^k configurations; in particular, a non-zero value is found for the probability of the $^3P_0-{}^1D_2$ transition in the p^2 configuration. This line was recently observed in O III by Bowen and Wyse.[2] Numerical computations are made of the transition probabilities for about fifty atoms in the p^k configurations. The formulae for the d^2 configuration are applied to the case of Fe VII, and give satisfactory agreement with the observed relative intensities. An application of the calculations is made to a question concerning the permitted lines of O III present in nebular spectra.

[1] E. U. Condon, Astrophys. J. **79**, 217 (1934).
[2] I. S. Bowen and A. B. Wyse, Pub. A. S. P. **50**, 348 (1938).

27. Twinning in Bismuth Crystals. ALFRED B. FOCKE, *Brown University.*—The segregation of impurities in very pure bismuth crystals offers a tool for a large scale study of the twinning process if polonium is used as one impurity. The range of the α-particles leaving the crystal gives a measure of the location of the polonium. This is found to be segregated into relatively small regions separated by specific distances dependent upon crystallographic direction. If the twinning process is atomic in nature, the effective distance between polonium groups should be unaffected by it. The results of this investigation show that this is not the case. In fact the spacing of the polonium groups when measured perpendicular to the imperfect cleavage plane is found to be $(0.86\pm0.03)\mu$ whether the face is one cut from an undeformed crystal, or formed by twinning from a perfect cleavage face. The normal spacing perpendicular to the perfect cleavage face is $(0.55\pm0.01)\mu$ in the undistorted crystal. It is found that the change of spacing due to twinning is reversible.

28. The Function of Anode Spots in the Glow Discharge. S. M. RUBENS AND J. E. HENDERSON, *University of Washington.*—Anode spots have been further investigated in nitrogen glows maintained in a large, spherical copper, discharge chamber with a disk anode at its center. Spots were grown on a flat probe mounted flush with the surface of the circular disk anode but insulated from it. When the probe potential is raised slightly above that of the anode a spot forms upon it. Plots of the probe current against the probe potential exhibit sharp peaks. These peaks account for the formation of many spots rather than a single large one. A study of the external circuit characteristics reveals that anode spots occur chiefly in a regime in which the voltage remains constant or increases but slightly with increasing current. The function of the spots is evidently that of furnishing sufficient positive ions to maintain a stable discharge. A theory is proposed which accounts for the formation and stability of the spots. As a consequence of this theory anode spots must appear whenever a critical current density at the anode is exceeded.

29. The Half-Life of B^{12}. R. A. BECKER AND E. R. GAERTTNER,[1] *California Institute of Technology.*—The half-life of the beta-ray active B^{12} produced according to the reaction $B^{11}+H^2\rightarrow B^{12}+H^1$ was measured by Crane *et al.*[2] with a cloud chamber, and estimated to be about 1/50 sec. The result however was open to the objection that the method of taking delayed expansions with a cloud chamber set only an upper limit on such a short half-life. To check this result we have re-measured the half-life by activating a rotating target of boric acid in the form of an annular ring of mean diameter 20 cm fused on an aluminum disk which was rotated 1800 r.p.m. with a synchronous motor. By observing the activity as a function of the angular displacement from the point of bombardment it was possible to follow the decay of the radiation. The ratio of the activities at different points on the target was measured with two Lauritsen electroscopes. The average of many measurements gave the value of 0.022 ± 0.002 sec. for the half-life of the radiation.

[1] H. H. Rackham Fellow, University of Michigan.
[2] Crane, Delsasso, Fowler and Lauritsen, Phys. Rev. **47**, 887 (1935).

30. Further Resolution of the 10μ and 16μ Ammonia Bands. E. F. BARKER AND H. Y. SHENG, *University of Michigan.*—Because of the existence of two minima in the potential function of NH_3, the energy levels for oscillations along the symmetry axis occur in pairs, and the parallel type bands are double. The separations of these pairs of levels for the vibration ν_3 are very sensitive to the height of the potential barrier, which in turn is considerably affected by centrifugal deformations. In consequence a new type of vibration-rotation interaction appears. An examination of the 10μ double band (ν_3) under the highest available resolution reveals many new details of structure. Lines corresponding to a given transition in J, originally observed as single, now appear as groups, the different members being associated with different values of K. The component band of lower frequency shows much more structure than does the other. In it, as theory predicts, the $K=0$ lines are missing whenever the initial value of J is odd. The band at 16μ arises from a transition for which the initial state is the upper level of the higher frequency 10μ band. Only a part of the negative branch

has been resolved, but it is found to fit consistently into the scheme. The following values (in cm^{-1}) for the vibrational terms W, and for $2B=h/4\pi^2A$, are computed for the molecule with $J=0$, from the pure rotation spectrum for the level 0_β and from the present observations for the other three states.

Level	W	$2B$
0_β	0.67	19.890
1_α	932.8	20.116
1_β	968.4	19.766
2_α	1597.9	

31. Phase Control Circuit and Mercury Arc Illumination of Cloud Chamber. Carl E. Nielsen, *University of California.*—An atmospheric pressure quartz capillary mercury arc has been used as a light source for a cloud chamber. It has been possible to get a 90° illumination intense enough and of short enough duration to take satisfactory drop count photographs. A spherical lens condensing system has been used. Comparison is made with an incandescent filament lamp and a low pressure mercury arc. In order to flash the arc on high voltage for one-half cycle of the 60-cycle power supply, a phase controlled tripping circuit has been designed. A gas discharge tube, thyratron, and ignitron are employed. Two alternate circuits for giving a phase controlled pulse of several cycles duration have been constructed.

32. The Gamma-Radiation from Nitrogen Bombarded by Deuterons. Louis A. Pardue[1] and E. R. Gaerttner,[2] *California Institute of Technology.*—The energies and the relative intensities of the gamma-rays emitted from nitrogen bombarded by deuterons of 700 kv have been measured by the positron-electron pairs and recoil electrons ejected from thin laminae placed inside a cloud chamber.[3] The distribution of pairs ejected from a lead lamina 0.026 cm thick reveals two strong components of quantum energy 7.2 ± 0.4 Mev and 5.3 ± 0.4 Mev, and a number of weaker components which may be attributed to radiation of about 4, 3, and 2 Mev. There are also a number of pairs which extend up to 11 Mev. The distribution of recoil electrons from a carbon lamina 0.12 cm thick indicates two strong groups of quantum energy 4.4 and 2.2 Mev. No attempt was made to extend the recoil measurements to higher energies. The 7.2-Mev radiation is attributed to the reaction

$$N^{14}+H^2\rightarrow C^{12}+He^4 \qquad (1)$$

because radiation of this energy has been observed in other reactions producing C^{12}.[3, 4] The 5.3-Mev radiation is attributed to an excited state of N^{15} of this energy according to the reaction

$$N^{14}+H^2\rightarrow N^{15}+H^1 \qquad (2)$$

in good agreement with the value of 5.4 Mev predicted by the range measurements of Cockcroft and Lewis.[5] An attempt will be made to correlate the energies and intensities of the gamma-rays produced by excited states in C^{12} according to several reactions.[3-5]

[1] On Sabbatical leave of absence from the Physics Department of the University of Kentucky.
[2] H. H. Rackham Fellow, University of Michigan.
[3] Fowler, Gaerttner and Lauritsen, Phys. Rev. **53**, 628 (1938); Phys. Rev. **55**, 27 (1939).
[4] Bothe, Zeits. f. Physik **100**, 273 (1936).
[5] Crockcroft and Lewis, Proc. Roy. Soc. **154**, 261 (1936).

33. The Mobility Spectrum of Atmospheric Ions. E. A. Yunker, *Stanford University* (*Introduced by N. E. Bradbury*).—The mobility spectrum of atmospheric ions is being studied by using the classical air blast method with the collecting electrode divided into segments for resolution. The apparatus is designed for continuous operation with photographic recording. The sensitivity is such that the range of mobilities from 2.0 to 5×10^{-4} cm/sec./volt/cm, when divided into eighteen groups, is covered in one hour. Simultaneous and continuous measurements of the density of atmospheric condensation nuclei using the cloud chamber expansion method[1] enable a study to be made of the change of small ions into large ions and of the mass and character of the condensation nuclei involved. Preliminary investigations have shown that the number of small ions changes markedly with the concentration of nuclei with appropriate changes in the magnitude of the local component of the earth's electric field. The ion spectrum appears to consist of rather prominent groups superimposed upon a general background.

[1] Bradbury and Meuron, Terr. Mag. **43**, 231 (1938).

34. Quantitative Analysis of Rubidium in Plant Sap by Spectrographic Means. Louis A. Strait, *University of California.*—The source of light is a condensed spark between an upper point electrode and a lower cylindrical electrode on which a small amount (0.04 cc) of the prepared plant sap is deposited. The cylindrical electrode of copper is mounted on a screw arrangement which allows uniform sparking of the complete area of the surface of the cylinder. The light from the spark is photographed with a quartz spectrograph of large dispersion. Photometric measurements are made of the relative intensities of the spectral lines λ4215.6 and λ4201.8 of rubidium and λ4101.8 of indium, which serves as internal standard. A working curve is determined from known concentrations of rubidium bromide introduced into prepared plant sap. Correction for the influence of varying amounts of potassium on the rubidium determinations is made by a method of excess. In preliminary testing of the method the accuracy of analysis is of the order of 10 percent. Aliquots of 0.04 cc of solution of prepared sap are used for a single analysis. A minimum concentration of $N/400$ rubidium is measurable. This corresponds with measurement in absolute amount of 0.085 mg of rubidium. The method can be adapted to simultaneous determination of potassium.

35. The Far Infra-Red Water Bands and Heat Transfer in the Atmosphere. Walter M. Elsasser, *California Institute of Technology.*—Thermal radiation at the temperatures prevailing in the atmosphere has its maximum near 10μ; consequently the rotational and the lowest vibrational water bands are the main carriers of heat radiation in the atmosphere. During the last two years extensive computations have been undertaken in order to apply spectroscopic results to the physical conditions under which water vapor radiates in the atmosphere. The absorption of the rotational band is obtained from the analysis of Randall, Dennison and collaborators. The envelope of the vibrational band at 6μ can be obtained from this by a

simple transformation since the two bands have parallel electric moments. The absolute intensity of this vibrational band has recently been measured by T. Strong of the California Institute. With these data as a basis the equations of radiative transfer have been integrated numerically for a large range of temperatures and optical thicknesses. The results are given in form of a graph-paper in which temperature and moisture appear as independent variables. If the vertical temperature-moisture relationship in any actual atmosphere is plotted on this paper, the radiative heating and cooling at any height can rapidly be obtained by a graphical quadrature.

36. The Dielectric Constant of Water Vapor at a Frequency of 42 Megacycles. ANGUS C. TREGIDGA, *California Institute of Technology.*—A heterodyne beat apparatus was constructed for the measurement of the dielectric constant of water vapor at 42 megacycles. One of the oscillators was crystal-controlled, the other having a tuned circuit containing a condenser which could be evacuated and filled with water vapor. A cathode-ray oscilloscope was used to indicate zero beat. Drift of the oscillators was eliminated from the results by plotting readings on a time base and alternating between vacuum and water vapor as rapidly as physical limitations would permit. Air was used as the calibration gas, because it is composed of nonpolar molecules. It should therefore have the same dielectric constant at this frequency as at the lower frequencies at which it has been measured by other investigarors. The Clausius-Mosotti relation was verified for water vapor at constant temperature, and the dielectric constant of water vapor at 100 degrees centigrade and 760 mm of mercury determined. It has the value 1.0060. This research was undertaken because of its connection with the transmission of radio signals of this frequency. The optical path for such waves in a medium of varying index of refraction is curved, and it was desired to know the magnitude of the curvature which a gradient of water vapor content in the atmosphere can produce.

37. Fine Structure in the Absorption and Emission Spectra of X-Rays. S. T. STEPHENSON, *State College of Washington.*—The K x-ray emission spectrum of pure copper has been studied. K absorption spectra of pure copper, of copper and selenium in cupric selenate, and of elements in other compounds have been obtained. The spectrograms were all taken with a focusing curved crystal (mica) spectrograph and analyzed with a recording microphotometer. Faint copper emission lines were found extending more than 300 volts to the short wave-length side of Cu $K\beta_2$. It is suggested that these lines are due to the transition of conduction electrons into the K shell. The positions of these lines have been compared with the Kronig type fine structure found in the absorption spectrum of copper. The results of this comparison point to the conduction electron origin of the emission fine structure. The absorption fine structures of two elements in the same crystalline compound have been studied for cupric selenate, cupric arsenate, rubidium bromide and other compounds. The structures in many cases are different for the two elements making up the compound. Similar discrepancies have been obtained by other investigators for a few compounds.

38. Experiments on the Scattering of Fast Neutrons. E. R. GAERTTNER,[1] LOUIS A. PARDUE,[2] AND J. F. STREIB, *California Institute of Technology.*—A description of a series of experiments on the scattering of fast neutrons in gases of low atomic number with a linear amplifier and a mechanical oscillograph will be given. Since the angular distribution of the scattered neutrons is reflected in the distribution in energy of the recoil nuclei, this experimental method also affords a means for studying the angular distribution of the scattered neutrons. An investigation of the scattering in helium of the low energy group of neutrons ($Q=0.9$ Mev) produced in the reaction $Be^9+H^2 \rightarrow B^{10}+n^1$ [3] has confirmed the existence of an anomalous scattering for neutrons of 1 Mev.[4] The position of the anomaly was found to be independent of the deuteron energy (500 kv–800 kv). The distribution of helium recoils indicates also a maximum at about 0.8 Mev. An attempt is now being made to extend the measurements to lower energies to investigate further the character of this anomalous scattering.

[1] H. H. Rackham Fellow, University of Michigan.
[2] On sabbatical leave from the Physics Department of the University of Kentucky.
[3] Bonner and Brubaker, Phys. Rev. **50**, 308 (1936).
[4] Staub and Stephens, Phys. Rev. **55**, 131 (1938).

39. Luminescence of Synthetic Halite Crystals. BRYON E. COHN, *University of Denver.*—Synthetic halite crystals were grown from sodium chloride melts to which had been added small amounts of manganese chloride. Crystal specimens were prepared which analyzed from 0 to 0.25 percent manganese. The specimens were analyzed by the periodate method. For the determination of luminescence crystals were cleaved to a uniform face area and thickness and were excited with ultraviolet light. The thermoluminescence emission was determined by photographic methods. Curves of luminescence are presented. Optima were observed at 0.0042 percent and at 0.05 percent manganese.

40. X-Ray Spin Doublet Splittings. R. F. CHRISTY AND J. M. KELLER, *University of California.*—Professor R. T. Birge[1] has suggested the possibility of a precision determination of the fine structure constant α from his recently compiled data on $L_{II}L_{III}$ x-ray spin doublet splittings. This method involves some theoretical information on the variation of the "screening constant" s with Z. We propose to write

$$\Delta = S(Z)[1-(b/Z)\varphi(\alpha^2Z^2)-(c/Z^2)\psi(\alpha^2Z^2)-\cdots],$$

where Δ is the observed $L_{II}L_{III}$ splitting, $S(Z)$ is that given by the Sommerfeld formula with $s=0$, and where the functional forms of $\varphi, \psi, \cdots$ are to be given theoretically. The determination of α would then involve a least squares solution for $\alpha, b, c, \cdots$. In this form of expansion, the term φ is given by the first order interaction energies of the L electrons with all other atomic electrons. We are determining its functional form using Dirac hydrogen-like

wave functions for charge Z and Breit's approximate Hamiltonian. The dependence of ψ and higher terms on α^2Z^2 is relatively unimportant and can be taken as that given by Sommerfeld's formula $S(Z-s)$ with constant s. We have calculated the first order electrostatic interaction due to the K and L shells, which provides the major portion of φ, and are now calculating smaller terms in φ due to the electrostatic interactions of higher shells and to the magnetic interactions.

[1] R. T. Birge, Bull. Am. Phys. Soc. Vol. 14, No. 2, abstract 47.

41. Recording Bragg Spectrometer for Use Between Room Temperature and Helium Temperature. A. GOETZ AND A. DEMBER, *California Institute of Technology.*—A Bragg spectrometer with stationary ionization chamber is described where the crystal is rigidly attached to a Heliquifier, so that neither the incident nor the reflected radiation has to pass through liquid gases. The helium liquifier is of the "single adiabatic expansion" type with a capacity of 80 cm³ and is arranged in such a manner that by means of liquid H_2, solid H_2, and ultimately liquid He, any temperature between 300 and <4.2°K can be attained. The adiabacy is sufficient to maintain temperatures between such fixed points constant for the time necessary for recording. The temperature is measured at the crystal with resistance thermometers and within the expansion chamber with a gas thermometer.

42. The Measurement of Intensity Profiles of Bragg Reflections from Calcite Between 300° and 4.2°K. A. DEMBER AND A. GOETZ, *California Institute of Technology.*—The intensity profiles of Mo $K\alpha_1\alpha_2$ radiation reflected from calcite are determined for different orders between room temperature and the boiling point of helium. To eliminate distortion due to the gradation of the emulsion and the indeterminacy by its graininess, inseparable from the use of photographic methods, an ionization chamber connected to a linear d.c. amplifier and galvanometer is used for recording the intensity distribution of the reflected radiation either as function of the position of the crystal within the rocking angle or across the angle of reflection for a stationary crystal. Consequently the recording speed can be set in fixed relation to the rotation of the crystal or the motion of a scanning slit in front of the ionization chamber. For recording the full profile of the Mo $K\alpha$ doublet the time necessary is approximately $3\frac{1}{2}$ min. which is sufficiently short for measurements under stable temperature conditions at and between the thermal fixed points of the gases used for the cooling of the crystal. From the integrated intensities of reflection the values of the characteristic temperature with and without zero point energy are calculated. The shape of the profiles is discussed.

43. Theory of X-Ray Lines Resulting from Double Ionization of the L-Shell. ROBERT D. RICHTMYER, *Stanford University.*—We describe theoretical calculations of the wave-lengths and intensities of some very faint lines in L-series x-ray spectra. The lines are produced by atomic transitions from initial states in which two electrons are missing from the L-shell; these initial states are in turn produced by Auger transitions which take place in atoms originally ionized in the K-shell. Very careful experimental work by Cecil Burbank and later by Werner Veith has brought out several of these lines photographically. The experimental and theoretical results agree within the estimated error of the calculations; furthermore this error is small enough to allow us to deduce a correlation of observed lines to theoretically predicted ones, the correlation being unique for most of the observed lines.

44. A New Method for the Measurement of Work Functions. WILBUR H. GOSS AND JOSEPH E. HENDERSON, *University of Washington.*—A new method for the measurement of work functions has been devised. It depends for its success upon the high energy cut-off in the normal energy distribution of field current electrons; this cut-off is quite sharp.* These high energy electrons are unable to enter a collector unless the potential of the collector is higher than that of the emitter by an amount at least equal to the work function of the collector. This should be true if the electrons "tunnel" the surface barrier of the emitter and go over the surface barrier of the collector. Thus the collector potential at which field electrons begin to be measured gives directly the collector work function. A tube has been built containing copper, platinum, and nickel, any of which can be used independently as a collector. Preliminary data show a progressive increase in the potential thresholds at which current is collected in line with accepted values of the work functions of these three elements and of approximately the accepted value.

* Jos. E. Henderson and R. K. Dahlstrom, Phys. Rev. **55**, 473 (1939).

45. Limiting Solutions for Collapsing Masses. H. SNYDER, *University of California (Introduced by J. R. Oppenheimer).*—Volkoff and Oppenheimer have shown that the general relativistic field equations do not possess any static solution for a spherical distribution of neutrons if the total mass is greater than $\sim 0.7\odot$. We have made a qualitative investigation of the behavior of non-static solutions under the assumption that the total loss of mass by radiation is small. The characteristics of the solutions are: (1) The radius of the star approaches its gravitational radius asymptotically with time, as measured by an observer at a great distance from the star. (2) An observer co-moving with the matter in the star would not be able to communicate with an observer outside the star after a finite time, as measured by a co-moving clock. Neglecting the pressure we have obtained analytic solutions which confirm the general behavior indicated above. If R is the radius of the star and R_0 the gravitational radius, then asymptotically

$$R/R_0 - 1 \sim \exp(-cT/R_0).$$

This characteristic time R_0/c is of the order 10^{-5} sec. for stars of the mass of the sun.

46. The Fields Involved in Field Emission. JOSEPH E. HENDERSON, *University of Washington,* AND K. V. MACKENZIE, *Oregon State Highway Department, Salem, Oregon.*—One of the noteworthy characteristics of the energy

distribution curves for field emission is the occurrence of a sharp maximum near the maximum energy observed. This maximum has been observed at various positions usually within a few volts of each other. By using a Fermi distribution and the transmission coefficient as given on the Fowler-Nordheim theory of field emission, it has been possible to solve for the position of the maximum as a function of the field present during emission. This yields values for the field of about 10^8 volts per cm. Assumption of an image force lowers the value of the field only slightly in the region where the maxima are observed. Comparison with the values obtained from the slopes of the corresponding log i versus $1/V$ curves is quite satisfactory. These values seem quite high unless the areas involved in emission are smaller than usually supposed.

47. On the Proper Energy of the Electron. G. M. VOLKOFF, *University of California.*—The method used by Serber[1] to evaluate the proper energy of the electron by introducing an off-diagonal distance into the commutation rules for the wave functions of the positron-electron field has been extended to include time-like off-diagonal distances. Following a suggestion of Dirac[2] for eliminating the singularities in the classical treatment of the radiation field of the electron by antisymmetrizing the solution in the retarded and advanced potentials, the present results are symmetrized in positive and negative values of the off-diagonal time. Calculations of the electrostatic energy of an electron at rest were made both with the negative energy states filled (positron theory), and empty (single electron), and are summarized in the table below.

	Electron Proper Energy Single Electron	Positron Theory
Serber's results for space-like off-diagonal distance R	$e^2/2R$	$-\frac{e^2}{\pi}\left[\log\frac{1}{2}CR-1+O(R)\right]$
Present results for time-like off-diagonal distance τ	$-\frac{e^2}{2}\left[\frac{3}{2}\tau+O(\tau^3)\right]$	$-\frac{e^2}{\pi}\left[\log\frac{1}{2}C\tau+1+O(\tau)\right]$

Although the introduction of an off-diagonal time removes infinite terms in the single electron case, positron theory still leads to a logarithmic singularity.

[1] R. Serber, Phys. Rev. **49**, 545 (1936).
[2] P. A. M. Dirac, Proc. Roy. Soc. **167A**, 148 (1938).

48. Forbidden Transitions in Nitrogen. JOSEPH KAPLAN, *University of California at Los Angeles.*—A number of new afterglow spectra in pure nitrogen and in nitrogen containing a small concentration of oxygen are presented. These include the weak high-pressure afterglow in nitrogen in very small bulbs in which the nebular transition $^2D\rightarrow{}^4S$ has been observed for the first time in the laboratory. The high relative intensity of the $^2P\rightarrow{}^4S$ line and the absence of first-positive bands are other important characteristics of this afterglow. The first observation of the transauroral line $^1S_0\rightarrow{}^3P_1$ of oxygen in a weak afterglow at medium pressures, accompanied by a strong emission of the Vegard-Kaplan bands and the green auroral line, is also included. The absence of the normally strong β bands of NO is an important and curious feature of this spectrum. The bearing of these spectra on the Cario-Kaplan theory of the Lewis-Rayleigh glow and on excitation processes in the earth's upper atmosphere is briefly discussed. There are indications that the strong relative intensities of forbidden lines in these and upper atmosphere spectra arise from the dissociation of molecules into metastable atoms rather than in direct excitation of atoms.

49. The Positron Spectra of N^{13} and Na^{22}. F. OPPENHEIMER AND E. P. TOMLINSON, *California Institute of Technology.*—A semi-circular focusing spectrograph of high resolution was used to examine the positron spectra and the gamma-rays of N^{13} and Na^{22}. The gamma-rays were examined by placing the source in contact with a one-half mil Pb foil. The positron distribution of Na^{22} has an upper limit of 0.55 Mev. The peak of the distribution is rather broad, suggesting a complex spectrum. However no low energy gamma-rays, corresponding to different components of the spectrum, were found. Only one gamma-ray at 1.3 Mev was found for Na^{22}. By comparing the intensity of this gamma-ray with that of the annihilation radiation it is found that there are $1.1\pm.1$, 1.3 Mev quanta per positron. The N^{13} positron spectrum is distinctly resolved into two components, the two peaks being at about 0.370 and 0.540 Mev. This complexity has already been reported by E. Lyman.[1] The peak of the lower energy component is very broad, suggesting that there may be other unresolved components of the spectrum. The gamma-ray, reported by Richardson,[2] at about 280 kev has been examined. It appears as a broad group of photoelectrons rather than as a sharp line such as is produced by the N^{13} annihilation radiation. The 250-kev radiation must be produced by two or more gamma-rays.

[1] E. M. Lyman, Bull. Am. Phys. Soc. **14**, 2, 19 (1939).
[2] J. R. Richardson, Phys. Rev. **55**, 609 (1939).

50. The Second Townsend Ionization Coefficient for Nickel Cathodes in Pure Hydrogen. DONALD H. HALE, *University of California.*—Measurements of the Townsend ionization coefficients in pure hydrogen for platinum and NaH cathodes have been reported.[1] An improved ionization chamber has been designed and the Townsend γ coefficient determined for a nickel cathode in pure hydrogen. It is found that the curve of values of α/p plotted as a function of X/p shows a negative slope in the range of values of X/p from 1000 to 1400 after which it again rises. The curve of values of γ plotted as a function of X/p shows the same general characteristics as the curve for the platinum cathode. However, the increase in the value of γ at the higher values of X/p is less rapid for the nickel cathode. A sparking potential curve has been calculated using the values of γ found in this work and is in agreement with the curves found experimentally except at values of $p\delta$ near the minimum sparking potential.

[1] Donald H. Hale, Phys. Rev. **55**, 815 (1939).

51. Gamma-Radiation from Fluorine plus Protons. C. C. LAURITSEN, W. A. FOWLER AND T. LAURITSEN, *California Institute of Technology.*—An investigation has been made of the gamma-radiation from fluorine bombarded with

protons at 330 kv and 950 kv, with a pressure Van de Graaff generator. Analysis of 38 pairs in cloud-chamber photographs at 330 kv gives a mean energy of 6.2 ± 0.2 Mev for the radiation, in agreement with earlier measurements, while the mean of 122 pairs obtained at the higher voltage, covering all resonances up to 1 Mev, is 6.3 ± 0.1 Mev. This result, which is in essential agreement with the work of Dee, Curran and Strothers,[1] indicates that the radiation is due to an excited state in O^{16} which is reached by the ejection of a short range alpha-particle from Ne^{20},[2] and that the various resonances represent similar states of the Ne^{20} nucleus.

Five pairs, corresponding to a gamma-ray of energy 10.5 Mev, were found at the higher bombarding voltage, but it is not certain whether they can be due to contamination or whether they arise from one of the intermediate resonances at 479 or 660 kv.

[1] Dee, Curran and Strothers, Nature **143**, 759 (1939).
[2] McLean, Becker, Fowler and Lauritsen, Phys. Rev. **55**, 796 (1939).

52. Infra-Red Pleochroism and Fermi Resonance Associated with CH_2 Groups in Crystals. JOSEPH W. ELLIS AND JEAN BATH, *University of California at Los Angeles.*—The near infra-red absorption spectra of two dissimilar organic crystals, pentaerythritol, $C(CH_2OH)_4$, and diketopiperazine, $(CH_2NHCO)_2$, have been obtained with plane polarized waves. Both crystals display marked pleochroism. Of particular interest is the region 1.7μ associated with the vibrations of the methylene groups, CH_2. Both spectra show a strong band at 1.703μ when the electric vector E parallels the bisector of the HCH angle. This practically disappears when E is perpendicular to this symmetry axis. We identify it as $2\nu_\tau$, the first overtone of the symmetrical valence vibration. Pentaerythritol gives a double band at 1.735, 1.763μ with components of equal intensities. These are excited by E in either its parallel or perpendicular positions but more efficiently in the latter instance. We interpret these as $[2\nu_\sigma, 4\delta_\tau]$, the first and third overtones, respectively, of asymmetrical valence and deformation vibrations. Fermi resonance must occur and equality in intensities indicates perfect superposition of the two frequencies. Diketopiperazine shows bands at 1.745, 1.754μ, the former strong when E is perpendicular to the symmetry axis and the latter strong when these are parallel. Our interpretation is similar to that for the 1.735, 1.763μ pentaerythritol bands, with the exception that Fermi resonance must be greatly reduced owing to a less exact superposition of $2\nu_\sigma$ and $4\delta_\tau$.

53. Resonance in the Production of Short Range Alpha-Particles from $F^{19}+H^1$. W. B. MCLEAN AND R. A. BECKER, *California Institute of Technology.*—Resonance in the production of the short range alpha-particles from $F^{19}+H^1$ recently reported from this laboratory[1] has been shown to coincide with the gamma-ray resonance at 330 kv[2] within ±5 kv. Cloud chamber determinations of yield curves requiring extended periods of observation are found to be feasible if the alpha-particle yields are measured as a function of the range of the scattered protons appearing on individual photographs. Relative voltage measurements were made with an inexpensive resistance voltmeter consisting of a circulating solution of xylol and alcohol. Variations in the specific resistance of the solution were compensated for by applying a known potential of the order of 3000 volts across a short section of the resistance column and balancing out the current in the column due to the high potential.

[1] McLean, Becker, Fowler and Lauritsen, Phys. Rev. **55**, 796 (1939).
[2] Hafstad, Heydenberg and Tuve, Phys. Rev. **50**, 504 (1936).

54. Photoconductivity of Tartaric Acid Crystals. JAMES J. BRADY AND JOHN D. TODD, *Oregon State College.*—Recent work[1] has shown that tartaric acid crystals, when illuminated, produce an electrical current without the aid of an external source of e.m.f. In the present work, we have investigated the effect of applying an external e.m.f. on the crystal. The dark current depends on the time the potential difference has been applied across the crystal. With 100 volts across the crystal for 24 hours, the dark current drops to less than one hundredth of its original value. The final value of the dark current depends on the magnitude of the potential difference. The application of voltages up to 300 has *no measurable* effect on the actinoelectric current for illumination with light in the visible part of the spectrum. The investigation was carried out at room temperature.

[1] J. J. Brady and W. H. Moore, Phys. Rev. **55**, 308 (1939).

55. Proton Activation of $_{48}Cd$ and $_{49}In$. S. W. BARNES, *University of Rochester.*—Indium activated by 7.2 Mev proton exhibits two activities, one due to In^{115*} and one due to Sn^{113}. The other two activities previously reported[1] have been shown to be due to impurities. Sn^{113} has a half-life of about 100 days and decays by K electron capture, emitting In K x-rays. An active In of 105 minutes' half-life with a γ-ray of 0.39 Mev has been chemically separated from an aged Sn^{113} sample. An exactly similar In has been formed by proton bombardment of Cd, which suggests the assignment of this activity to In^{113*}. The absence of Cd K x-rays indicates that In^{113*} decays to In^{113} with the emission of the 0.39 γ-ray. In addition Cd shows the expected In isotopes In^{111} $20m$ e^+, In^{114} $48d$ e^- and In^{116} $54m$ e^-. A positron emitter of 65 minutes' half-life with a maximum positron energy of 1.6 ± 0.3 Mev is found and tentatively assigned to In^{110}. Activities of $72s$ e^- and $2.7d$ e^- with γ's of 170 and 245 kev are ascribed to isomeric states of In^{113}.

[1] S. W. Barnes, Phys. Rev. **55**, 241 (1939).

56. Production of Secondary Electrons by High Energy Electrons. W. A. FOWLER AND C. W. SHEPPARD, *California Institute of Technology.*—In nearly two thousand traversals of a 0.033-cm lead foil by high energy electrons and positrons ($W\sim10$ Mev), we have observed the production of six secondary electrons with energy greater than 1 Mev. The cross section is thus $\sim5\times10^{-24}$ cm^2 and is of the order of the theoretical cross section $\sigma\sim2\pi r_0^2Z/W_s\sim10^{-23}$ cm^2 where W_s ($\ll W$) is the minimum observed secondary energy. Energy was approximately conserved in all cases but conservation of momentum apparently did not hold in several cases due probably to scattering in the lead foil. No authentic cases of pair production were observed, in

agreement with the small cross section (10^{-25}) for this process.

57. Experimental Studies of Energy Releases in Reactions of Light Nuclei. SAMUEL K. ALLISON, LESTER S. SKAGGS, AND NICHOLAS M. SMITH, JR., *University of Chicago.*—The study of the energy spectra of particles emitted from beryllium under proton bombardment has been continued, with the electrostatic analyzer previously described. Energy spectra have been obtained at proton energies or 262, 315, and 351 kv, and show quantitatively the conservation of energy and momentum in the two modes of disintegration. Approximately equal numbers of alpha-particles and deuterons are produced. The determination of the energy releases in the reactions $Li^7(p,\alpha)\alpha$ and $Li^6(d,\alpha)\alpha$ has been repeated by the range method in an absorption cell in which the only absorbing medium other than air is cellophane of 5 mm stopping power. Thin targets were used, heated to prevent carbon deposition, and the ranges were compared with those of the 8.5-cm particles from ThC′. Preliminary results are 17.31 Mev for the Li^7 reaction and 22.24 Mev for the Li^6 reaction.

AUTHOR INDEX TO ABSTRACTS OF THE STANFORD MEETING

Abbott, Frank R. and Joseph E. Henderson—No. 20
Allison, S. K., L. S. Skaggs and N. M. Smith, Jr.—No. 57
Anderson, Paul A.—No. 8
—— see Johnson, G. W.

Bagley, Dale—No. 13
Barker, E. F. and H. Y. Sheng—No. 30
Barnes, S. W.—No. 55
Bath, Jean—see Ellis, Joseph W.
Becker, R. A. and E. R. Gaerttner—No. 29
—— see McLean, W. B.
Boynton, W. P.—No. 21
Bradbury, N. E.—No. 1
Brady, James J. and John D. Todd—No. 54

Christy, R. F. and J. M. Keller—No. 40
Cohn, Bryon E.—No. 39
Corson, Dale R.—see Wilson, Robert R.

Dancoff, S. M.—No. 17
Davis, Leverett, Jr.—No. 10
Dember, A. and A. Goetz—No. 42
—— see Goetz, A.

Ellis, Joseph W. and Jean Bath—No. 52
Elsasser, Walter M.—No. 35

Fenn, W. H.—No. 6
Fine, Paul—No. 18
Fleming, G. M. and Joseph E. Henderson—No. 24
Focke, Alfred B.—No. 27
Foster, M. G. and A. Goetz—No. 4
Fowler, W. A. and C. W. Sheppard—No. 56
—— see Lauritsen, C. C.
—— see Sheppard, C. W.

Gaerttner, E. R., L. A. Pardue and J. F. Streib—No. 38
—— see Becker, R. A.
—— see Pardue, Louis A.
Goetz, A. and A. Dember—No. 41
—— see Dember, A.
—— see Foster, M. G.
—— see Gould, W. O.
Goss, Wilbur H. and Joseph E. Henderson—No. 44
Gould, W. O. and A. Goetz—No. 9

Hale, Donald H.—No. 50
Hane, W. A.—see Johnson, G. W.
Hellund, E. J. and E. A. Uehling—No. 14
Henderson, Joseph E. and K. V. MacKenzie—No. 46
—— see Abbott, Frank R.
—— see Fleming, G. M.
—— see Goss, Wilbur H.
—— see Rubens, S. M.
Houston, W. V. and S. Rubin—No. 16

Johnson, G. W., W. A. Hane and P. A. Anderson—No. 15

Kaplan, Joseph—No. 48
Keller, J. M.—see Christy, R. F.
Kirkham, Don—No. 19
Kyropoulos, S.—No. 23

Langer, R. M.—No. 12
Lauritsen, C. C., W. A. Fowler and T. Lauritsen—No. 51
Lauritsen, T.—see Lauritsen, C. C.

McLean, W. B. and R. A. Becker—No. 53
MacKenzie, K. V.—see Henderson, Joseph E.
Morrison, P.—No. 3

Nielsen, Carl E.—No. 31

Oppenheimer, F. and E. P. Tomlinson—No. 49

Pardue, Louis A. and E. R. Gaerttner—No. 32
—— see Gaerttner, E. R.
Pasternack, Simon—No. 26

Richtmyer, Robert D.—No. 43
Rubens, S. M. and J. E. Henderson—No. 28
Rubin, S.—see Houston, W. V.

Schiff, L. I.—No. 7
Sheng, H. Y.—see Barker, E. F.

Sheppard, C. W. and W. A. Fowler—No. 2
—— see Fowler, W. A.
Skaggs, L. S.—see Allison, S. K.
Smith, N. M., Jr.—see Allison, S. K.
Snyder, H.—No. 45
Stephenson, S. T.—No. 37
Strait, Louis A.—No. 34
Streib, J. F.—see Gaerttner, E. R.

Taub, A. H.—No. 22
Todd, John D.—see Brady, James J.
Tomlinson, E. P.—see Oppenheimer, F.
Townes, Charles H.—No. 5
Tregidga, Angus C.—No. 36

Uehling, E. A.—see Hellund, E. J.

Volkoff, G. M.—No. 47

White, John U.—No. 25
Wilson, Robert R. and Dale R. Corson—No. 11

Yunker, E. A.—No. 33

THE AMERICAN INSTITUTE OF PHYSICS

INCORPORATED

ADMINISTRATIVE STAFF

HENRY A. BARTON, *Director*

MADELINE M. MITCHELL, *Publications Manager*

Office: 175 Fifth Avenue, New York, New York

JOURNALS

THE PHYSICAL REVIEW

REVIEWS OF MODERN PHYSICS
JOHN T. TATE, *Editor*
J. W. BUCHTA, *Assistant Editor*

JOURNAL OF APPLIED PHYSICS
ELMER HUTCHISSON, *Editor*

THE JOURNAL OF THE OPTICAL SOCIETY OF AMERICA

THE REVIEW OF SCIENTIFIC INSTRUMENTS
F. K. RICHTMYER, *Editor*

JOURNAL OF THE ACOUSTICAL SOCIETY OF AMERICA
FLOYD A. FIRESTONE, *Editor*

THE JOURNAL OF CHEMICAL PHYSICS
HAROLD C. UREY, *Editor*
JOSEPH E. MAYER, *Assistant Editor*

THE AMERICAN PHYSICS TEACHER
DUANE ROLLER, *Editor*

GOVERNING BOARD

For The American Physical Society:

JOHN T. TATE, *Chairman*
University of Minnesota

GEORGE B. PEGRAM, *Secretary*
Columbia University

KARL T. COMPTON
Massachusetts Institute of Technology

For The Optical Society of America:

E. C. CRITTENDEN
National Bureau of Standards

A. C. HARDY
Massachusetts Institute of Technology

W. B. RAYTON
Bausch & Lomb Optical Company

For The Acoustical Society of America:

FLOYD A. FIRESTONE
University of Michigan

HARVEY FLETCHER
Bell Telephone Laboratories

WALLACE WATERFALL
The Celotex Corporation

For The Society of Rheology:

WHEELER P. DAVEY
Pennsylvania State College

MELVIN MOONEY
United States Rubber Products, Inc.

R. L. PEEK, JR.
Bell Telephone Laboratories

For The American Association of Physics Teachers:

PAUL E. KLOPSTEG
Central Scientific Company

FREDERIC PALMER, JR.
Haverford College

F. K. RICHTMYER
Cornell University

The American Institute of Physics is a membership corporation of which five societies are the founding members. These five societies are the principal national societies devoted to pure and applied physics in America. Their names, and those of their representatives who form the Governing Board of the Institute, are given above. The principal work of the Institute is the publication of journals sponsored by the societies or by itself. The names and the editors of the journals are also listed above.

The broad purpose of the Institute is to represent, in all matters of wide or common interest, the five thousand or more members and subscribers associated with the Founder Societies and the journals. It aims to advance the science and profession of physics, and to promote cooperation between pure research, the applied sciences and the industries. To achieve these aims, it is greatly in need of an endowment and is empowered by law to administer grants and funds of any kind.

CONTENTS

PHYS. REV. 56 (1939) OCTOBER 15

Hyperfine Spectra of Mg^{25}, Co^{59} and the Nuclear Moments of Mn^{55} . . . E. C. CRITTENDEN, JR. 709

Ionization of a Beam of Fast Neutrons . . . . . PAUL C. ARMSFIELD 714

Magnetic Moments of the Proton and the Deuteron. The Radio-frequency Spectrum of H_2 in Various Magnetic Fields . . . . . J. M. B. KELLOGG, I. I. RABI, N. F. RAMSEY, JR. AND J. R. ZACHARIAS 728

Note on the Scattering of Neutrons by Protons . . . . . C. KITTEL AND G. BREIT 744

On the Derivation of the Dispersion Formula for Nuclear Reactions . . . A. J. F. SIEGERT 750

Identification of Characteristic X-Rays Associated with Radioactive Decay . PHILIP H. ABELSON 753

On the Single Crystal X-Ray Diffraction Pattern of Calcite . . . . FRANKLIN MILLER, JR. 757

M_I and M_{II} X-Ray Absorption Edges of Lead . . . . . J. W. MCGRATH 765

Intensities of Hélium Lines . . . . . L. SIBAIYA 768

$^1\Sigma_u$-$^1\Sigma$ Transition of the C_2 Molecule . . . . . O. G. LANDSVERK 769

Note on Electronic States of Diatomic Carbon, and the Carbon-Carbon Band . . . . . ROBERT S. MULLIKEN 778

Band-Head Spectrum and Molecular Constants of Silicic Oxide . . . . . ALVIN H. NIELSEN AND WALTER GORDY 781

Radiative and Thermionic Characteristics of Uranium . . . W. L. HOLE AND R. W. WRIGHT 785

Electronic Energy Bands in Metallic Tungsten . . . . . MILLARD F. MANNING AND MARVIN I. CHODOROW 797

Spinor Equations for the Meson and Their Solution When No Field Is Present . A. H. TAUB 799

Improved Method of Making Permanent Electrets and Factors Which Affect Their Behavior . . . . . WILFRED M. GOOD AND J. D. STRANATHAN 810

Note on the Slide Theory of Diffusion . . . . . R. P. JOHNSON 814

Transport Phenomena in Mixtures of Gases . . . . . E. J. HELLUND AND E. A. UEHLING 818

Letters to the Editor:

Electrical Arc Source for the Cyclotron . . . . . EDWIN MCMILLAN AND W. W. SALISBURY 826

High Pressure Supersonic Reinforcement Vibration of the Ammonia Molecule . . . . . G. B. B. M. SUTHERLAND 826

Magnetic Anisotropy of Nickel at 20°K . . . . . E. J. WILLIAMS AND R. M. BOZORTH 827

Disintegration of Hafnium . . . . . BRUNO ROSSI, H. VAN NORMAN GILBERT AND J. BARTON HOAG 827

Magnetic Spectrograph Investigation of B^{10} Gamma-Radiation . . . . . G. E. VALLEY 828

Search for β- and Delayed γ-Radiation from the Deuteron-Neutron Reaction . . . . . M. H. KANNER AND W. T. HARRIS 829

Fast Neutrons from Fluorine Bombarded with Protons . . . W. A. FOWLER AND C. C. LAURITSEN 830

Fast Neutrons from Lithium Bombarded with Protons . . . . . W. A. FOWLER AND C. C. LAURITSEN 831

On the Stability of the Proton-Proton and Proton-Neutron Interactions . . . . . EUGENE W. BECKER AND HERBERT S. PLENDL 832

Proceedings of the American Physical Society:

Southeastern Section: University of Georgia Meeting, March 31 and April 1, 1939; Minutes and Abstracts 1–31 833

Stanford, California, Meeting, June 30–July 1, 1939: Minutes and Abstracts 1–37; Author Index . 849

LANCASTER PRESS, INC., LANCASTER, PA.